Non-contact Monitoring of Skin Perfusion as a Proxy for Haemodynamic Status



Mirae Harford

St Cross College

University of Oxford

A thesis submitted for the degree of

Doctor of Philosophy

Hilary 2023

This thesis is dedicated to
my parents
who taught me the joy and privilege of lifelong learning.

Declaration

I declare that this thesis is my own work and was performed while I was a full-time postgraduate student at the University of Oxford. All figures are original unless otherwise indicated. Where figures or tables have been adapted from work previously published elsewhere, this has been stated and referenced. Materials from Chapter 6 have been published. I was the sole producer of material for this paper, with co-authors having an advisory role. The word count (excluding tables, lists, figure legends, and references) falls under the 50,000 limit. None of the material presented here has been previously submitted for another degree or qualification.



Mirae Harford

March 2023

Acknowledgements

The completion of this thesis would not have been possible without the support of a large number of people.

First of all, I would like to thank my supervisors - Peter Watkinson and Lionel Tarassenko. Thank you for having been such inspiring, encouraging, and kind supervisors and mentors. I genuinely could not have wished for better. Thank you for this opportunity; I feel so blessed to have had these years of exploration!

I would also like to thank Duncan Young for his infinite wisdom and enthusiasm, and Kevin Marsh for having been an extremely supportive pastoral mentor. Thank you also to Stuart McKechnie and Chris Pugh who provided invaluable guidance through the transfer and confirmation of status process.

I gratefully acknowledge financial support from the NIHR Oxford Biomedical Research Centre.

I owe a great deal to my friends and colleagues at the Institute of Biomedical Engineering and the Critical Care Research Group. As much as I love the research field, the most wonderful aspect of immersing myself in the academic world has been the mega-brains I have had access to and the warm friendship and camaraderie these people have provided. Particular mention to Mauricio Villarroel and João Jorge who really took me under their wing and introduced me to the world of image analysis.

Outside of the research world, I am deeply thankful to my family and friends who have carried me through some of the more difficult times during my DPhil journey. Special thanks to my husband and best friend Phil who has kept our lives going over the last four years with patience, support, and love. Also to our children Ethan and Jemima, who make our lives infinitely better each day by just being themselves.

At the age of 12, I was moved from a small town in the outskirts of Seoul, South Korea to the UK by the two wisest and bravest people I know. My parents have given up so much to give me and my brother a chance at a better life and understanding of the world. This doctorate is a direct result of my parents' belief in me and their boundless love, and this thesis is dedicated to them.

Abstract

The examination of skin perfusion is a key component of haemodynamic assessment. The body is quick to redirect blood flow away from the skin during periods of haemodynamic instability, making it a sensitive site for an early detection of cardiovascular compromise. The clinical assessment of skin perfusion is mostly subjective. As an external organ, however, it is possible to objectively assess skin perfusion using video cameras operating both within and outside the visible light spectrum.

The use of video cameras in clinical monitoring has been explored in vital-sign estimation, and may offer both objectivity and higher sensitivity compared to the current subjective assessment of skin perfusion. However, its evolution as a monitor has been held back by practical challenges such as vulnerability to signal noise from movement and lighting changes. This thesis describes the Mapping Of Lower Limb skIn pErfusion (MOLLIE) study, in which phenylephrine and glyceryl trinitrate (GTN) were used to pharmacologically induce skin perfusion changes in healthy volunteers under controlled environmental conditions. The participants were monitored using a variety of video cameras.

Using this dataset, several streams of analyses are presented. First, image processing techniques are used to quantify clinically visible skin mottling. Following the measurement of these direct correlates of visually detected clinical findings, the remainder of the thesis demonstrates the detection of induced skin vasoconstriction and vasodilation which is not readily visible to the naked eye. A differential response to perfusion changes in different regions of skin is described, related to the underlying vascular anatomy of the skin.

This thesis argues that video cameras can provide additional insight into the haemodynamic status. It is only by combining the knowledge of skin as an organ and its blood supply with the available image processing techniques that we can fully understand the information present in the measured parameters at the skin surface and improvements can be made in skin perfusion monitoring.

Publications

Publications arising from or related to this thesis

- **Harford M.**, Catherall JA., Gerry, S., Young, JD., and Watkinson, PJ., 2019. Availability and performance of image-based, non-contact methods of monitoring heart rate, blood pressure, respiratory rate, and oxygen saturation: A systematic review. Physiological Measurement, 40(6):06TR01.

- **Harford M.**, Areia CM., Villarroel M., Jorge J., Davidson S., Finnegan E., Mahdi A., Young JD., Tarassenko L., and Watkinson PJ., 2019. A study protocol for an exploratory interventional study investigating the feasibility of video-based non-contact physiological monitoring in healthy volunteers by Mapping Of Lower Limb skIn pErfusion (MOLLIE). BMJ Open, 10(6):e036235.

- **Harford M.**, Villarroel M., Jorge J., Redfern O., Finnegan E., Davidson S., Young JD., Tarassenko L., and Watkinson PJ., 2022. Contactless skin perfusion monitoring with video cameras: tracking pharmacological vasoconstriction and vasodilation using photoplethysmographic changes. Physiological Measurement, 43(11):115001.

- Jorge J., **Harford M.**, Villarroel M., Chaichulee S., Davidson S., Finnegan E., Clark SH., Young JD., Watkinson PJ., and Tarassenko L., 2019. Non-contact assessment of peripheral artery haemodynamics using infrared thermography. IEEE Transactions on Biomedical Engineering, 68(1): 276-288.

- Jorge J., Villarroel M., Tomlinson H., Gibson O., Darbyshire JL., Ede J., **Harford M.**, Young JD., Tarassenko L., and Watkinson PJ., 2022. Non-contact physiological monitoring of post-operative patients in the intensive care unit. npj Digital Medicine, 5(1):4.

Conference abstracts

- **Harford M.**, Bedford J., Redfern O., Jorge J., Villarroel M., Tarassenko L., Young JD., and Watkinson PJ. Incidence of lower limb mottling in critical care patients and associated mortality risk. European Society of Intensive Care Medicine Annual Conference 2019, Berlin, Germany

Oral presentations

- **Harford M.** Biomedical engineering efforts for medicine of the future. Annual Mackintosh Conference 2020, Oxford, United Kingdom

Other publications and conference abstracts from the MOLLIE study

- Finnegan E., Villarroel M., Davidson S., Jorge J., **Harford M.**, Watkinson P., Young D., and Tarassenko L., 2021. Pulse arrival time as a surrogate of blood pressure. Scientific Reports, 11(1):22767.
- Finnegan E., Davidson S., **Harford M.**, Watkinson P., Tarassenko L., and Villarroel M., 2023. Features from the photoplethysmogram and the electrocardiogram for extimating changes in blood pressure. Scientific Reports, 13 (Article number 986).

Contents

List of Figures **xvi**

List of Tables **xix**

List of Abbreviations **xxi**

1 Introduction **1**

1.1 The clinical setting 4

1.1.1 The cardiovascular system 4

1.1.2 Approaches to haemodynamic monitoring in critical care . . 5

1.1.3 The value of skin perfusion assessment 9

1.1.4 Skin perfusion as a prognostic marker 15

1.1.5 Section summary 16

1.2 Anatomy of skin perfusion 16

1.2.1 Skin structure 17

1.2.2 Arterial perforators and skin macrocirculation 18

1.2.3 Anatomy of skin microcirculation 24

1.2.4 Section summary 25

1.3 Physiology of skin perfusion 26

1.3.1 Regulation of skin perfusion 26

1.4 Measurement of skin perfusion 27

1.4.1 Clinical/bedside assessment of skin perfusion 28

1.4.2 Skin perfusion monitoring tools 31

1.5 Summary and current gaps in knowledge 33

2 Usefulness of skin mottling assessment 35

2.1 Introduction . . . 35

2.2 Methods . . . 37

2.2.1 Study design . . . 37

2.2.2 Settings and data sources . . . 37

2.2.3 Participants . . . 38

2.2.4 Variables, data sources, and measurement . . . 38

2.2.5 Bias . . . 39

2.2.6 Study size . . . 39

2.2.7 Outcomes . . . 39

2.2.8 Statistical analyses . . . 39

2.3 Results . . . 40

2.3.1 Participants and descriptive data . . . 40

2.3.2 Main results . . . 41

2.3.3 Subgroup analysis . . . 42

2.4 Discussion . . . 42

2.5 Chapter summary . . . 45

3 Rationale and motivation for video camera-based skin assessment 47

3.1 Introduction . . . 47

3.2 Video camera as a skin perfusion assessment tool . . . 48

3.2.1 Video camera use for physiological monitoring . . . 49

3.2.2 Windkessel effect to contact PPG waveform . . . 50

3.2.3 Origins of PPGi . . . 52

3.3 Study introduction and rationale for study design . . . 56

4 Materials, methods, and the dataset 59

4.1 Ethical approval and recruitment 60

4.1.1 Ethical approval 60

4.1.2 Recruitment 60

4.2 Study setting 60

4.3 Participants and eligibility 61

4.4 Experimental timeline 62

4.5 Interventions 64

4.5.1 Drugs 64

4.5.2 Tourniquet 66

4.6 Monitoring instrumentation 68

4.6.1 Cameras 68

4.6.2 Reference monitors 71

4.6.3 Data collection set-up 73

4.7 Data storage 73

4.8 Analysis methods overview 74

4.8.1 Identification of periods of interest 75

4.8.2 Identification of region of interest (ROI) 75

4.8.3 RGB multi-channel analysis 76

4.8.4 Validity of frames included 76

4.9 Data display and summary statistics 77

4.9.1 Box and whisker plots 78

4.10 Acquired dataset from the MOLLIE study 78

4.10.1 Participant demographics 78

4.10.2 Evidence of drug effect 79

4.10.3 Camera data acquired 82

4.11 Chapter summary 83

5 Detection of skin mottling using non-contact image-based analysis 85

5.1 Introduction . . . 85

5.1.1 Rationale for approach . . . 86

5.1.2 Using the MOLLIE dataset to model skin mottling . . . 88

5.1.3 Hypothesis . . . 89

5.2 Analysis methods . . . 90

5.2.1 Selection of the region of interest for image processing . . . 90

5.2.2 Edge detection . . . 91

5.2.3 Clinical assessment . . . 94

5.2.4 Subgroup analysis using clinical labels . . . 97

5.3 Results . . . 98

5.3.1 Kirsch operator convolution . . . 98

5.3.2 Clinical classification of skin mottling changes and subgroup analyses . . . 101

5.4 Discussion . . . 105

5.5 From visible to non-visible parameters . . . 108

6 Detection of skin perfusion changes using photoplethysmographic imaging 109

6.1 Introduction . . . 109

6.1.1 Aims and hypotheses of this chapter . . . 112

6.2 Analysis methods . . . 114

6.2.1 AC amplitude . . . 115

6.2.2 DC component . . . 117

6.2.3 Hue, saturation, value (HSV) . . . 118

6.3 Statistical methods . . . 120

6.4 Results . . . 121

6.4.1 Change in pulsatile PPGi waveform amplitude (AC) . . . 121

6.4.2 Change in the DC component of PPGi . . . 126

6.4.3 Skin colour changes (hue and saturation) 127

6.5 Chapter summary 129

7 Skin changes according to perforator locations 132

7.1 Introduction 133

7.2 Localising perforators using thermal imaging 136

7.2.1 Introduction 136

7.2.2 Methods 138

7.2.3 Results 139

7.2.4 Section summary 141

7.3 Consistency of baseline skin radiance pattern and correlation between perforator locations and baseline skin radiance 143

7.3.1 Introduction 143

7.3.2 Methods 144

7.3.3 Results 147

7.3.4 Section summary 149

7.4 Thermal response to vasoconstriction and vasodilation 151

7.4.1 Introduction 151

7.4.2 Methods 153

7.4.3 Results 153

7.4.4 Section summary 156

7.5 Changes in laser speckle contrast imager (LSCI) 159

7.5.1 Introduction 159

7.5.2 Methods 161

7.5.3 Results 162

7.6 Changes occurring between the rest and peak periods in all sub-regions 165

7.6.1 Introduction 165

7.6.2 Methods 166

7.6.3 Results . . . 167
7.6.4 Section summary . . . 169
7.7 Chapter summary . . . 170

8 Implications of perforator locations on RGB imaging 173
8.1 Introduction . . . 174
8.2 Methods . . . 177
8.2.1 Selection of the region of interest . . . 177
8.2.2 Sub-region selection . . . 177
8.2.3 Comparison of ROI_{HIGH} and ROI_{LOW} . . . 178
8.2.4 Changes occurring between the rest and peak periods in all sub-regions . . . 179
8.2.5 Sub-region proximity to perforator locations defined in chapter 7 179
8.3 Results . . . 180
8.3.1 Locations of ROI_{HIGH} and ROI_{LOW} . . . 180
8.3.2 Absolute change in PPGi amplitude in the sub-regions . . . 182
8.3.3 Changes occurring between the rest and peak periods in all sub-regions . . . 183
8.3.4 Proximity of ROI_{HIGH} to perforator zones . . . 186
8.4 Discussion . . . 186

9 Conclusions 189
9.1 Conclusions . . . 189
9.1.1 Contributions of this thesis . . . 189
9.1.2 Limitations . . . 198
9.2 Future directions . . . 201
9.2.1 PPGi waveform analysis from the MOLLIE study dataset . . . 201
9.2.2 Analyses from the Arterial Perforator Imaging study . . . 201
9.2.3 Future clinical studies . . . 203
9.3 Concluding remarks . . . 206

Appendices

A Prognosis associated with skin mottling **208**

A.1 Systematic review of skin mottling literature 208

A.1.1 Introduction 208

A.1.2 Methods 208

A.1.3 Results 209

A.1.4 Discussion 212

B Ethics approval documents **213**

C MOLLIE study documents **216**

D HemaClear® figures **228**

E RGB to HSV conversion **231**

E.1 Introduction 231

E.2 Conversion algorithm 231

F Background radiance change **233**

G Consistency of baseline skin surface radiance **235**

H Additional analyses from ICU databases: skin mottling **237**

H.1 Included hospitals from eICU-CRD 237

H.2 Individual database results 238

H.3 UK versus US results 241

I Perforator locations on RGB imaging: further results **242**

I.1 Absolute change in PPGi amplitude in the sub-regions 242

I.1.1 Red channel 242

I.1.2 Blue channel 243

I.2 Percentage change in PPGi amplitude in the sub-regions 243

I.2.1 Green channel 243

I.2.2 Red channel 245

I.2.3 Blue channel 245

J Permissions **249**

Bibliography **268**

List of Figures

1.1 Microvasculature 9

1.2 Structure of the skin 17

1.3 Two types of arterial perforators 19

1.4 Schematic representation of the cutaneous perforator angiosomes . . 21

1.5 Laser speckle contrast imaging 33

4.1 Experimental timeline for drug infusion 64

4.2 Bayer filter pattern and pixel response curves 69

4.3 Experimental set-up 74

4.4 De-Bayer image processing 77

4.5 Changes in reference vital signs 81

5.1 The mottling score 87

5.2 Kirsch edge detection kernel 91

5.3 Demonstration of Kirsch operator 92

5.4 Evolution of mottling in MOLLIE dataset 95

5.5 Baseline Kirsch operator contrast 99

5.6 Changes in mean contrast to reflect mottling 100

5.7 Subgroup analysis according to clinical labels of skin mottling . . . 104

6.1 DC and AC components of photoplethysmography imaging (PPGi) waveform 111

6.2 Valid beats analysis of pulsatile peak-to-trough PPGi amplitude . . 117

6.3 HSV colour space 119

6.4 Peak-to-trough pulsatile AC amplitude during rest 122

6.5 Pre- to peak-infusion change in the amplitude of the pulsatile (AC) component 124

6.6 Correlation between AC component and LSCI 126

6.7 Correlation between DC component and LSCI 127

6.8 Colour hue and saturation response to vasoconstriction and dilation 128

7.1 Perforator progression 140

7.2 Perforator images 142

7.3 Sørensen-Dice similarity index 146

7.4 Example comparison of the $ROI_{HIGH\text{-}TEMP}$ and $ROI_{LOW\text{-}TEMP}$ 148

7.5 Example comparison of $ROI_{HIGH\text{-}TEMP}$ and perforator locations . . . 150

7.6 Radiance changes in response to phenylephrine and GTN 155

7.7 Flux changes in response to phenylephrine and GTN 163

7.8 Median change in radiance observed in response to phenylephrine and GTN: all time periods 168

8.1 Paired ROI_{HIGH} and ROI_{LOW} in 4 individuals 181

8.2 Differential response in RGB sub-regions: absolute change in PPGi amplitude 182

8.3 Change in peak-to-trough amplitude of the AC component of the PPGi waveform associated with phenylephrine and GTN: all time periods 184

9.1 Individual responses to phenylephrin and GTN 197

A.1 PRISMA flow diagram for skin mottling systematic review 210

A.2 Mortality odds ratio associated with any degree of skin mottling . . 211

D.1 HemaClear® 229

D.2 HemaClear® XL: applied skin pressure 230

F.1 Background radiance change from baseline 234

I.1 Differential response in RGB sub-regions: absolute change in PPGi amplitude 244

I.2 Differential response in RGB sub-regions (contd.) 247

I.2 Differential response in RGB sub-regions: relative change in PPGi amplitude 248

List of Tables

2.1 Characteristics of included patients 41

2.2 ICU and Hospital Mortality adjusted odds ratio comparing mottled and never-mottled groups 41

2.3 Mottling database: sensitivity analysis 43

4.1 MOLLIE: inclusion and exclusion criteria 62

4.2 RGB camera specifications 70

4.3 RGB configuration for MOLLIE 70

4.4 Thermal configuration for MOLLIE 71

4.5 Laser speckle contrast imager specifications 73

4.6 Laser speckle contrast imager configuration for MOLLIE study . . . 73

4.7 Summary participant demographics 79

5.1 Summary of mean Kirsch output changes 100

5.2 Phenylephrine session clinical mottling assessment 102

5.3 GTN session clinical mottling assessment 103

5.4 Summary RGB video camera ROI_{GLOBAL} results 105

6.1 Summary RGB video camera ROI_{GLOBAL} results 123

7.1 Sørensen-Dice similarity coefficient 145

7.2 Radiance changes for three regions 154

7.3 Flux changes for three regions 163

8.1 Differential response in RGB sub-regions: Phenylephrine 183

8.2 Differential response in RGB sub-regions: GTN 185

G.1 Sørensen-Dice similarity index 236

H.1 Characteristics of included hospitals from eICU-CRD 238

H.2 Skin mottling: UK versus US results 241

List of Abbreviations

AC . . . . . Alternating Current

ANP . . . . . Atrial Natriuretic Peptide

βHCG . . . . . beta Human Chorionic Gonadotrophin

BD . . . . . Becton Dickson

BIDMC . . . . Beth Israel Deaconess Medical Center

BMI . . . . . Body Mass Index

BNP . . . . . Brain Natriuretic Peptide

BSP-ML . . . Biomedical Signal Processing & Machine Learning

BP . . . . . Blood Pressure

CI . . . . . Confidence Interval

CCD . . . . . Charged-coupled device (image sensor)

CCRF . . . . . Cardiovascular Clinical Research Facility

CCU . . . . . Critical Care Unit

CMOS . . . . . Complementary Metal Oxide Semiconductor

CO . . . . . Cardiac Output

COVID-19 . . Coronavirus Disease 2019

CRT . . . . . Capillary Refill Time

CT . . . . . Computed Tomography

CUREC . . . . Central University Research Ethics Committee

DC . . . . . Direct Current

ECG . . . . . ElectroCardioGram

eICU-CRD . . eICU Collaborative Research Database

FICE . . . . . Focused Intensive Care Echocardiography

FLIR . . . . . Forward Looking InfraRed

GTN . . . . . Glyceryl TriNitrate

HR . . . . . Heart Rate

IBME . . . . . Institute of BioMedical Engineering

ICU . . . . . Intensive Care Unit

IQR . . . . . InterQuartile Range

ISRCTN . . . International Standard Randomised Controlled Trial Number

IR . . . . . Infrared

IV . . . . . IntraVenous

KLT . . . . . Kanade-Lucas-Tomasi

LDF . . . . . Laser Doppler Flowmetry

LDI . . . . . Laser Doppler Imaging

LED . . . . . Light-emitting diode

LOA . . . . . Limits of agreement

LOS . . . . . Length of stay

LSCI . . . . . Laser Speckle Contrast Imaging or Laser Speckle Contrast Imager

MAP . . . . . Mean Arterial Pressure

MIMIC . . . . Medical Information Mart for Intensive Care

MOF . . . . . Multi-organ failure

MOLLIE . . . Monitoring Of Lower Limb skIn pErfusion (study acronym)

NICU . . . . . Neuro Intensive Care Unit

NIR . . . . . Near-Infrared

NIRS . . . . . Near-Infrared Spectroscopy

NO . . . . . Nitric Oxide

OASIS . . . . . Oxford Acute Severity of Illness Score

OR . . . . . Odds Ratio

PAC . . . . . Pulmonary Artery Catheter

PD . . . . . PhotoDiode

PICRAM . . . Post-Intensive Care Risk-adjusted and Monitoring

PPG . . . . . PhotoPlethysmoGraphy or PhotoPlethysmoGram

cPPG . . . . . Contact PhotoPlethysmoGraphy

PPGi . . . . . PhotoPlethysmoGraphic Imaging (imaging waveform)

PTT . . . . . Pulse Transit Time

RECORD . . . REporting of studies Conducted using Observational Routinely-collected Data

RGB . . . . . Red Green Blue (camera colour channels)

RMSE . . . . . Root Mean Square Error

ROI . . . . . Region Of Interest

RR . . . . . Respiratory Rate

RRT . . . . . Renal Replacement Therapy

SpO_2 . . . . . Peripheral Oxygen Saturation

SQI . . . . . Signal Quality Index

SR . . . . . SteRadian

StO_2 . . . . . Tissue Oxygen Saturation

SV . . . . . Stroke Volume

$ScvO_2$ . . . . . Central venous Oxygen Saturation

SvO_2 . . . . . Mixed venous Oxygen Saturation

TEB . . . . . Thoracic Electrical Bioimpedance

TTE . . . . . Transthoracic Echocardiography

UK . . . . . United Kingdom

USA . . . . . United States of America

VIP . . . . . Vasoactive Intestinal Peptide

1

Introduction

Contents

1.1 The clinical setting 4
1.1.1 The cardiovascular system 4
1.1.2 Approaches to haemodynamic monitoring in critical care 5
1.1.3 The value of skin perfusion assessment 9
1.1.4 Skin perfusion as a prognostic marker 15
1.1.5 Section summary 16
1.2 Anatomy of skin perfusion 16
1.2.1 Skin structure 17
1.2.2 Arterial perforators and skin macrocirculation 18
1.2.3 Anatomy of skin microcirculation 24
1.2.4 Section summary 25
1.3 Physiology of skin perfusion 26
1.3.1 Regulation of skin perfusion 26
1.4 Measurement of skin perfusion 27
1.4.1 Clinical/bedside assessment of skin perfusion 28
1.4.2 Skin perfusion monitoring tools 31
1.5 Summary and current gaps in knowledge 33

Skin perfusion is of interest in several medical disciplines including dermatology, diabetology, rheumatology, plastic surgery, and critical care. The assessment methods and the implications of any abnormalities detected vary among the specialties listed. Given this broad usefulness of assessing the blood flow to the

skin, an objective, accurate, easy to use, and low-to-no risk skin perfusion monitor would be of high clinical value. Of the potential settings and clinical questions to investigate related to skin perfusion, I concentrate on the assessment of skin perfusion as a proxy marker of systemic haemodynamic status in acute care in this thesis. This concept of using the skin as a window to the underlying global circulatory status is deeply embedded in our clinical practice, originating back in the writings of Hippocrates [1]. Skin perfusion assessment as a haemodynamic marker in acute care also has some notable differences when compared to its use in the other clinical settings listed above, where the perfusion changes tend to occur over periods of months to years. In addition, the resulting changes in the other clinical settings are often chronic and irreversible [2, 3]. In contrast, the skin perfusion changes of interest in acute care tend to occur over minutes to hours and directly reflect the underlying haemodynamic status [4]. The skin perfusion changes I refer to throughout this thesis are likely to be transient and reversible. Clinical settings in which chronic skin perfusion changes are monitored have seen a recent rise in new measurement methods such as Laser Doppler Imaging (LDI) and Laser Speckle Contrast Imaging (LSCI) [5–7], with several of the developed tools or monitors now implemented in clinical practice [8]. In contrast, the assessment of skin perfusion for haemodynamic status has remained largely a clinical task and therefore often subjective and operator-dependent [4, 9]. In these acute settings, objective skin perfusion monitoring tools have not been incorporated into routine clinical practice [8, 10].

In this thesis, I first explore the clinical implications of documented subjective skin perfusion changes in critical care settings, using the incidence of recorded skin mottling and its association with patient outcomes. Using this visible examination feature as a marker of poor perfusion and circulatory failure [11, 12], I explore objective skin perfusion monitoring using non-contact video cameras. While currently available skin perfusion monitors tend to focus on the measurement of a single parameter (section 1.4.2), I aim to demonstrate that video cameras have

the additional advantage of potentially tracking several parameters concurrently. By combining the knowledge of *which* biological signals are measurable and *where* these signals are measured, video cameras as skin perfusion monitoring tools may provide additional information beyond that attainable from visual examination by clinicians. To demonstrate this concept, I designed a clinical study in which skin perfusion was pharmacologically manipulated under controlled settings while the skin was monitored using a variety of instruments.

To best apply the use of video cameras to the clinical aim of this thesis, current knowledge and published evidence from several disciplines will be combined. First, there is the known anatomy and physiology of the skin as an organ with its own blood supply and function (as opposed to simply a uniform barrier between the body and the external environment). As well as the anatomy and the physiology of skin, the status of the clinical monitoring of skin perfusion prior to this thesis is reviewed. These are covered in this introductory chapter in the following order:

- Section 1.1: Understanding the clinical setting and a description of the cardiovascular system;
- Section 1.2: A description of the relevant skin anatomy;
- Section 1.3: Discussion of the key aspects of cardiovascular and skin physiology;
- Section 1.4: A review of the currently available methods of skin measurement.

Following presentation of the clinical background in this chapter, the evidence for the usefulness of skin perfusion monitoring - particularly in critical care settings - is further explored in chapter 2. I then review the evolution of physiological monitoring using video cameras, the current gaps in knowledge, and the rationale for a further clinical study in which the remainder of the thesis is based in chapter 3. The anatomy and physiology of skin and its blood supply described in the remainder

of this chapter need to be well understood for the design of any skin-based monitors. This knowledge has not always been incorporated into the analysis of camera monitoring of physiological variables in the literature. This is also explored in chapter 3 to further justify the work presented in this thesis. Chapter 4 describes the methodology of the clinical study and the resulting dataset. In chapter 5, I propose an image analysis method to detect the clinically visible skin mottling previously discussed in chapter 2. The following three chapters (chapters 6 to 8) then go onto demonstrate detection of skin perfusion changes that cannot be appreciated by visual inspection, applying the knowledge of skin vascular anatomy to improve understanding of the signal detected at the skin surface. Finally, chapter 9 contextualises the results presented and proposes clinical applications in which the work discussed in this thesis may be extended to.

1.1 The clinical setting

1.1.1 The cardiovascular system

The human cardiovascular system is responsible for both the delivery of oxygen, glucose, and micronutrients to all living cells around the body and the concurrent removal of waste products from cellular activities [13]. It may be modelled as two unidirectional pumps (left and right ventricles) connected by a high-pressure network of pipes on one side (the systemic circulation) and a low-pressure network on the other side (the pulmonary circulation). Its normal function is critical for homeostasis.

The human cardiovascular system faces the challenging task of meeting the body's needs in a wide range of conditions. In order to efficiently meet these varying needs and respond to any changes promptly, the precise control of cardiovascular function is achieved via several related systems working in parallel. This is further explored in section 1.3.

1.1.2 Approaches to haemodynamic monitoring in critical care

The cardiovascular system has been described as a network, designed to optimally deliver oxygen and glucose to distal tissues. During any disease process, how well the cardiovascular system is adjusting to meet the varying demands of the body, and how much strain the system is under at any one time are key questions facing clinicians. As a result, inpatients in secondary care settings routinely undergo haemodynamic monitoring [14]. This ranges from simple bedside measurements of routine vital signs (e.g., heart rate (HR) and blood pressure (BP)) measured intermittently in all inpatients, to continuous invasive haemodynamic monitoring favoured in critical care settings [15]. Cardiovascular monitoring strategies can be broadly divided into those that monitor the cardiac pump output (i.e., the amount of blood leaving the heart) and the pressure in the larger vessels, or those that monitor the target destination (i.e., the amount of blood being received by the distal organs and tissues). These two approaches are discussed in turn in the following sections.

1.1.2.1 Global circulation

Traditional methods of cardiovascular monitoring rely on relatively simple bedside measurements of HR and BP. These global metrics have the advantage of being easy to estimate non-invasively. In hospital inpatients outside of the critical care environment who are not acutely unwell, intermittent measurements of these parameters usually provide an adequate picture of the patient's physiological status. However, in critical care settings - where patient physiology is severely deranged and where patients receive therapies that often affect these simple measurements (either directly or via physiological feedback loops) - these measurements alone may provide an incomplete picture [15]. The 1970s saw the introduction of pulmonary artery catheters (PACs) to critical care units that allowed accurate estimates of the volume of blood leaving the heart, using the thermodilution technique [16]. The use

of PAC fell out of favour over the following decades because of the high complication rates associated with their use and the lack of robust evidence to suggest that their use was beneficial [17]. More recently, the use of PAC has largely been replaced by less invasive cardiac output monitors using several alternative techniques [18, 19]:

- Lithium dilution technique;
- Pulse contour analysis;
- Bioimpedance or bioreactance monitoring;
- Transthoracic Doppler or oesophageal Doppler;
- Transthoracic or transoesophageal echocardiography.

All of these methods offer less invasive methods of monitoring the cardiac output compared to the PAC, but all have their own disadvantages or limitations and are often based on assumptions that may not always be valid [19]. Furthermore, it is increasingly understood that while these monitors can guide therapy, they also only reveal a part of the macrovascular haemodynamic status. For example, normal global circulation can co-exist with multi-organ failure [20]. Published literature increasingly demonstrates the critical role of the microvasculature - the smaller vessels in target organs where gas exchange takes place - and its association with patient outcomes [21, 22]. This information is not captured in cardiac output estimates. In contrast, peripheral assessment has been shown to both guide therapy and have strong association with outcomes where macrovascular haemodynamic measurements did not [20, 23]. Therefore, an objective measurement of peripheral perfusion in addition to the macrocirculatory parameters may prove useful for both guiding management and for clinical prognostication.

1.1.2.2 Organ perfusion and local oxygen delivery

An alternative approach to monitoring the global haemodynamic metrics is to assess the delivery end of the cardiovascular system. In clinical practice, individual organ perfusion monitoring is frequently used as a proxy measure of global haemodynamic function. This is further explored in section 1.1.3.2.

The sufficiency of global organ perfusion may be estimated by taking samples from major veins and analysing the returning blood content. Examples include measures such as plasma lactate, mixed venous oxygen saturation (SvO_2, now less frequently available with the decline of the use of PAC), or central venous oxygen saturation ($ScvO_2$, taken from an internal jugular venous catheter and strongly correlated with SvO_2 but easier to acquire [24]). Alongside the global output measurements discussed in section 1.1.2.1, these estimates can add further information on whether the cardiac output is meeting the body's needs by assessing how much oxygen is being extracted by the organs [25, 26].

However, this assessment of gross perfusion of the organs may also provide an incomplete picture. Although parameters such as serum lactate and the measures of venous oxygen content can be used as global tissue perfusion markers, they are not always well correlated with each other depending on the cause of cardiovascular failure [27]. As with the measurement of key organ functions, these metrics rely on either abnormal perfusion of a number of organs, or a global fall in oxygen delivery below a critical level where anaerobic respiration must take place. As such, they may not be a sensitive marker of tissue hypoperfusion. Venous oxygen content is not routinely used as it has been shown not to improve clinical outcomes [28]. Plasma lactate levels may be elevated for many reasons other than circulatory shock [29].

The circulation inside each solid organ can be further divided into organ macro- and microcirculation [30]. Gas exchange between the circulation and the receiving

cells takes place across the wall of capillaries that belong to the organ-specific microcirculation. The term 'microcirculation' refers to the terminal vascular network of the systemic circulation, consisting of vessels with diameter <20 micrometres (arterioles, capillaries, and post-capillary venules) [30, 31]. Although the existence of capillaries has been long described, a better understanding of how repeated subdivision of terminal arterioles interacts architecturally with the capillary bed has developed more recently [30, 32, 33]. This improved understanding of the anatomy of capillaries has led to a greater appreciation of the physiological and functional roles of these vessels.

There are several key points from the early literature on microcirculation that are relevant to this thesis.

1. Most capillary vessels (including capillaries in the skin that are further investigated in this thesis) do not lie in the direct path of blood flow between arterioles and venules, but are a separate network that may be in- or out of-circuit [32, 34]. The total amount of flow directed through the capillaries is controlled locally via precapillary sphincters that control the blood flow to the relevant capillary bed (figure 1.1). The flow may be diverted away from the capillaries via the 'short-circuit' vessels (labelled 'arteriovenous bypass' in figure 1.1).

2. The microvasculature is sensitive to local effects and conditions, sometimes more than it is sensitive to systemic stimuli [32].

3. Although 'microcirculation' refers to vessels with diameter <20 micrometres [30, 31] within each organ, the microvasculature in individual organs is highly specialised according to the specific function of the organ [30].

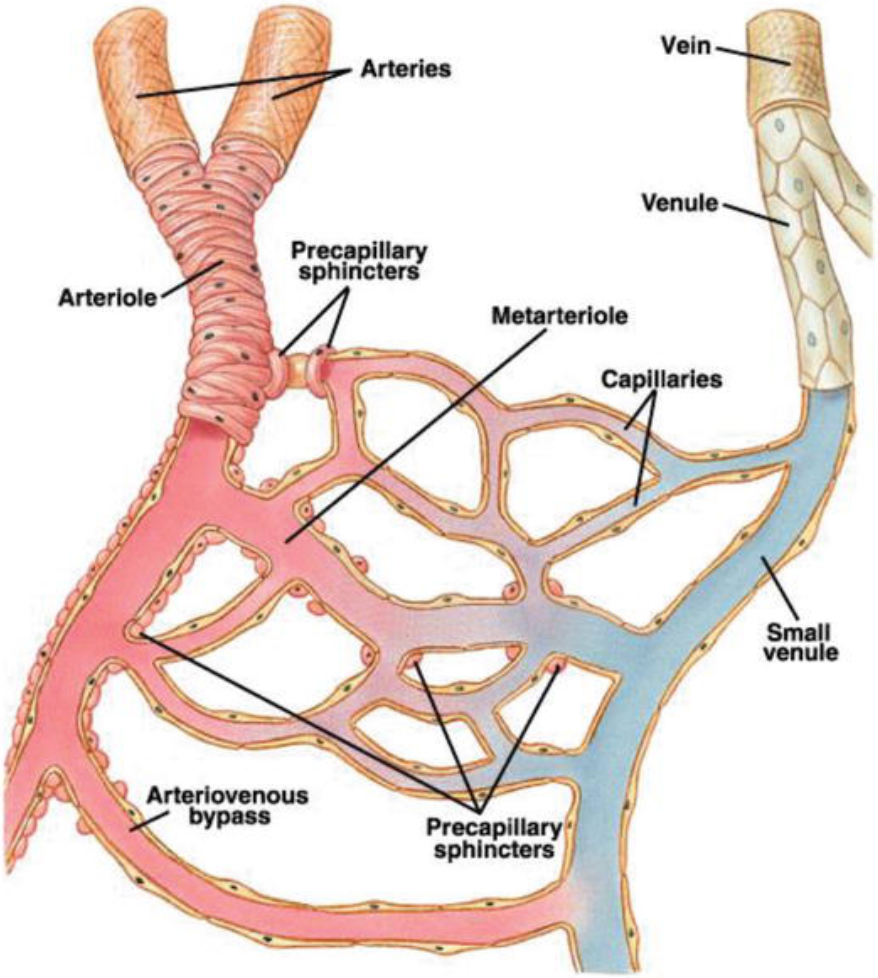


Figure 1.1: Microvasculature: The microcirculation is made up of terminal arterioles, collecting venules, and the thin walled capillaries lying in between. As shown, it is now understood that capillaries stem from terminal arterioles and drain into the venules but are not created by repeated division of arteries before joining up to become venules. Precapillary sphincters can control the relative amount of blood flow through the capillaries and the metarterioles (main arteriole branch from which capillaries are perfused from).
©2018 Fethi Gul, Omer Faruk Boran, and Reyhan Arslantas. Adapted from Gul *et al.*, [34]; originally published under CCBY 3.0 license. Available from: https://www.intechopen.com/books/6432.

1.1.3 The value of skin perfusion assessment

In view of the above, there are four main reasons why skin perfusion monitoring may be desirable in the context of haemodynamic assessment.

1. It provides an easy-to-access location for peripheral circulation measurement (section 1.1.3.1);

2. As a 'non-vital organ' [4], the skin is more likely to receive reduced blood supply during clinical deterioration (compared to organs such as the brain or the kidney), and reflect haemodynamic deterioration at an earlier point (section 1.1.3.2);

3. There are aspects of skin blood flow homeostasis that makes it an advantageous organ for haemodyamic monitoring (section 1.1.3.3);

4. Both the macro- and the microcirculatory components of skin blood flow are superficial. They can be monitored concurrently and may be amenable to non-invasive measurements due to their superficial location (section 1.1.3.4).

These key points are expanded in turn in the following subsections.

1.1.3.1 The peripheral circulation

The complex homeostatic control and feedback loops that keep the circulation stable in health and allow prompt response to any changes can also pose challenges during haemodynamic resuscitation when the system is failing. The assessment and support of the cardiovascular system during illness are fundamental to the delivery of critical care [35]. During haemodynamic collapse, the cardiovascular system may be supported using three main approaches. In order to increase organ perfusion, one can:

- increase the intravascular volume by administering fluids;

  or

- decrease the diameter of peripheral vessels to increase the pressure within the pipes by administering vasopressors;

  or

- improve the function of the pump driving the circuit by administering inotropes.

Often, a mixture of these approaches is required. A wrong decision regarding which of the three is most appropriate may be detrimental to patient care [36, 37]. For example, the administration of vasopressors to a fluid-depleted patient whose heart is failing will increase the afterload against which the heart must work, leading to further cardiac ischaemia and failure.

In order to diagnose which of the above therapies (or combination of therapies) is most appropriate, an accurate assessment of each of the three aspects (fluid balance, peripheral vessel status, and the cardiac function) is necessary. An objective estimation of fluid balance and cardiac function may be performed using multiple tools or techniques including pulse pressure variation and the cardiac output monitors described above (section 1.1.2.1) [18, 38]. In addition, both sets of data may be acquired non-invasively at the bedside and at regular intervals using transthoracic echocardiography, for example using Focused Intensive Care Echocardiography (FICE) [39]. In comparison, the peripheral circulation is currently largely left to be assessed visually by the clinician [4].

The peripheral circulation refers not only to the skin circulation but also to the distributed blood to all organs. However, the skin vasculature is more accessible to non-invasive monitoring compared to vessels supplying the internal organs.

1.1.3.2 Skin as a 'non-vital' organ

Referring to the skin as a 'non-vital' organ [4] is misleading as skin has critical functions. However, it is one of the first sites from which blood is diverted away during periods of haemodynamic deterioration [40]. Skin tissue can survive on a minimal amount of blood supply [41], but the blood flow to the skin in resting state can be many-fold higher than its basal requirements because of its role in systemic thermoregulation [41]. The total amount of blood in the skin during rest represents at least 9% of the total blood mass [42]. The delivery of blood

to the skin can increase to as much as 60% of the total cardiac output during hyperthermia [43]. The significant proportion of the total circulatory volume in the skin during rest and the low absolute requirement for skin homeostasis have implications during global haemodynamic struggle. When required, the blood flow to skin is redirected to core regions in a process called centralisation [40]. As the purpose of haemodynamic monitoring is to diagnose the risk of hypoperfusion of key organs as early as possible, skin may offer a better, more sensitive site for detecting mild haemodynamic compromise compared to monitoring internal organs [4].

Key organ function monitoring is already embedded in our clinical monitoring practice, based on the assumption that normal organ function can only be achieved when the blood supply to the organ is adequate. Examples include the assessment of the conscious level (brain), urine output (kidney), or serum liver enzymes or clotting parameters (liver). These markers are crude measurements of the optimal function of each of these organs. By the time an abnormality is detected, it is possible that the perfusion of those organs has been suboptimal for some time [44]. Minimising periods of organ hypoperfusion is desirable as there are long-term implications of even transient ischaemia for many internal organs [45, 46]. In a meta-analysis, Boyd *et al.*, [47] showed a significant mortality and morbidity benefit from improving tissue perfusion *before* the onset of apparent tissue hypoxia. A similar degree of resuscitation in patients who already have evidence of tissue hypoxia did not confer significant survival benefit. The benefits of early recognition of haemodynamic compromise by monitoring the perfusion of non-vital organs are well recognised [4].

1.1.3.3 Skin and autoregulation

The previous section (1.1.3.2) referred to other organs that are used for surrogate measures of adequate blood flow. In addition to the highlighted issue of a delay in displaying signs of hypoperfusion, several core organs show autoregulation in response to a reduction in perfusion pressure. Autoregulation is defined as the

intrinsic ability of an organ to maintain a constant blood flow despite changes in the perfusion pressure [48]. Different organs display a variable degree of autoregulation. The brain has several protective mechanisms that maintains steady flow between mean arterial pressure (MAP) values from 60 to 140 mmHg [49]. As a consequence, monitoring brain perfusion to direct haemodynamic resuscitation may lead to a late detection of any compromise (until a late point where a steady flow cannot be maintained, outside the limits of autoregulation) [50]. The renal and coronary circulation also show highly effective autoregulation [48]. Skeletal muscle and splanchnic circulations show moderate autoregulation [48, 51, 52].

The skin vascular bed behaves very differently from these other organs. The cutaneous vasculature displays little to no autoregulation [48, 53]. A perfusion pressure fall that would trigger autoregulation response in the other tissues mentioned above do not lead to similar changes in skin blood flow [54]. This lack of autoregulation makes skin a better site for early detection of a decrease in perfusion pressure compared to sites that rely on autoregulation.

1.1.3.4 Dual monitoring of macro- and microcirculation

Section 1.1.2.2 explained why the dual monitoring of both the organ macro- and microvasculature may be desirable. For most internal organs already discussed, this is difficult to achieve non-invasively. Organ-specific macro- and microcirculatory monitoring has been most explored for two internal organs: the brain and the kidney.

Measuring the total blood flow to the brain is a relatively easy task as the main afferent vessels are near the skin surface and accessible on either side of the neck [50]. Methods of assessing the cerebral microcirculation include oxygen microelectrodes, or non-invasive methods such as transcranial Doppler, laser Doppler flowmetry, diffuse reflectance spectroscopy, or near-infrared spectroscopy [55]. Therefore, although dual monitoring of the cerebral macro- and microcirculation is theoretically possible,

it requires the use of multiple instruments and a direct comparison of the adequacy of both circulations is difficult.

Dual monitoring of the renal system also poses further challenges. In a review of kidney perfusion monitoring in acute patients, Schneider *et al.*, [56] conclude that although dual monitoring techniques are available (e.g., renal artery Doppler, Scintigraphy, renal vein thermodilution), most are not possible at the bedside. In addition, the authors argue that the techniques require 'extensive patient manipulation' which make them impractical within the acutely ill population, and almost all estimate global organ flow rather than the microcirculatory perfusion of the kidney [56]. Other organs where microcirculatory changes are of interest and attempts have been made to monitor include the liver, the gut, and the eyes [30].

In comparison, the skin carries some advantages for dual monitoring of the macro- and microcirculation. Skin provides a large surface area where perfusion may be monitored. The skin's anatomical layout potentially allows dual monitoring of macro- and microcirculatory elements without invasive instrumentation (sections 1.2.2 and 1.2.3). However, traditional approaches to skin perfusion have not always divided skin blood flow into the macro- and microvasculature. In particular, the locations of the larger vessels that bring the blood to the skin surface are not usually considered in monitoring or clinical examination [40, 57]. For example, pulse oximeters are worn 'blindly' at the finger-tip (without a precise knowledge of the exact vasculature under the skin surface where the probe is worn), where there are a mixture of vessels. Arteries supplying the finger tip can vary in diameter between 0.1 and 0.5 mm [58]. Their locations are not considered in measurements made with pulse oximetry. This does not have clinical consequences when measuring the SpO_2, but may affect the use of the photoplethysmographic waveform (further described in section 3.2.2) for haemodynamic assessments. A blind selection of skin regions to monitor without considering the anatomy of the underlying vasculature has also

been used in video camera-based physiological monitoring. This is further discussed in chapter 7.

Unlike the brain and kidney, the skin plays a key role in thermoregulation [59]. As a result, both external and core temperature may need to be taken into account to inform interpretation of changes over time.

1.1.4 Skin perfusion as a prognostic marker

The previous section described the advantages of skin as a site for haemodynamic monitoring. A subjective assessment of skin perfusion is routine in bedside clinical examination [60, 61]. Several elements of clinical assessment are reliant on skin perfusion, including skin colour, temperature, capillary refill time (CRT) (further described in section 1.4.1). These parameters provide valuable information regarding the haemodynamic status. The skin is the first organ to reflect hypoperfusion in response to global haemodynamic compromise and the last to normalise following resuscitation [62]. In addition to the real-time guidance of clinical decision-making (section 1.1.3.1), evidence suggests that the duration of skin hypoperfusion and the response to resuscitation (and subsequent normalisation to normal skin blood flow) may be related to patient prognosis. Van Genderen *et al.*, [63] showed that following cardiac arrest there are profound changes in both skin perfusion and sublingual microcirculation, independent of the resuscitation and systemic haemodynamic parameters. Survival was associated with rapid normalisation of skin perfusion.

Shock is defined as circulatory failure resulting in inadequate cellular oxygen utilisation [64]. There is strong evidence for a dissociation between the macro- and microcirculation in patients with shock [65–67]. Although the two elements are clearly related and cannot be completely separated, taking the approach discussed in section 1.1.2.1 and only measuring macrohaemodynamic parameters has been shown

to provide limited information for guiding haemodynamic resuscitation [63, 65, 66]. Resuscitation strategies considering tissue perfusion assessments rather than the global metrics only (discussed in section 1.1.2.2) may improve outcomes [67].

1.1.5 Section summary

This section has described the cardiovascular system and how haemodynamic status may be assessed. The traditional approach of assessing global haemodynamic parameters or the macrovasculature alone may provide limited information. Section 1.1.3 presented four reasons why skin perfusion is a good candidate for macro- and microhaemodynamic assessments. As skin is an organ that responds early in haemodynamic compromise with relatively limited autoregulation, skin perfusion provides a sensitive site for haemodynamic monitoring. In addition to providing a picture of the current underlying status, the assessment of *peripheral* perfusion may also be a useful prognostic marker. In order to use skin perfusion as a parameter for macro-or microcirculation assessment, an understanding of the underlying anatomy is vital. This is described in the following section.

1.2 Anatomy of skin perfusion

The skin is the largest organ of the body and accounts for approximately 16% of our body weight. The average 70kg man has a skin surface area of 1.8m^2 [68], but there is considerable topographical variation in skin structure across the body. The skin anatomy relevant to this thesis and how this may relate to parameters that can be measured using video cameras is described in this section. The section is divided into three subsections. The overall skin structure is described first, followed by the macro- and microcirculation within the skin in turn. The results described in chapters 5 to 8 build on this anatomical background.

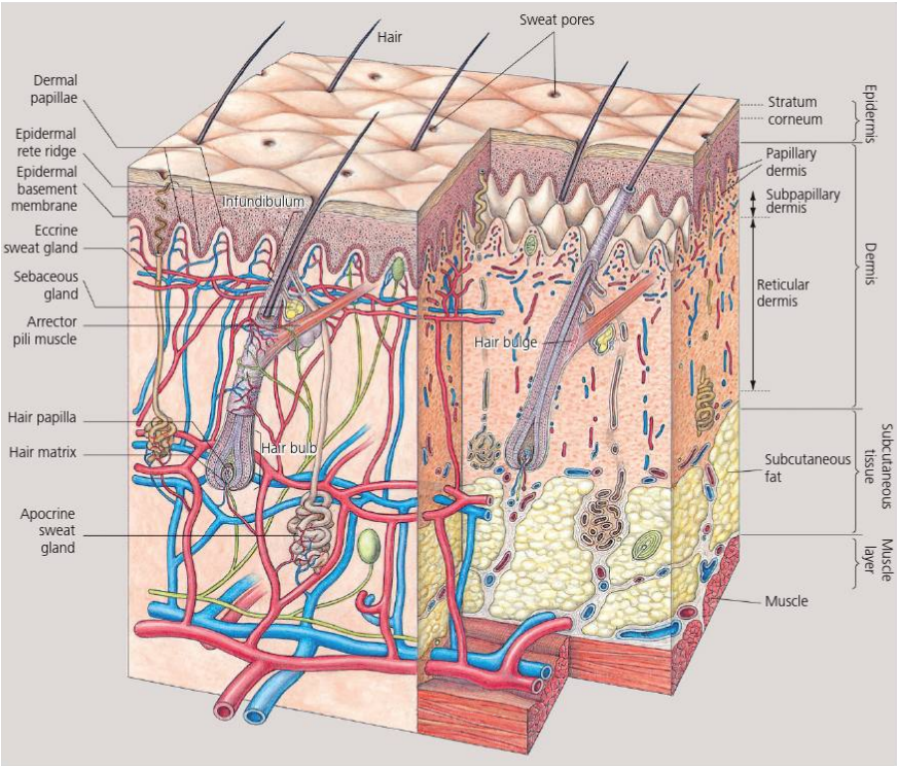


Figure 1.2: Structure of the skin. Image from Shimizu *et al.*, [71] with permission (appendix J).

1.2.1 Skin structure

Skin has three main layers; epidermis, dermis, and subcutaneous tissues (figure 1.2). The outermost layer - the epidermis - is made up almost entirely of keratinocytes (95%) and melanocytes (5%). As there are no blood vessels in this region, the cells in the epidermis receive oxygen by diffusion from the layers underneath [69] or directly from the atmosphere [70]. The most external blood vessels are contained within the second - dermal - layer. Here, two sheets or layers of vessels parallel to the skin surface are found. The third layer - the subcutaneous tissue - is made up predominantly of fat cells, separating the dermal layer from underlying muscles which are organised in compartments separated by fibrous septal tissues.

The two layers of superficial blood vessels (called the dermal and subdermal plexi, shown as collection of vessels at the superficial end of the dermis and at the dermal : subcutaneous fat junction on figure 1.2) play an important part in the

thermo-regulatory mechanism of the skin. The amount of blood flowing through these two capillary layers controls heat loss to the atmosphere. As shown in figure 1.1, fine control over the amount of blood delivered to the superficial capillaries is possible via the precapillary sphincters present at the arteriole : capillary interface.

In section 1.1.2.2, the concepts of skin macro- and microcirculation were introduced. The anatomical representations of these vessels are discussed in turn in the following two subsections.

1.2.2 Arterial perforators and skin macrocirculation

1.2.2.1 Description of perforators

The blood supply to an area of skin originates from a dominant arterial branch - an 'arterial perforator' - that stems from the underlying main artery. The literature recognises two distinct subtypes of perforator artery, distinguished by their location and vessel diameter. In the literature, a nominal cut-off of 0.5 mm or greater is used as the threshold for the definition of a perforator [72, 73].

The dominant or deep perforators (using the thigh as an example, the three perforating arteries that originate from the profunda femoris and *perforate* adductor magnus, figure 1.3) are the larger of the two perforator subtypes with diameter of 1.5 to 2.5 mm [74]. These larger arterial branches stem from major named arteries and perforate deeper structures such as muscle, and are easily visible both upon surgical dissection and using surface imaging such as Doppler sonography or Duplex scans [41]. These deep perforators are of critical importance in the design and surgical techniques of skin grafting. They are taken alongside skin graft to be anastomosed at the recipient site [75]. As such, it is important that the selected vessels are large enough to always remain open, even during global haemodynamic deterioration. Vasoconstriction in these vessels post graft transfer is the leading

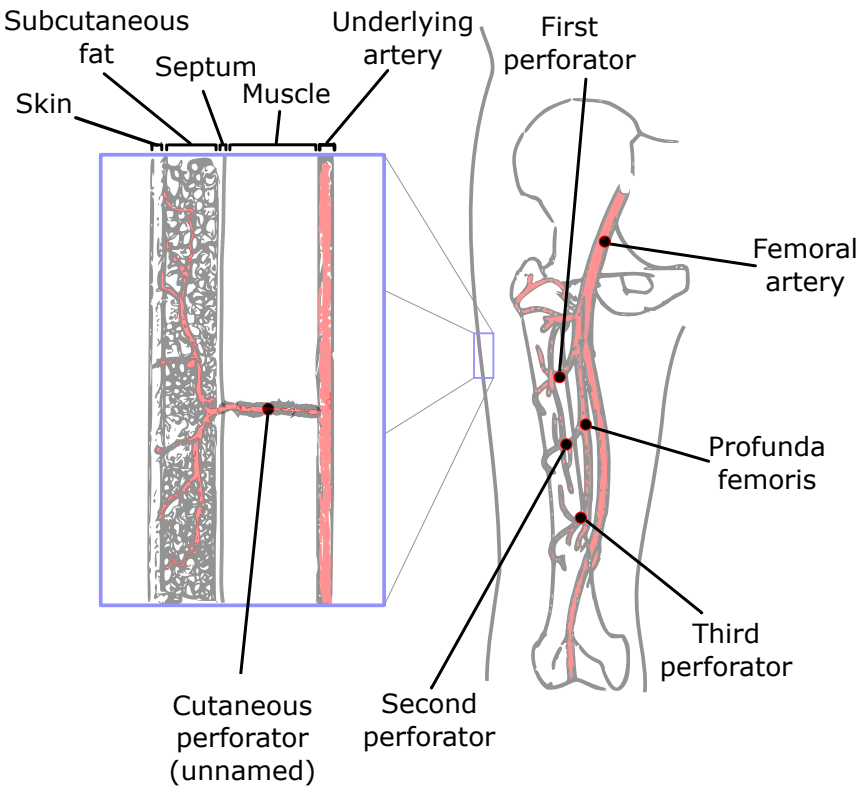


Figure 1.3: Two types of arterial perforators. Two types of arterial perforators are recognised in the literature and these are shown here using the thigh as an example. Deeper perforators originate from major arteries (e.g., deep perforators originating from the profunda femoris artery which is the main vascular supply to the thigh) and 'perforate' through deeper tissues. They can be easily visualised using techniques such as Doppler sonography or Duplex scans. They are labelled as the first, second, and third perforators in the figure. In contrast, cutaneous perforators that bring arterial blood up to the surface are smaller (<1.0 mm) and much more superficial. They cannot be reliably visualised using ultrasound techniques. An example of the location and the relationship with skin and subcutaneous fat layers (section 1.2.1 and figure 1.2) is shown inside the magnified rectangle on the left of the figure.

cause of graft ischaemia and subsequent failure [75]. The commonly used donor sites for skin flaps (e.g., antero-lateral thigh or the lower abdominal wall [41]) tend to have anatomically consistent and reliable deep arterial perforators [75].

At a more superficial level, smaller arterial perforators (usually <1.0 mm) *perforate* the septum that separates the subcutaneous layer of skin from underlying muscular compartments. These vessels (more numerous and widespread around the body surface compared to the deep perforators) deliver blood up to the cutaneous skin

layers by delivering blood into the two aforementioned layers of superficial capillaries (the dermal and subdermal plexi). These are usually referred to as 'cutaneous perforators' or 'septo-cutaneous perforators' in the literature to distinguish them from the deeper, larger dominant perforators [72, 76] (figure 1.3).

Each unit of skin area served by a cutaneous perforator vessel along with its blood supply is called an angiosome [72, 73, 76]. Each angiosome unit is supplied from its centre (figure 1.4), with blood flow from the middle of the angiosome to the outer periphery. This sub-unit arrangement at the skin surface is difficult to appreciate from surface anatomy alone. As a consequence, the arterial pulse may 'arrive' at two adjacent areas of the skin with a larger time difference than anticipated based on distance alone, if they are supplied by two different cutaneous perforators. Without the knowledge of the location of the underlying angiosomes or the inter-subject variability in this pattern, the baseline temporal sequence of skin perfusion measurements (using any technology to monitor the skin surface) cannot be accurately interpreted.

1.2.2.2 Clinical relevance of perforators

Both the deep and cutaneous perforators are of clinical relevance in flap surgery [76, 77]. The knowledge of which deeper perforator vessels supply the relevant skin regions is critical for the design and long term survival of skin flap transfers. The smaller cutaneous perforators are also of interest in plastic surgery [76], but identifying their locations and exact course prior to surgery is less critical for tissue survival. Smaller cutaneous perforators may be tied off during surgery, allowing the relevant arterioles to fill via the small vessels near the peripheries of the angiosome that are closed and not functional at baseline. These closed vessels dilate as needed to allow filling of a distal region from an alternative source, for protection against ischaemia when required. These vessels connect adjacent angiosomes and are named

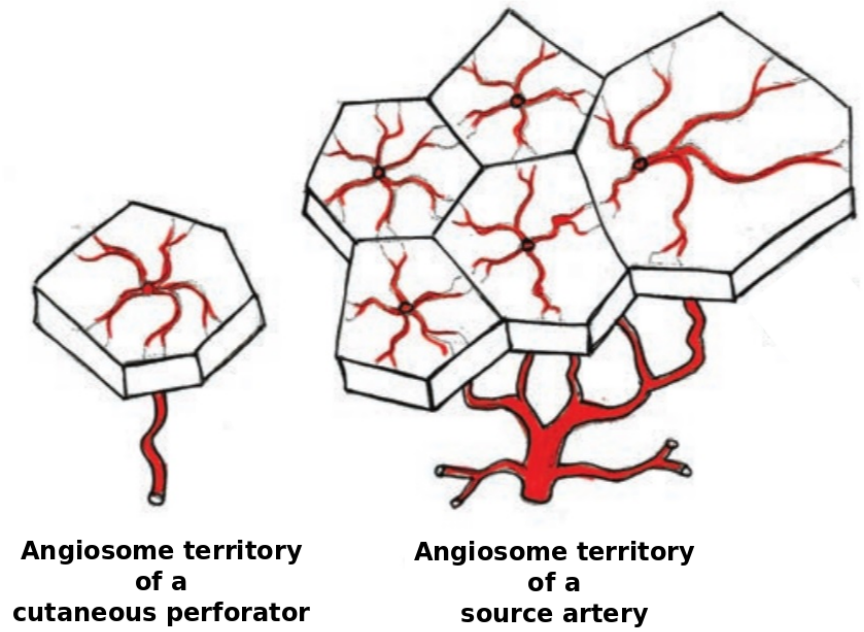


Figure 1.4: Schematic representation of the cutaneous perforator angiosomes. On the left, a single cutaneous perforator and its zone of supply ('angiosome') is shown. The figure on the right shows how multiple angiosome territory of a single cutaneous perforator interact with each other. Reproduced from Taylor *et al.*, [72] with permission (appendix J).

choke or linking vessels [78].

1.2.2.3 Watershed regions in the skin

The term 'watershed' is generally used in medicine to refer to the regions of the body that receive dual blood supply from the most distal branches of two (or more) source arteries. Two commonly discussed watershed zones in the body are the splenic flexure in the large bowel where watershed areas account for about 70% of all ischaemic colitis [79] and in the cerebral circulation where watershed infarcts occur in the distal fields of two arterial branches [80]. Being in the watershed anastomotic regions can be advantageous when one of the two feeding vessels are interrupted as flow can be maintained from the other source artery with normal flow. However, these areas are ironically more prone to ischaemia during systemic hypoperfusion as the region usually lies in the periphery zone for both source vessels and the blood

supply from both channels can be interrupted concurrently [79].

The concept of watershed zones in the skin was first proposed by McGregor *et al.*, [81]. In their investigations of skin flap territories, the authors demonstrated that the precise skin territories supplied by vessels are not clear-cut. In particular, the boundary of a territory was not fixed but could be altered by interfering with the flow of blood into an adjoining artery. The skin can be divided into regions which are reliably supplied by a named vessel all the time, and other regions which could be supplied by two or more vessels in the nearby region via choke vessels. In contrast to the colon or the brain which are prone to infarction from reduced blood supply [79, 80], the skin can survive during longer periods of reduction in flow [41].

The presence of arterial perforators and the watershed regions where choke vessels lie between adjoining perforators (figure 1.4) can form the theoretical basis for sub-regions within a patch of skin. Chapters 7 and 8 in this thesis consider how the sub-regions of skin immediately overlying the centre of a perforator vessel may behave differently from the watershed regions that lie between them.

1.2.2.4 Localisation of perforators

The gold standard method of localising perforators varies depending on the clinical indication for identifying the vessels [77, 82]. Direct visualisation during flap surgery (via exploratory incision) remains the gold standard in the field of plastic surgery where arterial perforators are most often discussed [77]. However, intra-operative localisation is known to be challenging due to a variability in the location and size of perforators [83, 84]. In addition, this invasive method of artery identification is only appropriate where surgical intervention is planned. It cannot be the standard method for localising perforators for other purposes.

Prior to the direct verification of the larger perforators during skin graft surgery, surgeons use various methods to ensure that there is a large artery present and to predict its approximate location. Several methods of localising arteries have been used in clinical practice and research. Commonly used techniques include acoustic Doppler sonography, colour duplex imaging, and computed tomography (CT) angiography [85, 86]. The preferred method of localisation depends on the flap being planned, with the Doppler sonography or colour duplex imaging being preferred for anterolateral thigh flaps [87–89] and CT angiography for abdominal flaps [90].

In contrast to the deep perforators, cutaneous perforators that are of interest in this thesis for the purpose of skin surface monitoring are more challenging to isolate using these methods. This is largely due to their smaller size. CT angiography can be used to assess arteries down to approximately 1mm in diameter [91]. Smaller vessels down to 0.1mm may be visualised using direct angiography [92] but this is more interventional and carries the risks of access and radio-opaque contrast-related complications [93].

Infrared thermography has been explored as a method of localising cutaneous perforators. These perforators have been described as 'hot spots' on the skin surface with faster re-warming back to baseline following cooling [78, 94]. In a review of diagnostic accuracy studies assessing the performance of thermography for perforator identification, Berner *et al.*, [77] showed that thermography for perforator localisation has high sensitivity (cumulative meta-analysis sensitivity of 95%) but relatively low specificity (65.6 to 98%, meta-analysis not possible). The vessel size threshold for accurate diagnosis of arterial perforators using thermography (using CT angiography as the reference comparator) has been shown to be approximately 1 mm [77, 78]. Several studies measured baseline skin surface temperature without intervention and reported high sensitivity when compared to perforator locations

identified using CT angiography and ultrasound Doppler [94–96]. Compared to these static localisation studies, the current body of literature supports a better thermographic perforator localisation performance using dynamic assessments [77]. The previous studies all achieved cooling of the skin surface using a cooling gel/water pack [78, 97], or a fan [82].

In summary, several methods have been used to localise deep and cutaneous perforators. Many imaging modalities used for deep perforator localisation are not appropriate for cutaneous perforators because of their smaller size. Cutaneous perforators may be localised using an infrared video camera with high sensitivity, with dynamic methods improving performance [77]. A clinical study which uses a novel dynamic method to locate perforators will be further described in chapter 4.

1.2.3 Anatomy of skin microcirculation

Skin microcirculation receives oxygenated blood from skin macrocirculation (i.e., cutaneous perforators described in the previous section 1.2.2). The microcirculation consists of the capillaries organised as two parallel sheets of vessels, named the dermal and subdermal plexi (section 1.2.1, figure 1.1). Smaller capillary loops then invaginate towards the epidermal layer, originating from the upper plexi [71] (figure 1.2).

The two layers of capillaries are in communication with each other. The blood flow into these capillaries are controlled via sphincters located at the capillary inflow origin of arterioles (figure 1.1). When external temperature is low, the sphincters contract, minimising flow through the capillaries and preventing heat loss. Blood is redirected via physiological arteriovenous bypass (figure 1.1) that redirects the flow into the venous circulation towards the heart. The skin vasculature is densely innervated by adrenergic axons [98]. The dense innervation allows precise control of

the amount of blood entering the superficial capillaries [99]. When the flow to the skin microvasculature is reduced for physiological reasons (e.g., low environmental temperature), constriction of the afferent entry junctions under nervous control leads to subsequent emptying of the capillaries and reduced flow in the microvasculature. During these responses, the endothelium (the lining wall of the microcirculation) remains normal despite the reduced perfusion. In contrast, certain pathological conditions are known to cause a constriction at the efferent or outflow end *prior to* a reduction from the afferent vessel [100]. This leads to a backlog of flow and stasis of blood along the capillary network [100, 101]. The static blood becomes further deoxygenated over time, leading to the darker colour within the microvasculature - a hallmark of skin mottling (see next chapter). The dermis and epidermis of skin then act as optical filters, causing the appearance of net-like streaks on the skin surface described as *livedo reticularis* or skin mottling [101]. This classical appearance of mottled skin likely represents static blood throughout the network of microvascular capillaries, across the two layers of superficial blood vessels with interconnecting vessels between them. The appearance of the linear streaks indicate abnormal endothelial function [12]. Subjective assessment of skin mottling (currently diagnosed visually by clinicians) has gained interest in critical care as a hallmark of microcirculatory failure [11, 12, 102]. This is further considered in a latter section on clinical perfusion assessment (section 1.4.1.2) and further explored in chapter 2.

1.2.4 Section summary

This section has presented an overview of the skin anatomy in relation to blood flow. Afferent skin blood flow occurs via vessels named cutaneous perforators, bringing blood from deeper arteries up to the skin surface. The perforators then supply capillaries organised into two parallel layers called the dermal and subdermal plexi. This anatomical arrangement beneath the skin surface is not clinically visible to the naked eye in health. However, the anatomical arrangement of vessels most likely contributes to the skin mottling appearance during circulatory failure [101]. The

presence of arterial perforators under some regions of the skin leads to non-uniformity on the surface. This is frequently not accounted for in skin perfusion monitoring. The relevance of this and the opportunity it presents are explored in chapters 7 and 8.

1.3 Physiology of skin perfusion

1.3.1 Regulation of skin perfusion

The precise control of skin blood vessel diameter is complex [43, 103]. As described in section 1.1.3.2, this control allows a large range in cutaneous blood flow. The following section briefly details the pathways that are particularly relevant to the study methodology in this thesis (described in chapter 4).

Sympathetic nervous system Two branches of the sympathetic nervous system innervate the cutaneous vasculature [103]. The first branch uses the neurotransmitter noradrenaline and has a vasoconstricting effect. Noradrenaline acts on adrenoceptors [104, 105], causing smooth muscle contraction on the vascular wall that ultimately leads to vasoconstriction. Vasopressors including noradrenaline, adrenaline, phenylephrine, and ephedrine exert their effect via this pathway [105]. The mechanism of action mainly limits this pathway vasoconstriction to the arterial branches with a contractile vascular wall.

The second branch has an opposite (vasodilating) effect, acting via a range of neurotransmitters including neuronal nitric oxide (NO), prostaglandins, substance P, and vasoactive intestinal peptide (VIP). This branch is not mediated via noradrenaline [106]. This action mediated via local release of vasoactive substances leads to more widespread action that include both the macro- and microvasculature.

Global hormone effects Both the heart and the vasculature are affected by hormones acting on specialised surface receptors and intracellular signalling systems [106]. The largest hormonal effects are exerted by noradrenaline, adrenaline, vasopressin (also known as anti-diuretic hormone), and renin.

Noradrenaline tends to have a main role as neurotransmitter, whereas adrenaline exerts its effects mainly as a hormone released from the adrenal medulla [105]. Other hormones involved in skin blood flow include atrial natriuretic peptide (ANP), brain natriuretic peptide (BNP) [107], endothelin [108], and thyroxine [109].

Other mediators A number of local mediators are involved in the maintenance of vascular tone. The above section discussed the role of noradrenaline. As well as sympathetically-mediated systemic release of substances such as NO, prostaglandins, substance P, and VIP, they can also be involved in the local mediation of blood flow. For example, external pressure applied to a skin area causes local release of both NO and prostaglandins [110]. By far the most dominant of these local mediators is NO, which acts as a pivotal signalling molecule that regulates blood flow [111]. NO activates soluble guanylyl cyclase, resulting an increased level of cyclic guanosine monophosphate. This in turn activates iron channels leading to a decrease in intracellular calcium, smooth muscle relaxation, and ultimately local vasodilation. As well as the natural role in regulation of blood vessel tone, the pathway is also activated in response to NO-containing metabolites such as glyceryl trinitrate (GTN).

1.4 Measurement of skin perfusion

Several skin perfusion monitoring methods are currently in use in clinical practice. In this section, the methods relevant to this thesis are described. Subjective clinical assessment of skin perfusion is the gold standard method in acute care settings [62], and this is covered first (section 1.4.1). Following the description of

several elements of the clinical assessment, currently available monitors in wider clinical settings are described, focusing on laser speckle contrast imaging (LSCI) in section 1.4.2.1. This tool is described in detail over other methods because a skin perfusion monitor using this technology is able to provide reference skin perfusion measurements as in the clinical study described in chapter 4. LSCI allows skin perfusion monitoring from a skin 'field' or larger region of interest (rather than a single spot) and provides images rather than just a single measurement [112]. It has lower intra-operator variability compared to several other available techniques.

1.4.1 Clinical/bedside assessment of skin perfusion

A clinician assesses several parameters concurrently to subjectively determine skin perfusion. These features can be categorised into visual clues - e.g., the skin colour (flushed/pale), skin mottling (present/absent or using the mottling score [11]) - and palpable clues including skin temperature (°C) and capillary refill time (seconds) [40, 60].

Four aspects of clinical assessment are particularly relevant in this thesis.

1.4.1.1 Skin colour

A subjective assessment of the general skin colour is a critical component of the cardiovascular examination [60]. Pallor is defined as 'abnormal paleness of the skin, due to reduced blood flow or lack of normal pigments' [113]. There are many additional causes of skin pallor beyond peripheral vasoconstriction (e.g., anaemia [60], acute limb ischamia [5], neurogenic [114]). In acute care, however, skin pallor is used as a clinical sign of shock and a reduction in skin circulation due to haemodyamic crisis [9]. More recently, however, the difference in the ability to detect skin pallor in different ethnic groups has been suggested as a contributing factor to the ethnic disparity in outcomes in healthcare settings [5]. An objective

measurement of skin colour and its changes is not currently available in acute care settings.

1.4.1.2 Skin mottling

Skin mottling is a blue discolouration of the skin with a distinctive net-like pattern. Although it can occur due to chronic vessel abnormalities e.g., vasculitis or hyperviscosity syndromes, in critical illness it is usually associated with cardio-circulatory failure [101, 115]. Mottling helps with prognostication in critically ill patients [11]. It is usually observed alongside skin pallor and reduced blood flow to the microvasculature. The capillary networks in the areas most distal to the cutaneous perforators are perfused via the smaller branches of terminal arterioles [72]. As discussed in section 1.2.2.3, these peripheral zones are particularly susceptible to reduced flow during systemic hypoperfusion.

There has been increased academic interest in the last decade in skin mottling in critically ill patients as a marker of microvascular dysfunction. In particular, it is thought to reflect microvascular hypoperfusion and endothelial dysfunction which predicts prognosis independently of global haemodynamic parameters [12]. A model describing the anatomy of skin mottling was proposed by Duval and Pouchot [101]. The authors describe mottling as an abnormal state where the increased venous pressure leads to visible static desaturated blood in a ring-like pattern in the superficial microvasculature.

Even in otherwise healthy subjects, exogenous administration of adrenergic agonists such as phenylephrine cause more potent cutaneous vasoconstriction in the lower limbs compared to upper limbs [116] in normothermia. As a consequence, micro-vascular hypoperfusion can lead to mottled skin appearance in the lower limb [105, 117]. In addition, the knee is thought to be the most vulnerable site for skin mottling secondary to a higher concentration of noradrenergic receptors in this

region [101].

A summary of the literature on skin mottling including a meta-analysis of the mortality data associated with skin mottling is included in Appendix A. Studies report a large variation in the estimated incidence and outcomes associated with skin mottling, but are in agreement that skin mottling is strongly associated with poor prognosis. The evidence for skin mottling assessment is further explored in chapter 2 and forms the basis for camera-based, objective mottling detection in chapter 5.

1.4.1.3 Skin temperature

Clinical assessment of skin temperature is a simple and non-invasive method of estimating peripheral perfusion. Clinically estimated subjective skin temperature has been shown to correlate to global parameters including cardiac output and cardiac index [118–120]. This association between clinical assessment of skin temperature and global parameters has not been matched by demonstrable link between objective skin temperature measurements and similar parameters [57]. For example, Woods *et al.*, [121] reported no significant correlation between core temperature (measured using a pulmonary artery catheter) and peripheral temperature (big toe temperature using a thermistor) gradients, and several haemodynamic parameters including cardiac index and systemic vascular resistance. In another study, skin temperature from five different locations (axilla, groin, patella, anterior ankle, and big toe) were shown not to correlate with cardiac index [122]. This disparity between the usefulness of subjective and objective skin temperature measurements is not fully understood. Contact skin temperature measurements can vary depending on the sensor type, method of attachment, and environmental factors. It is possible that the lack of support for objective skin temperature monitoring may be secondary to a variability in the location of, and the method of attachment of the probe for the skin temperature measurement in different studies [123]. It may also be the case

that the underlying arterial anatomy was not taken into account.

1.4.1.4 Capillary refill time

Capillary refill time (CRT) is an examination technique for the rapid assessment of peripheral perfusion. It is routinely assessed using the naked eye [124]. Manual pressure is applied to the ventral surface of a finger until the nail-bed is blanched. The pressure is maintained for 10 seconds before release. The CRT is the number of seconds until normal colour is restored. The normal upper limit is less than 3 seconds [125]. In the literature, it has been frequently used as a key non-invasive peripheral perfusion monitoring technique. Clinical assessment of the peripheral circulation including CRT has been shown to improve prediction of poor outcomes when compared to matched patient cohorts with the same global or macrovascular cardiovascular parameters [20].

1.4.1.5 Subsection summary

The four clinical parameters - skin colour, surface pattern (mottling), temperature, and refill time - provide rapid methods of assessing blood flow to the skin without the need for any equipment. Clinical assessment of these parameters has been shown to have prognostic value in addition to global haemodynamic parameters [63]. Objective measurements of these variables may provide information which is additional to macrohaemodynamic monitoring, but this transition has not been successful for skin temperature measurement using contact monitors such as thermistors (discussed in section 1.4.1.3).

1.4.2 Skin perfusion monitoring tools

Several non-contact methods of estimating skin blood flow exist currently. They provide real-time or close to real-time perfusion assessment in the dermis (figure 1.2) [5]. The commonest methods in clinical use are Laser Doppler Imaging (LDI) and

Laser Speckle Contrast Imaging (LSCI). Both of these non-contact methods have the advantage of offering 'field' imaging (rather than a single spot measurement). Field imaging improves the reproducibility of measurement compared to single spot measurement which can be more operator dependent and are affected by the incident angle and the pressure applied [126].

LDI has been used in the assessment of burns [127], rheumatological assessment of capillary dysfunction [126], and in intraoperative tissue monitoring [128]. However, it provides relatively low resolution images and requires long scanning time with moving laser probe [129]. The following section explains LSCI in more detail.

1.4.2.1 Laser speckle Contrast Imaging

A 'speckle' interference pattern is formed when laser interacts with tissue. Movement inside the tissue causes a blurring of this pattern and the degree of blurring and change in the speckle pattern may be used to estimate blood flow in the tissue. Since its initial description in 1970s, the method has been developed into clinically-approved monitors which are used in research and (limited) clinical settings [7]. An example set-up for LSCI is shown in figure 1.5.

LSCI is used for the assessment of the severity of small vessel and capillary dysfunction in rheumatology [130], non-contact depth of burn assessment in plastic surgery [131], assessing retinal flow in ophthalmology, and to ensure adequate anatostomosis and non-compromised flow in bowel surgery. These applications have been comprehensively reviewed elsewhere [7].

LSCI offers rapid image acquisition from a field in contrast to LDI [7, 129]. However, it is sensitive to movement artefacts as it cannot easily distinguish between the

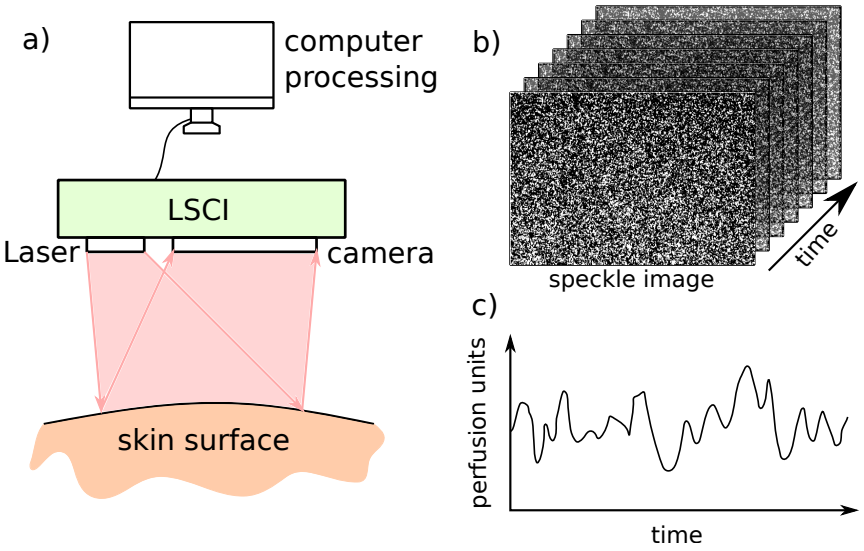


Figure 1.5: Laser speckle contrast imager (LSCI): principles. Laser speckle contrast imaging require a laser light source and a camera sensor that is sensitive to the wavelength of the laser. The laser illuminates a region of skin, and the speckle images from the illuminated skin are captured by the camera. The speckle images are processed by a dedicated computer. Example of speckle images are shown in b). The change or blurring of the speckle patterns are used to estimate blood flow.

movement of the red blood cells and larger-scale movement of the limb [7].

Several commercial products have been developed that use Laser speckle technology. Two clinically-approved commercial devices are moorFLPI-2 (Moor Instruments, Axminster, UK) and PeriCam PSI (Perimed AB, Jrflla, Sweden).

1.5 Summary and current gaps in knowledge

Evidence presented in this introductory chapter demonstrates that skin perfusion is a useful and clinically relevant parameter to monitor. Skin provides a convenient site for peripheral circulation assessment (section 1.1.3.1) with early changes during deterioration (section 1.1.3.2). It displays minimal autoregulation (section 1.1.3.3), and has accessible macro- and microcirculation components (section 1.1.3.4). Skin perfusion monitoring allows an assessment of the current haemodynamic status to guide management [62], and has been shown to prognosticate in critically ill

populations [20, 63, 132]. Objective skin perfusion monitors have been introduced (e.g., LSCI described in section 1.4.2.1), but this use is limited to settings for which the interest is in chronic changes (section 1.4.2.1). The distinction between the macro- and microcirculation in the skin is often not considered in either clinical assessment or other measurements of the skin surface using perfusion monitors.

Currently, skin perfusion in acute settings is assessed clinically. Despite being highly subjective, this clinical assessment of peripheral perfusion has been shown to out-perform macrovascular parameters in determining prognosis. In particular, skin mottling assessment has been further explored in the last decade as a marker of microvascular compromise, a trend monitor, and a prognostic tool. However, skin mottling can also be a marker of impending death [133], and whether it is simply associated with other signs of critical illness is not known. The next chapter explores whether skin mottling in critical care units - when considered separately from severity of illness - provides additional prognostic information.

2

Usefulness of skin mottling assessment

Contents

2.1 Introduction 35
2.2 Methods 37
2.2.1 Study design 37
2.2.2 Settings and data sources 37
2.2.3 Participants 38
2.2.4 Variables, data sources, and measurement 38
2.2.5 Bias 39
2.2.6 Study size 39
2.2.7 Outcomes 39
2.2.8 Statistical analyses 39
2.3 Results 40
2.3.1 Participants and descriptive data 40
2.3.2 Main results 41
2.3.3 Subgroup analysis 42
2.4 Discussion 42
2.5 Chapter summary 45

2.1 Introduction

The previous chapter described the advantages of skin perfusion assessment in acute care as a proxy measurement reflecting the underlying haemodynamic status. In contrast to other healthcare settings where monitors have been introduced for

objective assessment, the skin perfusion assessment in critical care is performed by the clinicians using clinical examination. Skin mottling has seen an increase in interest over the last decade with the growing recognition that it reflects microvascular hypoperfusion [12]. The associated microvascular malfunction and endothelial dysfunction play a critical role in sepsis [66, 134]. The mottling score has been proposed as a severity scale to describe the extent of mottling based on a visual assessment [11].

Skin discolouration in mottling has been attributed to stasis in the venous network which appears darker secondary to a high concentration of deoxygenated haemoglobin [135]. The microcirculatory failure appears to be a separate (although often concurrent) process to macrocirculatory hypoperfusion/failure. The latter is usually is associated with pale and cool distal skin rather than mottled skin. This distinction is supported by the classically described development of mottled skin, which tends to appear around the knee and spread over the lower limb followed by the upper limb and abdomen [101]. This typical sequence of mottling progression led to the grading system for its severity, called the mottling score [11], further described in chapter 5. The knee is thought to be the most vulnerable site for mottling appearance [101]. The presence of venous stasis may indicate microcirculatory failure alongside perfusion deficit, which have been shown to predict mortality, independent of clinical resolution of shock [136].

There is a large variability in the reported incidence of skin mottling in critical care settings from 2.5% [137] to 70% [11] (Appendix A). Many studies reporting on the incidence and associated prognosis of mottling are single-centre studies with a limited clinical population. The reported prognosis of mottled patients also varies, ranging from associated ICU mortality of 22% [138] to near 100% [139]. The assessment of skin appearance is part of routine critical care daily review [140]. A large-scale retrospective study using mottling documentation in electronic patient

records and multiple centres has not been performed, and may strengthen the evidence for association between skin mottling (a visible skin surface phenomenon) and clinical outcomes.

The retrospective study of three large ICU patient databases described below aimed to estimate the incidence of skin mottling and its association with patient outcomes when corrected for other measures of illness severity. I hypothesised that documented skin mottling would be associated with increased risk of ICU and hospital mortality when adjusted for illness severity, and that this pattern would be present across multiple ICU databases.

2.2 Methods

2.2.1 Study design

This is a multi-centre retrospective, observational study including two ICUs in the United Kingdom and 13 ICUs in the United States. Findings are reported following the REporting of studies Conducted using Observational Routinely-collected Data (RECORD) guideline [141].

2.2.2 Settings and data sources

The following three clinical databases were included:

- The Post-Intensive-Care Risk-adjusted Alerting and Monitoring (PICRAM) database [142], gathered in the UK between June 2008 and December 2015 in the adult critical care units in John Radcliffe Hospital and Churchill Hospital, Oxford;
- Medical Information Mart for Intensive Care (IV) (MIMIC-IV), a critical care database gathered between 2001 and 2019 at the Beth Israel Deaconess Medical Center (BIDMC) in Boston, MA, USA;

- The eICU Collaborative Research Database (eICU-CRD), a critical care database gathered between 2014 and 2015 from 208 hospitals across the USA. Of these, routine skin colour assessment data were available from 12 hospitals.

2.2.3 Participants

All adult patients aged 18 or over admitted to ICU were included. Where there were multiple admissions for the same patients, the first admission was used to minimise survivorship bias.

2.2.4 Variables, data sources, and measurement

From each database, the following variables were extracted: patient demographics (age, sex), organ support (vasoactive medication use, renal replacement therapy (RRT), ventilatory support), skin colour documented (with anatomical region if available), length of ICU stay, ICU mortality, and hospital mortality. The calculated OASIS score [143] was extracted where available, or manually computed using the components required. Where OASIS score components were missing, the best score possible for that domain was used [97, 143].

The presence of mottling was extracted from the documented limb skin assessment. Skin assessment occurred as part of the nursing assessment at a frequency set by the clinical need. Nursing staff documented the skin colour electronically, selecting from a pre-defined list of terms (that included 'mottled') in all three databases. Free-text descriptions were also possible in two of the databases. Any free-text entries were manually inspected and any term that resembled 'mottling' (including "mottled/marbled", "mottled and pale", and "slight mottling") was categorised as mottling. All patients were then coded dichotomously as 'never mottled' ('never-mottled' group) or 'mottled at some point during their ICU stay'

('mottled' group).

2.2.5 Bias

The databases included in this study were not created for the purpose of skin mottling assessment. The clinical team caring for each patient assessed the patient according to the clinical need and documented their findings, rather than follow a standardised protocol. Therefore, there is a potential for significant reporting bias. As mottling is easier to observe in lighter skin colours [144], it is possible that there is less accurate documentation of mottling in patients with darker skin colours.

2.2.6 Study size

Study size was determined by the size of the clinical databases.

2.2.7 Outcomes

The primary outcome was ICU mortality. ICU mortality was used because mottling is more likely to be associated with short-term or acute events, best reflected in ICU mortality. Secondary outcomes of interest were the overall incidence of mottling in ICU, ICU length of stay, and hospital mortality.

2.2.8 Statistical analyses

The results from the three databases were analysed separately and also pooled together, adding the database origin as a fixed effect variable. The odds of ICU and hospital mortality were estimated using logistic regression, with and without adjustment for the level of sickness using OASIS [143] and the need for organ support with vasopressors or RRT, neither of which are included in OASIS. ICU

length of stay was compared for patients who survived to discharge only.

The following sensitivity analyses were performed, applying more stringent criteria in each case to define mottling on ICU.

- Inclusion of only the patients who had documented lower limb mottling in the first 24 hours of their ICU stay, in order to exclude mottling that may occur purely in association with ICU treatments e.g., use of vasopressors.
- Exclusion of patients whose documentation of lower limb mottling only occurred in the 24-hour period preceding death on ICU, as skin mottling can be a pre-terminal clinical sign and may have been seen/documented in patients receiving palliative/expectant care.
- Excluding all patients with only one documentation of lower limb mottling when all other skin colour assessments were non-mottled, in order to exclude either very short duration of mottling or those that were recorded in error while selecting from a list on the electronic patient records.

R core v4.1.2 was used for for statistical analysis [145].

2.3 Results

2.3.1 Participants and descriptive data

Of the 208 hospitals included in eICU-CRD, skin assessment data was present in 12 hospitals' records. The hospitals included a mix of teaching and non-teaching hospitals of variable sizes and regions (appendix H). After exclusions, 8555, 53150, and 8891 index admissions to ICU were identified from PICRAM, MIMIC-IV, and eICU-CRD respectively. A total of 70596 patients entered the full analysis. The characteristics of included patients are shown in table 2.1.

Table 2.1: Characteristics of included patients

Variable		**PICRAM**	**MIMIC-IV**	**eICU-CRD**
N		8555	53150	8891
Age	Median (IQR)	63 (47-73)	66 (54-78)	65 (53-76)
Sex	Male (%)	5053 (59.1)	29797 (56.1)	4938 (55.5)
	Female (%)	3495 (40.9)	23353 (43.9)	3943 (44.3)
	Not coded (%)	3 (0.0)	0 (0.0)	10 (0.1)
Organ support	Ventilation (%)	4886 (57.1)	22456 (42.3)	1964 (22.1)
	RRT (%)	783 (9.2)	1189 (2.2)	82 (0.9)
	Vasopressor use (%)	2052 (24.0)	17267 (32.5)	3769 (42.4)
ICU score	OASIS (IQR)	33 (25-42)	30 (24-36)	29 (23-37)
Mottled		1120 (13.1)	1771 (3.3)	282 (3.2)
ICU LOS*	Median (IQR)	1.9 (1.0-3.9)	1.8 (1.1-3.4)	2.0 (1.1-3.7)
ICU mortality	(%)	914 (10.7)	3704 (7.0)	554 (6.2)
Hosp mortality	(%)	1328 (15.5)**	5515 (10.4)	803 (9.0)

*ICU length of stay (LOS) calculated from patients discharged from ICU alive only.
**No record of hospital mortality in 453 cases. Calculated from the 8102 records (94.7%) with hospital mortality data.

Table 2.2: ICU and Hospital Mortality adjusted odds ratio comparing mottled and never-mottled groups

	PICRAM	MIMIC-IV	eICU-CRD	**Combined**
ICU mortality	2.7	2.3	6.0	2.6
OR (95% CI)	(2.2 - 3.2)	(2.0 - 2.6)	(4.5 - 8.1)	(2.4 - 2.9)
Hospital mortality	2.81	2.2	4.9	2.5
OR (95% CI)	(2.3 - 3.4)	(1.9 - 2.4)	(3.7 - 6.5)	(2.3 - 2.7)

Adjusted for OASIS, vasopressor therapy, and renal replacement therapy.

2.3.2 Main results

Patients with at least one episode of mottling were more likely to require vasopressor therapy (64.6% vs 31.2%, $p<0.001$), more likely to be ventilated (78.5% vs 39.8%, $p<0.001$), and more likely to require renal replacement therapy (21.0% vs 2.1%, $p<0.001$).

The median length of stay (survivors only) in the mottled group was 4.8 (2.0 - 10.5) days. Never-mottled patients' median length of stay (survivors only) was 1.8 (1.0 - 3.4) days.

Within-ICU mortality was significantly higher in the mottled group, 36.6% compared to 5.9% in the never-mottled group (unadjusted OR 8.9, CI 8.2 - 9.6). Of the 5172 patients who died in ICU, 1162 (22.5%) had documented recording of mottling at some point during the length of stay. Adjusting for OASIS score, renal replacement therapy and vasopressor use reduced the association, but significant association with ICU mortality (OR 2.6, 95% CI 2.4 - 2.9) remained.

Hospital mortality was similarly significantly higher in the mottled group (unadjusted OR 7.2, CI 6.6 - 7.8). Adjusting for OASIS score and the therapies given in ICU showed persistent significant association with hospital mortality (OR 2.5, 95% CI 2.3 - 2.7). ICU and hospital mortality results from individual databases are shown in table 2.2.

2.3.3 Subgroup analysis

Sensitivity analysis of ICU mortality is shown in table 2.3. Using all 3 conditions, lower limb mottling was associated with significant increase in odds of ICU mortality.

2.4 Discussion

This large retrospective cohort study has shown that documentation of mottling on routine skin assessment while on ICU is associated with a 8.9-fold increase in ICU mortality odds. This association persisted when adjusted for illness severity on admission and levels of organ support required, and when sensitivity analysis was performed. The association between skin mottling and ICU mortality was

Table 2.3: Mottling database: sensitivity analysis

Analysis		**All databases**
Total: mottled patients		3173
A	n (included)	2015
	OR (95% CI)	2.2 (2.0 - 2.5)
B	n (included)	2795
	OR (95% CI)	1.4 (1.3 - 1.6)
C	n (included)	2239
	OR (95% CI)	2.5 (2.3 - 2.8)

A: Only include patients who had documented mottling in the first 24 hours of ICU admission.
B: Exclude those who were only documented as being mottled 24 hours prior to death on ICU.
C: Exclude single documentation of mottling.

comparable across the three databases (table 2.2).

A higher incidence of mottling on ICU was observed in the UK-based database (13.1%) compared to the two based in the US (4.0% and 3.2%). These differences between the databases may be due to higher illness severity in the UK ICU patient cohort, supported by higher ICU mortality, OASIS, and rates of vasopressor and renal support (Appendix H). A lower skin mottling incidence was observed in this study in comparison to two previous prospective studies that included all critical care admissions without pre-specified diagnoses [146, 147] and reported incidence rates of 29% and 31% respectively.

The differences observed have several explanations. The previous studies were conducted in France and the Netherlands respectively and it is possible that the cohort of patients admitted to ICUs in these countries are different. A direct comparison between the populations is not possible but the overall ICU mortality reported by Coudroy *et al.*, [146] is 14.7% compared to ICU mortality of 7.3% in the three databases included in our study. The eICU-CRD database in particular had low rates of organ support with only 22.1% receiving ventilatory support and

0.9% receiving renal replacement therapy. The demographic and patient type may also vary. Coudroy *et al.*, [146] report that 65/791 patients had septic shock and 283/791 were admitted with acute respiratory failure. Some have suggested that mottling may be associated with abnormal microvasculature as part of sepsis pathophysiology [148], potentially leading to the higher observation of mottling among septic cohorts [11, 144, 146, 149]. The difference in proportion of admissions with sepsis or septic shock may subsequently lead to different incidence. Mottling may have been under-recorded in our database due to the electronic documentation pathway which only allows one finding to be documented for the whole limb. Mild degree of mottling may therefore not have been captured.

As mottling is an assessment of the skin colour and pattern, it may be more challenging to diagnose in darker skin. Most skin mottling studies within critical care environment have been performed in Europe and North America, and many studies exclude darker skin [11, 12, 115, 139, 148]. The two studies based in Asia [150] and South America [151] vary from other studies both in form of incidence reported and mortality rates. Cheng *et al.*, [150] report mottling incidence of 4.8% among 126 patients admitted with sepsis or septic shock. De Moura *et al.*, [151] reported an incidence of 39.2% but patients with darker skin were also excluded from this study. The potential difficulty in assessing mottling visually in non-caucasian populations has not been explored in the literature but this may limit the use of skin mottling as a routine assessment tool if used in isolation. When used as part of an overall assessment of skin perfusion as suggested by Hariri *et al.*, [67], an assessment of mottling still may be useful as a finding independently associated with significantly increased mortality.

There are several limitations to the analysis presented in this chapter. The analysis was performed retrospectively and therefore unable to ensure uniformity in skin assessment and record keeping. The results represent an analysis of recorded skin

mottling rather than whether skin mottling was present according to specified criteria. Information available from all 3 databases was gathered for clinical use rather than for assessing skin mottling and associated outcomes. As nursing staff mainly selected the data entered from a pre-defined list of colours/observations, milder degree of mottling may not have been documented. Therefore, it is possible that my estimate of skin mottling incidence may be an underestimate of the true incidence. As it was not possible to identify patients with known vascular disease, I could not ascertain whether the patient had any underlying systemic disorders making them more prone to mottling (or have mottled skin at baseline). Prospective mottling studies that can control these factors have been done and agree with my findings that skin mottling is highly associated with morbidity and mortality [144, 146, 152].

The main strength of the analysis presented in this chapter is the large sample size representing non-selected ICU intake. In total, 70,596 patients were included in the analysis, compared to the largest study to date which included 791 patients [146]. The association between mottling appearance and mortality was assessed while accounting for other confounding factors. Despite the adjustment, mottling appears to be associated with increased mortality, independent of the severity of illness on admission and the need for cardiovascular and renal support. Mottling may provide a useful marker of severity of illness which is easy to detect non-invasively. The association found based on records from clinical practice rather than requiring any special study conditions is an additional strength of the analyses presented.

2.5 Chapter summary

The analysis presented in this chapter is the largest study of critical care skin mottling to date. Data from three large ICU databases were pooled to estimate mottling incidence in the populations and the associated changes in patient outcome.

Lower limb mottling is a clinical sign of poor perfusion to the skin. The presence of mottling in ICU was associated with a significant increase in ICU mortality, and this association was still present even when adjusted for the degree of sickness.

This work provides a backdrop of the current level of clinical skin perfusion monitoring (visual observation and documentation). The skin assessments from ICU databases analysed in this chapter have limitations as discussed in section 2.4. Despite being subjective and prone to documentation-related errors, the skin changes were associated with patient outcomes. Skin mottling that may be easily identified by bedside observers is a potentially crude measurement of skin perfusion abnormality, in a similar way to using GCS for brain perfusion or clotting parameters for liver perfusion (section 1.1.3.2). The association with patient outcomes may be clearer from objective measurements of skin perfusion. The following chapter introduces the concept of objective monitoring of these clinically measured variables using video cameras, and develops the rationale and motivation for the new avenue of research presented in this thesis based on the background introduced in chapters 1 and 2.

3

Rationale and motivation for video camera-based skin assessment

Contents

3.1 Introduction 47
3.2 Video camera as a skin perfusion assessment tool . . . 48
3.2.1 Video camera use for physiological monitoring 49
3.2.2 Windkessel effect to contact PPG waveform 50
3.2.3 Origins of PPGi 52
3.3 Study introduction and rationale for study design . . . 56

3.1 Introduction

The introductory chapter presented the rationale for skin perfusion assessment and the background anatomy and physiology relevant to blood flow to the skin. Chapter 2 then presented further supporting evidence for clinical assessment of the skin on the ICU; subjective observation and documentation of skin mottling in ICU patients were associated with adverse patient outcomes, even when adjusted for the degree of sickness at ICU admission.

On the basis that the utility of skin perfusion assessment has now been established, there are two elements of clinical skin perfusion monitoring that could be improved:

- **Objectivity:** The visual assessment on which the prior evidence is built [61, 62, 153] is operator dependent and subjective. Although subjective assessment has been shown to be clinically useful, adding objectivity to this assessment by *measuring* what the human eye is assessing (rather than using other measured macro- or microvascular parameters described in chapter 1 as proxy variables) may add further value.
- **Sensitivity:** Not all changes that occur at the skin surface are either visually detectable or palpable on examination by a clinician. For example, the changes in skin perfusion that occur over the course of one cardiac cycle described in section 3.2.2 cannot be visually appreciated. It is, however, possible to detect these changes using a video camera; this forms the basis of photoplethysmographic imaging [154]. Similarly, although thermal sensing is a critical component of the human hand function, the absolute sensitivity varies from person to person [155]. A thermal video camera can provide a higher sensitivity, detecting changes of under 0.02 °C [156] compared to a human palm sensitivity of approximately 0.5 to 1.5 °C [155].

Both of these improvements may be achieved using commercially available video cameras. This chapter describes the development of video camera monitoring to date and presents the rationale and motivation for the clinical study on which the remainder of the thesis is based.

3.2 Video camera as a skin perfusion assessment tool

Video cameras are an attractive solution to non-contact physiological monitoring. The gold standard objective skin perfusion measurement methods described in

section 1.4.2 are not in routine use within acute clinical settings. There are several potential reasons for this. The two methods based on laser properties (LDI and LSCI) currently have a narrow range of clinical use, estimating skin perfusion by measuring velocity of moving red blood cells. There is a complete lack of evidence for these monitors for acute skin perfusion monitoring for haemodynamic assessment, and their use in acute settings is practically limited by the device size and cost [5]. In comparison to settings where these tools have been employed (e.g., rheumatology clinics or burn depth assessments [7]), the skin perfusion changes that occur alongside global haemodynamic changes happen over a shorter timescale and can fluctuate rapidly depending on the clinical course and the resuscitation measures.

The use of video cameras may offer a potential solution to these challenges. A camera is an instrument that captures images by measuring light falling on a sensor. Most cameras in commercial use measure light in the visible spectrum, mimicking the function of our eyes. However, specialised cameras exist that can measure light reflection from different ranges of wavelengths within the electromagnetic spectrum, including near infrared (NIR) and infrared (IR). A camera/set of cameras therefore offer the potential to capture other clinically useful information concurrently.

3.2.1 Video camera use for physiological monitoring

In the last 20 years, substantial developments in camera technology have coincided with increased availability and affordability [157]. The attitude of the general public to camera-monitoring has also shifted in recent years, with growing acceptability despite early concerns regarding privacy and the potential for misuse [158, 159]. In addition, the appeal of telemedicine and remote monitoring of patients has increased in both hospital and other care settings, further highlighted most recently by the COVID-19 pandemic [160]. From a combination of these factors, there has been an increase in interest in using video cameras for physiological monitoring. Image-based monitors potentially allow multiple variables to be measured concurrently using a

non-contact sensor, avoiding complications associated with contact sensors such as tethering, skin irritation, and frequent loss of contact [161].

My 2019 systematic review of camera-derived vital-sign monitoring [161] revealed that 88% of published studies were conducted in academic settings, largely in healthy, young (18 to 40 years) populations. The most explored vital signs were heart and respiratory rate measurements, with 75% and 39% of published studies aiming to estimate the two respectively. Approximately half of the studies reported being able to estimate heart and respiratory rates within industry standard [162]. Evidence for camera-based monitoring of peripheral arterial oxygen saturation and blood pressure was relatively sparse [161].

Both heart rate and blood pressure monitoring from skin using RGB cameras are based on photoplethysmographic imaging (PPGi), relying on sensing the fluctuation in reflected light from the skin surface with video cameras. This technology is a recent development of contact photoplethysmography (cPPG), which was invented fifty years ago by Takyo Aoyagi [163].

3.2.2 Windkessel effect to contact PPG waveform

Left ventricular contraction generates the driving force required to move blood through the cardiovascular network described in section 1.1.2.1. The forward flow and the resulting pressure and volume waveforms generated are known to be a major (but not the only) source of the signal acquired using video cameras at the skin surface [154, 164, 165].

The cardiac cycle is composed of two distinct phases. During systole, the left ventricle ejects a volume of blood out through the aorta. Following systole, the left ventricle relaxes to re-fill during diastole. Throughout one cardiac cycle, all vessels

in circulation undergo changes. The changes that occur are dependent on the site of measurement, related to the distance from the heart and the route taken (i.e., the number of junctions and subsequent dampening effect) [166]. The elastic structure of the large arteries allows some give in the wall and they distend during systole. During the subsequent diastole, the distension recoils and the blood continues to move forward, giving a constant forward flow throughout the cycle. This is named the Windkessel effect [167]. The pulsatility along the arterial tree is preserved in dampened shape down to the capillary and the microcirculation.

Photoplethysmography (PPG) uses the change in light absorbance associated with the above changes in tissue blood volume during each cardiac cycle. The systolic increase in blood volume at the peripheral sites (e.g., skin) leads to more absorbance of light travelling through the biological tissue, compared to the diastolic phase. When the light transmitted through the peripheral site (e.g., finger, toe, or earlobe) is measured using a photodiode (PD) (as in a pulse oximeter), the resulting pulsatile waveform is called the PPG waveform. Pulse oximeters use two wavelengths of light (usually red and near-infrared) which are differentially absorbed by the oxygenated and de-oxygenated forms of the haemoglobin molecule responsible for oxygen transport in the blood [165]. The absorbance patterns of the two wavelengths are used to estimate the arterial oxygen saturation (SaO2) [165, 168].

Clinical pulse oximeters typically encase two light-emitting electrodes (LEDs) to generate the light beam to be transmited through the peripheral site and a photodiode on the opposite of, for example, a finger. The precise arrangement of the LEDs and the PDs can vary, but they are arranged so that the recorded PPG waveform represents changes in transmission of light. In contact PPG, the sealed casing in which the LEDs and PDs are placed around the finger reduces the effects of ambient light, motion artefacts, and other external noise. The principle of PPG may be applied to alternative arrangements with differing light source and sensor

arrangements.

3.2.3 Origins of PPGi

PPGi may be considered as a non-contact counterpart of the well-known and used contact photoplethysmography (cPPG). The first description of obtaining a waveform similar to cPPG using a video camera was in 2005 by Wieringa *et al.*, [169]. Instead of the light source and sensor that are built into a single finger probe or a clip described above, the set-up consisted of a light source distal from the skin surface and a video camera as the light detector. A range of variations on this set-up has been explored in the literature since, with light sources ranging from a dedicated single-wavelength light to ambient lighting or natural light, and a wide range of video cameras as the sensor, from monochrome video cameras measuring single-wavelength light intensity to cameras measuring light energy from outside the visible electromagnetic spectrum e.g., thermal or near infra-red (NIR) video cameras [161]. In contrast to cPPG where the waveform reflects changes in the absorption of light travelling through the biological tissue, the light intensity sensor in the camera measures the varying amount of light that is reflected by an object (the skin in this case).

There are several theoretical advantages of PPGi over cPPG. PPGi has the advantage of monitoring a larger body area, potentially allowing multiple regions to be monitored concurrently and compared using a single monitor [165]. It does not require contact with the skin surface which may be more comfortable for the patient, and avoids complications associated with contact monitors such as infection and pressure effects [170, 171]. Pressure on the skin surface can also affect perfusion to the area, which is the very signal being measured [170].

The cardiac rate fluctuation in skin reflectance is well described [154], but the precise source of the signal is not clear. There are four potential sources of this

fluctuation explored in the literature:

- Change in the volume of blood from systole to diastole, described in previous section [154, 169];
- Movement from nearby arteries close to the skin surface with systole and diastole, leading to a cardio-synchronous movement in the area being measured (region of interest (ROI)) [172];
- Movement of a body region due to volume changes in the total amount of blood (ballistocardiography) [173], most typically observed when measuring from the head and neck region.
- Change in colour as new oxygenated blood arrives with each cardiac pulse [174].

All four factors would cause a cardiac-synchronous variation in reflectance from the skin and all likely make some contribution to the PPGi waveform measured, with the proportion of the effect depending on the location of the ROI. For example, a ROI over a superficial artery is likely to have a larger component from movement compared to regions distal from large arteries [175].

Heart rate is directly estimated from the frequency of the PPGi waveform, with studies reporting on methods of eliminating motion artefacts and optimal peak detection algorithms [176–178]. Heart rate monitoring using PPGi measurement currently performs within clinically acceptable limits under experimental conditions. The video-camera derived estimates have been shown to be less accurate in studies performed in clinical environments [161].

In addition to heart rate estimation, several studies have used camera-derived pulse transit time (PTT) for blood pressure estimation [179–182]. PTT is the time delay of the pressure wave created by the left ventricle, often measured using contact

methods between the R wave of ECG waveform and the peak of the cPPG waveform at a distal site (usually a fingertip) [165, 183]. The use of PTT to estimate blood pressure is well explored in the literature, with systolic blood pressure typically showing an inverse relationship with PTT [183]. Several studies were able to show accuracy within clinically acceptable limits (a mean error ± standard deviation of 5 ± 8 mmHg) [181, 182]. However, these studies do not meet all the criteria for blood pressure monitoring in clinical settings that also specify the size of trials and details of how the reference measurements are recorded [184].

In summary, beyond heart rate and respiratory rate, video-derived monitoring is not at the stage where it can be easily translated to clinical application, although the advantages of incorporating this type of monitoring is clear. This topic is further comprehensively reviewed by Steinman *et al.*, 2021 [185].

3.2.3.1 Challenges in video camera monitoring

In the previous section, the differences between the arrangement of light source and sensor in a pulse oximeter and those used in video camera monitoring studies were discussed. Despite the advantages offered by the non-contact nature of the set up, the distance between the skin and both the light source and the light detector makes the latter system more prone to interference.

A thematic analysis of the challenges associated with camera studies were included in my systematic review of vital-sign monitoring using video cameras [161]. The challenges in physiological monitoring using video cameras can be categorised into practical aspects of data acquisition, data processing, and socio-economical.

The commonest data acquisition limitations reported by studies include:

- Sensitivity to artefacts, such as movement or lighting changes;
- Frequent loss of signal, related to the above reason;
- The reliance on constant lighting;
- Poorer signal acquisition from subjects with darker skin tones.

Data processing challenges relate to efficient processing of noisy data, the video file size generated, and the challenge in continuous monitoring. As a consequence, studies report difficulty in performing real-time analysis and translation to clinical settings. However, a number of recent studies have demonstrated accurate real-time heart rate monitoring from video cameras [186–189]. Socio-economical factors include the potential invasion of privacy and concern regarding patient confidentiality, costs of video camera monitors, and the possibility of providing this type of monitoring at scale.

The practical and data processing challenges may be resolved by further innovation or careful selection of the settings in which monitoring systems may be used. The latter challenges are in constant flux and require not just quantitative research but also work with human factors and qualitative researchers for smooth transition and integration of novel technologies. The concept of video-based vital-sign monitoring has recently been shown to be acceptable to ICU staff with perceived benefits to both patients and staff [190].

Studies that monitor the skin using video cameras for the purpose of vital-sign monitoring have tended to select ROIs based on the availability of the skin region, ease of access, or surface anatomy. How the locations of the arterial perforators that bring arterial blood to the skin surface affect video camera measurements at skin surface in both the visible and outside the visible electromagnetic spectrum is

not yet known.

3.3 Study introduction and rationale for study design

An objective of this thesis is to describe which features quantifiable using red/green/blue (RGB) and thermal video cameras change following induced variation in skin perfusion. As discussed earlier in this chapter, the use of video cameras for haemodynamic monitoring has been primarily focused on heart rate and respiratory rate estimation. In the development of video camera-derived vital-sign monitoring, the direction of progress has been in:

- Improving the accuracy of estimation in noisy environments, e.g., using motion-robust algorithms, with the goal of translation into clinical settings. This has been achieved in several clinical areas including outpatient clinics [191], renal dialysis units [192], neonatal critical care [193–195], and adult critical care [196, 197].
- Estimation in real-time [186, 189, 198].

Far less has been published on further exploration of PPGi features. The experimental methods used to induce changes in vital-sign have tended to introduce even more movement artefacts in the PPGi signal [161], frequently leading to PPGi waveforms containing much motion-induced noise [199, 200].

Whether any of the features of the hypothetical 'noise-free' PPGi waveform change during any increase or decrease in skin perfusion remains largely unexplored. Furthermore, the selection of ROI from which PPGi is measured has traditionally been based on either the availability or the ease of exposure of the anatomical region

(e.g., face or arm) or because of large vessels present in the region (e.g., side of the neck and vascular structures [201, 202]). The ROI selection in most studies does not consider the blood supply to the ROI itself and the knowledge of the arterial perforator vessel supplying it. In chapter 1, I explored the macro- and microvascular anatomy of the blood supply to the skin. Incorporating knowledge of perforator locations in the selection of ROI and the subsequent analysis of PPGi waveforms may provide further insight into how the most superficial vessels of the skin are perfused and the interaction between skin macro- and microvasculature.

Studies consistently cite movement artefacts and sensitivity to ambient lighting changes as key limitations in video camera monitoring [161]. I designed the Mapping of Lower Limb skIn pErfusion (MOLLIE) study to build a dataset with a) varying skin perfusion states and b) localisation of arterial perforators in the same healthy individuals. In the first part of the study, I induced peripheral perfusion changes pharmacologically in order to minimise movement artefacts. I used intravenous phenylephrine and glyceryl trinitrate (GTN) infusions to achieve vasoconstriction and vasodilation respectively. In the second part of the study in the same participants, I used a timed tourniquet release technique to locate arterial perforators [203]. I registered the study on ISRCTN (ISRCTN10417167) and published the protocol [203]. Chapter 4 describes the MOLLIE study in full, and presents a summary of the resulting dataset.

Two video cameras were selected for the clinical study. The first video camera was a 3-channel (red/green/blue or RGB) colour video camera. The second camera was an infrared camera. Throughout the remainder of this thesis, the two cameras are referred to as RGB and thermal cameras respectively. They are further described in section 4.6.1. In addition to the two video cameras, a commercial laser speckle contrast imager (LSCI, section 1.4.2.1) was used to concurrently measure skin perfusion using an existing imaging method. The LSCI monitor is further described

in section 4.6.2.3.

Using the created dataset, several streams of analyses were performed to demonstrate the potential of video camera-derived monitoring. The streams each address one of the two improvements that video camera monitoring may add to clinical assessment (section 3.1). Staying with the theme of skin mottling as a clinical sign of microvascular failure further explored in chapter 2, the first stream of analysis is on using video camera images for skin mottling assessment. As mottling is a visible clinical sign, the primary aim of this analysis was to add objectivity to a visible sign. In addition, however, I also aimed to explore whether mottling appearance could be detected earlier using video camera monitoring with higher sensitivity. This analysis is described in chapter 5.

Chapter 6 then explores how the PPGi waveform (not visible to the naked eye) changes in response to the pharmacologically induced vasoconstriction and dilation. In this chapter, the PPGi waveform parameter changes are computed from a large region of the thigh without consideration of the location of cutaneous perforators within the region. Chapter 7 then presents data from the thermal camera to locate skin regions overlying the perforator and regions distal to the cutaneous perforators. This information is then incorporated into PPGi waveform analysis in chapter 8.

4

Materials, methods, and the dataset

Contents

4.1 Ethical approval and recruitment 60
4.1.1 Ethical approval 60
4.1.2 Recruitment 60
4.2 Study setting 60
4.3 Participants and eligibility 61
4.4 Experimental timeline 62
4.5 Interventions 64
4.5.1 Drugs 64
4.5.2 Tourniquet 66
4.6 Monitoring instrumentation 68
4.6.1 Cameras 68
4.6.2 Reference monitors 71
4.6.3 Data collection set-up 73
4.7 Data storage 73
4.8 Analysis methods overview 74
4.8.1 Identification of periods of interest 75
4.8.2 Identification of region of interest (ROI) 75
4.8.3 RGB multi-channel analysis 76
4.8.4 Validity of frames included 76
4.9 Data display and summary statistics 77
4.9.1 Box and whisker plots 78
4.10 Acquired dataset from the MOLLIE study 78
4.10.1 Participant demographics 78
4.10.2 Evidence of drug effect 79
4.10.3 Camera data acquired 82
4.11 Chapter summary 83

In this chapter, the methodology used in the MOLLIE study and the resulting dataset are described.

4.1 Ethical approval and recruitment

4.1.1 Ethical approval

The Oxford University Research and Ethics Committee/Clinical Trials and Research Governance (R63796/RE001) approved the study following a CUREC 3 ethical review process for licensed drug administration to healthy volunteers (Appendix A). The study followed Good Clinical Practice guidelines and conformed to the standards set by the Declaration of Helsinki.

4.1.2 Recruitment

Participants were recruited via an in-person approach, poster adverts, and snowball recruitment. All participants who expressed interest were enrolled serially as long as they were eligible according to the inclusion/exclusion criteria (section 4.3).

4.2 Study setting

The study took place at the Cardiovascular Clinical Research Facility (CCRF) within the John Radcliffe Hospital, Oxford, United Kingdom. The CCRF is a dedicated research environment with expertise in echocardiography, exercise physiology, and vascular assessments. The facility is well equipped for potential haemodynamic resuscitation to safely support cardiovascular clinical studies. The location was chosen for the MOLLIE study to maximise the cardiovascular safety of the study participants. The clinical staff at the CCRF checked the haemodynamic resuscitation

equipment daily which was on standby for immediate use as necessary.

Two dedicated rooms within the CCRF were used for all study recordings. In-built blackout blinds minimised natural light in the study area as much as possible and controlled the lighting for image acquisition. Illumination was delivered by the ceiling fluorescent lighting and a dedicated 5600K light-emitting diode (LED) mosaic panel light (Limelite 30cm Mosaic Panel, Bowens, London, UK) with 576 diodes over a 30 x 30 cm^2 area, held by a stand located at the foot of the examination bed. Vibration noise was minimised by switching off air-conditioning units in the research area and keeping the room as quiet as possible.

4.3 Participants and eligibility

Healthy participants aged between 18 and 65 years inclusive took part in the study. As this was an unexplored field, the effect size was not known and it was not possible to calculate a sample size. The target number of participants was set at 30 based on a balance of adequate study size to describe inter-subject differences and to include sufficient numbers of males and females and potential skin types, with practical considerations of data size for data storage, analysis, and running of the study. Details of study inclusion and exclusion criteria are shown in table 4.1. Any participants for whom the known side-effect profile of phenylephrine and GTN may be more noticeable or harmful were excluded from the study. Participants removed lower limb body hair 24 to 48 hours prior to the study visit to improve the quality of the skin images taken and to reduce the amount of noise from fine hair movement in the images. Participants avoided caffeine intake for 4 hours prior to the study visit [204].

All participants who expressed an interest in taking part were sent a copy of the participant information sheet and the consent form (available as Appendix

Table 4.1: Inclusion and exclusion criteria

Inclusion criteria
• Healthy adults aged 18 to 65 years • Willing and able to give informed consent for participation in the study • Willing to remove hair on lower limbs by shaving or waxing 24 hours prior to the study visit
Exclusion criteria
• Participants whose anatomy, condition, or other required monitoring precludes the use of the camera equipment or the thoracic bioimpedance monitor device. Examples include skin disorders such as eczema, scleroderma, or psoriasis • Any degree of lower limb amputation • History of surgical intervention to the thigh/knee/lower leg, except for procedures not expected to permanently change blood flow pattern to the lower limb skin e.g., knee arthroscopy • Allergy to silver chloride ECG sensors • Hyperthyroidism (intravenous phenylephrine contraindicated) • Any regular medication except oral contraception • Pregnant* or breastfeeding • History of or current neurological condition affecting peripheral circulation • History of cardiovascular disease where phenylephrine or glyceryl trinitrate (GTN) are contraindicated • History of severe headaches
*In addition to the screening questionnaire, a urinary pregnancy test was performed for all female participants on the day of the study visit prior to the experiment.

B) electronically. Participants had at least 24 hours to read and consider the documents. Participants then underwent screening via a telephone consultation to confirm eligibility, further discuss the details of the study, answer any remaining questions, and schedule the experimental visit.

4.4 Experimental timeline

Each eligible participant attended for one in-person visit. The study visit began with informed consent taken by me, a final eligibility check, measurement of height (cm), weight (kg), Fitzpatrick skin scale (I-VI), Von Luschan skin scale (1-36), and baseline vital-sign observations including heart rate (beats per minute), blood pressure (mmHg), respiratory rate (breaths per minute), and peripheral oxygen saturation (%). All female participants took a urinary βHCG test to rule out

pregnancy before proceeding with the study.

A cardiovascular examination was performed at the beginning of the study visit to detect any underlying abnormalities that would make the drug infusions potentially unsafe. The baseline heart rate and mean arterial pressure (MAP) were used to calculate the individual maximum allowed deviation (30%) during drug infusions for safety [203].

Participants lay down on the study bed (semi-recumbent position, figure 4.3). A Becton Dickson (BD) Venflon (BD, Eysins, Switzerland) intravenous cannula with injection port (size 22G blue 25mm) was placed in the participant's right antecubital fossa using a sterile non-touch technique. The intravenous cannula was kept in place using a Smith & Nephew IV3000 transparent dressing. All video camera and reference monitoring equipment were placed as per manufacturer instructions. Once all equipment was in place, the computer workstations were time-synchronised using the network time protocol [205]. The study visit timing was tightly controlled using an electrical timer with an audible cue for each step of the experimental timeline. I led all study visits and subsections of the study with technical assistance from the Oxford Biomedical Signal Processing Machine Learning Group (BSP-ML), Institute of BioMedical Engineering (IBME). The additional staff provided practical assistance in commencing multiple monitors at the same time point and optimising the camera set-up.

The monitored experimental period began with a 5-minute rest with no interventions. Following the rest period, phenylephrine hydrochloride was administered intravenously over a 15-minute period. The dose escalation protocol is described in subsection 4.5.1 and shown in figure 4.1. Once the infusion stopped, the participants continued to be monitored for a further 8-minute period, designated as the 'washout' period. Participants were then given a break of 15 minutes to rest (during which

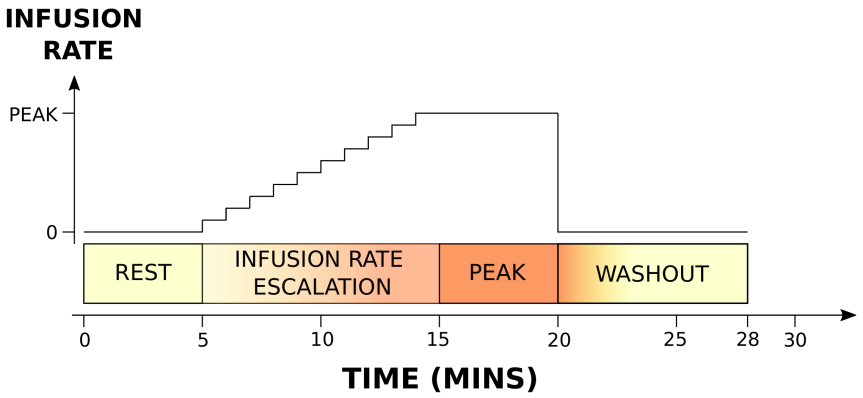


Figure 4.1: Experimental timeline for each drug infusion session, adapted from Finnegan *et al.*, [206]

they were allowed to move) before starting the GTN session following the same timeline. After a further 15-minute break, the re-filling pattern of the lower limb was studied using a thigh tourniquet. A combined limb exsanguinator/thigh tourniquet (HemaClear®) was used, as described in section 4.5.2. The tourniquet was applied following the manufacturer's instructions (appendix D) and released while assessing the refill pattern using video cameras. All participants were reviewed medically before they left the study session. All participants followed the same timeline and neither the participants nor researchers were blinded to the treatments given.

4.5 Interventions

Two categories of interventions were used in the MOLLIE study as detailed in this section.

4.5.1 Drugs

Two intravenous infusions were given to all participants to induce vasoconstriction and vasodilation. Intravenous infusions were used to induce physiological changes as the drug dose (and therefore the magnitude of effect) could be controlled away from the bedside to achieve the desired clinical effect while the participants remained still.

The design also minimised noise in the imaging dataset from nearby movement and shadow artefacts. The drug infusions were given alongside an additional infusion of 0.9% normal saline solution running at 100mL.hr^{-1}. The additional continuous fluid infusion was given to aid and ensure continuous drug infusion delivery through an extension set and dual intravenous cannula port. This set-up was chosen to improve the intravenous delivery of small volumes of GTN (which is known to be difficult and inaccurate [207]). An Alaris^{TM} CC Plus Syringe Pump with Guardrails^{TM} Safety Software was used to accurately control the drug infusion rates.

4.5.1.1 Phenylephrine

Phenylephrine is a synthetic alpha-1-adrenoceptor agonist. It acts selectively on the alpha-1 adrenoceptors present on the wall of peripheral blood vessels (both arterial and venous) without having significant direct effect on the cardiac myocytes [208]. It has the clinical effect of increasing blood pressure via peripheral vasoconstriction and also causes reflex bradycardia. It is used to treat hypotension associated with spinal or epidural anaesthesia.

Phenylephrine hydrochloride - provided as 10 mg.mL^{-1} clear colourless solution - was used in the study. One mL of phenylephrine hydrochloride was diluted in 100 mL of 0.9% saline to create concentrations of 100 mcg.mL^{-1}. A labelled 50 mL BD Plastipak Luerlock syringe was connected to a double-lumen extension (with the second lumen connected to the 0.9% saline infusion). The infusion commenced at 0.2 mcg.kg^{-1}.min^{-1} (calculated using actual body weight) and the rate was increased by 0.2 mcg.kg^{-1}.min^{-1} increments every minute for 10 minutes. The maximum infusion rate was indexed to the actual body weight at 2 mcg.kg^{-1}.min^{-1}. Once the maximum rate was reached after 10 minutes of infusion, the infusion and all monitoring continued for a further 5 minutes at stable maximum rate. The maximum absolute initial infusion rate was set at 14 mcg.min^{-1} (regardless of participant body weight), and the maximum absolute peak infusion rate was set at 140 mcg.min^{-1}. These

limits corresponded to no further increase above 70kg body weight. The maximum rates were chosen with guidance from the pharmacology advisory team as part of the CUREC Review for the study.

4.5.1.2 GTN

GTN is a nitrate which causes the relaxation of vascular smooth muscles causing arterial and venous dilation. Like other nitrates, GTN acts by generating nitric oxide (NO) which then acts directly on the vascular smooth muscle to activate the intracellular guanylate cyclase pathway leading to vasodilation (section 1.3) [209].

A ready-diluted GTN solution provided at a concentration of 1 $mg.mL^{-1}$ was used in the study. A labelled 20 mL BD Plastipak Luerlock syringe was used for the GTN infusion. Two different size syringes (50ml and 20ml for phenylephrine and GTN respectively) were used to minimise the risk of drug errors. The infusion commenced at 0.15 $mcg.kg^{-1}.min^{-1}$ and the rate increased by 0.15 $mcg.kg^{-1}.min^{-1}$ every minute for 10 minutes. The maximum infusion rate was indexed to the actual body weight at 1.5 $mcg.kg^{-1}.min^{-1}$. Once the maximum rate was reached, the infusion and all monitoring continued for a further 5-minute period. The maximum absolute initial infusion rate was set at 10.5 $mcg.min^{-1}$, and the maximum absolute peak infusion rate was set at 105 $mcg.min^{-1}$. These limits corresponded to no further increase beyond 70kg body weight, similar to the phenylephrine infusion protocol. The limits were chosen for participant safety, with guidance from the pharmacology advisory team as per phenylephrine.

4.5.2 Tourniquet

Right lower limb exsanguination and thigh tourniquet application followed by timed tourniquet release was used to identify arterial perforator locations in the thigh and lower leg [203]. The reperfusion phase post-tourniquet release was recorded

using the dual camera set-up described in section 4.6.1. As discussed in chapter 1, previous studies aiming to locate these vessels used cold gel or a water pack applied to the skin [210, 211] or a fan held close to the skin [212] to cool the skin surface then track the rewarming of the skin using video thermography ('dynamic thermography'). Limb exsanguination and tourniquet application were used in the MOLLIE study as it provided advantages over the cooling methods. Consistent uniform cooling of the full leg using external cooling methods across participants at a defined time was found to be difficult to achieve. By achieving standardised baseline conditions where the leg was as empty of blood as practically achievable, I hypothesised that the reperfusion phase would give higher resolution images of the perforators. Standardising the timing of perforator imaging across the participants achieved logistical advantages for the study.

Several methods of achieving limb exsanguination were trialled before selecting a final method. The following methods were considered and tested: leg elevation alone, Esmarsh bandage (P3 Medical, Bristol, United Kingdom), Rhys Davies Exsanguinator (AneticAid, Baildon, United Kingdom), and HemaClear® exsanguinator and tourniquet (Oneg HaKarmel Limited, Grandville, MI, USA). Elevation alone did not achieve significant limb cooling/emptying. Esmarsh bandage and Rhys Davies Exsanguinators both left linear streaks on the skin following application which affected the subsequent camera imaging. These two methods also did not achieve uniform exsanguination and were operator-dependent. In addition, leg elevation, Esmarsh bandage, and Rhys Davies exsanguinators all require a separate surgical tourniquet to be applied after exsanguination, whereas this function was integrated into the design of the HemaClear® exsanguinator, which was therefore chosen for the MOLLIE study.

HemaClear® consists of an elastic silicone ring, a stockinette, and straps that aid the device application [213]. In clinical settings, it is usually used during limb

surgery to achieve a bloodless surgical field [214] or for auto-transfusion during haemodynamic resuscitation [215]. By pulling on the straps, the device can be unrolled along the limb from distal to proximal. The device is usually provided in several sizes to cater for different limb circumferences (14 to 85cm). The extra-large size was used in the study which provided adequate exsanguination and tourniquet pressure (above systolic blood pressure). The pressures exerted by the extra-large HemaClear® are shown in appendix (figure D.2, appendix D).

The HemaClear® was placed on the right thigh of the participant following manufacturer instructions (figure D.1, appendix D). Once in place, the stockinette over the leg was removed, leaving the exsanguinated leg with the silicone ring tourniquet *in situ*. All monitoring started as soon as the stockinette was removed, and the leg was monitored for a further 30-second period with the tourniquet *in situ*. The tourniquet was then released by cutting the silicone ring using a scalpel as per manufacturer instructions.

Following the tourniquet release, The leg was monitored for 4 further minutes. This duration was selected based on previous evidence regarding the rewarming phase of the perforator angiosomes over time. In a study of the dynamic assessment of perforator locations [78], the temperature rise in skin regions overlying perforators was tracked for up to 240 seconds. The authors showed a logarithmic increase in skin temperature of perforator angiosomes following external cooling. The same timeline was followed to capture the dynamic phase of skin temperature changes.

4.6 Monitoring instrumentation

4.6.1 Cameras

Two video cameras were used to capture image data; an RGB (colour) camera and a thermal camera. Each camera was controlled by a designated computer workstation.

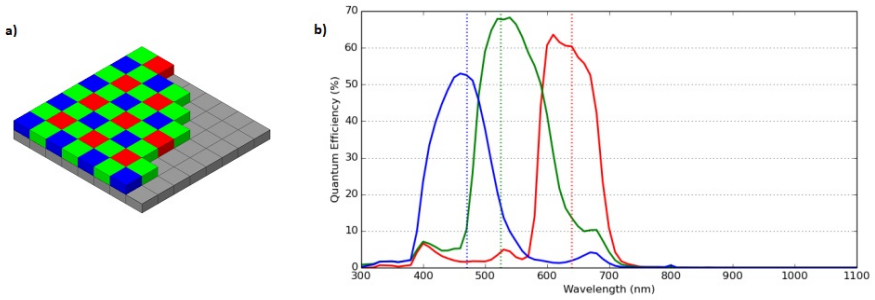


Figure 4.2: RGB camera sensors a: Bayer filter pattern used in the RGB camera sensor; b: Response curve for the three colour channels [216]

4.6.1.1 RGB camera

A Grasshopper3 GS3-U3-51S5C visible spectrum camera was used to collect the RGB data (table 4.2). The camera was fitted with a 16mm lens (VS Technology SV-1614H 1/1.2" 16mm F1.4 Manual Iris C-Mount Lens, 5 megapixel). The layout and the response curve for the three channels are shown in figure 4.2. The camera was placed 70cm vertical to the skin surface of the right knee (figure 4.3). The RGB camera selection including technical specifications was led by the BSP-ML Group, who also wrote the software controlling the RGB camera function.

Two different camera configurations were used for the drug and tourniquet sessions as detailed in table 4.3. A higher frame rate was used for the tourniquet release session as rapid changes were expected immediately following the tourniquet removal.

4.6.1.2 Thermal camera

A commercial thermographic video camera (A6750sc, FLIR systems, Oregon, USA) was used to collect thermal imaging data. The camera was placed vertically 55cm away from the skin surface (figure 4.3), as close to the RGB camera as possible to maximise the anatomical area being recorded. The thermal video camera has an in-built cooled FLIR Indium Antimonide (InSb) detector, providing a high thermal sensitivity of <20 mK. Further imaging specifications are shown in table 4.4. The

Table 4.2: RGB camera: features and specifications

Item	Details
Camera family	Grasshopper3
Model number	GS3-U3-51S5C-C
Manufacturer	Point Grey Research, FLIR Systems
Type	Colour Camera
Megapixels	5.0 MP
Imaging sensor	Sony IMX250
Type of sensor	Progressive scan CMOS
Type of shutter	Global
Image size (pixels)	2448 x 2048
Pixel size (micrometres)	3.45 x 3.45
Maximum frame rate	75 per second (at maximum resolution)
Video output	USB 3.0

Table 4.3: RGB camera configurations used in MOLLIE study

Item	Drug session	Tourniquet session
Frame rate (fps)	60	140*
Frame width	1280	1280
Frame height	960	960
Pixel format	RAW_16	RAW_16
Shutter (ms)	16	7

*Above the maximum frame rate stated in table 4.2 as lower resolution frames were used

thermal camera measured electromagnetic radiance from the skin, expressed in units of watts per steradian per square metre ($W.SR^{-1}.m^{-2}$).

The ResearchIR Max software provided by FLIR was used to control the thermal camera function.

For all the thermal data presented (mainly limited to chapter 7), the term 'radiance' is used. Thermal video cameras create images by measuring the infrared radiation. The camera software converts this to estimated surface temperature. This conversion requires a calibration of the thermal camera and a measurement of the emissivity of the material [217], which represents the relationship between the temperature and the object's radiance. Although the human skin is generally accepted to have a high emissivity, the exact value can vary from individual to individual [218]. The

Table 4.4: Thermal camera: features, specifications, and configurations used in the MOLLIE study

Item	Details
Detector type	FLIR Indium Antimonide (InSb)
Spectral range (micrometres)	1 to 5
Thermal sensitivity	<20mK (typically 18mK)
Readdout	Snapshot
Frame rate (fps)	60
Frame width	640
Frame height	512

raw radiance data was used to monitor relative changes rather than the converted skin temperature data, to minimise the number of assumptions being made (with variable inter-subject effects).

4.6.2 Reference monitors

4.6.2.1 Philips

The reference vital signs (heart rate, ECG waveform, respiratory rate, peripheral oxygen saturation (SpO_2), finger PPG waveform) were measured and recorded using a Philips IntelliVue MX800 patient monitor (Philips, Eindhoven, Netherlands). The monitor was used alongside a Philips IntelliVue MMX Multi-Measurement Module and a Masimo SET SpO_2 Vuelink IntelliVue Measurement Module (Masimo, Irvine, CA, USA). Vital signs were recorded using a Philips re-usable adult SpO_2 sensor (M1191BL), Comfort Care re-usable Adult NIBP cuff (M1574A), and ECG Cable 3 Leadset Grammer IEC ICU (M1672A) connected to an ECG Cable 3 Lead (M1669A). IxTrend software (Ixellence GmbH, Germany) was used to transfer and save the data from the Philips patient monitor onto a dedicated workstation hard drive.

4.6.2.2 CardioScreen

A commercially-available thoracic bioimpedance monitor (CardioScreen 1000, Medis, Germany) was used to estimate the stroke volume/cardiac output continuously using impedance cardiography. The device estimates cardiac output by measuring the electrical impedance across the thorax, which in turn is affected by the volume of blood in the chest at any one time [219]. The change in impedance with each cardiac cycle is used to estimate the stroke volume. This thoracic bioimpedance monitor has previously been shown to provide reliable haemodynamic trend monitoring in healthy individuals [220]. Four dual sensors were placed on the left lateral thorax and left side of the neck, following manufacturer instructions. The Arterial Compliance Modulation earlobe-sensor was placed on the left earlobe. The monitor was controlled using the manufacturer's own software (Cardio-Vascular-Lab) installed on a separate portable computer. Following each study session, session data was exported from the Cardio-Vascular-Lab to the secure external hard drive as comma-separated values files.

4.6.2.3 Laser speckle contrast imager (LSCI)

A commercial laser speckle contrast imager (moorFLPI-2, Moor Instruments, Axminster, UK) was used to collect reference skin perfusion data, reporting flux in proprietary perfusion units. The device estimates blood flow velocity by quantifying the extent of blurring of dynamic speckles caused by the motion of red blood cells moving through the vessels [221]. The principles of laser speckle contrast imaging were described in section 1.4.2.1. Device specifications are shown in table 4.5. The monitor was placed so as to maximise the overlap between the skin area monitored by the LSCI monitor with the regions recorded by the RGB and thermal cameras. The camera component was positioned 25cm away from the skin surface, following the manufacturer's guidance (figure 4.3). Two different configurations were used for the drug infusion and tourniquet release sessions (table 4.6). A higher frequency perfusion estimation was used for the tourniquet release session (25Hz vs 5Hz) to

Table 4.5: Laser speckle contrast imager: features and specifications

Item	Details
Measured parameter	Flux (range 0-5000PU)
Laser source	Near Infra-red laser diode 785 nm
Laser specifications	Class 1 per IEC 60825-1:2007
Scan area	15 x 20 cm
Image resolution	580 x 752 pixels
Maximum image acquisition rate (fps)	25

Table 4.6: Laser speckle contrast imager configurations

Item	Drug session	Tourniquet session
Image acquisition rate (fps)	5	25
Processing window	Spatial	Spatial
Time constant* (s)	3.0	0.1

*Image acquisition time constant for time resolution

improve the time resolution of any changes immediately following the tourniquet release.

The moorFLPI-2 Research Software (manufacturer's own) was used to control the laser speckle imager and for image acquisition. The software was also used to export the perfusion imaging data to a secure external hard drive.

4.6.3 Data collection set-up

The bedside set up for study recordings is shown in figure 4.3. The study recordings were acquired over 12 days, and every effort was made to keep the equipment in the same location throughout the study.

4.7 Data storage

A storage cluster hosted at the IBME Data Centre was used to store all data from the MOLLIE study. Video data was captured in real time onto internal hard drives.

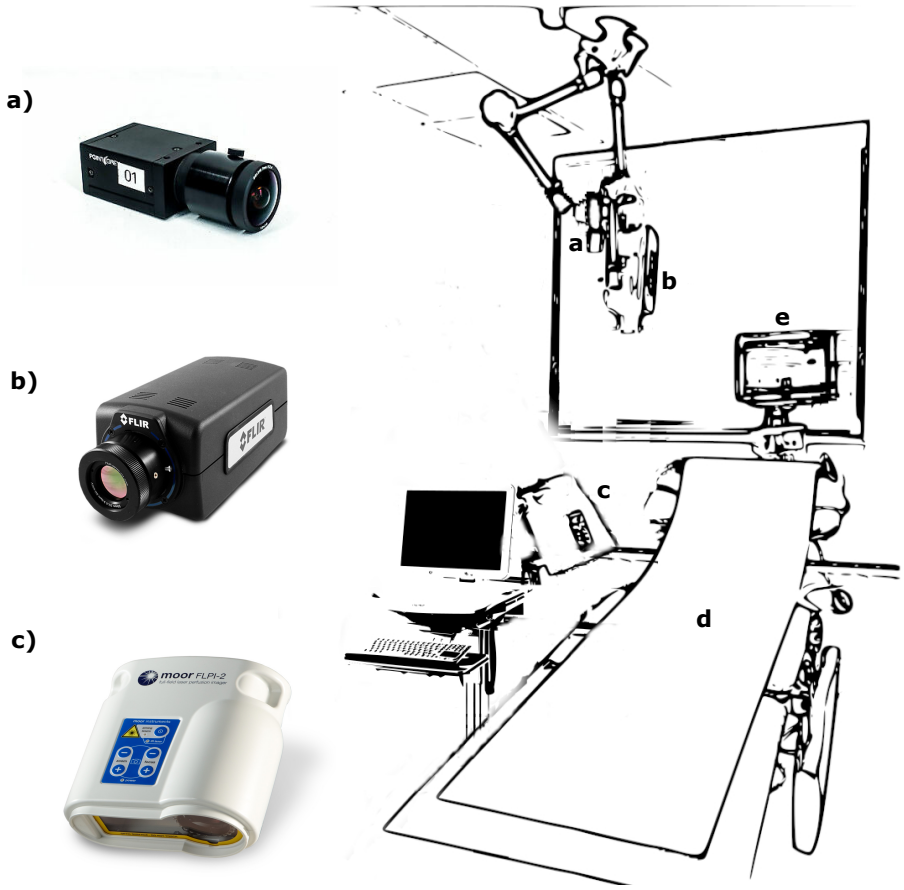


Figure 4.3: Experimental set-up a: RGB camera; b: thermal camera; c: laser speckle contrast imager; d: study bed (head up at 30 degrees); e: Philips Intellivue vital-sign monitor. Cameras were positioned to record full frame with larger dimension from thigh to knee of the right leg.

The BSP-ML Group transferred the data to the storage cluster using a secure portable hard drive.

4.8 Analysis methods overview

In this section, general analysis methodology used throughout this thesis is presented. Each results section in chapters 5 to 8 contains further methodology specific to the results presented in those chapters. Image analyses were performed using Matlab (R2020b). Members of the BSP-ML Group wrote the original code for processing video camera images and updated the software to apply to the MOLLIE study data.

4.8.1 Identification of periods of interest

Unless otherwise stated, the 'rest' period and 'peak' drug effect period are compared for each drug infusion session throughout the thesis. These two terms are used consistently throughout chapters 5 to 8. 'Rest' was defined as the 2-minute period between minutes 2 and 4 of the drug infusion sessions, during which participants were being recorded but no drugs were being infused (figure 4.1). This period was chosen to allow for the participants to settle into the experimental routine, and to avoid any movement noise associated with starting the infusion at t = 5 minutes (e.g., shadow effect from nearby movement). 'Peak' was defined as the 2-minute period between minutes 17 and 19 of each drug infusion session, during which the maximum rate of infusion was being administered. This period was chosen to avoid any noise from the preparation to stop drug infusion between minutes 19 and 20, but to allow as much time as possible for the maximum rate of drug infusion to have the desired clinical effect. Where a participant was unable to tolerate the drug infusion but was able to complete the session at a lower infusion rate, the same period (minutes 17 to 19) was used as the peak period.

4.8.2 Identification of region of interest (ROI)

4.8.2.1 RGB data

In sections where 'global' results are discussed (e.g., ROI_{GLOBAL}), the ROI was the anterior surface of the thigh of the right leg. The regions were selected manually over the thigh using the first RGB video frame of each session. The ROI consisted of the largest rectangle that could be fitted over the exposed skin captured on video images, leaving an edge of at least 20 pixels on all four sides to ensure that the entire ROI remained visible and only included skin throughout the experimental period (accounting for involuntary rotational or axial movements of the leg). The knee region was avoided due to the contour of the knee where a shadow cast by the patella was visible (example shown later in figure 6.8). An ROI tracking algorithm (customised for the MOLLIE data analysis by the BSP-ML Group) based on the

Kanade-Lucas-Tomasi (KLT) algorithm for feature tracking [222, 223]) was used to track the position and shape of the ROI throughout the experimental sessions.

4.8.2.2 Thermal data

In sections where 'global' results are discussed (chapter 7), the ROI was again the anterior thigh of the right leg. As with the RGB global ROI described in the previous section, the ROI for the thermal camera was manually selected over the anterior surface of the thigh using the first thermal video frame of each session. The ROI consisted of the largest rectangle that could be fitted over the exposed skin, leaving an edge of at least 10 pixels on all four sides to ensure that the ROI remained visible. A smaller number of pixels were left along the edge for thermal imaging compared to RGB data because of the smaller resolution of the image (640 x 512 versus 1280 x 960) captured by the thermal camera.

4.8.3 RGB multi-channel analysis

The RGB camera (PointGrey GS3-U3-51S5C-C) sensor uses a Bayer colour filter array with filter pattern consisting of half green, one quarter red, and one quarter blue ('GBRG' pattern). Raw data from each colour channel were analysed, leading to three single-channel images from every RGB image taken (matrices containing pixel intensity readings). Each colour channel provided images that were 25% of the size of the original images. This separation of RGB colour images to three separate colour channel images is referred to as 'debayering' and the images are referred to as 'debayered' images. This process is illustrated in figure 4.4.

4.8.4 Validity of frames included

Throughout the experimental period, the participants were asked to remain as still as possible. However, it was not possible to prevent all movement. The presence of

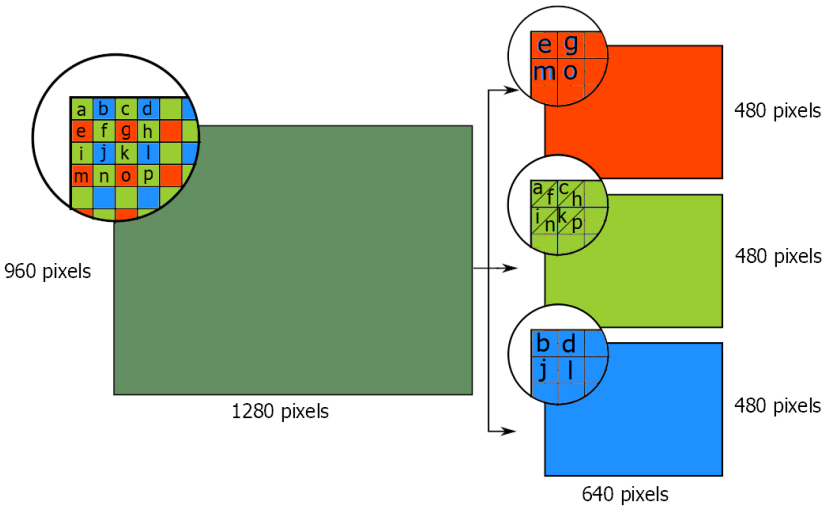


Figure 4.4: De-bayer image processing: The original RGB images are acquired at 1280x960 pixel resolution in the Bayer pixel pattern. The light intensities detected at each wavelength are gathered to form red/green/blue channel images, each of which is 25% of the original image size. For the green channel, two diagonally-positioned pixel intensities are averaged.

movement artefact in the video data was estimated using a proxy measurement. As well as performing feature tracking using the KLT algorithm [222, 223] described in section 4.8.2, estimates of the displacement of skin edges between consecutive frames [224] were used as an additional check for movement. Customised algorithms developed by the BSP-ML Group were used for this purpose. Outliers (defined in the algorithm as 2 standard deviations or more away from the mean) in eigen feature displacement was taken as an indication of large movement artefact. Any frames including these outlier features were excluded from analysis for both RGB and thermal imaging.

4.9 Data display and summary statistics

Throughout the results chapters, similar data display methods are used. In this section, the definitions used within the plots are defined.

4.9.1 Box and whisker plots

Box and whisker plots are used in results chapters 5 to 8. The following definitions were followed to produce the box and whisker plots:

- Central line in the box indicates the median;
- Bottom and top edges of the box indicate the 25th and 75th percentiles respectively;
- The whiskers extend to the most extreme data points not considered outliers. The standard Matlab definition of 'outliers' is used as following: greater than 1.5 x interquartile range away from the upper quartile, or less than 1.5 x interquartile range away from the lower quartile. In normally distributed data, the whisker is expected to include from 2.7 to 99.3 percent of the dataset.

Where the box and whisker plot included data from both phenylephrine and GTN sessions, grey indicated the phenylephrine session and white indicated the GTN session.

Where appropriate, the mean of the data set was marked using an x within the box and whisker plots.

4.10 Acquired dataset from the MOLLIE study

4.10.1 Participant demographics

Thirty participants were recruited. Summary demographics are given in table 4.7.

All study visits took place in November and December 2019. The effect of skin colour on the estimation of vital signs was not analysed due to the predominant representation of skin types I and II in our dataset (table 4.7) and limited participant numbers not powered for this analysis.

Table 4.7: Summary demographics of included participants

Age (years)	29 (25-34)*	
Sex (M/F)	16/14	
Weight (kg)	67 (56-75)*	
Height (cm)	171 (162-177)*	
BMI (kg.m-2)	21.7 (20.3-25.1)*	
Fitzpatrick	Type I	9
	Type II	10
	Type III	6
	Type IV	3
	Type V	2
	Type VI	0
Von Luschan	8 (7-10)*	

*Median (Interquartile range)

Two drug infusions were given to all 30 participants. Twenty-eight participants received and tolerated the full planned regimen of both infusions up to the highest level and stable infusion at the maximum dose. Two participants reported nausea and headache during the escalation phase of the GTN infusion at dose escalation levels 8 and 10. As stated in the protocol, the infusion rate was immediately reduced to the previous asymptomatic infusion rate - to levels 7 and 9 respectively - with resolution of the symptoms. These lower maximum tolerated rates were then continued as the stable maximum rate. As stated in the protocol [203] and section 4.5.1, the same timeline was kept for these cases, stopping infusion at t = 20 mins. Both participants consented to remain in the study and to have their data included in the final analysis; they completed the protocol time course using the highest tolerated infusion rates.

4.10.2 Evidence of drug effect

The participants received two standard regimen drug infusions with the doses determined by their actual weight (except where they weighed 70kg or above, where no further escalation in infusion rate was allowed as per safety review of the drug infusion protocol, described in section 4.5.1). Although each drug was expected to

have a similar physiological effect in different participants, the absolute degree of response to the infusion was expected to vary. Previous work has shown variable participant responses to set doses of phenylephrine and GTN [225, 226].

The following three elements were taken as evidence that the two infusions used in the MOLLIE study had the desired directional effect on skin perfusion.

4.10.2.1 Previous literature

Both phenylephrine and GTN are frequently utilised in experimental and clinical settings. Their mechanisms of action are well understood and their effects in healthy volunteers are well documented [227–231].

4.10.2.2 Macrodynamic effects

Macrodynamic responses to the two infusions are shown in figure 4.5. The two infusions caused an opposite effect response in three vital signs (HR, CO, BP). These are described below:

Heart rate At session A baseline, the median/IQR HR was 66 (57-70) beats per minute (bpm). During peak phenylephrine infusion, the median/IQR HR decreased by 15 (13-20) bpm. At session B baseline, the median/IQR HR was 62 (57-68) bpm. During peak GTN infusion, this increased by 14 (8-17) bpm.

Mean arterial pressure At session A baseline, the median/IQR MAP was 69 (63-76) mmHg. During peak phenylephrine infusion, the median/IQR MAP increased by 13 (7-20) mmHg. At session B baseline, the median/IQR MAP was 66 (62-71) mmHg. During peak GTN infusion, this decreased by 12 (6-18) mmHg.

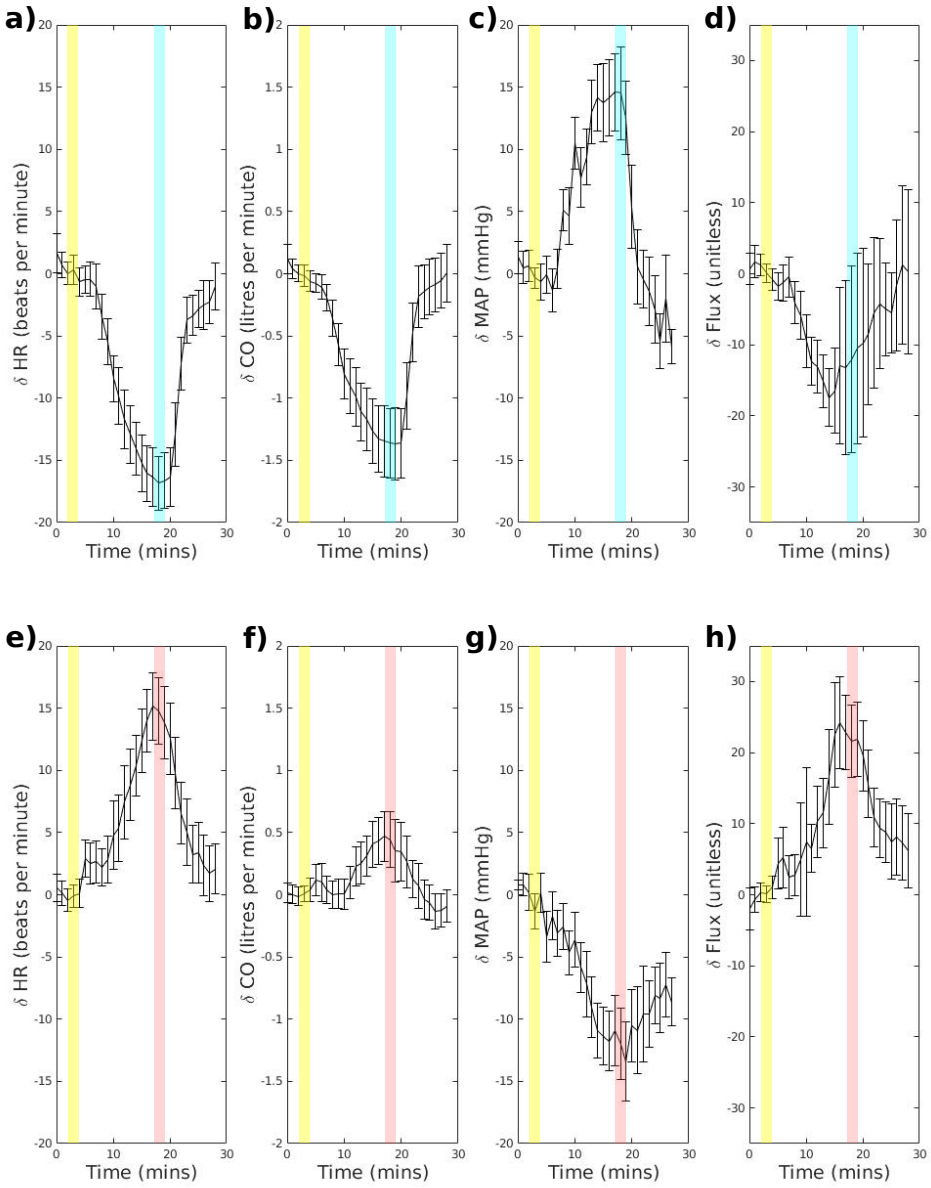


Figure 4.5: Changes in reference haemodynamic variables during the phenylephrine (a) - (d) and GTN (e) - (h) infusion protocol. For each minute of the experimental period, the mean deviation from the rest period is shown as a solid line with error bars indicating standard error of the mean. Heart rate: (a) and (e); mean arterial pressure: (b) and (f); cardiac output: (c) and (g); flux measured by laser speckle contrast imager: (d) and (h). The periods of interest are highlighted as follows: rest period from minutes 2 to 4 (yellow), peak phenylephrine effect from minutes 17 to 19 (blue), peak GTN effect from minutes 17 to 19 (pink).

Cardiac output At session A baseline, the median/IQR cardiac output was 5.7 (5.1-6.7) L.min^{-1}. During peak phenylephrine infusion, the median/IQR cardiac output decreased by 1.3 (0.7-1.6) L.min^{-1}. At session B baseline, the median/IQR cardiac output was 5.7 (5.1-6.5) L.min^{-1}. During peak GTN infusion, this increased by 0.3 (0.1-0.7) L.min^{-1}.

4.10.2.3 Microcirculatory effects

The LSCI monitor (described in section 4.6.2.3) tracked skin perfusion changes from the anterior thigh skin regions recorded with the two cameras. In addition to the macrohaemodynamic changes described in the previous section, opposite direction changes were observed using this reference skin perfusion monitor, as expected.

The median/IQR skin perfusion at rest in session A was 117.5 (103.2-145.3) flux units. At peak phenylephrine effect, this decreased by 14.0 (9.8-23.8) flux units. The median/IQR skin perfusion at rest in session B was 115.1 (97.0-128.4) flux units. At peak GTN effect, this increased by 17.8 (8.9-25.9) flux units (figure 4.5).

4.10.3 Camera data acquired

The following video sessions were obtained and analysed. This section describes the entire dataset analysed in the remainder of this thesis.

4.10.3.1 Phenylephrine infusion session

All 30 participants underwent the phenylephrine session uneventfully. From the session the following data was acquired:

- RGB: 30 x 28 minutes
- Thermal: 24 x 28 minutes, 6 x early termination due to camera overheat. All 6 sessions that were terminated early contain the initial rest and the drug

infusion periods but terminated during the 8-minute washout period.

4.10.3.2 GTN infusion session

28 participants underwent the GTN session uneventfully. Two participants developed side effects at levels 8 and 10. As per protocol, the infusion rates were lowered to the prior asymptomatic rate (levels 7 and 9) with resolution of symptoms at the reduced infusion rates. Both participants completed the sessions with lower dose of GTN infusion as maximum dose. The following data was acquired:

- RGB: 30 x 28 minutes
- Thermal: 26 x 28 minutes, 2 x early termination due to camera overheat. Both sessions contain the infusion periods but terminated early during the 8-minute washout period. 2 sessions failed to record due to thermal camera fan error.

4.10.3.3 Tourniquet release session

All 30 participants underwent the tourniquet session uneventfully. From the session the following data was acquired:

- RGB: 30 x 4 minutes
- Thermal: 29 x 4 minutes. 1 session failed to record due to thermal camera fan error.

4.11 Chapter summary

This chapter has covered the design of the MOLLIE study and the methodology used to acquire the dataset analysed and discussed in the following chapters. By giving two drug infusions with opposite physiological effects while controlling factors that are expected to affect camera data, I aimed to acquire an idealised dataset

of increased and decreased skin perfusion in the same individuals. In addition to the two drug infusions causing perfusion changes, the same participants underwent application and release of an arterial tourniquet to identify the locations of perforator vessels (described in section 1.2.2).

The study was designed to achieve controlled and safe range of increased and decreased skin perfusion states in healthy volunteers (as described in section 3.3). The two drug infusions were associated with expected macrovascular changes in opposite directions. The resulting changes from baseline were significant but not as deranged as we would expect to find in acutely haemodynamically compromised patients in critical care settings.

The aim of the thesis as stated in chapter 3 was to use video cameras to achieve both objectivity and improved sensitivity in skin perfusion monitoring compared to clinical assessment. The previous chapter showed that patients with documented evidence of skin mottling had worse outcome compared to patients without mottling, even when adjusted for severity of illness. Video camera diagnosis of skin mottling has not previously been described. Clinically used vasopressors are known to cause a reduction in skin perfusion [105, 117]. Given the usefulness of visually-detected skin mottling, it follows that measurement of skin mottling using video cameras may offer similar clinical insight in addition to the estimation of macrohaemodynamic parameters.

The next chapter further explores whether skin mottling which was considered as a binary - present or absent - clinical sign in chapter 2 can be quantified using video camera images.

5

Detection of skin mottling using non-contact image-based analysis

Contents

5.1 Introduction 85
5.1.1 Rationale for approach 86
5.1.2 Using the MOLLIE dataset to model skin mottling . . . 88
5.1.3 Hypothesis 89
5.2 Analysis methods 90
5.2.1 Selection of the region of interest for image processing . 90
5.2.2 Edge detection 91
5.2.3 Clinical assessment 94
5.2.4 Subgroup analysis using clinical labels 97
5.3 Results 98
5.3.1 Kirsch operator convolution 98
5.3.2 Clinical classification of skin mottling changes and subgroup analyses 101
5.4 Discussion 105
5.5 From visible to non-visible parameters 108

5.1 Introduction

In chapter 2, pooled data from three international databases showed an association between documented lower limb skin mottling and increased odds of ICU mortality,

hospital mortality, and increased ICU length of stay.

If clinically detected mottling carries prognostic value (chapter 2 and appendix A), an objective measurement and detection of mottling may allow earlier diagnosis and intervention. Although the human eye has a high number of receptors with theoretically high resolution [232], it is not an objective sensor. The human eye is highly developed as a sensor for visual processing (rather than accurate image capture), and is prone to biases [233]. A video camera-based detection method for skin mottling is proposed in this chapter, with a view to establishing direct correlates of the visual detection of skin mottling. Changes in these parameters from baseline to the periods corresponding to peak phenylephrine and GTN infusion (defined in section 4.8.1) are presented.

5.1.1 Rationale for approach

Each image from the RGB camera can be described as a 2D matrix capturing the amount of light reflected from the skin surface, which is then received by the corresponding location sensor in the camera. In image processing, a kernel (also referred to as a mask or a convolution matrix) is used to interact with the raw image matrix to change the image. The exact components of the kernel dictate the interaction's effect on the original image, which can include blurring, sharpening, and emphasising edges. Image processing by applying kernels to all individual pixels within the image is widely used in multiple medical settings to process the raw image data to improve the analysis or interpretation. Examples include the use of edge detection in retinal imaging [234], brain tumour detection [235], and lung computed tomography analysis [236].

In the detection of skin mottling, the challenge may be simplified to the detection of contrast (or the edge created at the point of maximal contrast) present on the skin surface. In this chapter, the term 'contrast' is used to mean the difference

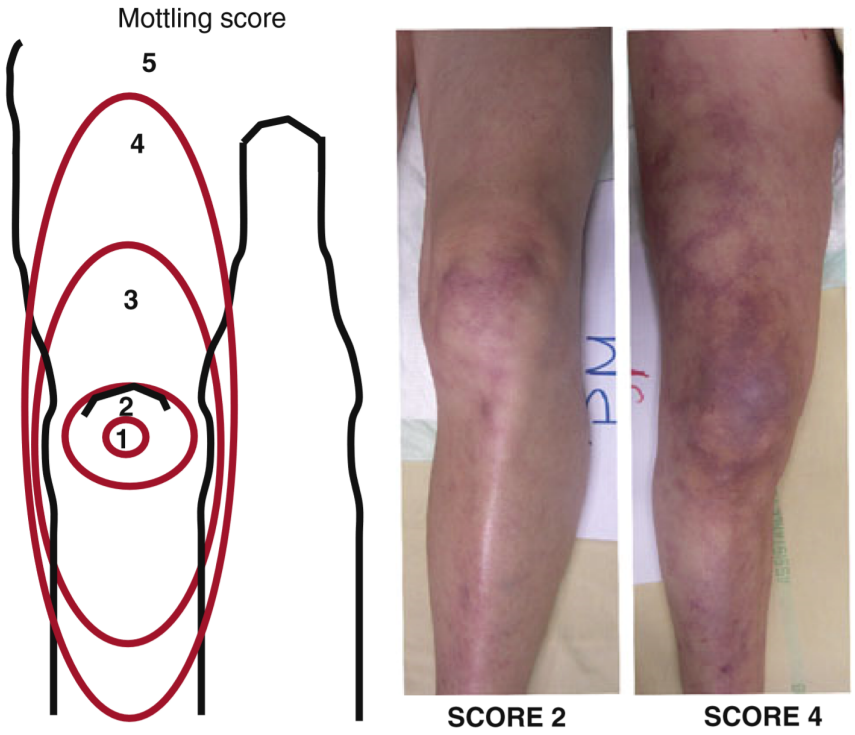


Figure 5.1: The mottling score is based on a mottling area extension on the legs. The score may range from 0 (no mottling) to 5 (severe mottling that goes beyond the fold of the groin). Two examples of mottling scores are shown on the right. Image from Ait-Oufella *et al.*, [11] with permission (appendix J).

between the reflected light intensity measured by a camera pixel against the eight neighbouring pixels surrounding it. Both the colour of the mottled lines (i.e., the contrast between the darker regions and the background skin between the linear streaks) and the anatomical extent of mottling (i.e., the size of the skin area affected) could indicate evolution or progression of skin mottling [101]. The extent/size of the mottled skin area centred around the knee has previously been proposed as a quantification tool ('the mottling score' [11], figure 5.1). The tool has been shown to have good inter-observer reproducibility (kappa 0.87, 95% CI (0.72-0.97)) despite relying on a subjective clinical assessment [11]. The severity of mottling according to the mottling score is associated with mortality in critically ill patients [144, 237]. Skin mottling may be quantifiable earlier and more objectively using an appropriate image convolution method to assess the amount of edges present within a set region of interest on the skin surface.

Previous work in video camera-based vital-sign monitoring (section 3.2) describes between-subject variations in the absolute light intensity measured from the skin surface. The factors affecting this signal can be categorised into subject-related factors (e.g., skin colour) or environmental factors (e.g., the light source, the interaction between the light and skin surface, shadows) [154, 161, 164]. This is further described in chapter 6. The same factors may also cause between-subject variation in the total amount of edges or contrast from a selected region of interest (ROI). In addition, the absolute baseline contrast of a skin region may also vary because of permanent skin features such as moles or scars (leading to the presence of permanent 'edges' in that region). Edges present due to these permanent features would be expected to remain stable under controlled lighting and movement. In contrast, any new appearance of skin mottling in response to the phenylephrine infusion (causing vasoconstriction) was expected to be associated with an increase in the total amount of edges within a given region when compared to baseline or resting state.

5.1.2 Using the MOLLIE dataset to model skin mottling

Based on the known mechanism of action of phenylephrine [105] and the side effect profile of clinically used vasopressors [117], the intravenous phenylephrine infusion used in the MOLLIE study was expected to induce (mild) skin mottling in the healthy participants. The effect of intravenous GTN on skin was more difficult to predict when it comes to mottling changes. Published studies on skin response to GTN frequently use the drug via transdermal delivery [238]. In the MOLLIE study, intravenous GTN was used instead for global haemodynamic effect without interacting directly with the region of monitored skin (section 4.5.1). Using a patch would have made direct camera measurement of the affected skin area impossible, as well as introduce potential confounding factors from skin reaction to a foreign body placed on the surface. Skin mottling is a sign of microvascular failure (section 1.2.3) [100–102], and GTN has been explored as a method of recruiting

the microcirculation by vasodilating the microvasculature in septic patients [239]. Therefore, GTN was expected to have grossly opposite changes to those induced by phenylephrine (although the mechanism of action is not directly opposite, as described in section 1.3.1). Although skin mottling was previously considered as a binary clinical sign that was either present or absent [101], the more recent evidence for mottling severity assessment [11, 115, 146] suggests that the clinical sign may be better considered as a continuous spectrum - one that becomes visually detectable above a threshold. The methodology presented in this chapter therefore assumed an opposite action of GTN compared to that of phenylephrine, making skin 'less mottled' compared to the baseline.

5.1.3 Hypothesis

I hypothesised that the peak phenylephrine infusion in the MOLLIE study would be associated with an increase in the total amount of edges within a pre-set skin ROI. The absolute baseline contrast in the lower limb images was expected to vary among the individuals for the reasons stated in section 5.1.1. On the other hand, any new skin mottling (due to phenylephrine-induced vasoconstriction) was expected to be associated with an increase in the amount of edges in the designated ROI from baseline. Conversely, I hypothesised that peak GTN infusion would be associated with a decrease in the amount of edges detected in a region due to vasodilation and increased perfusion in the microvasculature.

If mean contrast from a ROI measures correlates of the linear streaks visible to the human eye in skin mottling, the amount of increase and decrease in the total amount of edges within a designated ROI associated with phenylephrine and GTN infusions respectively would be expected to correlate with the *degree* of mottling change assessed by clinicians (and their visual assessment). Therefore, I expected a greater increase in the total amount of edges within an ROI in the subset of participants in whom mottling was visually detected in response to peak phenylephrine infusion.

Similarly, I expected a greater decrease in the total amount of edges within an ROI in participants in whom clinical changes were visually detected in response to peak GTN infusion.

5.2 Analysis methods

The RGB camera data from the MOLLIE study dataset described in chapter 4 was used in the following analysis. The analysis was performed using the RGB dataset as it most closely resembles the visual detection of skin mottling appearance used clinically (compared to thermal and laser speckle contrast imaging data).

5.2.1 Selection of the region of interest for image processing

Skin mottling is classically described as a phenomenon starting around the knee (figure 5.1) [11, 101]. However, the knee region is more contoured with variable depth across the surface compared to the thigh region (which is relatively flat). This makes the knee region more prone to movement and shadow artefacts (demonstrated in the images of the leg in figure 6.8 in the next chapter). The selection of a global ROI from the thigh was described in section 4.8.2. The largest rectangle that could be fitted was manually selected as the ROI, avoiding the contoured knee region and the associated shadow artefacts. These rectangular ROIs were labelled as $\mathrm{ROI}_{\mathrm{GLOBAL}}$, and the region was tracked using feature tracking as described in section 4.8.2. I also use these regions of interest in future chapters, referred to as $\mathrm{ROI}_{\mathrm{GLOBAL}}$.

The classical description of the spread or progression of mottling appearance from knee to thigh with worsening microvascular compromise [11, 101] suggests that similar underlying microvascular processes that occur at the knee leading to early mottling may also occur in the thigh regions at a latter/more severe point of haemodynamic deterioration. Although image analysis from the knee region may

$$\begin{bmatrix} 5 & 5 & -3 \\ 5 & 0 & -3 \\ -3 & -3 & -3 \end{bmatrix}$$
(a) North-west

$$\begin{bmatrix} 5 & 5 & 5 \\ -3 & 0 & -3 \\ -3 & -3 & -3 \end{bmatrix}$$
(b) North

$$\begin{bmatrix} -3 & 5 & 5 \\ -3 & 0 & 5 \\ -3 & -3 & -3 \end{bmatrix}$$
(c) North-east

$$\begin{bmatrix} -3 & -3 & 5 \\ -3 & 0 & 5 \\ -3 & -3 & 5 \end{bmatrix}$$
(d) East

$$\begin{bmatrix} -3 & -3 & -3 \\ -3 & 0 & 5 \\ -3 & 5 & 5 \end{bmatrix}$$
(e) South-east

$$\begin{bmatrix} -3 & -3 & -3 \\ -3 & 0 & -3 \\ 5 & 5 & 5 \end{bmatrix}$$
(f) South

$$\begin{bmatrix} -3 & -3 & -3 \\ 5 & 0 & -3 \\ 5 & 5 & -3 \end{bmatrix}$$
(g) South-west

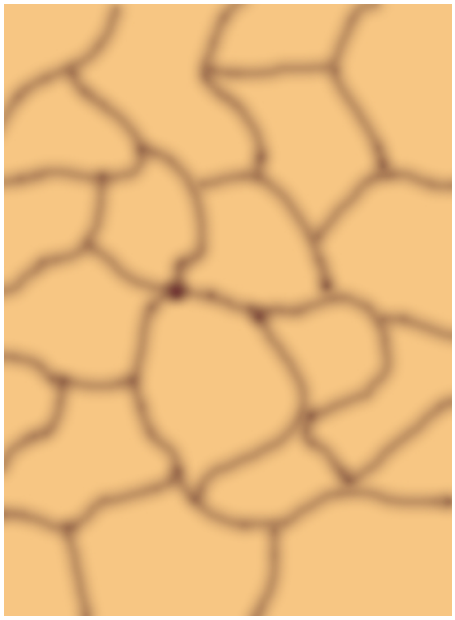
$$\begin{bmatrix} 5 & -3 & -3 \\ 5 & 0 & -3 \\ 5 & -3 & -3 \end{bmatrix}$$
(h) West

Figure 5.2: Kirsch edge detection kernel: These eight filters (a)-(h) are applied to the image matrix, taking each pixel of the original image in turn. The centre 0 of each filter (a)-(h) overlies the pixel being analysed, and the pixel intensity difference (contrast) between it and the neighbouring eight pixels are calculated using the multiplier represented by the -3s and 5s. All eight filters are applied to each pixel of the image, except the outermost pixels of the image where not all input values from the neighbouring pixels are available. The maximum value of the 8 kernel outputs is retained for the final image. The operator has the overall effect of finding and accentuating edges, looking in 8 compass directions as labelled. Also see figure 5.3.

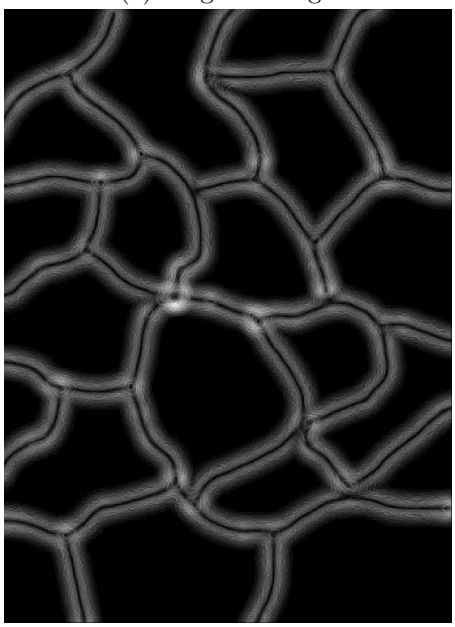
represent mottling changes better, the additional artefacts from the surface contours were expected to make the subsequent interpretation of camera image results from the MOLLIE study more difficult. On balance, an assumption was made that participants who develop knee mottling may also display subclinical changes in the ROI_{GLOBAL} that may not be apparent visually but could be identified using the image processing methods described below.

5.2.2 Edge detection

An edge detection algorithm was used to detect contrast within the skin ROI. Edge detection was performed using the Kirsch compass kernel algorithm which is available as open-source software [240] (figures 5.2 and 5.3). The kernel was designed to find the maximum edge strength (defined as the largest absolute difference in pixel intensity between a pixel and the eight neighbouring pixels) in multiple directions. This detector was selected based on its strong performance when the edges are not strictly linear [241]. De-bayered RGB images (described in section 4.8.3) were used. Kirsch compass kernel convolution was performed on all available pixels of the image, presented as a 2D matrix. The three colour channel data (red, green,



(a) Original image



(b) Post-convolution

Figure 5.3: Demonstration of Kirsch operator in practice. The original image (drawn to imitate skin mottling) is shown in (a). (b) shows a post-convolution image using the Kirsch operator as shown in figure 5.2. In (b), black indicates 0, and bright white indicates the largest value. Any areas of uniform colour in (a) are shown black in (b) as the contrast value calculated using the operator is 0 (no difference between the centre pixel and its 8 neighbouring pixels). This includes the centre of each of the lines in (a). In contrast, any edges where a contrast is present between a pixel and its neighbours are shown in white. Sharper contrast (e.g., the circular bright area, centre left) is shown in brighter white post convolution. As demonstrated, the strength of the Kirsch operator is its performance across the different directions in which the edge may appear.

and blue) were analysed separately.

For each image from the periods of interest (defined in section 4.8.1), the Kirsch operator was applied to the tracked $\text{ROI}_{\text{GLOBAL}}$ (defined in section 4.8.2), taking each pixel within the ROI in turn. The outermost edge rows and columns were exempt from the kernel application as the operator requires inputs from all 8 directions for each pixel (figure 5.2). Figure 5.3a was created for illustrative purposes, to demonstrate the application of the kernel and the resulting image highlighting edges. Figure 5.3b shows the output of the convolution kernel. The contrast was standardised across participants by dividing the magnitude of the Kirsch operator output for each pixel by the raw pixel intensity (i.e., measure the relative contrast between each pixel and its 8 neighbouring pixels). This step was included so that smaller magnitude contrast between neighbouring pixels could be detected in darker images. The total amount of edges within the image was estimated using the mean of the Kirsch operator output from the entire ROI ($\text{ROI}_{\text{GLOBAL}}$). This value was used as a surrogate measure of the total amount of 'contrast' present in each ROI frame. The mean was used instead of the sum of the kernel outputs to standardise across different ROI sizes.

For each participant, the two periods of interest were compared - the 'rest' and 'peak' periods (described in section 4.8.1) - from each drug infusion session. The mean Kirsch operator output from all pixels in the ROI was calculated for each image frame within the periods of interest. The mean of all 7200 frames in each 2-minute period of interest was taken as the mean Kirsch operator output. The two rest phase results (from the phenylephrine and GTN sessions) for each individual were compared using a paired t-test, with the null hypothesis that the mean contrast in a region of skin shall not significantly change across the two rest phases despite a small shift in leg positions between the two infusion sessions.

The mean change in Kirsch operator contrast values were tested for normality using the Kolmogorov-Smirnov test. The comparison between the rest and peak phenylephrine and GTN periods was made using the Wilcoxon sign-rank test.

5.2.3 Clinical assessment

In section 5.1.3, I stated that the increase and decrease in contrast (measured as the change in the mean Kirsch operator contrast described in section 5.2.2) was expected to be related to visible changes in the skin when the corresponding parameter is being measured using video camera data. Detection of skin mottling using the mean contrast method would be supported by increased contrast detection in participants who were classified as 'mottled' by clinicians in comparison to those who were 'not mottled'. This hypothesis was tested using subgroup analyses. The subgroups were determined based on clinical assessment from multiple clinicians, performed as following.

For each drug session from each participant, paired image sets were created with one image taken at t = 3 minutes (half way through the 'rest' period defined in section 4.8.1) and one image taken at t = 18 minutes (half way through the 'peak' period defined in section 4.8.1). Each image was labelled using the participant number and a 4 digit code. The code label was used to blind the assessor on whether the session image was from phenylephrine/GTN, or rest/peak period. The paired images from each session were then presented sequentially, but with randomised order (either rest period image first or peak infusion period image first).

Two critical care clinicians not familiar with the MOLLIE dataset were invited to review the paired images. As the MOLLIE study design only allowed limited changes in global haemodynamics for participant safety (up to 30% variation in HR or MAP allowed, described in section 4.5.1) and the participants remained well

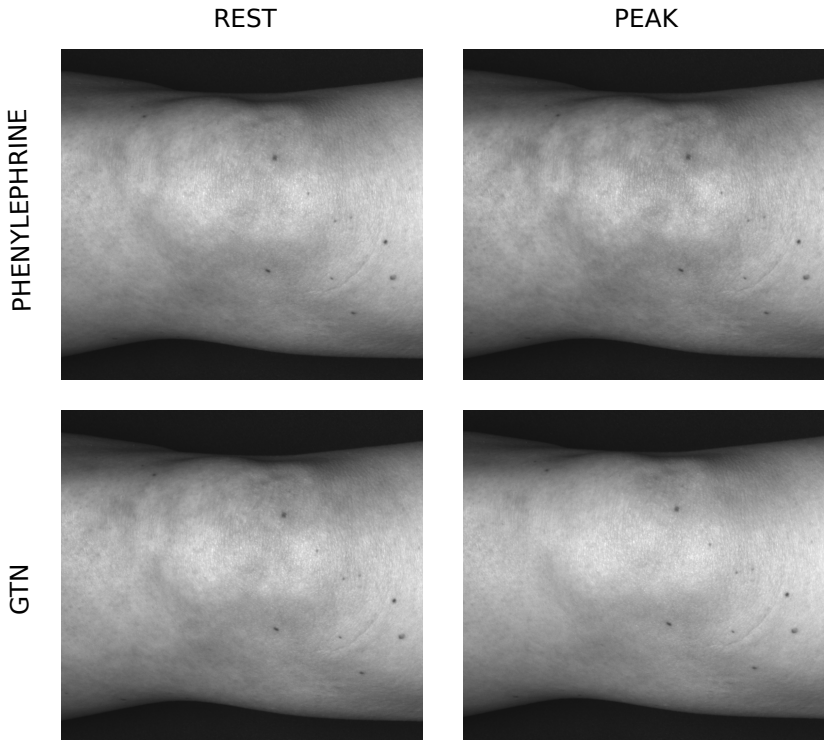


Figure 5.4: Example of skin mottling from the MOLLIE dataset: The four images are taken from one participant's phenylephrine and GTN sessions. The two images on the left are taken during rest, while the two images on the right are from the peak drug infusion duration. The top row images are from the phenylephrine infusion session, while the bottom row images are from the GTN session. Maximum mottling appearance seen around the knee (top right); less prominent net-like bruising over the knee during rest (top left and bottom left); improved appearance during peak GTN infusion (bottom right).

throughout, severe mottling as encountered in critical care settings was not expected to be found in the MOLLIE dataset. The mottling score (section 5.1.1, figure 5.1) was originally designed for use in critical care and incorporates very severe mottling (scores of 4 and 5) [11]. This scale was not used for the clinical assessment in this dataset, as the majority of the severity range the mottling score assessment tool was originally developed to capture was not expected to be present in the MOLLIE dataset. Instead, a binary classification of 'mottled' or 'not mottled' was used.

Originally, I had planned to assess the phenylephrine infusion sessions only and

compare two subgroups: the group for which the participants develop skin mottling (determined visually by clinicians), and a group of participants without skin changes. The paired images from the GTN sessions were originally generated as a control set for the phenylephrine images. However, a review of the images revealed that some participants had a rest state skin appearance consistent with mottling when compared to the corresponding peak GTN infusion images. As described in section 5.1.2, there is some evidence to suggest that GTN may induce opposite changes to phenylephrine by improving microcirculatory flow. Therefore, *post-hoc* changes were made to this clinical skin image diagnosis methodology to assess GTN sessions for a 'disappearance of mottling changes' (opposite direction change from the phenylephrine session). An example leading to the addition of this *post-hoc* analysis is shown in figure 5.4.

For each paired image, the clinicians were asked to review the images for changes between the two images that they would classify/diagnose as skin mottling. If such a difference existed, the assessors were asked to indicate which of the two images contained visible mottling changes. The two clinicians reviewed the images at two different time points without consulting each other. Where there was disagreement between the two assessors, a third critical care clinician reviewed the images and their assessment outcome was used. The two (or three) assessors reviewed the paired images for a relative assessment, rather than considering individual images for skin mottling. This method was used as the mild degree of skin change may otherwise be difficult to appreciate without context/a comparator image.

The assessors performed the binary classification (mottled or not mottled) using the whole leg image (including the $\mathrm{ROI}_{\mathrm{GLOBAL}}$ and the knee) rather than limited to the $\mathrm{ROI}_{\mathrm{GLOBAL}}$ alone for several reasons. The edge detection algorithm was applied to $\mathrm{ROI}_{\mathrm{GLOBAL}}$ (rather than the knee) for the reasons cited in section 5.2.1. However, only a mild degree of mottling changes was expected to occur in the MOLLIE study

dataset based on the limited dose of drugs given and the limited haemodynamic variation allowed using the drug infusion because of participant safety (4.5.1). Based on the traditional description of skin mottling evolution [101] and the mottling score [11], the visible mottling changes (identifiable using clinician vision) were expected to be limited to the knee, rather than extend to the thigh. Limiting the visual classification to only ROI_{GLOBAL} was expected to lead to very few sessions being labelled as 'mottling'. In the introductory section of this chapter (section 5.1.3), I hypothesised a relationship between skin mottling in the *participants* (rather than in the same skin area) and the objectively assessed mottling (section 5.2.2). This hypothesis was based on whether any 'subclinical' mottling changes in the thigh (anticipated to be present in participants with knee mottling) may be detected as changes in the mean kirsch operator contrast.

Based on the clinical assessments by the two (or three) assessors who had no knowledge of the drug infusion given, I created two subgroups for phenylephrine session data and two subgroups for GTN session data. The phenylephrine sessions were split into those for which the participants developed mottling in response to phenylephrine (rest session determined 'not mottled', peak session determined 'mottled'), and into those for which the participants did not. They were labelled as 'new mottling' and 'no change' subgroups respectively. Following the hypothesis presented in section 5.1.3, the GTN sessions were similarly split into subgroups for which the participants had reverse changes (rest session determined 'mottled', peak session determined 'not mottled') and those for which the participants did not. They were labelled as 'less mottling' and 'no change' groups respectively.

5.2.4 Subgroup analysis using clinical labels

Cohen's kappa coefficient was used to assess the agreement between the two clinicians. The mean Kirsch operator contrasts for the subgroups were compared using the Wilcoxon rank sum test. This non-parametric test was chosen because of the smaller,

potentially unequal sample size in the two groups following subgroup classification.

Any participants who were in both the 'new mottling' subgroup in the phenylephrine session and the 'less mottling' subgroup in the GTN session would have had labels of 'not mottled' in phenylephrine rest session and 'mottled' in GTN rest session. These participants' mean Kirsch operator contrast from their two rest periods were further compared using the Wilcoxon rank sum test. This was performed to assess whether an objective difference existed between the images recorded during the two rest periods for the participants for whom the clinical assessors had judged the GTN rest period images to be mottled.

5.3 Results

5.3.1 Kirsch operator convolution

The changes in mean Kirsch operator contrast across the 30 participants were not normally distributed (Kolmogorov-Smirnov test $p < 0.0001$ in both phenylephrine and GTN sessions).

There was no significant difference between the rest period mean Kirsch operator contrast in phenylephrine session and the corresponding contrast in GTN session rest period (figure 5.5).

Table 5.1 shows the rest period mean Kirsch operator output, the peak period mean Kirsch operator output, and the absolute and relative changes for each of the three colour channels. Phenylephrine infusion was associated with a significant increase in mean Kirsch operator output in all three colour channels, with the greatest relative and absolute changes observed in the red and blue wavelengths. Conversely, GTN infusion was associated with a significant decrease in mean Kirsch operator

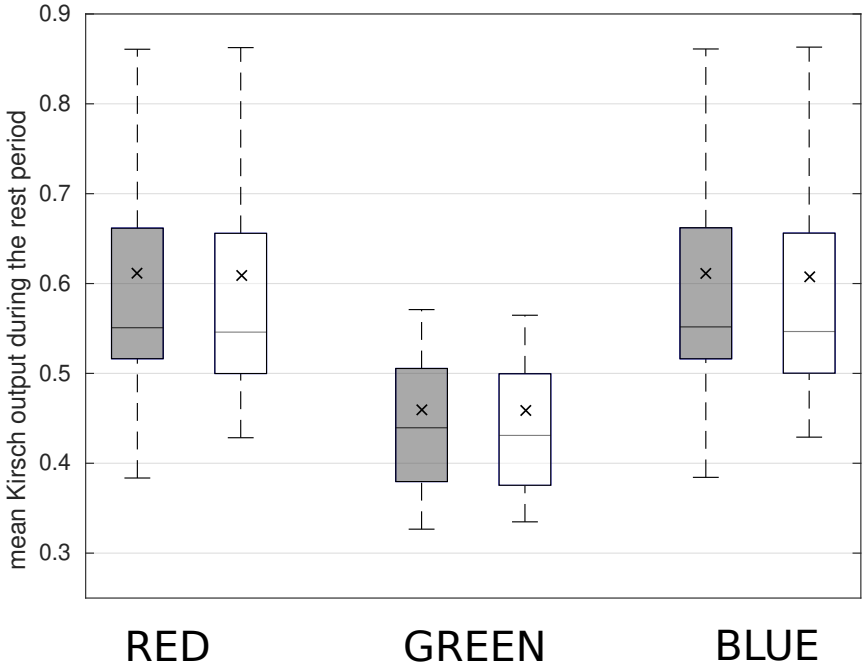


Figure 5.5: Baseline Kirsch operator contrast. Results from all 30 participants. Across the three colour channels, the rest period mean Kirsch contrast operator was compared for phenylephrine sessions (grey) and GTN sessions (white). The box and whisker plot components were defined in section 4.9.1. x within each box indicates the population mean. No significant differences were found for the rest periods between the two drug sessions within each colour channel. Difference between the two rest periods for each channel: red 0.0049 ($p = 0.18$); green 0.0085 ($p = 0.18$); blue 0.0051 ($p = 0.22$).

output in all three colour channels. The greatest relative and absolute changes were observed in the red and blue wavelengths.

A summary of the mean Kirsch output changes in all 30 participants is shown in figure 5.6.

Table 5.1: Summary mean Kirsch output changes

Phenylephrine				
	Rest (SD)	Peak (SD)	Absolute change (95% CI)	Percentage change (%)
Red	0.614 (0.21)	0.626 (0.21)	+0.012 (0.0067, 0.017)	+2.0
Green	0.459 (0.13)	0.465 (0.12)	+0.006 (0.0029, 0.0085)	+1.2
Blue	0.614 (0.21)	0.626 (0.21)	+0.012 (0.0070, 0.017)	+2.0
Glyceryl trinitrate (GTN)				
	Rest (SD)	Peak (SD)	Absolute change (95% CI)	Percentage change (%)
Red	0.611 (0.21)	0.604 (0.21)	-0.0071 (-0.010, -0.0041)	-1.2
Green	0.456 (0.13)	0.453 (0.13)	-0.0029 (-0.0043, -0.0015)	-0.6
Blue	0.611 (0.21)	0.604 (0.21)	-0.0072 (-0.010, -0.0043)	-1.2

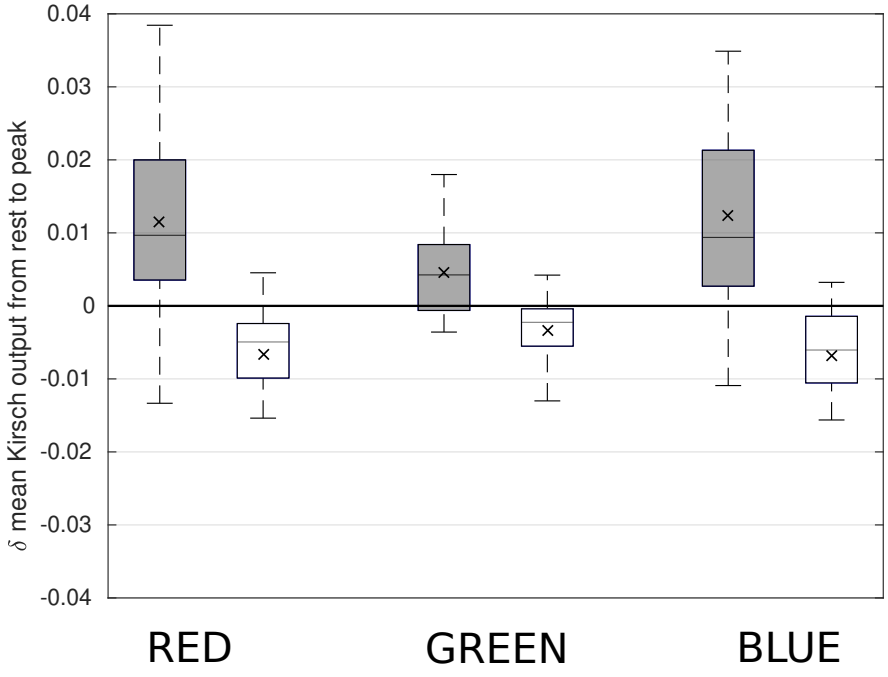


Figure 5.6: Changes in mean contrast to reflect mottling. Results from all 30 participants. δ in y axis label represents 'change in'. Across all three colour channels, vasoconstriction induced by phenylephrine (grey) was associated with an increase in the mean contrast in the thigh skin region of interest. Conversely, vasodilation induced by GTN (white) was associated with a decrease in the mean contrast in the thigh region of interest. The largest relative change was seen in the red and blue channels.

5.3.2 Clinical classification of skin mottling changes and subgroup analyses

5.3.2.1 Phenylephrine sessions

Both assessors labelled 11 phenylephrine sessions as 'not mottled' in the rest period and 'mottled' in the peak period. The 11 sessions were assigned to the 'new mottling' subgroup. 6 sessions were labelled as 'not mottled' in the rest period and 'mottled' in the peak period by one of the two assessors. One of these sessions was subsequently categorised as belonging to the 'new mottling' group following a third assessor review. 13 sessions were labelled as 'not mottled' by both assessors. The Cohen's kappa coefficient for the main two assessors was 0.60. The full clinical assessments are shown in table 5.2.

The differences between the subgroups for each colour channel are shown in figure 5.7a and reported in table 5.4.

5.3.2.2 GTN sessions

Both assessors labelled 16 GTN sessions as 'mottled' in the rest period and 'not mottled' in the peak period. The 16 sessions were assigned to the 'less mottling' subgroup. 7 sessions were labelled as 'mottled' in the rest period and 'not mottled' in the peak period by one of the two assessors. One of these sessions was subsequently categorised as belonging to the 'less mottling' subgroup following a third assessor review. 7 sessions were labelled as 'not mottled' by both assessors. The Cohen's kappa coefficient for the main two assessors was 0.49. The full clinical assessments are shown in table 5.3.

The differences between the subgroups for each colour channel are shown in figure 5.7b and reported in table 5.4.

Table 5.2: Phenylephrine session clinical mottling assessment

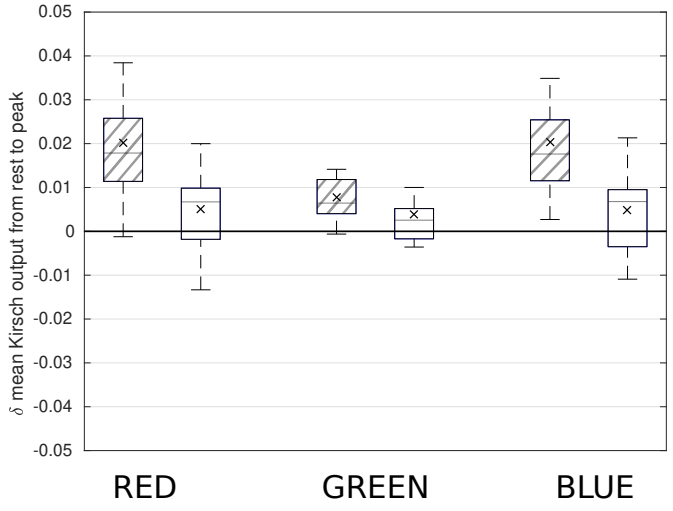
Part. no.	Assessor 1		Assessor 2		Assessor 3 (if needed)		Group (M/ NC)
	Rest	Peak	Rest	Peak	Rest	Peak	
1	NC	NC	NC	NC			NC
2	NC	NC	NC	NC			NC
3	NC	NC	NC	NC			NC
4	NC	NC	NC	NC			NC
5	NC	NC	NC	NC			NC
6	NC	NC	Unmottled	Mottled	Unmottled	Mottled	M
7	NC	NC	NC	NC			NC
8	NC	NC	NC	NC			NC
9	Unmottled	Mottled	NC	NC	NC	NC	NC
10	NC	NC	NC	NC			NC
11	NC	NC	NC	NC			NC
12	Unmottled	Mottled	Unmottled	Mottled			M
13	Unmottled	Mottled	Unmottled	Mottled			M
14	NC	NC	NC	NC			NC
15	Unmottled	Mottled	Unmottled	Mottled			M
16	Unmottled	Mottled	NC	NC	NC	NC	NC
17	Unmottled	Mottled	Unmottled	Mottled			M
18	NC	NC	NC	NC			NC
19	Unmottled	Mottled	Unmottled	Mottled			M
20	Unmottled	Mottled	Unmottled	Mottled			M
21	Unmottled	Mottled	Unmottled	Mottled			M
22	Unmottled	Mottled	Unmottled	Mottled			M
23	NC	NC	NC	NC			NC
24	NC	NC	Unmottled	Mottled	NC	NC	NC
25	NC	NC	Unmottled	Mottled	NC	NC	NC
26	Unmottled	Mottled	Unmottled	Mottled			M
27	NC	NC	NC	NC			NC
28	Unmottled	Mottled	NC	NC	NC	NC	NC
29	Unmottled	Mottled	Unmottled	Mottled			M
30	Unmottled	Mottled	Unmottled	Mottled			M

NC = 'No change'.
Groups: M = 'New mottling' subgroup; NC = 'No change' subgroup.

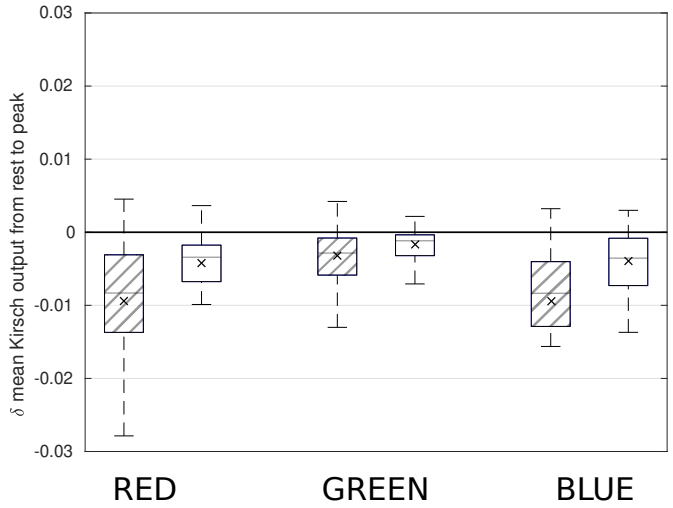
Table 5.3: GTN session clinical mottling assessment

Part. no.	Assessor 1		Assessor 2		Assessor 3 (if needed)		Group (M/ NC)
	Rest	Peak	Rest	Peak	Rest	Peak	
1	Mottled	Unmottled	Mottled	Unmottled			M
2	NC	NC	NC	NC			NC
3	NC	NC	NC	NC			NC
4	Mottled	Unmottled	NC	NC	NC	NC	NC
5	Mottled	Unmottled	Mottled	Unmottled			M
6	Mottled	Unmottled	Mottled	Unmottled			M
7	Mottled	Unmottled	Mottled	Unmottled			M
8	NC	NC	Mottled	Unmottled	NC	NC	NC
9	Mottled	Unmottled	Mottled	Unmottled			M
10	NC	NC	Mottled	Unmottled	NC	NC	NC
11	Mottled	Unmottled	Mottled	Unmottled			M
12	Mottled	Unmottled	NC	NC			NC
13	NC	NC	NC	NC			NC
14	Mottled	Unmottled	NC	NC	Mottled	Unmottled	M
15	NC	NC	Mottled	Unmottled	NC	NC	NC
16	NC	NC	NC	NC			NC
17	Mottled	Unmottled	Mottled	Unmottled			M
18	Mottled	Unmottled	Mottled	Unmottled			M
19	Mottled	Unmottled	Mottled	Unmottled			M
20	Mottled	Unmottled	Mottled	Unmottled			M
21	NC	NC	Mottled	Unmottled	NC	NC	NC
22	NC	NC	NC	NC			NC
23	Mottled	Unmottled	Mottled	Unmottled			M
24	NC	NC	NC	NC			NC
25	Mottled	Unmottled	Mottled	Unmottled			M
26	Mottled	Unmottled	Mottled	Unmottled			M
27	Mottled	Unmottled	Mottled	Unmottled			M
28	NC	NC	NC	NC			NC
29	Mottled	Unmottled	Mottled	Unmottled			M
30	Mottled	Unmottled	Mottled	Unmottled			M

NC = 'No change'.
Groups: M = 'Less mottling' subgroup; NC = 'No change' subgroup.



(a) Phenylephrine session subgroups



(b) GTN session subgroups

Figure 5.7: Subgroup analysis according to clinical observations. The changes in mean Kirsch output from baseline (measured during the rest period) to peak drug effect period. δ in y axis labels represents 'change in'. (a) shows changes associated with phenylephrine infusion, while (b) shows changes associated with GTN infusion. Each panel shows results from the three colour channels (red, green, blue) in turn. Hatched box and whisker plots show subgroups visually determined to have mottling changes as agreed by the two (or three) clinical assessors. In (a), this represents the subgroup of 12 sessions judged to show a change (increase in mottling with respect to the rest period). The clear boxes represent the subgroup of 18 sessions judged to have no change. In (b), the hatched boxes represent the 17 sessions judged to show a change (decrease in mottling with respect to the rest period), while the clear boxes represent the subgroup of 13 sessions judged to show no change. This is explained in section 5.2.3. The significance of the difference between the subgroups is also reported in table 5.4.

Table 5.4: Summary RGB video camera ROI_{GLOBAL}: change in mean Kirsch contrast from 'rest' to 'peak' period

	Phenylephrine			GTN		
	New mottling	No change	Difference (p value*)	Less mottling	No change	Difference (p value*)
Red	+0.0179	+0.0067	0.0112 (0.004)	-0.0083	-0.0034	0.0049 (0.10)
Green	+0.0064	+0.0025	0.0039 (0.036)	-0.0028	-0.0012	0.0016 (0.26)
Blue	+0.0176	+0.0068	0.0108 (0.0033)	-0.0083	-0.0035	0.0048 (0.079)

*Reports p values from Wilcoxon rank sum test

5.3.2.3 Comparison between the two rest periods

The detailed individual assessor results are given in tables 5.2 and 5.3.

Of the 12 participants assigned to the 'new mottling' group following phenylephrine session review (section 5.3.2.1), 7 were also in the 'less mottling' group from the GTN session review. There were no significant differences between the mean Kirsch operator contrast from their phenylephrine and GTN rest period images. For the red/green/blue channels, the differences were 0.0031 ($p = 0.80$), 0.0040 ($p = 0.98$), and 0.0029 ($p = 0.80$) respectively.

5.4 Discussion

There are two key findings of interest presented in this chapter.

1. **Objective skin mottling assessment:** In this chapter, a potential method of quantifying skin surface changes using video camera images was proposed. A simple edge detection image processing method was applied to skin regions of the thigh. A significant increase in the mean 'contrast' was observed for the ROI_{GLOBAL} with phenylephrine infusion, and a decrease in the same parameter was observed with GTN infusion. These changes were detected from ROI_{GLOBAL}, rather than the knee where skin mottling is typically described to develop first. While these results suggest that there may be an association

between contrast/edges present in skin images and clinical mottling, it is not possible to prove that it is strictly the mottling appearance that is being quantified. The subgroup analyses presented in section 5.3.2 further support the mean contrast method. There was a significantly greater increase in mean Kirsch operator output in the 12 participants who had clinician-determined new mottling in comparison to the 18 participants in whom no new mottling was detected visually. This was the case across all three colour channels (table 5.4). In the GTN sessions, there was a greater decrease in mean Kirsch operator output in the 17 participants who had clinician-determined reduction in mottling appearance in comparison to the 13 participants who did not (table 5.4) across all three colour channels, although the differences were not statistically significant. Even in the participants in whom no changes were observed by the clinicians, the direction of change in mean Kirsch operator output was the same: an increase associated with phenylephrine and a decrease associated with GTN (figure 5.7). These changes may represent subclinical or pre-mottling changes and may be a useful clinical signal to be explored.

2. **Skin mottling physiology:** Figure 5.5 showed that there were no significant differences between the mean Kirsch operator output during the rest period in phenylephrine and GTN sessions. The rest sessions compared the same anatomical areas (ROI_{GLOBAL}), but were recorded at two different time points and movement was allowed between the two sessions (see section 4.4). From the dataset, 7 participants were assigned into the 'new mottling' subgroup in the phenylephrine sessions and the 'less mottling' subgroup in the GTN sessions. As described in section 5.2.3, the two rest periods from these two individuals were differently labelled ('unmottled' in phenylephrine rest period and 'mottled' in GTN rest period). There were no statistical differences between the Kirsch operator contrast between the rest periods in these 7 participants (section 5.3.2.3).

All participants received phenylephrine first followed by GTN (as described in section 4.4). Therefore, it is possible that more participants had skin mottling during the GTN rest period as it always followed the phenylephrine infusion. However, there were no statistical differences between the objectively assessed edges/contrasts using the mean Kirsch operator contrast. In addition, the participants' HR, MAP, CO, and perfusion according to the LSCI monitor had all recovered to their pre-phenylephrine infusion baseline values as presented in section 4.10.2.

I propose that these results show both the subjective nature of a visual skin mottling assessment (different labelling based on visual assessment across the two rest periods depending on the comparator image), and a continuous spectrum of skin 'mottling'. 17 participants who had normal range vital signs and had not been given any drug infusions at the time (sections 4.4, 4.5.1, and 4.8.1, figure 4.1) were labelled as having skin mottling during the rest period of their GTN infusion session.

Skin mottling detection using visible spectrum cameras has not previously been reported. Ferraris *et al.*, [115] demonstrated that the presence of any degree of lower limb skin mottling in 46 critical care patients was associated with lower skin temperature, measured using a thermal camera. However, there was no correlation between the mottling score and the skin temperature. There are several possible reasons why their study did not demonstrate an association. The study estimated an average temperature for each of the mottling zones (figure 5.1). Non-uniformity in surface temperature (measured using infrared thermography) is discussed in chapter 7. This is not taken into consideration in a mottling zone classification that relies on surface anatomy. The mean skin temperature estimates in the Ferraris *et al.*, [115] study based on the five mottling zones may be inaccurate as the perforator locations were not taken into account.

5.5 From visible to non-visible parameters

The methods in this chapter use simple image processing techniques to quantify clinically visible examination findings. The application of Kirsch operator convolution is computationally simple and can easily be implemented in real-time. The standardised mean contrast values during the rest periods were consistent for each individual across the two drug infusion sessions despite changes in participant position and shadow, suggesting that they are robust to small changes in these.

This chapter explored measuring direct correlates of visually detected clinical findings using video cameras. As mentioned in the introductory section, video camera monitoring offers both objectivity and greater sensitivity to change compared to direct human vision. The next chapter explores how the pulsatile changes measured by photoplethysmographic imaging (introduced in section 3.2.3) respond to pharmacologically-induced vasoconstriction and vasodilation through the infusion of phenylephrine and GTN described in chapter 4.

6

Detection of skin perfusion changes using photoplethysmographic imaging

Contents

6.1 Introduction 109
6.1.1 Aims and hypotheses of this chapter 112
6.2 Analysis methods 114
6.2.1 AC amplitude 115
6.2.2 DC component 117
6.2.3 Hue, saturation, value (HSV) 118
6.3 Statistical methods 120
6.4 Results 121
6.4.1 Change in pulsatile PPGi waveform amplitude (AC) . . 121
6.4.2 Change in the DC component of PPGi 126
6.4.3 Skin colour changes (hue and saturation) 127
6.5 Chapter summary 129

6.1 Introduction

In chapters 1 and 2, I evidenced why monitoring skin perfusion is clinically useful (section 1.1.3) and explained the cardiovascular changes during systole and diastole that lead to both contact (cPPG, section 3.2.2) and imaging photoplethysmographic (PPGi) waveforms (section 3.2.3). The primary clinical use of cPPG is in monitoring

peripheral arterial oxygen saturation (SpO_2) [242]. However, increasingly PPG has found an additional role in cardiovascular assessments [165]. There are several attractions of exploring the use of PPG waveforms in cardiovascular monitoring. Pulse oximetry is already routine in clinical monitoring. It is economical, non-invasive, and simple [243]. The cPPG waveform morphology is known to vary according to the underlying systemic haemodynamic status [243, 244].

The PPG waveform is composed of a fluctuating component (the alternating current, 'AC' component) superimposed on a baseline non-fluctuating component (the direct current, 'DC' component) [168]. In transmittance mode, the AC component makes up a smaller proportion of the absorption of the light from the red and infra-red light-emitting diodes (LEDs) transmitted through the body segment, for example the finger. This component is pulsatile in nature, in time with the cardiac cycle. The changes represent the volume of blood in the arterial circulation of the body segment that fluctuates with each heart beat. The DC component results from all other tissues that lie in the path of the light, representing the overwhelming proportion of light absorption (>99%). In pulse oximetry, this component is often used to calibrate the signal, with the pulsatile (AC) component at the two wavelengths being subsequently analysed to derive the SpO_2 estimate [245, 246]. In contact pulse oximetry, both the light sources and the light sensor are in contact with the skin and are encased in a finger probe unit or a clip. An automatic gain control circuit is used to adjust the light intensity provided by the LED according to the size of the body segment (typically the finger) through which the light is transmitted (and to a lesser extent the colour of the skin) [245]. The gain control mechanism also standardises the amplitude of the pulsatile component of the PPG waveform and enables optional waveform shape assessment [165]. The amplitude of the pulsatile waveform is known to indicate perfusion pressure of the region where the pulse oximeter probe is worn [165, 168, 243].

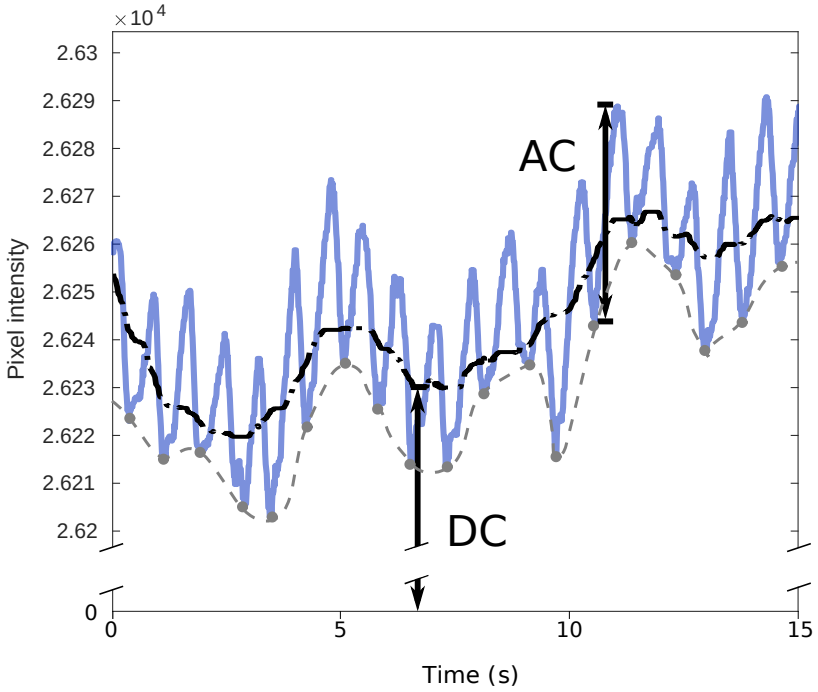


Figure 6.1: DC and AC components of photoplethysmography imaging (PPGi) waveform, using example data from the study. The AC component amplitude is the peak-to-trough amplitude of the pulsatile AC waveform, taken from a trough to the next peak as demonstrated (labelled 'AC'). There are two definitions of the DC component commonly used in the literature - the mean value of the overall waveform may be computed (black dash-dotted line, labelled 'DC'), or the baseline of the pulsatile waveform (grey dashed line) may also be computed using a trough detection algorithm. The mean pixel intensity was used as the DC component in the MOLLIE study, corresponding to the first definition. There is very little difference in practice between the two definitions, as the AC component amplitude is of the order of 0.1% of the DC component, as shown here. The lighting was controlled and movement constrained in the MOLLIE study experimental design to minimise the environmental effect on the DC component. Figure reproduced from Harford *et al.*, [247].

In contrast to cPPG, the light source in PPGi is not in contact with the skin (section 3.2.3). Studies use either a dedicated light source of known or controlled wavelength or use constant ambient lighting [161]. Non-contact video cameras act as the light sensor. The main strength of this non-contact system is that the set-up does not affect the very signal being acquired. Any haemodynamic information in the AC and DC components is unaffected by pressure exerted by the sensor itself. In addition, it does not constrain physical activities for the subject being monitored [154], and avoids complications associated with the contact nature such as infection

control [193].

In this chapter, the analysis of PPGi from the MOLLIE study is presented, framing the results in terms of traditionally recognised cPPG terminology (the AC and DC components). The effect of drug-induced vasoconstriction and vasodilation on the PPGi waveform baseline (DC component) and the cardio-synchronous fluctuations (AC component) are analysed separately. As demonstrated in figure 6.1, there are two common definitions of the DC component of the PPG waveform used in the literature. In some of the PPG literature, the DC component is defined as the mean of the pulsatile waveform (labelled 'DC' in figure 6.1) [248, 249]. This measurement is conceptually similar to the mean arterial pressure (MAP) of an arterial blood pressure waveform. Alternatively, the DC component may be defined as the baseline of the pulsatile waveform (grey line in figure 6.1) [168, 250]. In the analysis presented in the current chapter, the former definition is adapted and this parameter is referred to as the 'DC component' from this point onwards.

6.1.1 Aims and hypotheses of this chapter

As discussed in section 3.3, the MOLLIE study was designed to create a multiple imaging modality (RGB and thermal) dataset whilst minimising the impact of environmental noise. The overall aim of the current chapter is to compare any PPGi waveform changes associated with one infusion with respect to changes during the other infusion, which are expected to have the opposite effect (section 4.5.1). The evidence for opposite clinical effects induced by the two drugs was given in section 4.10.2 and demonstrated in figure 4.5. Several PPG waveform parameters are recognised in the literature [165]. In the analyses to be presented in this chapter, the metrics are limited to the peak-to-trough amplitude of the AC component (labelled 'AC' in figure 6.1) and the DC component (labelled 'DC' in figure 6.1), to follow the AC and DC terminology used in the description of PPG waveforms in

the scientific literature [165].

In section 1.4.2.1, laser speckle contrast imaging (LSCI) was introduced as an objective skin perfusion monitor. Further technical specifications were described in section 4.6.2.3. Figure 4.5 showed that LSCI-measured skin perfusion decreased in response to phenylephrine and increased in response to GTN. In addition to describing the changes in the AC and DC components of the PPGi waveform as described in the previous paragraph, this chapter presents the correlation between these changes and the changes in skin perfusion measured by the LSCI monitor between the rest and peak drug effect periods (as defined in section 4.8.1).

Light intensity changes in any one of the single colour channels of the RGB camera reflect the changes over a narrow bandwidth centred on the channel wavelength (figure 4.2), rather than skin *colour* changes. However, skin colour (rather than the intensity change at the wavelength of, for example, 540 nm for the green channel) is a more clinically relevant and relatable attribute. To test whether any observed changes in the DC component indicates skin *colour* change, the RGB pixel intensity values (raw measurements from the RGB camera as described in section 4.6.1) were converted to hue/saturation/value (HSV) colour space. A further description of this colour space and the reason for using the HSV representation is included in the analysis methods section which follows below (section 6.2.3).

Hypothesis I hypothesised that phenylephrine would lead to a decrease in the peak-to-trough amplitude of the pulsatile AC component of the PPGi waveform as it causes arterial and venous peripheral vasoconstriction [105, 251]. The vasoconstriction was expected to result in a reduced volume of blood in the skin during systole and consequently a smaller change in blood volume from systole to diastole. I hypothesised that GTN would lead to an increase in the peak-to-trough amplitude of the pulsatile AC component of the PPGi waveform as it is a known vasodilator [251].

Peripheral vasodilation from GTN's active metabolite nitric oxide was expected to lead to an increase in the volume of blood in the skin during systole and consequently a larger change in blood volume from systole to diastole. I further hypothesised that the phenylephrine infusion would be associated with a decrease in the DC component (figure 6.1) attributed to the reduction in blood volume in the peripheral tissues, while GTN infusion would be associated with an increase due to the increase in blood volume.

I hypothesised that the two drug infusions would induce opposite direction changes in hue and colour saturation from the baseline. The direction of change in hue was difficult to predict as it is a circular scale and the precise hue change depends on the rest state measurement (as further described in section 6.2.3 and appendix E). However, phenylephrine and GTN infusions were expected to be associated with opposite direction changes in hue. I expected phenylephrine infusion to lead to a decrease in the colour saturation (representing local anaemia or paler skin), while GTN would lead to an increase in the colour saturation (opposite response from phenylephrine).

In addition to the population changes hypothesised above in response to phenylephrine and GTN, I hypothesised that there would be a positive correlation between the magnitude of the AC and DC changes and the magnitude of change in perfusion flux measured using LSCI.

6.2 Analysis methods

Further to the general methods described in chapter 4, additional steps in analysis particularly relevant to the results presented in this chapter are described below.

For the current work, the available thigh skin surface area as a whole (referred to as $\mathrm{ROI}_{\mathrm{GLOBAL}}$ as described in section 5.2.1) was selected rather than focusing on

specific perforator locations. This is in line with methodology used in previously published studies [192, 252]. The relevance of arterial perforators is left to be explored in chapters 7 and 8.

6.2.1 AC amplitude

Previous works have demonstrated the presence of pulsatile PPGi waveform in all three colour channel outputs of the RGB video camera [192, 252]. The green channel has been shown to provide the strongest pulsatile PPGi waveform. This is thought to be related to the proximity of the spectral range of the green channel to the absorption peak of oxyhaemoglobin [253, 254].

The amplitude of the AC component of the PPGi waveform was defined as the height or peak-to-trough displacement of its pulsatile component, measured in 16-bit pixel intensity units. The peak-to-trough amplitude of the PPGi waveform for each colour channel was analysed using the de-bayered images created using the method described in section 4.8.3. All three colour channel results were analysed in parallel, but the green channel results were used as the primary outcome.

A rectangular skin region selected from the skin of the thigh (using the selection, fitting, and tracking methodology previously described in section 4.8.2) was defined as $\mathrm{ROI}_{\mathrm{GLOBAL}}$. The non-uniform blood arrival at different parts of an angiosome was described in chapter 1. The timing of the pulse arrival has previously been shown to be related to the arrival of blood at the specific part of the skin surface. As a result, the peaks of the PPGi waveform occurs at different times even within a limited skin region [255]. It was therefore necessary to construct PPGi waveforms locally (using smaller sub-regions where the pulse arrival was more likely to be nearly the same throughout the sub-region) and align the waveform peaks for the different sub-regions before averaging the pulsatile waveform amplitudes. This

enabled the computation of the average peak-to-trough displacement of the pulsatile component of the PPGi signal from the ROI_{GLOBAL}. Sub-regions consisting of 5 x 5 same colour channel pixels (from de-bayered images) were used for the local construction of PPGi waveforms. For each subsection ROI, the PPGi waveform was isolated using the following steps. BSP-ML researchers wrote a customised peak onset detection algorithm for this analysis, based on the algorithm initially described in the literature by Zong *et al.*, [256] and later extended by Villarroel *et al.*, [194]. The algorithm was used to detect the onset of each pulsatile signal. 'Pulsatility' was defined as the fluctuation in the signal in physiological HR range in adults, set to be above 30 beats per minute and below 180 beats per minute. The MOLLIE study dataset did not contain HR values outside this range, according to the reference HR monitor. Filtering using high-pass and low-pass filters based on these HR limits attenuated any non-HR frequency components. Each PPG waveform was reviewed using a beat-to-beat signal quality assessment algorithm based on previously published methods [257, 258]. A signal quality index (SQI) varying between 0 and 1 was computed, with 0 representing poor signal quality and 1 representing a noise-free signal. Any beats with SQI 0.8 or below were excluded from the analysis, in line with previously published works [192, 194, 252]. The analysis was repeated for the 3 colour channels.

The algorithm for PPGi waveform processing used the following method to determine the pulsatile PPGi (AC) amplitude. A 20-second window was used to determine the average peak-to-trough amplitude for the valid beats (SQI > 0.8) within that time window (shown by the red rectangle in figure 6.2). The computed average amplitude for the time window was displayed at the centre of the 20-second time window. The process was then repeated for the next 20-second window, beginning 1 second after the start of the previous window (shown by the green rectangle in figure 6.2). The peak-to-trough amplitude for ROI_{GLOBAL} for each second of the experimental period was computed using this algorithm.

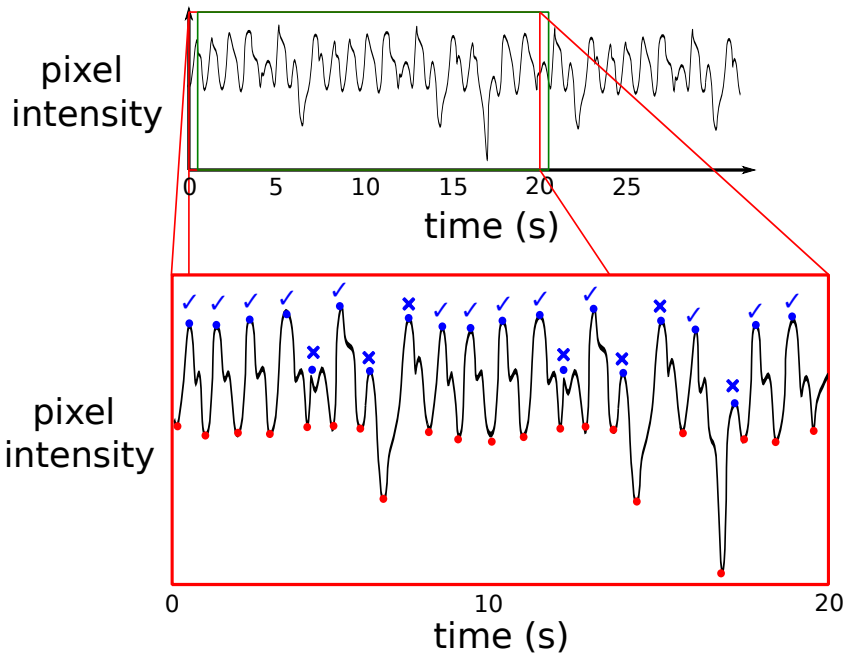


Figure 6.2: Valid beats anaysis of pulsatile peak-to-trough PPGi amplitude. Pulsatile PPGi waveforms from each 5x5 pixels ROI were analysed using previously published techniques [259]. These waveforms were processed for onset detection (red dots) [252, 256] and peak detection (blue dots). A signal quality index (SQI) varying between 0 and 1 was computed for each individual waveform, and only valid beats (SQI $>$ 0.8) were included. Within each 20 second window, the mean peak-to-trough amplitude was calculated and displayed at the centre of the window (at 10 seconds for the red window). This process was repeated with a 1-second shift with respect to the previous windows. On this example, the green rectangle would be analysed using the same process next and displayed at 11 seconds.

6.2.2 DC component

The intensity of the overall RGB signal from all pixels[1] within the tracked $\text{ROI}_{\text{GLOBAL}}$ of the thigh (section 4.8.2) was used to measure changes in the DC component of the PPGi waveform. In contrast to the AC analysis, the sub-regional variability in pulse arrival time across the ROI did not significantly impact the DC analysis. This is because out-of-phase pulsatile components in sub-regions do not impact the mean of the overall waveform, the DC component. Therefore, the DC results were computed directly from the tracked $\text{ROI}_{\text{GLOBAL}}$ by taking the mean raw pixel intensity of the selected skin region, rather than performing local averaging before

[1]Raw intensity calculated using mixing ratio of R:G:B = 0.30:0.59:0.11 [260]

combining these to compute the global mean.

6.2.3 Hue, saturation, value (HSV)

The pixel intensities recorded in each colour channel reflect changes in the level or intensity of light received by the colour sensor in the video camera at a particular wavelength (e.g., 540 nm for the green channel, figure 4.2). An increase or decrease in the 'pixel intensity' for the green channel could arise from changes in the light source, any interference in the light path from the light source to the skin or from the skin to the camera sensor, or changes occurring in the skin. Published literature uses the term 'microblush' [261] to refer to the fluctuation in colour as a result of the latter; i.e., changes arising from the changes from systole to diastole. This term suggests that the largest change will be observed in the red channel. However, analysis of a single channel (centred around any wavelength) cannot distinguish whether the change occurs in the colour spectrum or is caused by a change in the distance to the video camera or the orientation of the skin with respect to the camera, for example.

To test whether any observed changes indicate colour change, the RGB data was converted to another colour representation - hue, saturation, and value (HSV). This alternative method of characterising an image was initially described by Smith [260]. In this model, instead of describing colours using a combination of the three primary light colours (red, green, and blue), colours are captured as a three-dimensional description as follows:

- Hue (H) - the dimension with the colour or the colour name. The colour spectrum in the HSV model is expressed as a number from 0 to 360 degrees and is continuous as shown in figure 6.3. Matlab image processing software represents the hue by a unitless number between 0 and 1 that corresponds to a position on the circle. As the hue increases from 0 to 1, the colour transitions

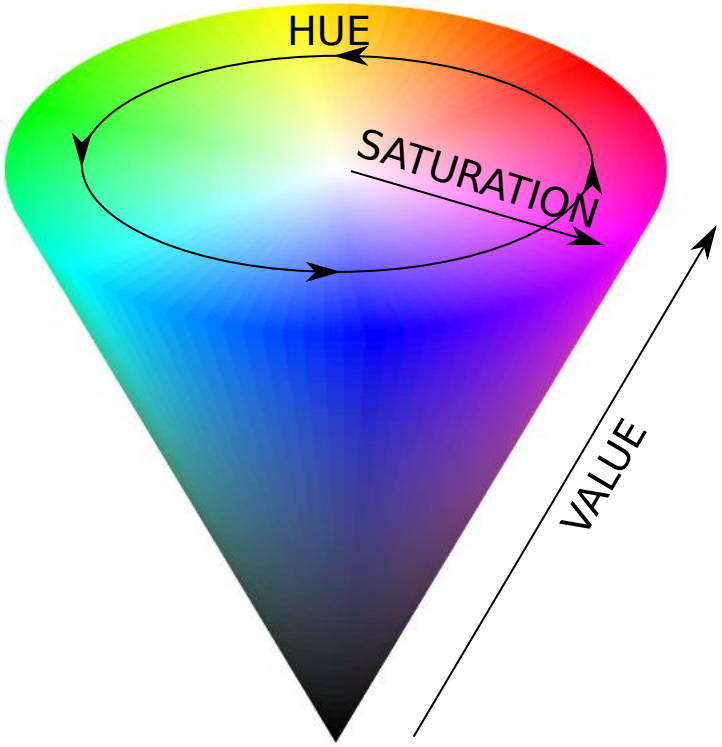


Figure 6.3: Hue, saturation, value (HSV) colour space. HSV is a method of describing colour, as a combination of the colour type (hue, e.g., red, yellow, or blue), vibrancy (saturation), and brightness (value). As demonstrated by the cone, the hue spectrum is continuous, whereas the saturation and value components are linear. [260]

around the circle anti-clockwise, transitioning from red, orange, yellow, green, cyan, blue, magenta, and back to red;

- Saturation (S) - the departure of a hue from achromatic (from white or grey). Matlab image processing software represents the saturation by a unitless number from 0 to 1. Achromatic proportion is represented by the centre of the circle in figure 6.3;

- Value (V) - the departure of a hue from black, shown as change from the tip of the cone (black) to brightness in figure 6.3. Matlab image processing software represents the value as a unitless number from 0 to 1. I did not include the value as a secondary outcome measure as I aimed to assess the colour of skin

independent of the luminance of the environmental lighting (which is mainly captured by the value component).

Compared to other colour spaces, HSV has been shown to best capture skin colour changes [262]. The de-bayered RGB pixel data was converted to HSV using the original algorithms proposed by Smith [260] and the 'rgb2hsv' Matlab image processing package. Details of the algorithm are available under the section 'RGB to HSV Algorithm (Hexcone Model)' of the original paper [260]. The conversion from three-channel RGB images to HSV colour space is further described in appendix E.

6.3 Statistical methods

The measured variables were reported using the following format as appropriate: mean (standard deviation); median (interquartile range).

Paired values from 'rest' and 'peak' periods of interest (as defined in section 4.8.1) were computed for the following variables:

- Amplitude of the peak-to-trough pulsatile PPGi waveform (AC in figure 6.1);
- DC component of the PPGi waveform (DC in figure 6.1);
- Colour hue;
- Colour saturation.

The paired rest and peak values corresponding to each of the above parameters for the phenylephrine and GTN sessions were compared. The two-tailed Wilcoxon signed-rank test was used to test for the significance of the drug-induced changes from rest to peak drug effect. Both the absolute and relative changes associated with the two drug infusions were computed.

The peak-to-trough amplitudes of the pulsatile PPGi waveform during the two rest periods were compared using the paired t-test. This comparison assessed the within-person consistency in the peak-to-trough amplitude of the PPGi waveform (AC) during rest in two separate sessions (phenylephrine and GTN).

The use of the LSCI monitor to measure reference skin perfusion changes from the anterior thigh region (overlapping with the RGB camera monitoring) was described in section 4.6.2.3. The relationship between the drug-induced change in peak-to-trough pulsatile AC amplitude in the green channel and the drug-induced change in reference skin perfusion made with the LSCI was assessed using Pearson's correlation coefficient. Similarly, the relationship between the drug-induced change in the DC component of the PPGi waveform and the drug-induced change in reference skin perfusion using the LSCI was assessed using Pearson's correlation coefficient.

6.4 Results

The demographic data of included participants and vital-sign changes were presented in section 4.10.

6.4.1 Change in pulsatile PPGi waveform amplitude (AC)

A pulsatile signal (defined in section 6.2.1) at the cardiac frequency was observed in all 3 colour channels. During the rest period, the green channel provided the strongest plethysmographic signal with the greatest peak-to-trough pulsatile PPGi amplitude (figure 6.4).

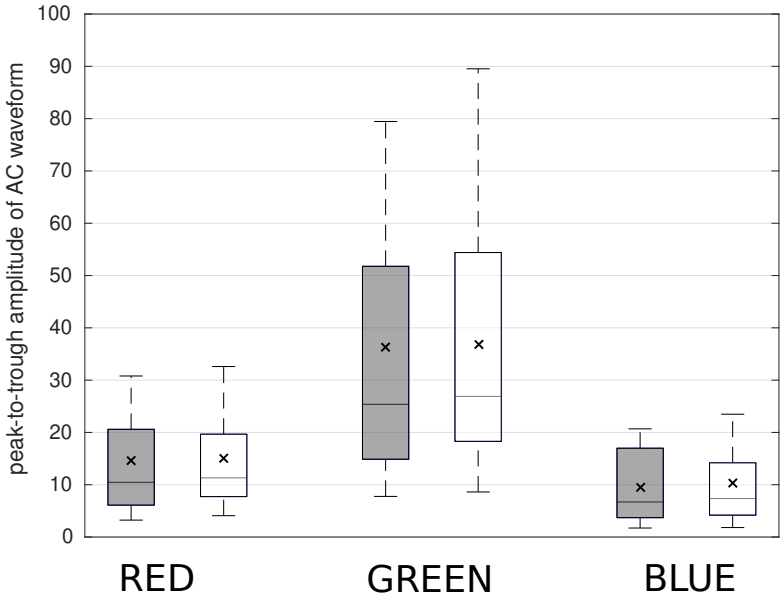


Figure 6.4: Peak-to-trough pulsatile AC amplitude during rest. The box and whisker plots (components defined in section 4.9.1) show the range of computed PPGi waveform amplitudes measured at rest. The mean peak-to-trough pulsatile AC PPGi amplitude is indicated by an x inside each distribution box. The peak-to-trough amplitude of the AC waveform during the phenylephrine rest phase is shown in grey, and is shown in white for the GTN rest phase. Measured in absolute variation in pixel intensity, the largest pulsatile waveforms were observed in the green channel. A wide range of rest state peak-to-trough PPGi amplitudes were observed across the participants. However, there were no significant changes between the rest/baseline state amplitude between phenylephrine and GTN sessions for each participant (red: $p = 0.16$, green: $p = 0.30$, blue: $p = 0.46$).

6.4.1.1 Green channel

Absolute changes During the peak phenylephrine effect, the change in peak-to-trough amplitude of the AC waveform averaged across all participants was a decrease of 15.4 (95% CI 9.4 - 21.4) pixel units ($p < 0.001$) from the baseline. During peak GTN effect, the corresponding change was an increase of 11.6 (7.0 - 16.2) pixel units ($p < 0.001$) from the baseline.

Percentage changes During the peak phenylephrine effect, the change in peak-to-trough amplitude of the AC waveform from the baseline averaged across all participants was a decrease of 34.7 % (95% CI 22.5 - 46.9). During the peak

Table 6.1: Summary RGB video camera ROI_{GLOBAL} results

Outcome variables	Colour channel	Phenylephrine	GTN
Peak-to-trough amplitude of AC waveform	Red	-17.0 (0.04)	+33.8 (<0.001)
	Green	-34.7 (<0.001)	+30.7 (<0.001)
	Blue	-34.5 (<0.001)	+33.7 (<0.001)
PPGi waveform DC	N/A*	-2.1 (<0.001)	+0.5 (0.03)
Colour hue**		-0.0013 (<0.001)	+0.0006 (0.017)
Colour saturation**		-0.0022 (<0.001)	+0.0005 (0.19)

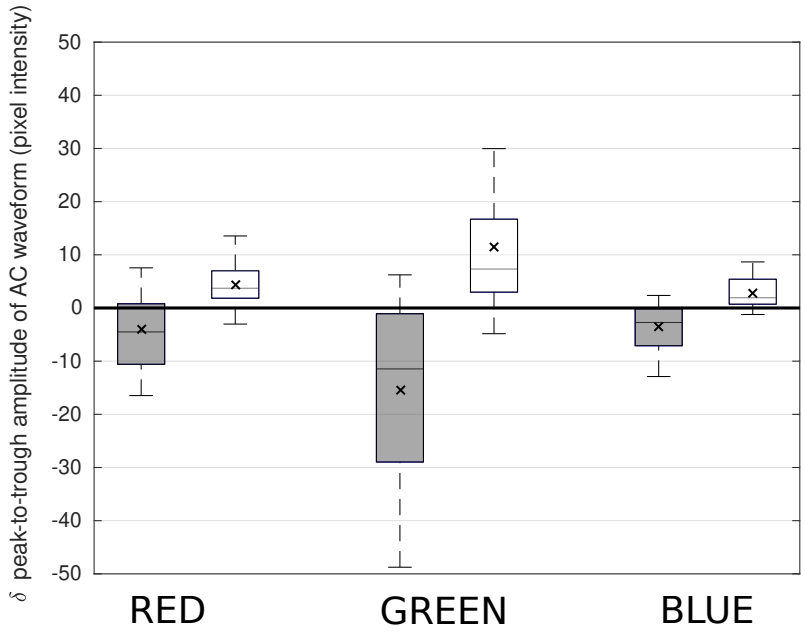
Peak-to-trough amplitude of PPGi waveform (AC) and PPGi waveform DC report relative changes (%) while colour hue and saturation report absolute changes.
*Raw pixel intensity used
**Hue and saturation values post conversion from RGB to HSV as described in sections 6.2.3 and appendix E.

GTN effect, the corresponding change was an increase of 30.7 % (21.8 - 39.5). Both changes were statistically significant ($p < 0.001$) (table 6.1).

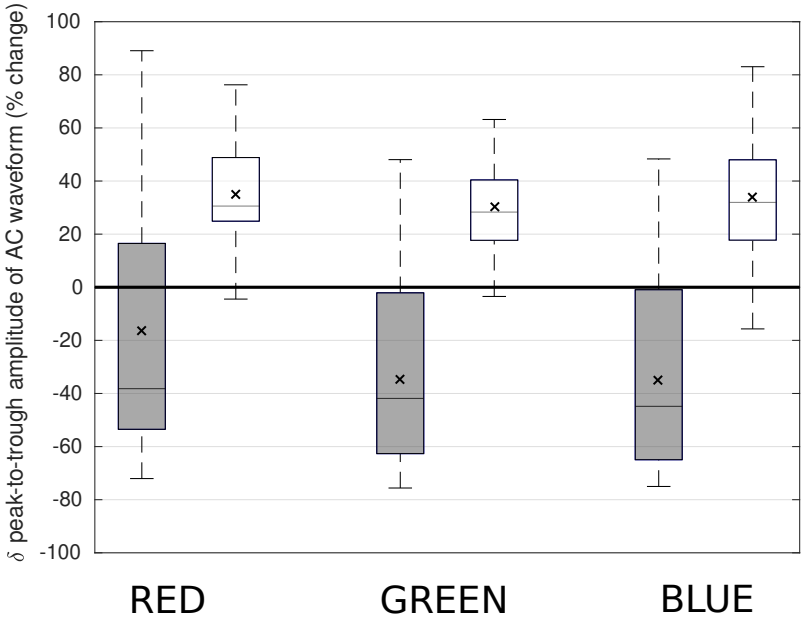
6.4.1.2 Red channel

Absolute changes During the peak phenylephrine effect, the change in peak-to-trough amplitude of the AC waveform averaged across all participants was a decrease of 4.4 (95% CI 2.1 - 6.6) pixel units ($p = 0.002$) from the baseline. During the peak GTN effect, the corresponding change was an increase of 4.7 (3.0 - 6.5) pixel units ($p < 0.001$) from the baseline.

Percentage changes During the peak phenylephrine effect, the change in peak-to-trough amplitude of the AC waveform from baseline averaged across all participants was a decrease of 17.0 % (95% CI 22.5 - 46.9) in the red channel ($p = 0.043$). During the peak GTN effect, the corresponding change was an increase of 33.8 % (21.8 - 39.5) ($p < 0.001$).



(a) Absolute change in peak-to-trough amplitude of the AC waveform



(b) Percentage change in peak-to-trough amplitude of the AC waveform

Figure 6.5: Pre- to peak-infusion change in the amplitude of the pulsatile (AC) component of the PPGi waveform for the three colour channels. δ in y axis label represents 'change in'. (a) Absolute change in amplitude across the three colour channels. (b) Percentage change in amplitude across the three colour channels. Responses to phenylephrine and GTN are shown in grey and white respectively. The mean changes are shown by an x inside each box.

6.4.1.3 Blue channel

Absolute changes During the peak phenylephrine effect, the change in peak-to-trough amplitude of the AC waveform averaged across all participants was a decrease of 4.1 (95% CI 2.4 - 5.8) pixel units ($p < 0.001$) from the baseline. During the peak GTN effect, the corresponding change was an increase of 3.4 (2.0 - 4.9) pixel units ($p < 0.001$) from the baseline.

Percentage changes During the peak phenylephrine effect, the change in peak-to-trough amplitude of the AC waveform from baseline averaged across all participants was a decrease of 34.5 % (95% CI 22.5 - 46.9) in the blue channel. During the peak GTN effect, the corresponding change was an increase of 33.7 % (21.8 - 39.5). Both changes were statistically significant ($p < 0.001$).

6.4.1.4 Summary of AC component changes

The greatest absolute change in peak-to-trough amplitude of the PPGi waveform in response to the drug infusions was observed in the green wavelength for both phenylephrine and GTN infusions (figure 6.5a). The percentage changes in peak-to-trough amplitude of the AC component (from rest state peak-to-trough amplitude, shown in figure 6.4) were comparable across the three colour channels for both phenylephrine and GTN infusions but marginally greater in the blue channel (figure 6.5b, table 6.1).

6.4.1.5 Correlation between AC component and LSCI

There was a positive correlation between the reference skin perfusion measured using the laser speckle contrast imager (section 4.6.2.3) and the change in peak-to-trough pulsatile AC amplitude (r = 0.82) across the phenylephrine and GTN sessions. The relationship is shown in figure 6.6.

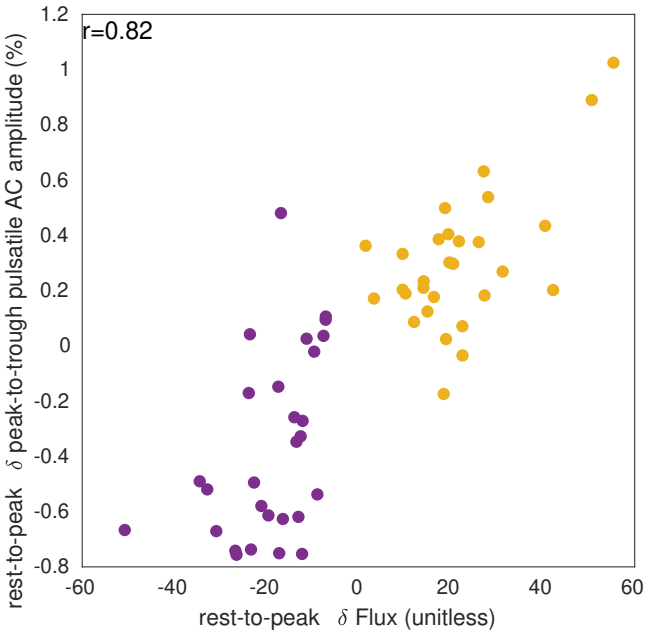


Figure 6.6: Correlation between the drug-induced change in peak-to-trough pulsatile AC amplitude (green channel) and drug-induced change in skin perfusion measured by the LSCI monitor. δ in y axis label represents 'change in'. Purple indicates measurements taken from phenylephrine sessions, and amber indicates measurements taken from GTN sessions. Each participant contributed a purple and an amber point. The overall correlation coefficient between the two was r = 0.82.

6.4.2 Change in the DC component of PPGi

Absolute changes During the peak phenylephrine effect, the change in the DC component of the overall RGB signal from its baseline, averaged across all participants, was a decrease of 518.6 (95% CI 297.5 - 739.6) pixel units ($p < 0.001$). During the peak GTN effect, the corresponding change was an increase of 166.7 (30.8 - 301.6) pixel units ($p = 0.013$) from the baseline value.

Percentage changes During the peak phenylephrine effect, the change in DC component of the PPGi waveform from the baseline, averaged across all participants, was a decrease of 2.1 % (95% CI 1.2-3.0) ($p < 0.001$). During the peak GTN effect, the DC component increased by 0.5 % (0.1-1.2) ($p = 0.026$) from its baseline value.

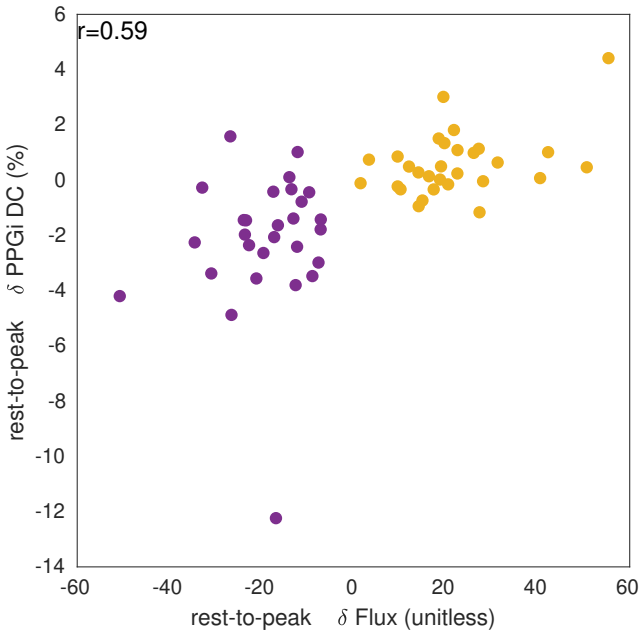


Figure 6.7: Correlation between the drug-induced change in DC component of the PPGi waveform and the drug-induced change in skin perfusion measured by the LSCI monitor. δ in y axis label represents 'change in'. Purple indicates measurements taken from phenylephrine sessions, and amber indicates measurements taken from GTN sessions. Each participant contributed a purple and an amber point. The overall correlation coefficient between the two was r = 0.59.

6.4.2.1 Correlation between DC component and LSCI

There was a positive correlation between the reference skin perfusion measured using the laser speckle contrast imager (section 4.6.2.3) and the change in the DC component of the PPGi waveform but with a lower correlation coefficient then for the AC component (r = 0.59) across the phenylephrine and GTN sessions. The relationship is shown in figure 6.7.

6.4.3 Skin colour changes (hue and saturation)

During the peak phenylephrine effect, colour hue decreased significantly from the baseline value by 0.0013 (95% CI 0.0008 - 0.0018) and saturation by 0.0022 (0.0011 - 0.0033). During the peak GTN effect, colour hue increased significantly from the baseline value by 0.0006 (0.00014 - 0.0011) but there was no significant change in

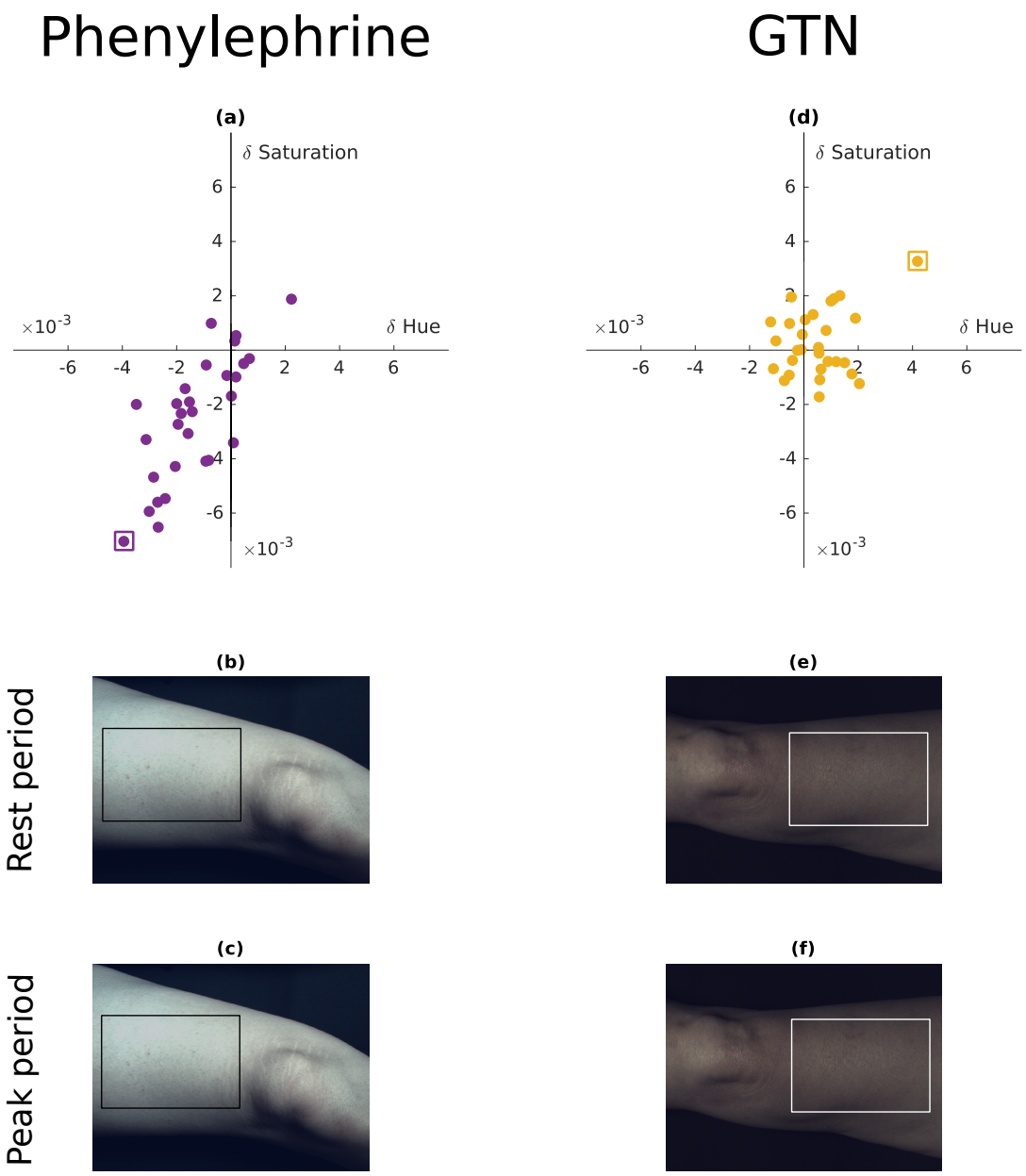


Figure 6.8: Colour hue and saturation response to vasoconstriction and dilation Skin appearance changes quantified in hue and saturation changes from rest to maximum drug effect periods. δ in x and y axis label in (a) and (d) represents 'change in'. (a) and (d) show the change in hue/saturation space from rest (origin) for all 30 participants. (b)-(c) and (e)-(f) show the images taken from the two participants with the largest degree of response (marked by squares in (a) and (d)). Regions of interest used from the sessions are marked as rectangles in (b), (c), (e), and (f). The dark ring cast by the patellar shadow was avoided when selecting the region of interest.

saturation (+0.0005, 95% CI -0.0001 - 0.0012). The changes in hue and saturation with associated significance are reported in table 6.1.

6.5 Chapter summary

Vasoconstriction and vasodilation induced by phenylephrine and GTN were associated with significant changes in both the AC and DC components of the PPGi waveform acquired from the ROI_{GLOBAL} of the thigh. During peak vasoconstriction induced using phenylephrine, all four outcome measurements (peak-to-trough pulsatile AC amplitude, PPGi waveform DC component, hue and colour saturation) decreased significantly when the changes were averaged across all participants (table 6.1). During peak vasodilation induced using GTN, all but one (colour saturation) outcome measurements increased significantly when the changes were averaged across all participants. This study demonstrates that drug-induced changes in skin perfusion can be detected as significant changes in the PPGi waveform acquired from a skin region. Both the peak-to-trough pulsatile AC amplitude changes and the PPGi waveform DC changes were positively correlated with changes measured using an LSCI monitor to collect reference skin perfusion measurements (figures 6.6 and 6.7).

The changes in skin colour hue and saturation from baseline were statistically significant when measured using video cameras. Despite the small p-values for the computed changes in hue and saturation, these changes would not be visible to a clinician monitoring the colour of the patient's skin. Example cases with the greatest change in hue and saturation from baseline and their corresponding images are shown in figure 6.8, where the photographs do not suggest major visible changes. Given that the cardio-synchronous colour changes from skin (a basis for PPGi) are imperceptible to the human eye [263], it is unsurprising that the drug-induced changes are difficult to identify using human vision despite the relevant signals

changing significantly when measured using an RGB camera.

Creating haemodynamic changes using drug infusions administered centrally (rather than local administration using patches) while keeping the participants still is a novel experimental method. Exercise and the Valsalva manoeuvre have been used to induce changes in physiology in previous video camera studies [161, 179, 264, 265]. These studies were not able to demonstrate changes to the AC and DC components of the PPGi waveforms as the chosen experimental methods caused movement artefacts. In addition, the complex effect of sympathetic and parasympathetic pathway activation on skin perfusion (described in section 1.3) was not taken into account. In the MOLLIE study, skin perfusion changes were induced using intravenous phenylephrine and GTN while limiting movement.

Movement artefact outside controlled conditions remains a significant factor to resolve. Settings in which patient movement is limited – such as critical care units or operating theatres – may permit perfusion monitoring using the methods described here. The results presented in this chapter suggest that PPGi waveform analysis may offer a sensitive tool to monitor within-patient changes in skin perfusion.

A large variation was observed in individual data both in the amplitude of the pulsatile signal (as defined in section 6.2.1, figure 6.4) and in the magnitude of the change in the PPGi waveform's AC and DC components in response to the drug infusions (figure 6.5). Although the experimental design in the MOLLIE study controlled for movement and lighting, movement artefacts were still present. There were also inter-subject variations in the rest state raw pixel intensity from the ROI_{GLOBAL} and the rest state peak-to-trough pulsatile AC amplitude (figure 6.4) along with the size (and in a few cases direction) of changes observed (figure 6.5) with drug infusions. This variation would need to be better understood for monitoring to be useful when applied to individual subjects. The large variation in

rest state measurements also suggests that this type of monitoring would currently perform better as a trend monitor.

Changes in the PPGi waveform area and width - two other commonly used PPG features - were not explored in this thesis for several reasons. Both phenylephrine and GTN affect the heart rate [105]. The waveform width and area calculations are usually calibrated for this when measured from contact PPG waveforms [266, 267]. Both phenylephrine and GTN have been shown to affect the PPG and arterial pressure waveform morphology in contact PPG [206, 268], but the effect of the drugs on PPGi waveform morphology is unknown. The PPGi waveform is more sensitive to environmental noise due to the distance between the light source, the skin, and the sensor (video camera). Quantification of the PPGi waveform shape has been shown to be challenging [269] in comparison to contact PPG. Although waveform morphology changes are not explored in this thesis, future work may use this dataset to do so (chapter 9).

This chapter has reported on the changes in amplitudes - for both the AC and DC components - observed from averaged global skin ROI. The next two chapters explore whether further improvements on monitoring skin perfusion can be made by localising perforator arteries.

7

Skin changes according to perforator locations

Contents

7.1 Introduction 133
7.2 Localising perforators using thermal imaging 136
7.2.1 Introduction 136
7.2.2 Methods 138
7.2.3 Results 139
7.2.4 Section summary 141
7.3 Consistency of baseline skin radiance pattern and correlation between perforator locations and baseline skin radiance 143
7.3.1 Introduction 143
7.3.2 Methods 144
7.3.3 Results 147
7.3.4 Section summary 149
7.4 Thermal response to vasoconstriction and vasodilation 151
7.4.1 Introduction 151
7.4.2 Methods 153
7.4.3 Results 153
7.4.4 Section summary 156
7.5 Changes in laser speckle contrast imager (LSCI) . . . 159
7.5.1 Introduction 159
7.5.2 Methods 161
7.5.3 Results 162
7.6 Changes occurring between the rest and peak periods in all sub-regions 165
7.6.1 Introduction 165

7.6.2 Methods 166
7.6.3 Results 167
7.6.4 Section summary 169
7.7 Chapter summary 170

7.1 Introduction

In the previous chapter, I showed that pharmacologically induced increase and decrease in skin perfusion were associated with changes in the amplitude (both the AC and DC components) of the PPGi waveform. The peak-to-trough amplitude of the AC component of the PPGi waveform decreased with phenylephrine infusion and the resulting vasoconstriction. Conversely, the AC component increased in response to GTN infusion and the resulting vasodilation. Opposite changes were observed in the DC component of the PPGi waveform baseline in response to the two drug infusions. The DC value decreased with the phenylephrine infusion, and increased with the GTN infusion. Subsequent analysis in the HSV colour space (section 6.4.3) showed a significant change in colour hue, suggesting that the observed increase and decrease in the PPGi DC component at least partially reflects changes in skin colour.

In the above analyses presented in chapter 6, PPGi waveforms were constructed by averaging light intensity measurements from a large or *global* region of interest (that I defined as $\text{ROI}_{\text{GLOBAL}}$) of the thigh, in line with previous PPGi analyses [192, 252]. Although the peak-to-trough AC amplitude analysis initially involved the construction of local PPGi waveforms using 5 x 5 pixel sub-regions (described in section 6.2.1), the *average* peak-to-trough AC amplitude across the entire $\text{ROI}_{\text{GLOBAL}}$ was reported. This approach of averaging measurements taken from a broader region is similar to the skin assessment performed in clinical settings. When assessing a patient, clinicians tend to make an overall judgement by observing the general appearance of a larger region of skin (e.g., skin of the upper or lower limb) and palpating the skin over the same area [60]. When comparisons between two regions

are made, these tend to be the assessment of the same global region at two different time points (e.g., before and after resuscitation measures such as fluid challenges or the start of therapies), or the assessment of two regions distal from each other. Examples of the latter may include a comparison of skin temperature of the periphery against core regions, such as limbs versus chest and abdomen, or a comparison between proximal leg with respect to the feet. In chapter 5, video camera analysis of skin mottling was explored, adding objectivity to the visual processing performed by the human eye. In chapter 6, drug-induced changes in amplitude parameters that cannot be quantified visually were explored. In this chapter, I continue to build the argument for the strengths of video camera monitoring by exploring the additional benefits of spatial acuity and concurrent multiple region analysis.

Blood arrives at the skin surface via cutaneous perforator vessels (section 1.2.2, figure 1.3), before the vessels branch out to supply the remainder of the angiosome (a skin unit supplied by a single perforator branch, figure 1.4). This anatomical arrangement and the centre-to-peripheral blood flow within each angiosome leads to non-uniformity at the skin surface. This non-uniformity was the basis in section 6.2.1 of the justification for the peak-to-trough amplitude of the PPGi waveform having to be measured locally before being averaged over the entire ROI_{GLOBAL}. The presence of perforators close to the skin surface presents a potential opportunity to assess the macrocirculation by limiting the ROI (the skin region within which the reflected light intensity is analysed) to just the 'perforator zones', rather than measuring from the entire ROI_{GLOBAL} as per the approach adapted in chapter 6. The term 'perforator zones' is used from this point onwards to refer to the skin regions immediately overlying the cutaneous perforators that bring arterial blood close to the skin surface before branching out. In this chapter, I explore how these zones may be identified and whether these sub-regions behave and respond differently to the sub-regions most distal from the perforators (i.e., the skin watershed regions, defined in section 1.2.2.3). The overarching hypothesis for the work presented in this chapter is that there is variability in sub-region response to

the pharmacologically-induced vasoconstriction and vasodilation in the MOLLIE study. I anticipate that this variability is related to the locations of the cutaneous perforators.

Video camera identification of perforator zones for the purpose of skin flap planning has been explored in the literature with varying success [77] (section 1.2.2). The classification of skin surface into perforator zones and non-perforator/watershed zones, and the subsequent tracking of these sub-regions is a novel approach. Several related questions must be explored in turn to support the hypothesis of a differential behaviour of skin sub-regions and whether there is any clinical value in monitoring them. Therefore, this chapter is divided into several smaller sections. The overarching line of enquiry and the sequence of questions are first addressed in the section below. Each question is then expanded in the sections that follow.

Sequence of questions

1. Section 7.2: Where are the cutaneous perforators and what can we learn from their appearance?
2. Section 7.3: Can regional skin thermal radiance during the rest periods be used to locate the perforator zones? Are these locations consistent? If consistent, do these zones align with perforators identified in section 7.2?
3. Section 7.4: Do the different sub-regions defined in section 7.3 behave differently in response to pharmacologically-induced vasoconstriction and vasodilation?
4. Section 7.5: Do the regional differences explored in section 7.4 also exist in the laser speckle contrast imager data?
5. Section 7.6: What happens to the measurements made in the local sub-region response during the drug infusion phase?

7.2 Localising perforators using thermal imaging

7.2.1 Introduction

The results of the tourniquet release session from the MOLLIE study are presented in this first section. The rationale for using a tourniquet for perforator localisation was covered in section 4.5.2. The best evidence available on localising perforators using video is so far limited to thermal camera imaging, previously discussed in section 1.2.2.4 [77, 82, 270]. Therefore, this section (and the subsequent sections in this chapter except section 7.5) focuses on the description of the thermal data from the MOLLIE study and whether a thermal camera can be used to identify the likely locations of cutaneous perforators.

Thermal camera monitoring of an exsanguinated limb using a HemaClear® followed by tourniquet release (section 4.5.2) is a novel method, designed to collect high-resolution images of the 'hot spots' previously correlated with the locations of cutaneous perforators (section 1.2.2.4). As the MOLLIE study used a new approach, the precise time taken for the cutaneous perforators and the surface capillary networks to re-fill after tourniquet release was unknown, as was the time taken for new (warm) blood flow in the vessels to cause an increase in local temperature and increased thermal radiance which could be detected using a thermal camera. Chubb *et al.*, [78] monitored the re-warming phase of manually-cooled skin (using cool water at a temperature between 20 and 22°C) and showed that the skin areas overlying cutaneous perforators warm up back to pre-cooling baseline radiance at a faster rate than the non-perforator regions. The study showed that the exact timing of skin re-warming (in regions both overlying the perforators and distal to the perforators) was variable between patients. The authors used 5-second non-overlapping time windows for analysis to account for the inter-person variability. They described the re-warming trend of perforator angiosomes to be approximated by a logarithmic function ($R^2 = 0.85$) [78].

I hypothesised that:

- Limb exsanguination and timed tourniquet release would lead to the fastest increase in radiance being found in the perforator zones, where blood would be expected to arrive first [72, 78]. This is in line with observed patterns from previous studies of thermographic localisation of perforators [77, 78, 82].
- The MOLLIE study would provide higher resolution images of the 'hot spots' (indicating perforator locations [77, 82]) than previous studies. I expected higher resolution surface images of cutaneous perforators in the MOLLIE study compared to previous imaging studies presented in section 1.2.2 for several reasons:

    1. I expected a greater increase in thermal radiance from baseline in the perforator zones using the limb exsanguination/tourniquet release technique (compared to external cooling methods [82, 270]) because of the period of ischaemia while the tourniquet was in place, and the subsequent reperfusion response (causing rebound hyperaemia) [271];
    2. More uniform venous drainage from the superficial vessels and subsequent cooling of the skin surface was expected from the use of HemaClear® exsanguinator/tourniquet (c.f., use of a cooling gel or water pack [78, 97]) as it is designed to apply consistent pressure on the skin surface. Similar uniformity may be more difficult to achieve using the local cooling methods adapted in the previous studies;
    3. A higher resolution thermal camera was used in the MOLLIE study than in the previous studies of thermographic identification of perforators (640 x 512 in the MOLLIE study compared to previous studies 320 x 240 [82], 256 x 256 [95], or 80 x 60 [94]). Previous studies identified regions of higher radiance but the images did not have sufficient resolution compared to the background skin to characterise the shape of the perforators. If the identified 'hot spots' are related to the presence of perforators, I

expected to see branching shapes with a core region and linear extension of the 'hot spots' [94] towards the edges of angiosomes, as described in the anatomy literature (see section 1.2.2, e.g., figure 1.4).

7.2.2 Methods

The tourniquet application and release were performed according to the steps described in section 4.5.2.

Precise timing (following tourniquet release) for image analysis was not determined *pre-hoc* due to a lack of consensus from previous studies regarding the best time window to use, and the difference between the methodology of the MOLLIE study and the previous methods of skin cooling [77, 82, 270]. Instead, the duration of monitoring after tourniquet removal was chosen using the results from our previous studies, selecting the longest period over which change in skin temperature over perforator zones was observed (up to 240 seconds, see section 4.5.2).

Grey-scale was used to represent skin radiance in the thermal images, with white indicating the highest radiance and black indicating the lowest radiance. Based on the results of previous studies [82, 270], the perforators were expected to appear whiter than the surrounding skin using this scale.

All thermal video images were visually inspected following the tourniquet release and the pattern of progression across the participants was qualitatively described. As with the previous study by Chubb *et al.*, [78], 5-second time windows centered from 2.5 seconds to 237.5 seconds following the tourniquet release were used. From each time window, the median radiance for each pixel (section 4.6.1) was computed to generate a series of perforator location images for all participants. The appearance changes were qualitatively described looking for common patterns in response across

the participants. Quantitative analysis was not attempted. As the assessment was qualitative and the images were averaged using 5-second non-overlapping windows, the timing of changes reported were approximate.

7.2.3 Results

In total, the data from 29 tourniquet release sessions were recorded using the thermal camera. The data were not recorded in one session as a result of unrecognised camera failure (section 4.10.3).

The precise timing associated with the appearance of the perforators on thermal imaging results were variable, but followed a similar pattern in appearance across the participants when 5-second windows were used. These are demonstrated in the images captured following the tourniquet release, shown in figure 7.1.

Following the tourniquet release, the following trend in the hot spot appearance was observed over the 240 seconds of monitoring. In the paragraph below, the time points indicate the centre of the corresponding 5-second window.

- **10 seconds post tourniquet release:** Dense and small filled-circular regions of increased radiance appear.
- **25 seconds post tourniquet release:** Development of branched shapes surrounding the circular regions seen previously, appearing as linear regions of high radiance.
- **40 seconds post tourniquet release:** Blurring of the outline of the branched shapes.
- **from 120 seconds post tourniquet release:** No further changes in radiance from this point to the end of the monitoring period at 240 seconds post

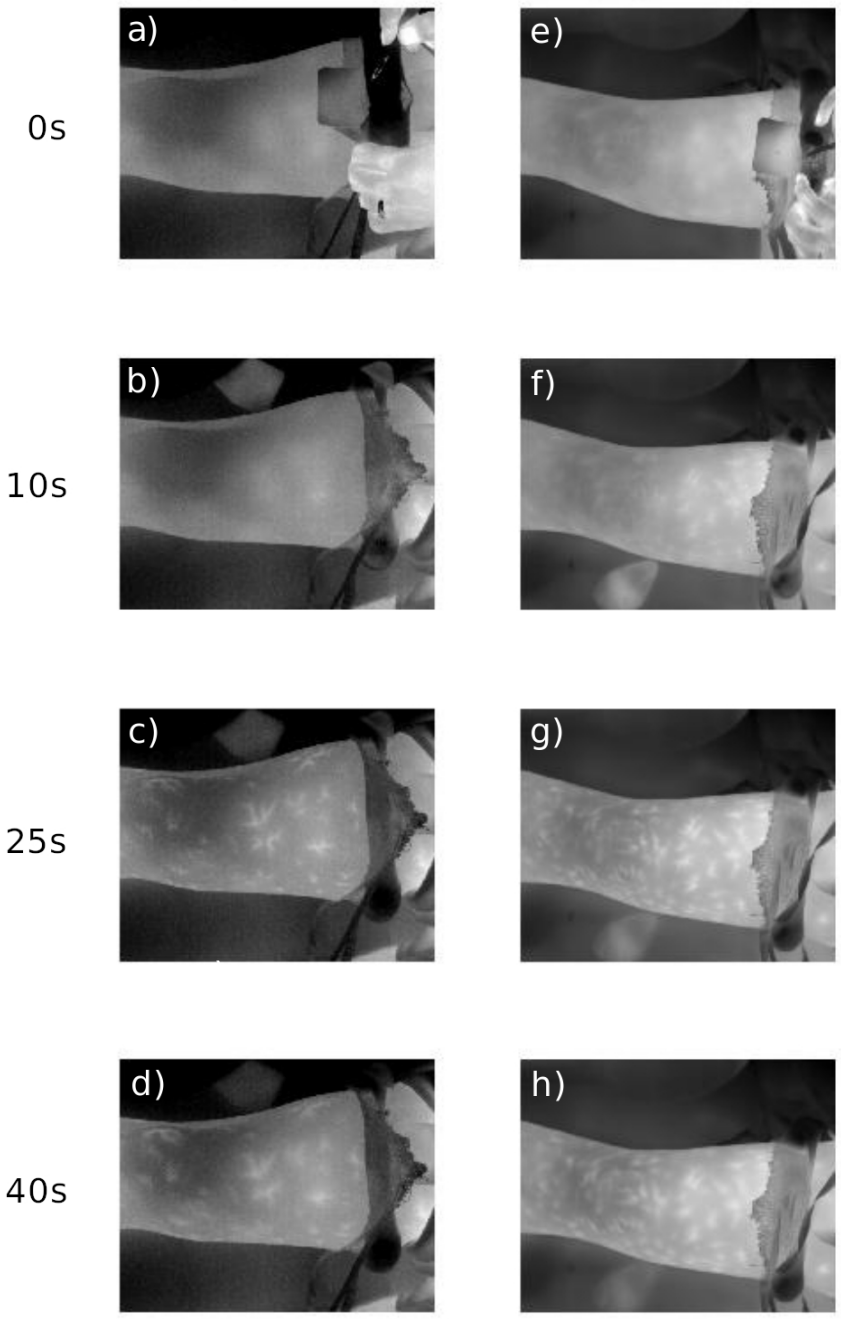


Figure 7.1: Perforator progression Progression of heat spots (white) following tourniquet release. Regions of higher radiance are shown in white, lower radiance in black. The images are taken from two participants, each represented as a column. At baseline (row 1), no clear outline of perforators is visible, but regions of higher radiance are seen in the thigh. The areas of higher radiance (appearing whiter) tend to be the areas where perforators go on to appear. At 10 seconds post tourniquet removal (row 2), white dots representing discrete regions of increased radiance appear (higher radiance appearing white). At 25 seconds (row 3), branches radiating from the dots observed in row 2 are seen. Over the following minute (row 4), the contrast between the branches and the background become more blurred.

tourniquet release.

Examples of the evolution of these three stages are shown in figure 7.1.

Variable patterns of perforator locations were observed among the participants, with no consistent overlap in locations. There was a range from individuals with a small number of larger cutaneous perforators to those with smaller, more evenly spread perforators. Examples are shown in figure 7.2.

7.2.4 Section summary

'Hot spots' were observed on the skin of the thigh following the tourniquet application and release, as previously described in the literature (1.2.2). Previous studies have demonstrated a spatial correlation between 'hot spots' and cutaneous perforator locations identified using other imaging techniques such as ultrasound Doppler or CT angiography (section 1.2.2.4). The images acquired in the MOLLIE study were of higher resolution compared to previously published images of cutaneous perforators [212, 272]. In comparison to the previous images which showed blurred approximate locations of where cutaneous perforators are present [77, 94], changes in the morphology of hot spots over the 240-second monitoring period post tourniquet release was observed in the MOLLIE study dataset.

The images collected (figures 7.1 and 7.2) agreed with previous report [78] that some skin regions rewarm faster from uniform skin cooling. In addition, changes in the shape of the hot spots over time was observed with an evolution from a dot of concentrated higher radiance followed by the appearance of high radiance linear streaks away from this central dot. This dynamic component supports an anatomical basis for these spots, with expected re-filling pattern of vascular network from exsanguination. Hot spot morphology and the associated changes

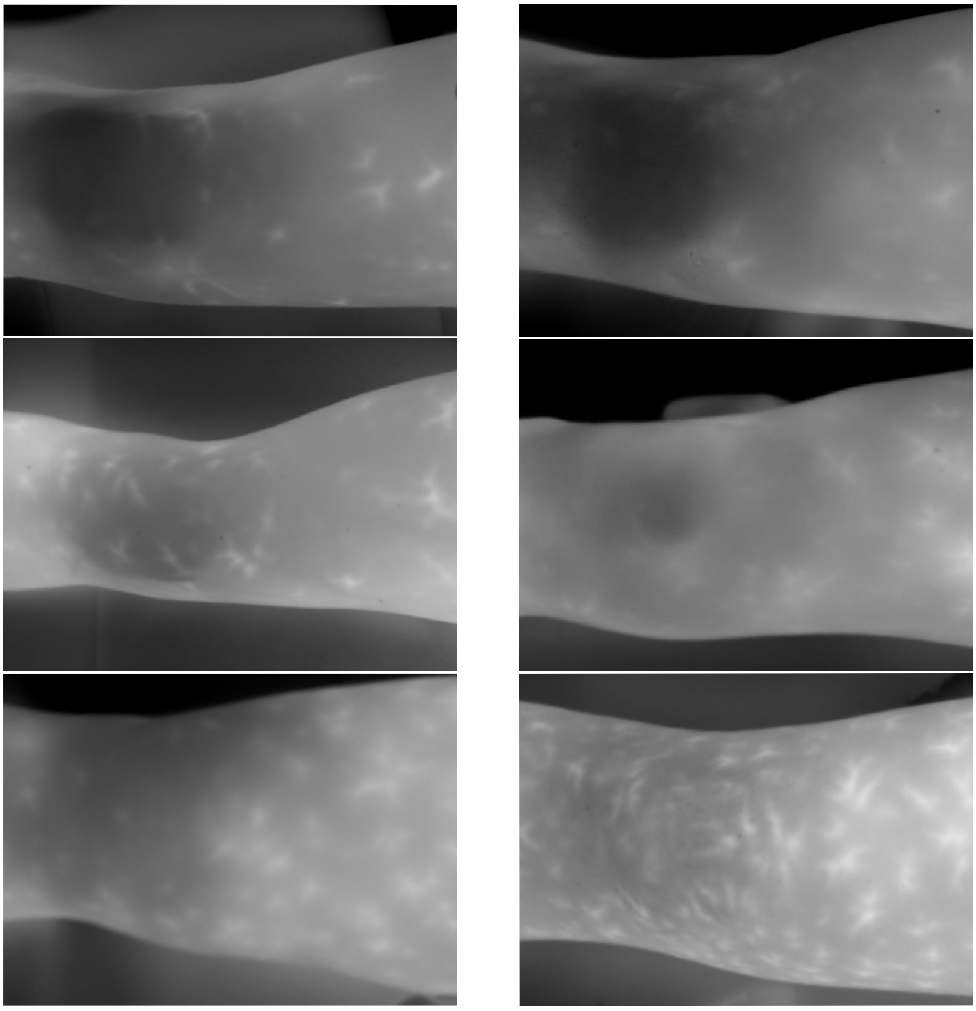


Figure 7.2: Perforator images at same time point for six participants The precise number and size of perforators were variable across the participants. In this figure, perforators from six different participants are demonstrated, all taken at the same time point (t=25 seconds) following the tourniquet release. A range of values for the number, size, and spatial distribution of perforators was observed.

over time were similar to the traditional description of perforator anatomy [72] with a perforator vessel reaching the dermis at the centre of the perforator before branching out towards the edge of the angiosome (figure 1.4).

7.3 Consistency of baseline skin radiance pattern and correlation between perforator locations and baseline skin radiance

7.3.1 Introduction

Previous works have demonstrated that tracking the rewarming phase after localised skin cooling can be used to localise perforators [78, 82, 273] (section 1.2.2.4). In addition to the studies that measure dynamic changes in skin temperature for perforator localisation, further evidence has shown that perforator zones have higher temperature than non-perforator/watershed zones even at rest-state. So far, the evidence for resting state temperature for perforator localisation has been limited to body regions clinically relevant for flap surgery; the inferior epigastric vessel region [274] and the lateral thigh [94]. These studies demonstrated a relationship between skin sub-regions of higher rest-state temperature or radiance and perforator locations (identified intra-operatively [274] or using pre-operative Doppler ultrasound [94]).

In this section, the baseline patterns and variations in skin surface radiance from the anterior thigh monitored in the MOLLIE study are presented. The images from the rest period from the phenylephrine and GTN sessions (prior to the drug infusion, defined in section 4.8.1) are analysed for this purpose. The additional localisation methods (such as exsanguination/tourniquet release used in the MOLLIE study or dynamic rewarming following localised cooling in previous studies) may be difficult to perform in standardised format in clinical settings and are likely to be time-consuming. The ability to locate or determine the perforator zones from resting state monitoring without intervention would widen the usability of this monitoring method in clinical settings.

Two sub-regions within the thigh were classified based on the rest period skin thermal radiance. The sub-regions with the highest and lowest decile rest period

skin radiance were selected and labelled as sub-regions. I hypothesised that if the baseline skin radiance variation was because of, or related to, the presence of perforators, the regions of highest and lowest temperatures would remain consistent between the two drug session rest periods. I additionally hypothesised that the locations of $ROI_{HIGH\text{-}TEMP}$ (sub-regions with the highest baseline radiance) may represent perforator locations identified in section 7.2 - the regions with the greatest increase in radiance following the tourniquet release.

7.3.2 Methods

7.3.2.1 Selection of $ROI_{HIGH\text{-}TEMP}$ and $ROI_{LOW\text{-}TEMP}$

A large rectangular area over each participant's thigh was selected as described in section 4.8.2.2, following the similar process of ROI selection in the RGB imaging data analysis presented in chapter 6. The entire global region was labelled as ROI_{GLOBAL}, using the same terminology as in chapter 6. Equal-size ROI_{GLOBAL} regions from the phenylephrine and GTN sessions were selected for each participant.

The ROI_{GLOBAL} was divided into 10 x 10 pixel sub-regions, following the method previously used in chapter 6 (described in section 6.2.1). For each 10 x 10 pixel ROI, the mean radiance from the 2-minute rest period (defined in section 4.8.1) was computed. All the mean 10 x 10 radiance values within ROI_{GLOBAL} for each session were then ranked from the highest mean radiance sub-region to the lowest mean radiance sub-region. Using this ranking, the following two sub-regions were identified for each session:

- Sub-regions consisting of the top decile rest period radiance (i.e., the warmest regions at rest). These sub-regions were labelled as '$ROI_{HIGH\text{-}TEMP}$'.
- Sub-regions consisting of the bottom decile rest period radiance (i.e., the coldest regions at rest). These regions were labelled as '$ROI_{LOW\text{-}TEMP}$'.

Table 7.1: Sørensen-Dice similarity coefficient: Proposed interpretation of the values [275].

Coefficient	Interpretation
0	"No agreement"
0 to 0.2	"Slight agreement"
0.2 to 0.4	"Fair agreement"
0.4 to 0.6	"Moderate agreement"
0.6 to 0.8	"Substantial agreement"
0.8 to 1.0	"Almost perfect agreement"

The highest and lowest deciles consisted of multiple 10 x 10 pixel areas. Some of the 10 x 10 pixel sub-regions in the highest decile were expected to be clustered together around a single perforator.

7.3.2.2 Consistency of baseline skin surface radiance

The two ROI_{GLOBAL} locations from each participant's two drug infusion session were manually aligned to account for any large movements that occurred between the two sessions. The locations of $ROI_{HIGH\text{-}TEMP}$ and $ROI_{LOW\text{-}TEMP}$ from each drug infusion session were reproduced as binary (consisting of only 0s and 1s) images. Two binary images (one with the $ROI_{HIGH\text{-}TEMP}$ locations and another with the $ROI_{LOW\text{-}TEMP}$ locations) for each of the two drug infusion rest periods were generated for each participant. In the first binary image, a value of 1 was assigned to all $ROI_{HIGH\text{-}TEMP}$ sub-regions and a value of 0 assigned to all other regions (the bottom 90% radiance sub-regions). In the second binary image, a value of 1 was assigned to all $ROI_{LOW\text{-}TEMP}$ sub-regions and a value of 0 was assigned to all other regions (the top 90% radiance regions). For each participant, the similarity between the $ROI_{HIGH\text{-}TEMP}$ from the phenylephrine and GTN sessions rest periods was compared using the two corresponding binary images. The similarity between the $ROI_{LOW\text{-}TEMP}$ from the phenylephrine and GTN sessions rest periods were also compared using the two corresponding binary images. The similarity between each pair of binary images was assessed using the Sørensen-Dice similarity index (see

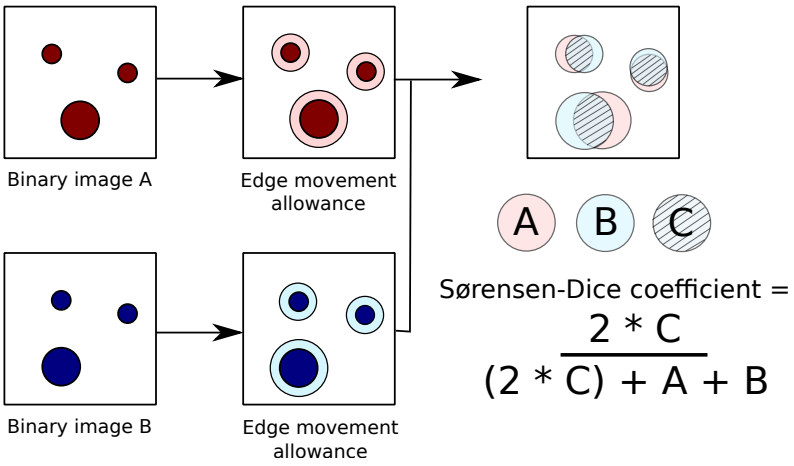


Figure 7.3: Sørensen-Dice similarity index

table 7.1) [276, 277]. An allowance of 10 x 10 pixel distance was used to account for any small degree of movement not adequately covered using manual alignment. The similarity index indicates the degree of overlap between the zones, with 0 indicating no agreement and 1 indicating perfect alignment (figure 7.3). The Sørensen-Dice similarity index is used extensively to test the performance or accuracy of image segmentation/anatomical labelling in medical imaging [275, 278]. The interpretation of the Sørensen-Dice similarity coefficient depends on the ease of segmentation, but a widely used set of categories is given in table 7.1. Similarity scores for the $ROI_{HIGH\text{-}TEMP}$ and $ROI_{LOW\text{-}TEMP}$ distributions were independently calculated.

7.3.2.3 Similarity between $ROI_{HIGH\text{-}TEMP}$ from rest periods and hot spot regions following tourniquet release

A formal comparison between the locations of $ROI_{HIGH\text{-}TEMP}$ from the two rest periods and the perforator zones seen following the tourniquet release described in section 7.2 was not performed for several reasons. Compared to the two rest sessions, more movement occurred between the drug infusion sessions and the tourniquet session owing to the physical application of the tourniquet. It was also difficult to manually realign the leg to the previous position (during the drug infusion phase)

because of the movement limitations while the participants had the tourniquet *in situ*. In addition, it was not always possible to place the tourniquet more proximally than the ROI_{GLOBAL} selected on the drug infusion sessions (demonstrated in figure 7.5c and d).

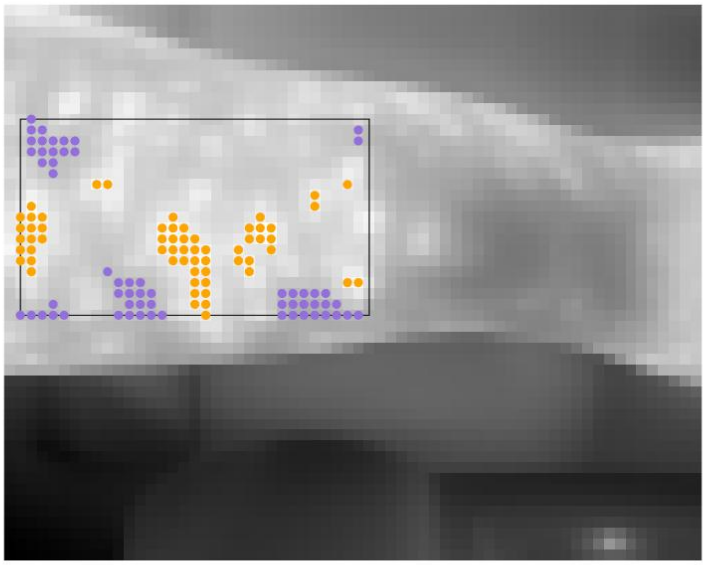
Images from the monitoring period following tourniquet release were labelled with the locations of $ROI_{HIGH\text{-}TEMP}$ and $ROI_{LOW\text{-}TEMP}$ like the rest-period images. Images centered 25 seconds post tourniquet release (with median radiance values from a 5-second window as described in section 7.2) were used for this analysis. This time period was used as it was where the branch pattern of the perforators was most clearly visualised (on subjective assessment). The largest ROI_{GLOBAL} that could be fitted distal to the tourniquet stockinette location was selected using the median radiance images, as demonstrated in figure 7.5d. The methods described above were used to label $ROI_{HIGH\text{-}TEMP}$ and $ROI_{LOW\text{-}TEMP}$ to identify the relevant sub-regions in the post-tourniquet release images. The images were compared visually without formal alignment and an example is shown in the following results section below.

7.3.3 Results

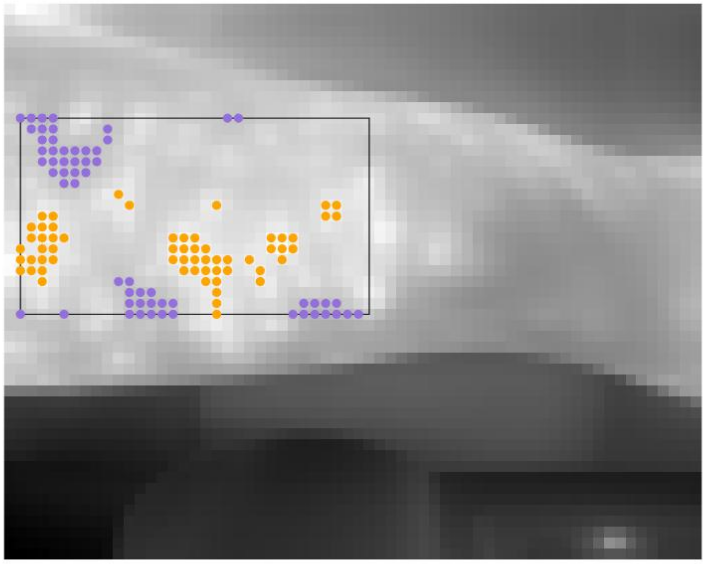
7.3.3.1 Consistency of baseline skin surface radiance

Matched rest period thermal images from phenylephrine and GTN sessions were available from 28 participants (section 4.10.3).

The designated $ROI_{HIGH\text{-}TEMP}$ and $ROI_{LOW\text{-}TEMP}$ sub-regions were located in clusters. Examples of spatial distribution are shown in figures 7.4 and 7.5. The $ROI_{HIGH\text{-}TEMP}$ and $ROI_{LOW\text{-}TEMP}$ areas showed high intra-person consistency in location when measured across the two rest periods from the phenylephrine and GTN sessions. The mean Sørensen-Dice similarity index was 0.67 (IQR 0.54 to 0.83) for $ROI_{HIGH\text{-}TEMP}$, classified as "substantial agreement" according to table 7.1. The mean Sørensen-Dice



(a) Phenylephrine session rest



(b) GTN session rest

Figure 7.4: Example comparison of the $ROI_{HIGH\text{-}TEMP}$ and $ROI_{LOW\text{-}TEMP}$. The two images are generated as the mean radiance for all frames within the 2-minute rest periods defined in section 4.8.1. $ROI_{HIGH\text{-}TEMP}$ is indicated by amber dots, and $ROI_{LOW\text{-}TEMP}$ is indicated by purple dots. A high degree of overlap between the zones in (a) and (b) was observed across the 28 participants with rest period thermal data from both drug infusion sessions.

similarity index was 0.80 (IQR 0.69 to 0.91) for $ROI_{LOW\text{-}TEMP}$, classified as "almost perfect agreement".

Figure 7.4 shows an example of the $ROI_{HIGH\text{-}TEMP}$ and $ROI_{LOW\text{-}TEMP}$ agreement, with Sørensen-Dice similarity index of 0.68 and 0.77 respectively. The data for this participant is shown as the median similarity index values reported for all 28 participants for $ROI_{HIGH\text{-}TEMP}$ sub-regions (appendix G).

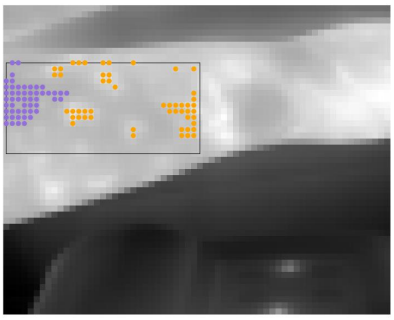
7.3.3.2 Similarity between $ROI_{HIGH\text{-}TEMP}$ from rest periods and hot spot regions following tourniquet release

A formal similarity assessment between $ROI_{HIGH\text{-}TEMP}$ and the perforator zones identified in section 7.2 was not performed for reasons that were explained in section 7.3.2.3. However, an example of alignment is shown in figure 7.5.

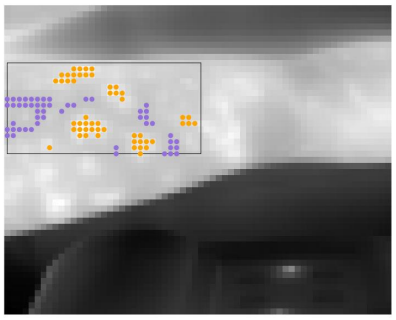
7.3.4 Section summary

I observed a 'substantial agreement' (mean Sørensen-Dice similarity index of 0.67) between the locations of $ROI_{HIGH\text{-}TEMP}$ from the two rest periods (from phenylephrine and GTN sessions). I also observed an 'almost perfect agreement' (mean Sørensen-Dice similarity index of 0.80) between the locations of $ROI_{LOW\text{-}TEMP}$ from the two rest periods. A consistency in the spatial location of the two sub-regions supports an anatomical basis for the differential baseline skin surface radiance. Intra-person consistency in the sub-regions would be necessary for sub-region tracking for clinical monitoring. Future work will involve checking this consistency in a subset of the study participants with a further agreement measurement after a 2-year interval (described in the future work in section 9.2.2).

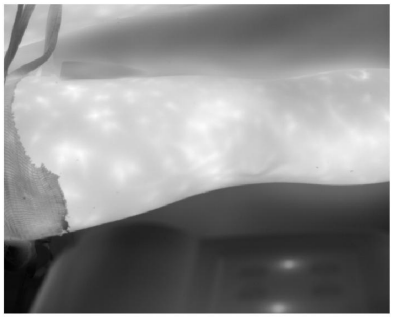
Quantification of the similarity between $ROI_{HIGH\text{-}TEMP}$ and the hot spot locations from section 7.2 was not attempted due to the practical challenges discussed above



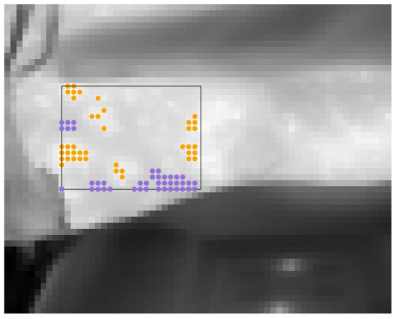
(a) Phenylephrine session rest



(b) GTN session rest



(c) Tourniquet session image at peak perforator appearance



(d) Top and bottom decile at 25 seconds post tourniquet release

Figure 7.5: Example comparison of $ROI_{HIGH\text{-}TEMP}$ and perforator locations. The top row images show rest period $ROI_{HIGH\text{-}TEMP}$ (amber) and $ROI_{LOW\text{-}TEMP}$ (purple) from the phenylephrine (a) and GTN (b) rest periods as per figure 7.4. The black rectangles show the ROI_{GLOBAL}. (c) shows the perforator location image taken at 25 seconds post tourniquet removal, where the branch patterns are most clearly demonstrated. In (d), the rectangle shows the ROI_{GLOBAL} most similar to (a) and (b) as allowed by the tourniquet location. The top and bottom decile radiance sub-regions are demonstrated (top decile = amber, bottom decile = purple). (c) and (d) demonstrates that comparison of the same anatomical area across the drug infusion and tourniquet release sessions was difficult. The tourniquet in this case could not be placed proximal to the ROI selected in (a) and (b), so the selected area on (d) is smaller than the areas selected in (a) and (b). However, the five common regions of higher baseline/rest period radiance shown in (a) and (b) are also seen in (d).

and demonstrated in figure 7.5, which shows the difficulty of comparing areas due to the locations of tourniquet.

The results described in this section demonstrate constant locations for the sub-regions in different images, even though the hot spots following tourniquet release and the baseline $ROI_{HIGH\text{-}TEMP}$ sub-regions cannot be directly united. However, it is the changes in the $ROI_{HIGH\text{-}TEMP}$ and $ROI_{LOW\text{-}TEMP}$ in response to increasing drug infusion doses that would truly demonstrate the usefulness of sub-region monitoring. This is explored in the next section.

7.4 Thermal response to vasoconstriction and vasodilation

7.4.1 Introduction

The previous section identified two sub-regions that show good agreement across two rest periods (during the phenylephrine and GTN sessions). In this section, the thermal radiance response of the same two sub-regions $ROI_{HIGH\text{-}TEMP}$ and $ROI_{LOW\text{-}TEMP}$ (that can be selected *a priori* by using baseline skin radiance) to the pharmacologically-induced vasoconstriction and vasodilation is described.

The results from ROI_{GLOBAL} are also investigated as these represent what would be obtained using traditional measurement methods (global averaging) in video camera studies. As described in section 7.3.2.1, $ROI_{HIGH\text{-}TEMP}$ and $ROI_{LOW\text{-}TEMP}$ are sub-regions within ROI_{GLOBAL} (top and bottom deciles). This means there is an overlap in the regions represented. ROI_{GLOBAL} was included as a comparator rather than a sub-region representing the remaining 80% of ROI_{GLOBAL}, because the state of the art in camera monitoring is the use of ROI_{GLOBAL} [279, 280].

I hypothesised that phenylephrine and GTN would have the overall effect of decreasing and increasing skin radiance based on their known mechanism of action and physiological effects as a vasoconstrictor and a vasodilator respectively [105]. I further hypothesised that if perforators are indeed responsible for the consistent spatial variability in skin surface radiance during the resting state (as described in section 7.3), phenylephrine's vasoconstrictive effect (and subsequent decrease in skin radiance from a reduction in the influx of warm blood) would be more pronounced in the regions overlying cutaneous perforators represented by $ROI_{HIGH\text{-}TEMP}$. Therefore, I expected the decrease in radiance associated with the phenylephrine infusion to be greater in $ROI_{HIGH\text{-}TEMP}$ than $ROI_{LOW\text{-}TEMP}$. I anticipated this as the starting radiance was higher in $ROI_{HIGH\text{-}TEMP}$, and because I expected the action of phenylephrine to be more pronounced on the macrovasculature (on arterial perforators, where it is expected to cause vasoconstriction). I expected any effect on the microvasculature (or the capillary networks, possibly better represented by $ROI_{LOW\text{-}TEMP}$, as discussed in section 7.4.4) to be downstream of the primary effect on the macrovasculature.

I further hypothesised that the GTN infusion would be associated with a greater magnitude increase in radiance in $ROI_{HIGH\text{-}TEMP}$ (where it would cause vasodilation of the perforator vessels) than in $ROI_{LOW\text{-}TEMP}$. However, the differential effect of GTN on the two sub-regions was more difficult to predict compared to the phenylephrine infusion due to its less localised site of action as discussed in sections 1.3.1 and 4.5.1. As well as a downstream increase in flow in the microvasculature (better represented by $ROI_{LOW\text{-}TEMP}$), GTN may also have a direct vasodilatory effect on the capillaries themselves [209, 231, 281]. This, added to the lower baseline temperature in $ROI_{LOW\text{-}TEMP}$ made the response to GTN in the two sub-regions more difficult to predict.

7.4.2 Methods

The primary outcome was the computed mean thermal radiance from two ROI defined in section 7.3: $ROI_{HIGH\text{-}TEMP}$ and $ROI_{LOW\text{-}TEMP}$. In addition, the results from ROI_{GLOBAL} are also computed and reported.

For each participant, the median (IQR) radiance of the three regions was calculated for the 2-minute rest period and the 2-minute peak drug effect period (section 4.8.1). The change in radiance was calibrated using the changes in background radiance (appendix figure F.1). This step was added to account for the changes in the environmental temperature secondary to the computing equipment and dedicated lighting used. Details of the calibration method and the observed change in background temperature are included as appendix F.

The radiance differences between the rest and peak infusion periods for both drugs across all included participants were analysed using the Wilcoxon sign rank test.

The difference between the changes in radiance in $ROI_{HIGH\text{-}TEMP}$ and $ROI_{LOW\text{-}TEMP}$ was compared using the Wilcoxon rank sum test.

7.4.3 Results

All radiance values are reported in $W.sr^{-1}.m^{-2}$.

The mean change in the background radiance during the phenylephrine session (comparing the rest period and peak drug effect period data) was +24.6 (95% CI 16.7 - 32.6). The mean change in background radiance during the GTN session was +17.3 (7.7 - 26.9) (appendix F).

Table 7.2: Radiance changes for ROI_{GLOBAL}, $ROI_{HIGH\text{-}TEMP}$, and $ROI_{LOW\text{-}TEMP}$. Values presented as mean (p-value).

	Phenylephrine	GTN
ROI_{GLOBAL}	-16.5 (0.15)	+58.2 (<0.001)
$ROI_{HIGH\text{-}TEMP}$	-46.4 (<0.001)	+47.5 (<0.001)
$ROI_{LOW\text{-}TEMP}$	-6.8 (0.86)	+51.7 (<0.001)

7.4.3.1 $ROI_{HIGH\text{-}TEMP}$

The median $ROI_{HIGH\text{-}TEMP}$ radiance at rest during the phenylephrine session was 6843 (IQR 6729 - 7055). During the peak phenylephrine effect, the calibrated[1] median change in $ROI_{HIGH\text{-}TEMP}$ radiance was a decrease of 46.4 (IQR 19.3 - 85.7) from baseline ($p < 0.001$) (table 7.2).

The calibrated median $ROI_{HIGH\text{-}TEMP}$ radiance at rest during the GTN session session was 6948 (IQR 6779 - 7169). During the peak GTN effect, the calibrated median change was an increase of 47.5 (IQR 28.3 - 106,5) from baseline ($p < 0.001$).

7.4.3.2 $ROI_{LOW\text{-}TEMP}$

The median $ROI_{LOW\text{-}TEMP}$ radiance at rest during the phenylephrine session was 6475 (IQR 6366 - 6680). During peak phenylephrine effect, the calibrated median change in $ROI_{LOW\text{-}TEMP}$ radiance was an increase of -6.5 (IQR -26.3 - 31.6) from baseline ($p = 0.86$).

The median $ROI_{LOW\text{-}TEMP}$ radiance at rest during the GTN session was 6562 (IQR 6406 - 6760). During the peak GTN effect, the calibrated median change was an increase of 51.4 (IQR 26.8 - 83.6) from baseline ($p < 0.001$).

[1] with adjustment for background temperature change, appendix F

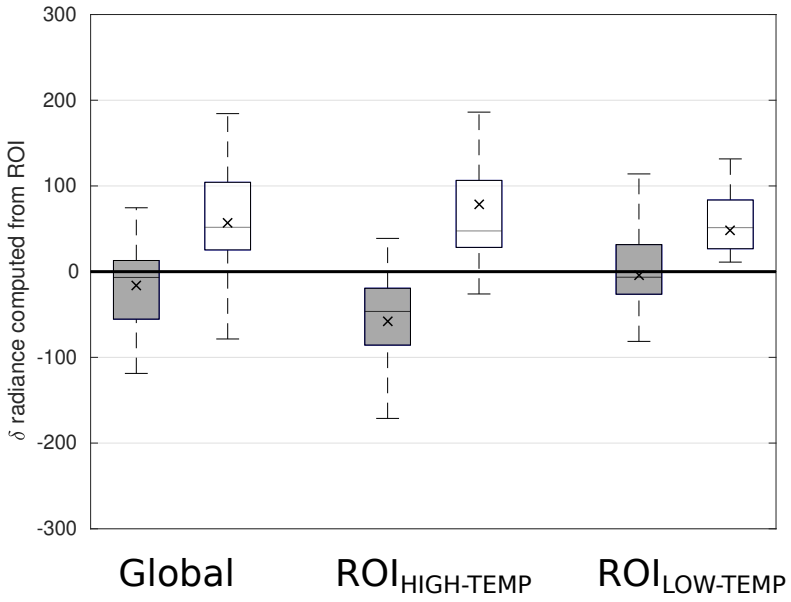


Figure 7.6: Radiance changes in response to phenylephrine (grey) and GTN (white). The box and whisker plots demonstrate observed changes between the rest and peak drug infusion periods (section 4.9.1). δ in y axis label represents 'change in'. Phenylephrine infusion was associated with a decrease in radiance in $ROI_{HIGH\text{-}TEMP}$ but no change in radiance in $ROI_{LOW\text{-}TEMP}$. GTN was associated with an increase in radiance in both sub-regions, but greater increase in $ROI_{HIGH\text{-}TEMP}$. Changes in radiance are in $W.sr^{-1}.m^{-2}$. Mean values are indicated as x.

7.4.3.3 ROI_{GLOBAL}

The median global radiance at rest during the phenylephrine session was 6703 (IQR 6580 - 6901). During peak phenylephrine effect (period defined in section 4.8.1), the calibrated median change in ROI_{GLOBAL} radiance was a decrease of 6.8 (IQR -55.4 - 13.0) from baseline ($p = 0.15$).

The median global radiance at rest during the GTN session was 6810 (IQR 6603 - 6932). At peak GTN effect, the calibrated median change was an increase of 51.7 (IQR 25.4 - 104.2) from baseline ($p < 0.001$).

7.4.3.4 Difference between $ROI_{HIGH\text{-}TEMP}$ and $ROI_{LOW\text{-}TEMP}$

During the peak phenylephrine effect, the median difference between the change in $ROI_{HIGH\text{-}TEMP}$ radiance and $ROI_{LOW\text{-}TEMP}$ radiance was 50.1 (IQR 8.4 - 102.8) ($p < 0.001$). During the peak GTN effect, the corresponding difference was 16.1 (IQR -23.8 - 51.1) ($p = 0.71$).

7.4.4 Section summary

In this section, the thermal radiance responses of two skin sub-regions to pharmacologically-induced vasoconstriction and vasodilation - $ROI_{HIGH\text{-}TEMP}$ and $ROI_{LOW\text{-}TEMP}$ - were compared, with the global thigh region response (ROI_{GLOBAL}) also reported.

My first hypothesis (presented in section 7.4.1) was that the phenylephrine infusion would be associated with a global decrease in skin thermal radiance and the GTN infusion would be associated with a global increase in skin thermal radiance. Although there was a decrease in skin radiance in ROI_{GLOBAL} associated with phenylephrine infusion, this was not statistically significant ($p = 0.15$). In contrast, the GTN infusion was associated with a significant increase in skin radiance in ROI_{GLOBAL} ($p < 0.001$).

The second part of my hypothesis was that the sub-regions of the skin defined using the baseline skin radiance - $ROI_{HIGH\text{-}TEMP}$ composed of the top 10% baseline radiance regions and $ROI_{LOW\text{-}TEMP}$ composed of the bottom 10% baseline radiance regions - would differ in response to phenylephrine and GTN. A statistically significant difference between $ROI_{HIGH\text{-}TEMP}$ and $ROI_{LOW\text{-}TEMP}$ was observed in response to phenylephrine. During the peak phenylephrine response, the change in $ROI_{HIGH\text{-}TEMP}$ radiance was a significant decrease of 54.8 $W.sr^{-1}.m^{-2}$ ($p < 0.001$), despite no significant change in ROI_{GLOBAL}. My hypothesis that the perforator zones (represented by $ROI_{HIGH\text{-}TEMP}$, suggested by the results in section 7.3) would

show greater magnitude decrease in radiance compared to the regions further away from the perforators ($ROI_{LOW\text{-}TEMP}$) was demonstrated to be correct.

In contrast, both sub-regions - $ROI_{HIGH\text{-}TEMP}$ and $ROI_{LOW\text{-}TEMP}$ - showed a significant increase in skin radiance in response to the GTN infusion. There was no significant difference between the responses of the sub-regions to GTN infusion ($p = 0.71$).

There are several potential reasons why there was a significant difference between sub-regions in response to phenylephrine but not to GTN.

- **Drug action**: Phenylephrine and GTN have generally opposing effects on the cardivascular system [105], but are not exactly opposite in their mechanism of action. They exert their clinical effect via different pathways. Phenylephrine acts selectively on the noradrenergic channels leading to vasoconstriction, whereas GTN acts via the generation of nitric oxide and can have a more widespread effect [209] (section 1.3.1). Phenylephrine would therefore be expected to act more selectively on the afferent arteries sensitive to noradrenergic vasoconstriction [105], whereas GTN has been shown to be less selective in effect sites (due to the less selective effect of nitric oxide). It is possible that the phenylephrine's effect was more pronounced over the perforator zone, leading to a greater magnitude decrease in radiance. The reduction in afferent flow would eventually be expected to reduce flow to the watershed areas (represented by $ROI_{LOW\text{-}TEMP}$), but it is possible that this was not observed in the MOLLIE dataset due to a combination of short duration of infusion and relatively low starting temperature in these zones (bottom 10% resting state skin radiance) prior to the administration of phenylephrine. GTN has been explored for clinical use in septic patients to increase microvascular flow [239], suggesting that its site of action is both macro- and microvascular. This may have led to the observed concurrent increase in radiance in both

the $ROI_{HIGH\text{-}TEMP}$ and $ROI_{LOW\text{-}TEMP}$ sub-regions.

- **Hysteresis**: There may be an intrinsic difference between vasoconstriction and vasodilation processes that do not exactly mirror each other. The increase and decrease in blood vessel diameter may be affected by a different balance of forces, leading to a hysteresis effect [282]. When hysteresis is observed in physiology, it typically refers to an opposite direction state change that does not follow the same pattern. It is present in several physiological settings with the best known example being lung compliance (differential curve for inspiration and expiration [283]). Loading and unloading processes on the elastin in the vascular wall (responsible for the variation in blood vessel diameter) has been shown to display hysteresis with different curves depending on the direction of change [284].

- **Measurement modality**: Monitoring skin radiance is a) a proxy measurement for blood flow or perfusion (relying on heat transfer from blood to tissue), and b) susceptible to influence from the environmental temperature. Both could play a role in the observed asymmetrical response of the two sub-regions to phenylephrine and GTN. As the regions were defined using their baseline temperature, the heat transfer between blood and tissue is not along an equal gradient which will affect the rate of temperature (and thermal radiance) change [285]. In addition, there was an increase in the background temperature of the room (estimated from the increase in background radiance measured using the thermal camera) which could have had an effect on both the $ROI_{HIGH\text{-}TEMP}$ and $ROI_{LOW\text{-}TEMP}$ results.

The following two sections further investigate the different response observed between the $ROI_{HIGH\text{-}TEMP}$ and $ROI_{LOW\text{-}TEMP}$ sub-regions.

7.5 Changes in laser speckle contrast imager (LSCI)

7.5.1 Introduction

In the previous section, the sub-regions of skin with the highest temperature at baseline ($ROI_{HIGH\text{-}TEMP}$) were shown to respond differently to the sub-regions with the lowest temperature at baseline ($ROI_{LOW\text{-}TEMP}$) during phenylephrine-induced reduction in skin perfusion. This sub-region difference was not perceptible when the global averaging method (the approach presented in chapter 6) was used as demonstrated by the regional responses to phenylephrine. Despite a significant decrease in response to phenylephrine in $ROI_{HIGH\text{-}TEMP}$ ($p < 0.001$), the ROI_{GLOBAL} radiance did not change significantly ($p = 0.15$).

In section 1.4.2.1, LSCI monitoring was introduced as a clinically validated method of estimating skin perfusion (flux measured in proprietary perfusion units) using the speckle property of laser when it interacts with living tissue. A commercial LSCI monitor was used in the MOLLIE study as a reference local perfusion change monitor as described in section 4.6.2.3. Chapter 6 then presented the positive correlation between the drug-induced changes in skin perfusion measured using this instrument with the two PPGi waveform parameters computed (peak-to-trough amplitude of the AC component and the magnitude of the DC component of the PPGi waveform). Both parameters showed a positive correlation with skin perfusion changes measured by the LSCI monitor. The changes in the peak-to-trough amplitude of the AC component of the PPGi waveform had a stronger correlation with flux changes (r = 0.82) compared to the DC component (r = 0.59).

As described in section 4.6.2.3, the LSCI monitor software (Moor Measurement Software version 3.0) estimates flux from a manually-selected ROI, automatically averaging across the entire selected ROI [112]. The default method of perfusion analysis using this tool is to average across a large area rather than select sub-regions.

This mirrors the 'global averaging' prevalent in the PPGi literature, represented in this chapter by the ROI_{GLOBAL} measurements. Sub-region differences in flux using laser speckle contrast imager have not previously been explored. However, the manufacturer software allows export of the flux estimates prior to the global averaging, maintaining the spatial information. Using this function, the time-stamped 'flux images' were exported from the LSCI monitor, with each pixel representing the local/sub-regional flux estimates. In this section, analysis of this LSCI dataset mirrors the sub-region analysis presented above for thermal imaging sections (7.3 and 7.4).

I hypothesised that the response of sub-regions measred with the LSCI monitor would mirror the variable sub-region responses seen with thermal imaging. As with the latter, I expected the sub-regions with the highest flux at baseline (which I expected to be over the perforator zones) to respond with a greater decrease in flux in response to phenylephrine compared to the sub-regions with the lowest flux at baseline (which I expected to be over the watershed zones of the skin). Based on the responses observed in section 7.4, the response to GTN was expected to be less variable in the lower and upper decile sub-regions. In the previous section summary (section 7.4.4), several potential reasons were proposed to explain why the differential response in these sub-regions in phenylephrine infusion were not seen with the GTN infusion. If it was because of a difference in the drug action (and specificity of the site of action), a greater sub-region difference during the phenylephrine session compared to the GTN session would be seen in the LSCI data (as in the thermal data). On the other hand, if the observed behaviour arose because of the characteristics of the thermal imaging modality, the LSCI data would show the expected greater magnitude difference between sub-regions. LSCI provides a direct measurement of flow (section1.4.2.1) rather than measuring a proxy parameter, and it is less affected by increases in environmental radiance.

7.5.2 Methods

The images acquired using the Moor FLPI-2 laser speckle contrast imager were analysed using methods similar to those used for thermal image data analysis (described in section 7.4). The flux measurements were exported as a series of 2D matrices, with each image pixel representing the flux value from the local skin area. The largest rectangular ROI that could be fitted over the skin of the thigh was manually selected, leaving at least 10 pixels from the skin edge to ensure that the rectangle does not leave the skin region as a result of a small degree of involuntary movement. The rectangular ROI_{GLOBAL} selection method was similar to those used for the RGB and thermal image data described in section 4.8.2.

Two sub-regions from the rectangular ROI_{GLOBAL} were selected using the following steps. ROI_{GLOBAL} was divided into 10 x 10 square sub-regions. For each sub-region, the mean flux was computed using all measurements recorded during the 2-minute 'rest' period. The average baseline sub-region flux was then used to rank the sub-regions from areas with the highest rest period flux to the lowest rest period flux.

Two sub-regions were defined following the methods used in section 7.3:

- $ROI_{HIGH\text{-}FLUX:}$ A sub-region consisting of the top decile rest flux (i.e., the areas with the highest blood flow at rest);
- $ROI_{LOW\text{-}FLUX:}$ A sub-region consisting of the bottom decile rest flux (i.e., the areas with the lowest blood flow at rest).

The primary outcome was the computed mean flux from the two sub-regions. In addition, the same parameter from the whole region - ROI_{GLOBAL} - was also computed, to reflect the change observed if the entire area was averaged as per the standard method in the literature. For each participant, the change in mean

flux for the three regions from the rest period to the peak drug effect period was calculated. These differences for both drugs across all participants were analysed using the Wilcoxon sign rank test. All flux values are reported using the unit PU (Perfusion Units[2]).

7.5.2.1 Alignment of sub-regions across modality

Alignment between the top and bottom decile zones labelled using the thermal camera and the LSCI was not attempted because the two sets of images are too different from each other. The camera set-up and the optimal distance from the skin for best image resolution are not the same for the two imaging modalities. The two cameras were placed at different angles to capture the thigh images without interfering with data collection using the other device.

7.5.3 Results

Laser speckle data was obtained from all 30 participants (section 4.10.3).

7.5.3.1 $\text{ROI}_{\text{HIGH-FLUX}}$

The mean global flux at rest during the phenylephrine session was 167.9 (95% CI 149.3 - 186.5) flux units. During the peak phenylephrine effect, the median change in $\text{ROI}_{\text{HIGH-FLUX}}$ flux was a decrease of 23.1 (IQR 14.3 - 32.8) ($p < 0.001$).

The mean global flux at rest during the GTN session was 173.1 (95% CI 146.0 - 200.1). During the peak GTN effect, the corresponding change was an increase of 22.1 (IQR 13.5, - 27.2) ($p < 0.001$).

[2]Proprietary units. The mean flux is a dimensionless unit measuring microcirculatory blood flow, calibrated in the factory [286]

Table 7.3: Flux changes for ROI_{GLOBAL}, $ROI_{HIGH\text{-}FLUX}$, and $ROI_{LOW\text{-}FLUX}$. Values presented as mean (p-value).

	Phenylephrine	GTN
ROI_{GLOBAL}	-14.8 (<0.001)	+18.9 (<0.001)
$ROI_{HIGH\text{-}FLUX}$	-23.1 (<0.001)	+22.1 (<0.001)
$ROI_{LOW\text{-}FLUX}$	-9.0 (<0.001)	+11.8 (<0.001)

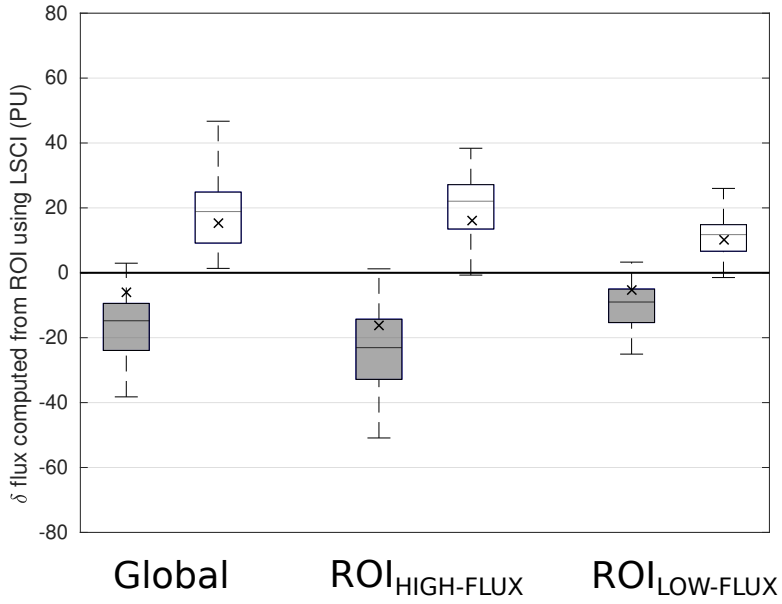


Figure 7.7: Flux changes in response to phenylephrine and GTN. The box and whisker plots demonstrate observed changes between the rest and peak drug infusion periods (section 4.9.1). δ in y axis label represents 'change in'. The mean changes are shown as an x. Phenylephrine infusion was associated with a decrease in skin flux in both $ROI_{HIGH\text{-}FLUX}$ and $ROI_{LOW\text{-}FLUX}$, but the decrease in the $ROI_{HIGH\text{-}FLUX}$ was greater. Similarly, GTN infusion was associated with an increase in skin flux in both sub-regions, but a greater magnitude increase in $ROI_{HIGH\text{-}FLUX}$.

7.5.3.2 $ROI_{LOW\text{-}FLUX}$

The mean global flux at rest during the phenylephrine session was 76.5 (95% CI 67.0 - 86.1) flux units. During the peak phenylephrine effect, the change in $ROI_{LOW\text{-}FLUX}$ flux was a decrease of 9.0 (IQR 5.0 - 15.3) ($p < 0.001$).

The mean global flux at rest during the GTN session was 77.9 (95% CI 89.0 - 110.9). At peak GTN effect, the corresponding change was an increase of 11.8 (IQR 6.7 -

14.8) ($p < 0.001$).

7.5.3.3 $\mathbf{ROI_{GLOBAL}}$

The mean global flux at rest during the phenylephrine session was 119.6 (95% CI 107.1 - 132.0) flux units. During the peak phenylephrine effect, the median change in ROI_{GLOBAL} flux was a decrease of 14.8 (IQR 9.4 - 23.9) ($p < 0.001$).

The mean global flux at rest during the GTN session was 122.9 (95% CI 103.8 - 142.0). During the peak GTN effect, the corresponding change was an increase of 18.9 (IQR 9.2 - 24.9) ($p < 0.001$).

7.5.3.4 Difference between $\mathbf{ROI_{HIGH\text{-}FLUX}}$ and $\mathbf{ROI_{LOW\text{-}FLUX}}$

During the peak phenylephrine effect, the mean difference between the change in $ROI_{HIGH\text{-}FLUX}$ flux and $ROI_{LOW\text{-}FLUX}$ flux was 12.9 (IQR 7.1 - 22.7) ($p < 0.001$). During the peak GTN effect, the corresponding difference was 9.1 (IQR 5.2 - 13.5) ($p = 0.001$).

7.5.3.5 Section summary

In this section, the sub-region differences in skin flux response to phenylephrine and GTN were described. As I hypothesised, the areas with the highest rest period flux ($ROI_{HIGH\text{-}FLUX}$) showed the greater magnitude decrease in flux in response to phenylephrine compared to the areas with the lowest rest period flux ($ROI_{LOW\text{-}FLUX}$). These responses were similar to those observed for $ROI_{HIGH\text{-}TEMP}$ and $ROI_{LOW\text{-}TEMP}$ (section 7.4) with the thermal imager.

In contrast to the findings from thermal data presented in section 7.4, $ROI_{HIGH\text{-}FLUX}$ showed a significantly greater increase in flux in response to GTN in comparison to

$ROI_{LOW\text{-}FLUX}$. There are several potential explanations for this. With the thermal data, there was an increase in the background/environmental temperature which may have acted as a confounding factor. A calibration step was added to account for this (figure F.1), but it is possible that the increase in background temperature had a similar effect on the response observed in the two sub-regions.

The difference in GTN response may also be secondary to a difference between skin temperature response to vasodilation and LSCI-measured change in skin blood flow. Conductive heat transfer to the skin surface may occur from GTN-induced vasodilation in the deeper tissues, leading to a generalised increase in temperature in both $ROI_{HIGH\text{-}TEMP}$ and $ROI_{LOW\text{-}TEMP}$ sub-regions.

7.6 Changes occurring between the rest and peak periods in all sub-regions

7.6.1 Introduction

If the two sub-regions within an area of skin do respond differently as shown in sections 7.4 and 7.5, there is a potential clinical utility in first identifying the skin sub-regions with the greatest magnitude change and monitoring them instead of monitoring the global region. The results presented in the previous two sections suggest that ROI_{GLOBAL} changes may be reduced in comparison to the changes seen in perforator regions. In this final section of this chapter, I explore the different response profiles of the sub-regions.

Throughout chapter 6 and in the current chapter to this point, the data for the rest and the peak periods from the drug infusion sessions have been compared. This simplified analysis has been performed as the rates of change were expected to vary from person to person, and the main concern was the *direction* of change for all parameters presented. The differential response in skin regions presented

in sections 7.4 and 7.5 suggested that the sub-regions with the highest baseline skin radiance ($ROI_{HIGH\text{-}TEMP}$) and baseline flux ($ROI_{HIGH\text{-}FLUX}$) have a greater response to induced changes in the underlying circulation in comparison to the sub-regions with the lowest baseline skin radiance ($ROI_{LOW\text{-}TEMP}$) and baseline flux ($ROI_{LOW\text{-}FLUX}$). The direction of change remained the same across the sub-regions.

A greater magnitude change in certain sub-regions (that may be identified *a priori* based on measurements during the rest state as performed in section 7.3) offers a potential method of detecting small changes earlier by monitoring more sensitive regions and hence having a greater signal-to-noise ratio. Sub-regions with greater response may additionally show deviation from baseline at an earlier point, allowing earlier detection of changes and more sensitive trend monitoring. I hypothesise that the sub-regions with greater magnitude response ($ROI_{HIGH\text{-}TEMP}$ and $ROI_{LOW\text{-}TEMP}$) would show earlier response to pharmacologically induced vasoconstriction and dilation, further supporting the use of sub-region monitoring. I explore this question using the thermal camera data, by considering skin radiance changes occurring during the dose escalation phase of the two drug infusion sessions.

Plotting the changes over the 10 escalation steps leading to the peak changes explored in section 7.4 can also support the assumption that the peak drug effect period selected were the periods with maximum vasoconstriction and vasodilation. In addition, instead of comparing the $ROI_{HIGH\text{-}TEMP}$ and $ROI_{LOW\text{-}TEMP}$ only, I also use the data from the middle 80%.

7.6.2 Methods

The same analysis method as described in section 7.4 was used. In addition to the rest and peak periods (defined in section 4.8.1), ten additional periods of interest were added, each taken from the step-wise increase in dose occurring every minute

(figure 4.1, from t = 5 minutes to t = 15 minutes labelled 'infusion rate escalation'). Each escalation period was one minute in length, consisting of 3600 thermal camera images collected at 60Hz (section 4.6.1). The same $ROI_{HIGH\text{-}TEMP}$ and $ROI_{LOW\text{-}TEMP}$ regions previously defined in section 7.3 were tracked. As described in section 4.10.3, two participants did not tolerate the escalation in GTN dose. They only contributed data points up to their maximum level of escalation they tolerated (levels 7 and 9).

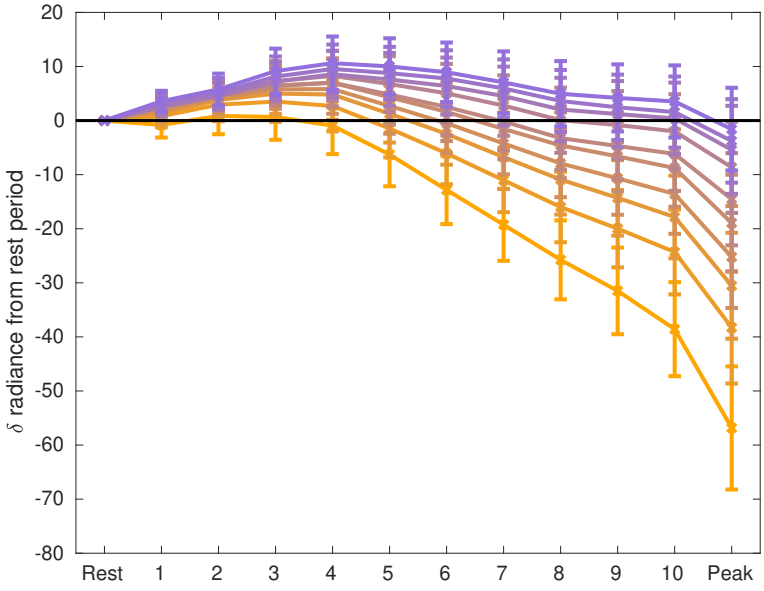
In addition to the two previously defined ROIs, a further 8 sub-regions also classified according to the baseline or rest state skin radiance were used in the analysis. The sub-regions were defined as decile groups. $ROI_{HIGH\text{-}TEMP}$ represented the top 10% baseline radiance ROIs, then another subgroup represented the 10 to 20^{th} centile baseline radiance ROIs and so on, down to $ROI_{LOW\text{-}TEMP}$ representing the 90 to 100^{th} (or the bottom 10%) baseline skin radiance ROIs.

In line with the analysis presented in section 7.4, the calibrated median changes were plotted, after adjusting for the increase in background radiance (Appendix F). Alongside the median changes, the standard errors were plotted in the figures to show the range of values surrounding the median.

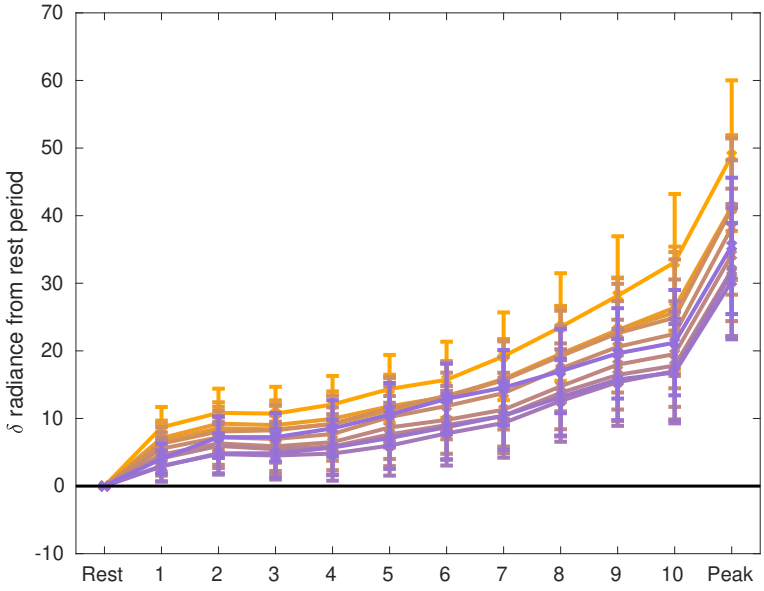
The analysis presented in this section was performed for both a sense-check of the sub-region differences presented in section 7.4 and to display the pattern of change between the two periods of interest (defined in section 4.8.1), rather than to discover the precise dose where the differences between the sub-regions becomes statistically significant (which would not be clinically meaningful beyond the data presented).

7.6.3 Results

The skin radiance change from baseline measured for the ten sub-regions for the phenylephrine and GTN sessions at each dose increment are shown in figure 7.8.



(a) Phenylephrine session changes



(b) GTN session changes

Figure 7.8: Median change in radiance observed in response to phenylephrine and GTN: all time periods. δ in y axis label represents 'change in'. Instead of comparing only the two periods of interest ('rest' and 'peak' defined in section 4.8.1), all values from the step-wise increase in drug infusion rates were included in this analysis to determine the progression and determine how the results from $ROI_{HIGH\text{-}TEMP}$ (amber) and $ROI_{LOW\text{-}TEMP}$ (purple) compared to the remaining 80% of sub-regions within ROI_{GLOBAL}. The middle 8 sub-regions are colour-coded as a gradient from $ROI_{HIGH\text{-}TEMP}$ (amber) to $ROI_{LOW\text{-}TEMP}$ purple. The 10 steps along the x-axis shows the drug dose escalation levels up to level 10 ('peak'). Step 10 represents t = 14 to 15 - the first minute at the maximum infusion rate. The error bars represent standard errors.

7.6.3.1 Phenylephrine

An initial increase in radiance was present in most of the sub-regions when compared to the rest period. As shown in figure 7.8a, the changes in skin radiance in the sub-regions followed the order of baseline radiance deciles. The sub-region with the highest baseline radiance ($ROI_{HIGH\text{-}TEMP}$, represented in amber) showed the greatest decrease in radiance in response to phenylephrine. The sub-region with the lowest baseline radiance ($ROI_{LOW\text{-}TEMP}$, represented in purple) showed the least decrease in radiance in response to phenylephrine. The sub-regions lying between displayed responses between these two extremes, with the order following the original ranking order (represented as the graded colour changes from amber to purple).

7.6.3.2 GTN

The 10 sub-region responses to GTN are shown in figure 7.8b. An increase in skin radiance was observed in all 10 sub-regions. The greatest magnitude increase in radiance in response to the GTN infusion was observed in $ROI_{HIGH\text{-}TEMP}$, and the smallest magnitude increase in radiance was observed in $ROI_{LOW\text{-}TEMP}$. Compared to the phenylephrine infusion plot (figure 7.8a), there was a smaller range of sub-region responses to GTN.

7.6.4 Section summary

The analysis shown in this section contextualises the results previously presented in section 7.4. I have shown that the previously reported difference between $ROI_{HIGH\text{-}TEMP}$ and $ROI_{LOW\text{-}TEMP}$ were preceded by divergent results during the drug escalation phase. This was clearer for phenylephrine infusion sessions (figure 7.8a) where greater differences between the two extreme sub-regions were observed, compared to the GTN infusion sessions (figure 7.8b).

The change in radiance value between level 10 and 'peak' period following linear trends prior to level 10 may be accounted for by the larger gap between these two periods of interest. Level 10 occurred between minutes 14 to 15 (the first minute of the maximum infusion rate), while the 'peak' period was taken from the constant maximum infusion period (section 4.8.1, figure 4.1).

In both phenylephrine and GTN infusion sessions, the two extreme deciles defined using baseline features ($ROI_{HIGH\text{-}TEMP}$ and $ROI_{LOW\text{-}TEMP}$) demonstrated the greatest and the least change in response to both drug infusions. The magnitude of the skin radiance change was ordered according to baseline temperature in the phenylephrine sessions. This was more difficult to appreciate in the GTN session where the responses were less variable across the sub-regions, although there was a greater increase in $ROI_{HIGH\text{-}TEMP}$ in comparison to $ROI_{LOW\text{-}TEMP}$.

The decision to use deciles (as opposed to other percentage subsets) for sub-region response was not based on physiological reasons. However, the difference between the decile sub-regions does seem to be greatest between the top decile and the next, with smaller differences between the sub-regions with the lower baseline skin radiance (represented by the purple lines in figure 7.8). This was easier to appreciate in the phenylephrine results for which sub-region variation was greater.

7.7 Chapter summary

In this chapter, a series of related analyses from thermal and LSCI imaging from the MOLLIE study have been presented. At the beginning of the chapter, I hypothesised that sub-regions of skin will respond differently to the pharmacologically induced vasoconstriction and vasodilation, and that the difference in response will be related to the locations of the cutaneous perforators.

The first section verified the previous findings that thermal video cameras can be used to visualise the variable rate of rewarming from a uniformly cooled state. The regions with the highest rate of rewarming have previously been shown to correlate well with the locations of cutaneous perforators [78, 94]. Higher-resolution images of the previously described 'hot spots' (section 1.2.2.4) were obtained (compared to previous thermographic cutaneous perforator studies), with the changes in shape of the hot spots from a single dot followed by linear streaks branching out from the dot. The shapes were suggestive of a vascular morphology, following the literature description of arterial perforators (section 1.4). The consistency of baseline radiance patterns was shown by selecting the top and bottom decile sub-regions using rest state data (prior to drug infusions). A statistically significant sub-region difference in response to phenylephrine infusion using both thermal and LSCI imaging was observed. In contrast, the same two sub-regions showed a statistically significant difference in flux changes associated with the GTN infusion, but not skin radiance difference.

In section 7.4, several potential mechanisms for the significant difference in magnitude of sub-region differences to phenylephrine but not GTN were proposed. Results in section 7.6 showed that the similarity between the two sub-regions in response to GTN was maintained throughout the experimental period. The statistically significant difference in flux response to GTN (section 7.5) suggests that the use of thermal imaging as a modality may have played a role. It may be that thermal radiance from skin is not a direct proxy measurement for skin perfusion.

The sub-region differences described in this chapter would be difficult to appreciate from a purely clinical assessment. Within-region skin temperature gradients (e.g., comparing sub-regions within the thigh) are likely to be difficult to identify clinically because of limitations in both the thermal sensitivity resolution and the spatial acuity of clinical assessment by a clinician's hand. High resolutions in both

elements are required to detect whether temperature gradients exist within a region of skin solely using clinical examination. This sensory detection resolution - dependent on the density of innervation - has been studied using Weber Two-Point Discrimination Test [287, 288]. The result shows a high variation in sensitivity across the body, and is significantly worse on the human palm (used for skin temperature assessment) compared to the fingertip [289]. The difference between $\text{ROI}_{\text{HIGH-TEMP}}$ and $\text{ROI}_{\text{LOW-TEMP}}$ was statistically significant (figure 7.8) but may be difficult to gauge clinically.

The skin regions overlying the localised arterial perforators may reflect the macrocirculation more closely, with closer agreement to the global haemodynamic changes. The regions most distal to the perforators ($\text{ROI}_{\text{LOW-TEMP}}$) may be more reflective of the microvasculature, representing flow in the smallest vessels. As well as selectively allowing more sensitive monitoring of the global changes (by tracking $\text{ROI}_{\text{HIGH-TEMP}}$), the results point to a new hypothesis that a dual/concurrent monitoring of the macro- and microvasculature may be possible using video cameras. This is particularly exciting given the emerging evidence that a loss of coherence between the macro- and microcirculation is associated with increased morbidity and mortality [22, 290].

The next chapter returns to the data collected by the RGB camera, first presented in chapter 6. Building on the regional differences observed in thermal camera and laser speckle contrast imager data, the chapter will explore whether baseline features measured using the RGB camera can similarly be used to classify sub-regions, and whether these sub-regions show differential response to induced vasoconstriction and vasodilation.

8

Implications of perforator locations on RGB imaging

Contents

8.1 Introduction 174
8.2 Methods 177
8.2.1 Selection of the region of interest 177
8.2.2 Sub-region selection 177
8.2.3 Comparison of ROI_{HIGH} and ROI_{LOW} 178
8.2.4 Changes occurring between the rest and peak periods in all sub-regions 179
8.2.5 Sub-region proximity to perforator locations defined in chapter 7 179
8.3 Results 180
8.3.1 Locations of ROI_{HIGH} and ROI_{LOW} 180
8.3.2 Absolute change in PPGi amplitude in the sub-regions . 182
8.3.3 Changes occurring between the rest and peak periods in all sub-regions 183
8.3.4 Proximity of ROI_{HIGH} to perforator zones 186
8.4 Discussion 186

8.1 Introduction

Chapter 6 reported a change in both the peak-to-trough amplitude (AC) and the baseline (DC) of the PPGi waveform in response to phenylephrine and GTN infusions. The changes measured were the spatially averaged responses from ROI_{GLOBAL}, selected as the largest rectangle that could be fitted over the anterior thigh (e.g., figure 6.8). In chapter 7, a series of results using thermal and laser speckle contrast imaging (LSCI) data suggested the existence of sub-regions within ROI_{GLOBAL}. These results were the basis for the hypothesis that the pharmacologically-induced changes observed from ROI_{GLOBAL} consisted of averaged results from sub-regions with larger magnitude change ($ROI_{HIGH\text{-}TEMP}$ in thermal imaging and $ROI_{HIGH\text{-}FLUX}$ in LSCI) and other sub-regions with smaller magnitude change ($ROI_{LOW\text{-}TEMP}$ in thermal imaging and $ROI_{LOW\text{-}FLUX}$ in LSCI). Figure 7.8 showed that the sub-regions displayed a graded response to the underlying haemodynamic changes, the magnitude of which was related to baseline or rest state parameters measured from those sub-regions.

A large shift in underlying physiology may be detected using the global averaging method, as demonstrated in chapter 6. However, smaller changes or changes selectively affecting either the perforator zones or non-perforator zones (as defined in section 7.1) may be lost in the gross average signal represented by ROI_{GLOBAL}. The results presented in chapter 7 indicated that perforator and non-perforator zones behaved differently in response to induced skin perfusion changes. Section 7.3 indicated a close spatial relationship between the locations of perforators estimated using the tourniquet release technique and the sub-regions with the highest resting state thermal radiance. Although identification of perforator zones using LSCI was not attempted in the previous chapter, the top and bottom decile sub-regions defined *a priori* using baseline perfusion flux were similarly different in their responses to phenylephrine and GTN.

The average PPGi waveform responses associated with phenylephrine and GTN infusions measured from ROI_{GLOBAL} may also represent averaged results from sub-regions with greater and smaller magnitude responses to the pharmacologically induced variation in perfusion. This hypothesis is explored in the current chapter.

Rationale for hypothesis The AC amplitude of the pulsatile PPGi waveform measured from a region of interest (ROI) represents the magnitude of the difference between the peak and trough reflected light intensity from that region of skin. The regions with the highest AC amplitude at rest are likely to represent skin regions with the highest degree of cardiosynchronous pulsatility.

The anatomy of skin and the arterial blood supply was reviewed in section 1.2. Arterial blood supply to the skin surface is provided by cutaneous perforators. The current understanding of skin perfusion anatomy suggests that maximum changes in both the RGB and temperature signals within the cardiac cycle would occur where the cutaneous perforators are located, close to the skin surface. These superficial arteries (skin macrocirculation) have a higher degree of pulsatility and pressure variation compared to the capillary networks making up the skin microcirculation (section 1.3). Therefore, greater response to the two infusions would be expected in these sub-regions than the sub-regions maximally distant from a perforator. These latter sub-regions will be least able to respond to the infused agents, being dependent on the perfusion status of the cutaneous perforators. The thermal and LSCI results presented in chapter 7 did follow this pattern.

If skin perfusion anatomy and the presence of cutaneous perforators are responsible for the response patterns observed in the thermal and LSCI data, I would expect the same response pattern in the RGB data, with greater magnitude changes in the zones representing perforator locations. Although each camera in the MOLLIE study monitored the thigh skin from a different angle (figure 4.3), I would expect

a reasonably close agreement between the locations of the high-response decile sub-regions across different imaging modalities. The agreement between the thermal and LSCI data was not explored as the cameras were too distal from each other, with different ROI_{GLOBAL} sizes for the two modalities. The ROI overlap between the RGB and thermal camera data is greater, and so the agreement between the high-response decile sub-regions for the two modalities is explored in this chapter.

Hypothesis I hypothesised that the sub-regions of skin with the greatest PPGi waveform pulsatility at baseline (greatest peak-to-trough amplitude of the AC component of the PPGi waveform) will show a greater variation in pulsatility in response to pharmacologically induced vasoconstriction and vasodilation compared to the sub-regions of skin with the smallest waveform pulsatility at baseline (lowest magnitude of AC component).

Based on the rationale described above that the greater pulsatility is seen for the cutaneous perforator locations and the least pulsatility from regions distal from them, I hypothesised that these two sets of sub-regions selected on the basis of baseline PPGi waveform amplitude will represent the extremes of the variation in response to the drug infusions. I hypothesised that a graded variation in response to the drugs would be observed across all 10 decile sub-regions defined using the baseline AC amplitude of the PPGi waveform (in line with results of section 7.2.3, also displayed in figure 7.8).

I further hypothesised that the sub-regions with the greatest AC amplitude for the PPGi waveform pulsatility at baseline would be spatially consistent in an individual between the two drug sessions. I expected the sub-regions with the smallest AC amplitude at baseline to be similarly consistent across the two drug sessions. In addition, I hypothesised that there would be a spatial agreement between the sub-regions with the greatest PPGi waveform pulsatility (largest peak-to-trough

amplitude for the AC component) and the previously identified $ROI_{HIGH\text{-}TEMP}$ from section 7.4.

8.2 Methods

The RGB camera images previously analysed in chapter 6 were re-analysed using the sub-region methodology described in chapter 7. Throughout this chapter, ROI_{GLOBAL} refers to the same tracked regions analysed in chapter 6.

8.2.1 Selection of the region of interest

The de-bayered image files generated using the steps described in section 4.8.3 were used for separate processing of the three colour channels. The global ROIs used in chapter 6 (ROI_{GLOBAL}) were split into smaller 30 x 30 square ROIs (equating to 15 x 15 square in the de-bayered images as a result of the GBRG layout of the three-colour pixels, see figure 4.4). This ROI size was selected as a compromise between the requirement to have a sufficiently large ROI to generate a pulsatile PPGi waveform with good signal-to-noise ratio and the requirement to have numbers of sub-regions comparable to those used in the analyses of the thermal and LSCI data.

8.2.2 Sub-region selection

The sub-region analysis of chapter 7 was repeated to assess local (sub-region) responses in RGB data using the AC amplitude of the in PPGi waveform. In line with previous methodology, a baseline parameter was required with which to define the sub-regions *a priori*. Sub-regions were selected using the previously computed AC amplitude of the local PPGi waveform, a necessary step in the average peak-to-trough waveform amplitude calculations in chapter 6 (as described in section 6.2.1). The mean peak-to-trough waveform amplitude (AC component) for each 30 x 30 pixel ROI sub-region was computed for all images from the 2-minute rest period.

The 30 x 30 sub-regions were then ranked, from the sub-region with the highest AC component amplitude to the sub-region with the smallest AC component amplitude. The following two sub-region groups were defined for each session. Those with:

- The top decile rest/baseline peak-to-trough waveform amplitude, labelled 'ROI_{HIGH}'.
- The bottom decile rest/baseline peak-to-trough waveform amplitude, labelled 'ROI_{LOW}'.

Any ROI in the top or bottom decile was selected, whether or not it was part of a spatial cluster. Consistency between the locations of ROI_{HIGH} and ROI_{LOW} for each participant across the two drug sessions was assessed using the Sørensen-Dice similarity index (as described in section 7.3 and figure 7.3). An allowance of 15 x 15 pixel distance was used to account for any minor movement between the two drug sessions when calculating the Sørensen-Dice similarity index.

8.2.3 Comparison of ROI_{HIGH} and ROI_{LOW}

The primary parameter of interest was the absolute change in the peak-to-trough amplitude of the AC component of the PPGi waveform. The change in the amplitude was measured from the baseline (rest period, as defined in section 4.8.1) to the time of the peak drug effect. The mean peak-to-trough amplitude of the AC component was calculated for each 2-minute period of interest using the estimates from the 20-second running windows shown in figure 6.2. As in chapter 7, the two extreme sub-region responses were compared against each other, and the statistical significance of change in each sub-region from baseline to peak drug effect was assessed using the Wilcoxon sign rank test. As in section 7.4, the difference in response between ROI_{HIGH} and ROI_{LOW} was assessed using the Wilcoxon rank sum

test.

The changes in the red and blue channels were reported as secondary outcomes.

8.2.4 Changes occurring between the rest and peak periods in all sub-regions

In section 7.6, the full response profiles between the rest and peak periods of interest were presented by analysing the step-wise drug infusion escalation period (figure 7.8). The response from the remaining 80% of sub-regions were also described by plotting all 10 decile sub-region responses. In order to determine whether the sub-region differences observed in thermal imaging are replicated when using the AC amplitude of the PPGi waveform, the same analysis method was employed for the RGB video camera data analysis.

The same methodology as in section 8.2.2 was used, but with the analysis extended to include all 10 deciles. As with the analysis of section 7.6, the data from the previously defined rest and peak periods of interest and from the additional time periods taken from t=5 to t=15 were analysed.

8.2.5 Sub-region proximity to perforator locations defined in chapter 7

The agreement between the locations of ROI_{HIGH} (from the RGB camera dataset) and the locations of $ROI_{HIGH\text{-}TEMP}$ (from the thermal camera dataset, defined in section 7.3) was assessed using the Sørensen-Dice similarity index (figure 7.3).

As the two cameras recorded images taken from different camera angles and positions (figure 4.3), the images were not perfectly aligned. In addition, the images from the two cameras were acquired at different resolutions (960 x 1280 pixels for the

RGB camera images and 512 x 640 pixels for the thermal camera images). The locations of perforators in the thermal images were determined from binary images (consisting of 0s and 1s) as described in section 7.3.2.2. The locations of ROI_{HIGH} were also used to generate binary images, using 1 for the ROI_{HIGH} sub-regions and 0 for all other regions. The two sets of binary images from the two imaging modalities had different sizes because of the different image resolutions for the two modalities.

In order to fairly compare the similarity in locations, the ROI_{GLOBAL} regions were aligned manually for each participant using the raw leg images but without knowledge of the ROI_{HIGH} or $ROI_{HIGH\text{-}TEMP}$ locations. The offsets between the corners of the rectangular regions (ROI_{GLOBAL}) were measured and manually compensated for. The binary images from the two modalities were scaled to have equal size to allow a fair similarity index calculation.

8.3 Results

RGB video camera images from all 30 participants were available for analysis.

8.3.1 Locations of ROI_{HIGH} and ROI_{LOW}

The mean Sørensen-Dice similarity index between phenylephrine and GTN rest periods was 0.67 (95% CI 0.63 to 0.71) for ROI_{HIGH} and 0.73 (95% CI 0.69 to 0.78) for ROI_{LOW}. Both correspond to "substantial agreement" according to the previously used Sørensen-Dice similarity index interpretation table (table 7.1). Three examples of designated sub-regions according to the AC mplitude of the PPGi waveform are shown in figure 8.1 for a visual comparison.

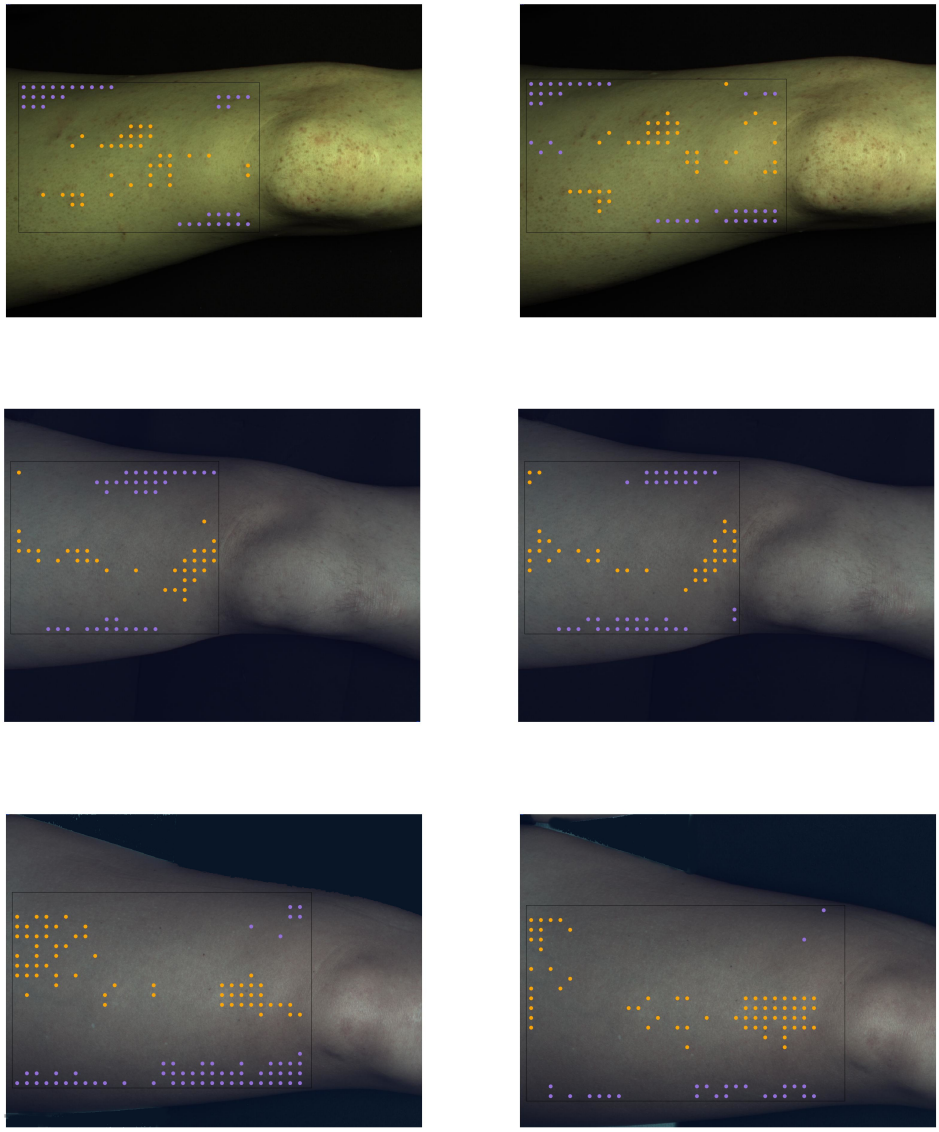


Figure 8.1: Paired ROI_{HIGH} (amber) and ROI_{LOW} (purple) in 3 individuals. The left-hand column (a) shows the phenylephrine rest session, and the right-hand column (b) shows the GTN rest session. Across all 3 participants, there is consistency in the zones with highest and lowest PPGi waveform AC amplitude.

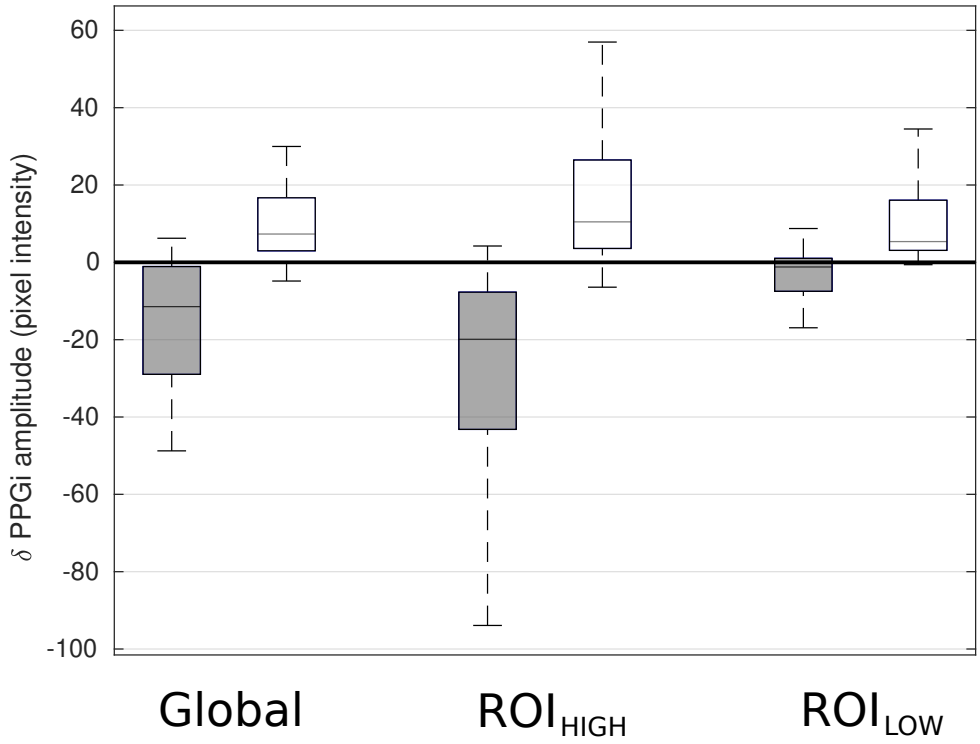


Figure 8.2: Differential response in RGB sub-regions: Rest-to-peak absolute change in PPGi waveform AC amplitude. δ in y axis label represents 'change in'. Phenylephrine session results are shown in grey; GTN session results are shown in white. The ROI_{GLOBAL} response previously presented in chapter 6 is shown first on the left. The PPGi amplitude changes in the two sub-regions are shown as ROI_{HIGH} and ROI_{LOW}. The two sub-regions defined using baseline/resting state PPGi waveform amplitude show different responses to both phenylephrine and GTN, with more marked responses for ROI_{HIGH}.

8.3.2 Absolute change in PPGi amplitude in the sub-regions

During the peak phenylephrine effect, the median absolute change in the peak-to-trough amplitude of the AC waveform in ROI_{HIGH} from its baseline value in the green channel was a decrease of 19.9 (IQR 7.7 - 43.2) pixel units ($p < 0.001$). The corresponding change in ROI_{LOW} was a decrease of 1.2 (IQR -7.5 to 1.0) pixel units ($p = 0.15$) from baseline. The two responses were significantly different from each other ($p < 0.001$). The mean absolute changes are shown in table 8.1.

During the peak GTN effect, the median absolute change in peak-to-trough

Table 8.1: Differential response in RGB sub-regions: Phenylephrine

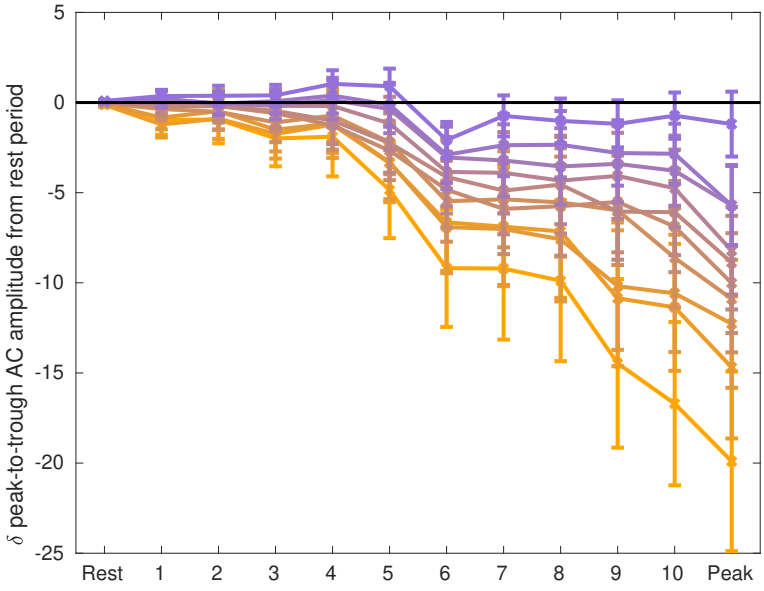
Colour channel	ROI	Mean change (pixel intensity)	Difference from ROI_{HIGH} (p value)
Red	ROI_{GLOBAL}	-4.4	
	ROI_{HIGH}	-7.3	
	ROI_{LOW}	+0.9	+8.2 (<0.001)
Green	ROI_{GLOBAL}	-15.4	
	ROI_{HIGH}	-27.7	
	ROI_{LOW}	-2.4	+25.3 (<0.001)
Blue	ROI_{GLOBAL}	-4.1	
	ROI_{HIGH}	-6.0	
	ROI_{LOW}	-0.4	+5.6 (<0.001)

amplitude of the AC waveform in ROI_{HIGH} from its baseline value in the green channel was an increase of 10.5 (IQR 3.6 - 26.5) pixel units ($p < 0.001$). The corresponding change in ROI_{LOW} was an increase of 5.4 (IQR 3.1 - 16.1) pixel units ($p < 0.001$) from baseline. The two responses were not significantly different ($p = 0.42$). The mean absolute changes are shown in table 8.2.

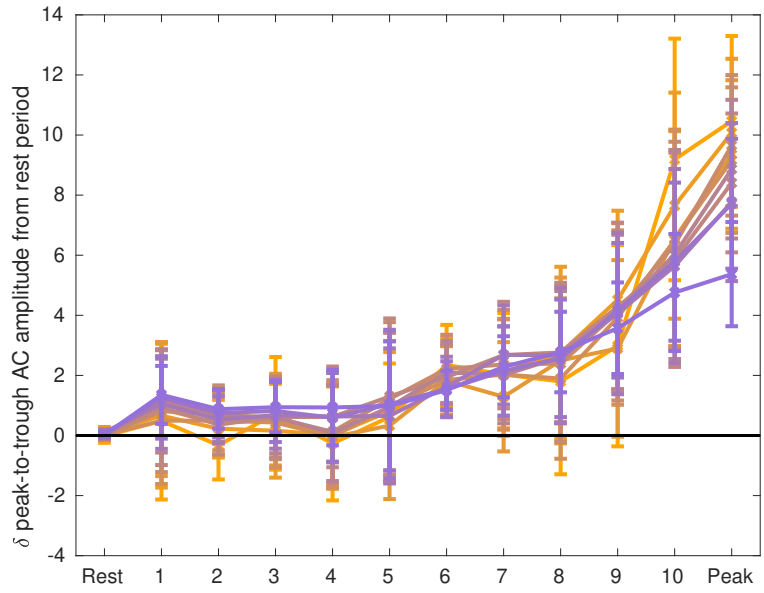
Corresponding results for red and blue channels are shown in tables 8.1 and 8.2, and further expanded in appendix I. Percentage changes in the PPGi AC amplitude values in the sub-regions in all three channels are also presented in appendix I.

8.3.3 Changes occurring between the rest and peak periods in all sub-regions

The changes in peak-to-trough amplitude of the AC component of the PPGi waveform in the 10 sub-regions from baseline to peak infusion period are plotted in figure 8.3.



(a) Phenylephrine session changes



(b) GTN session changes

Figure 8.3: Median change in peak-to-trough amplitude of the AC component of the PPGi waveform, observed in response to phenylephrine and GTN: all time periods. δ in y axis label represents 'change in'. Instead of comparing only the two periods of interest ('rest' and 'peak' defined in section 4.8.1), all values from the step-wise increase in drug infusion rates were included in this analysis to track the progression over time and determine how the results from ROI_{HIGH} (amber) and ROI_{LOW} (purple) compare to the remaining 80% of sub-regions within ROI_{GLOBAL}. The 10 steps along the x-axis shows the drug dose escalation levels up to level 10 ('peak'). Step 10 represents t = 14 to 15 - the first minute at the maximum infusion rate.

Table 8.2: Differential response in RGB sub-regions: GTN

Colour channel	ROI	Mean change (pixel intensity)	Difference from ROI_{HIGH} (p value)
Red	ROI_{GLOBAL}	+4.7	
	ROI_{HIGH}	+6.4	
	ROI_{LOW}	+4.2	-5.2 (0.16)
Green	ROI_{GLOBAL}	+11.6	
	ROI_{HIGH}	+14.5	
	ROI_{LOW}	+10.2	-4.3 (0.42)
Blue	ROI_{GLOBAL}	+3.4	
	ROI_{HIGH}	+5.1	
	ROI_{LOW}	+2.7	-2.4 (0.11)

8.3.3.1 Phenylephrine

A decrease in the peak-to-trough amplitude of the AC component was observed in response to phenylephrine across all 10 sub-regions. The magnitude of this decrease was related to the baseline amplitude that was used for the ranking of the sub-regions as described in section 8.2.2. The sub-region with the greatest baseline amplitude (ROI_{HIGH}) showed the greatest magnitude decrease in the peak-to-trough amplitude. The sub-region with the smallest baseline amplitude (ROI_{LOW}) had the smallest magnitude decrease in the peak-to-trough amplitude. The response curves for the regions falling between the two extreme deciles fell between the response curves for ROI_{HIGH} and ROI_{LOW} (figure 8.3a).

8.3.3.2 GTN

The 10 sub-region responses to GTN are shown in figure 8.3b. All 10 sub-regions showed an increase in the peak-to-trough amplitude of the AC component of the PPGi waveform associated with the GTN infusion. The responses of the sub-regions were uniform throughout the majority of the dose escalation phase. By the peak infusion point (point 10 and 'peak' periods), ROI_{HIGH} had a greater magnitude increase in the peak-to-trough amplitude of the AC component compared

to ROI_{LOW}, but the differences were smaller compared to the differences observed in the phenylephrine session (figure 8.3a). As with the thermal responses seen in figure 7.8b, the responses of the middle sub-regions fell approximately in the order of the original classification although the curves were closer together with heavily overlapping error bars.

8.3.4 Proximity of ROI_{HIGH} to perforator zones

The Sørensen-Dice similarity index between ROI_{HIGH} (RGB) and $ROI_{HIGH\text{-}TEMP}$ (thermal) was 0.44 (95% CI 0.38 to 0.51). This indicated 'moderate agreement' between the two sub-regions (table 7.1).

8.4 Discussion

There are several novel findings presented in this chapter.

1. There are sub-regional differences in the AC amplitude of the PPGi waveform. The sub-regions with the top 10% largest AC amplitudes at baseline were consistent in each individual across the two drug sessions (figure 8.1). These sub-regions were defined using the baseline AC amplitude computed using the video camera images from a 2-minute period. Across two drug session rest periods, participants showed substantial agreement in both ROI_{HIGH} and ROI_{LOW} locations within ROI_{GLOBAL}. A moderate agreement was observed between ROI_{HIGH} and $ROI_{HIGH\text{-}TEMP}$ using the Sørensen-Dice similarity index.

2. A significant difference was observed between the ROI_{HIGH} and ROI_{LOW} responses to phenylephrine-induced vasoconstriction. ROI_{HIGH} had a greater magnitude absolute and percentage decrease in peak-to-trough amplitude of the AC component in comparison to the values for ROI_{LOW}. Skin sub-region differences in the AC amplitude of PPGi waveform have not previously been demonstrated.

3. Both ROI_{HIGH} and ROI_{LOW} showed a significant increase in the AC amplitude as a result of the GTN infusion. The absolute increases between the two sub-regions were not significantly different across all three channels. In the green channel, ROI_{LOW} showed a significantly greater percentage increase in the AC component amplitude in comparison to equivalent value for ROI_{HIGH}. This was not replicated in the red and blue channels. A similar type of response in the sub-regions associated with the GTN infusion was previously reported for thermal imaging (section 7.4).

ROI selection for video camera-based monitoring has so far been largely convenience-based. Regions in prior work have been selected either based on which skin regions are practically available for recording data, or chosen for the highest quality waveforms detected [259]. In this chapter, a greater change in response to phenylephrine was detected in a sub-region of skin defined *a priori* from its baseline AC amplitude of the PPGi waveform. The values of the AC amplitude for ROI_{HIGH} showed a greater decrease in response to phenylephrine than the values for ROI_{GLOBAL}. A decrease in the signal-to-noise ratio by including the values from regions with minimal response in ROI_{GLOBAL} data leads to a decrease in the sensitivity of RGB camera detection of perfusion changes. As discussed in chapter 1, improving the signal-to-noise ratio is an important part of any physiological measurement from video camera images [291].

Regional differences in the AC component of the PPGi waveform are also of interest in the context of the use of pulse transit time to estimate blood pressure from PPGi data. Pulse transit time measured using electrocardiography and contact PPG (usually from the fingertip) has previously been shown to be inversely correlated with systolic blood pressure under most conditions [206]. Based on this principle, previous work has used video camera-derived pulse transit time from PPGi to estimate blood pressure [179, 180]. It has been shown that pulse arrival at the skin

surface is dependent on the ROI selection [255]. ROI selection for image-derived pulse transit time measurement is particularly important in view of the findings presented in this chapter. The distance between the ROIs selected for transit time measurements and the distance from the ROI to the cutaneous perforator that supplies the ROI would be expected to affect the pulse arrival time. Pulse transit time computation from perforator zones may be better correlated with the contact PPG measurements of pulse transit time.

In this chapter - as in the previous chapter - two sub-regions were compared by selecting the top and bottom deciles of a baseline parameter. In both chapters, the underlying assumption was that $ROI_{HIGH\text{-}TEMP}$, $ROI_{HIGH\text{-}FLUX}$, and ROI_{HIGH} all correlate with the location of the perforator zone. In contrast, the data from $ROI_{LOW\text{-}TEMP}$, $ROI_{LOW\text{-}FLUX}$, and ROI_{LOW} provide different information. Across all three imaging modalities, phenylephrine effects on the two sub-regions were greater than the GTN effects. The changes observed in the non-perforator sub-regions may be more reflective of the skin microcirculatory response, compared with the perforator zones that directly overlie arteries and more closely reflect the macrocirculation.

This gradient between the sub-regions may be used clinically. As mentioned in chapter 1, poor macrocirculation is associated with poor microcirculation, but it is possible to have microcirculatory dysfunction co-existing with normalised macrocirculation [65]. Monitoring the coherence between macro- and microcirculation has been proposed as being particularly important in sepsis [22, 290]. Treating skin sub-regions as eing representative of either the macro- or the microcirculation and studying the gradient between the responses as presented in this chapter may provide further information to infer the underlying haemodynamic status.

9 Conclusions

Contents

9.1 Conclusions 189
9.1.1 Contributions of this thesis 189
9.1.2 Limitations 198
9.2 Future directions 201
9.2.1 PPGi waveform analysis from the MOLLIE study dataset 201
9.2.2 Analyses from the Arterial Perforator Imaging study . . 201
9.2.3 Future clinical studies 203
9.3 Concluding remarks 206

9.1 Conclusions

9.1.1 Contributions of this thesis

Skin perfusion is a dynamic process in a constant flux, changing over multiple time scales. Changes occur within each cardiac cycle, reflected in the cardiac-synchronous signal represented by the PPGi waveform. The frequency of this waveform is used for heart rate and respiratory rate estimation using video cameras with a high degree of accuracy [161] (section 3.2). Skin perfusion changes also occur acutely over a longer time frame of minutes to hours depending on the fluid balance and haemodynamic status of the subject, and chronically over months to years as a result

of chronic disease states [2, 3]. During acute skin perfusion changes in response to varying cardiac output, the vessel anatomy of perfusion remains the same. The two main variables leading to skin perfusion changes are the diameter of the involved blood vessels and the number of capillary network vessels recruited. A fine control of both elements by global and local mechanisms (discussed in section 1.3) leads to a rapid and appropriate response to global haemodynamic status. In contrast, chronic perfusion changes are usually attributed to irreversible changes in the vasculature as a result of a disease process (e.g., diabetes or rheumatological conditions [292]). These chronic changes have thus far been the focus in the development of perfusion monitoring tools such as laser speckle contrast imager [7].

The aim of this thesis was to focus on the shorter term changes in skin perfusion that occur in association with underlying haemodynamic status, and improve upon the current clinical, subjective assessment. The overarching hypotheses at the start of the thesis were:

- Video camera monitoring adds objectivity to the currently available and used visual clinical assessment of the skin.
- Pharmacologically induced vasoconstriction and vasodilation are associated with opposite direction changes in several parameters that can be measured using video cameras.
- The location of cutaneous perforators affect the signals acquired at the skin surface.
- The location of cutaneous perforators should be taken into account during region of interest selection for tracking/monitoring of haemodynamic status.

Before analysing the video data, the usefulness of skin perfusion assessment in the form of skin mottling detection was presented in chapter 2. Three large critical care databases were reviewed for documentation of skin mottling in the lower limbs.

Having mottled skin was associated with increased odds of adverse outcomes even when adjusted for the severity of illness. This is in line with previous reports that clinical assessment of mottling can outperform some of the macrohaemodynamic parameters in predicting patient outcomes [9, 61].

The MOLLIE study combined two experimental methods to create a dataset on which to test my hypotheses. Peripheral vasoconstriction and vasodilation were induced in healthy subjects using two intravenous drug infusions. Phenylephrine and GTN were chosen because of their well-described clinical effects and safety profile in healthy populations. The two infusions had largely opposite clinical effects as predicted. Following the drug infusion sessions, a lower limb tourniquet was applied and removed under monitoring to locate cutaneous perforators. Known sources of commonly encountered signal noise, such as variable lighting and subject movement, were controlled to create the best-possible dataset for hypothesis testing.

From chapter 5 onwards, the focus of analysis shifted first from using cameras to measure direct correlates of visible parameters (i.e., skin mottling), followed by measuring parameters not visible to the naked eye. In chapter 5, an image analysis method for skin mottling assessment using edge detection algorithms was proposed. Phenylephrine infusion was associated with an increase in the (mean) amount of edges or contrast within a skin region. Conversely, GTN infusion was associated with a decrease in the same parameter. The magnitude of the increase in the amount of edges/contrast was greater in the subgroup who were clinically determined to show new skin mottling, compared to the control subgroup who did not. The work presented suggests that the proposed image analysis method corresponding to visual diagnosis may be implemented using video camera imaging, with potentially increased sensitivity. The edge/contrast changes were measured from the thigh region, using the hypothesis that sub-clinical changes may occur in

the thigh although mottling is known to be first noted around the knee [11, 101].

In chapter 6, I demonstrated changes in overall skin perfusion detected using the same parameters as in contact photoplethysmographic (cPPG) waveform analysis. Photoplethysmographic imaging (PPGi) waveforms were computed from the global thigh skin region (ROI_{GLOBAL}). Methods for processing the PPGi waveform for vital sign monitoring have been extensively studied [161]. Two features of the PPGi waveforms from the MOLLIE study participants were shown to change in response to the two drug infusions. The change in reflected light intensity measured by the video camera pixels during each cardiac cycle - measured as the peak-to-trough amplitude of the pulsatile PPGi waveform - decreased in response to phenylephrine (vasoconstriction) and increased in response to GTN (vasodilation). Similarly, the baseline of the PPGi waveform (DC) decreased in response to phenylephrine and increased in response to GTN. To further characterise this latter change in the DC component, the measured RGB values were converted to an alternative colour space (HSV) known to best indicate skin *colour* changes independent of ambient luminance [262]. The changes in the DC baseline of the PPGi waveform were shown to include skin colour changes, with significant changes occurring along the colour hue dimension. The hue changes were in opposite direction with phenylephrine and GTN infusions.

Building on the global changes shown in chapter 6, chapter 7 presented a series of results from thermal and laser speckle imaging modalities, building the argument that sub-regions of the thigh responded differently to the drug-induced haemodynamic changes. The chapter began by reporting high-resolution images of cutaneous perforators acquired following limb exsanguination, application of a thigh tourniquet, and timed release of the tourniquet. The consistency of resting state skin radiance (measured at baseline) was subsequently demonstrated, highly suggestive of a relationship between the baseline/resting state patterns in radiance and the locations

of cutaneous perforators. The top decile sub-region defined using the baseline skin radiance ($ROI_{HIGH\text{-}TEMP}$) showed a greater magnitude decrease in temperature in response to phenylephrine infusion in comparison to the bottom decile sub-region ($ROI_{LOW\text{-}TEMP}$). This sub-region difference between skin areas that could be assigned *a priori* from baseline parameters was replicated in the laser speckle contrast imager (LSCI) results, where the $ROI_{HIGH\text{-}FLUX}$ regions showed a greater magnitude decrease in flux in response to phenylephrine and a greater increase in flux in response to GTN. Finally, analysis of the full study period including the 10-step drug dose escalation showed a range of responses in the 10 decile sub-regions defined using baseline skin radiance, confirming the differential response of the sub-regions.

The analysis presented in chapter 8 was based on the methodology of the previous chapter, but applied to the RGB image data presented in chapter 6. Differential arrival times for the PPGi waveform on the skin surface had previously been demonstrated [255], but an underlying explanation (anatomical or otherwise) for these differences and their implications for clinical monitoring had not previously been explored. Based on the results presented in chapter 6, sub-regions were determined using the peak-to-trough amplitude of the AC component of the PPGi waveform. This metric had already been shown to decrease on average across ROI_{GLOBAL} in response to phenylephrine and increase on average in response to GTN (chapter 6). The results of the sub-region ROI analyses for the RGB data mirrored the results of chapter 7 for the thermal data. The sub-regions with the greatest peak-to-trough amplitude of the PPGi waveform at baseline (ROI_{HIGH}) showed greater magnitude absolute changes in response to drug-induced vasoconstriction and vasodilation compared to the sub-regions with the smallest peak-to-trough amplitude of the pulsatile PPGi waveform at baseline (ROI_{LOW}). The locations of these sub-regions were highly consistent in each individual.

Across the three imaging modalities presented in this thesis (RGB, thermal, and LSCI), the patterns in sub-region responses to phenylephrine were highly consistent. In contrast, the sub-region responses to GTN were less consistent across the three imaging modalities. RGB and thermal imaging both demonstrated non-significant differences between the corresponding top and bottom decile sub-regions, although the difference between the sub-regions was significant for LSCI. In section 7.4, several potential explanations for the observed differences in the sub-region response patterns to the phenylephrine and GTN infusions were proposed. Which of these factors is most responsible is unclear, but it may be a combination of the differential specificity of site of action of the two drugs [105], and an intrinsic hysteresis effect in the vasodilation and vasoconstriction of vessels [284]. The existence of sub-regions within the skin which can be explained by the anatomy of skin surface perfusion has several clinical implications for the development of video camera monitoring of physiological variables. These are presented in the next section.

9.1.1.1 Clinical

The results presented in this thesis have several clinical implications.

Skin perfusion assessment is a routine element of cardiovascular examination. The current gold standard method of skin perfusion measurement in acute care is a subjective assessment based on metrics such as skin colour, temperature, and capillary refill time [4] (section 1.4.1). This subjective assessment has been shown to be a good [9, 61] or better [20] indicator of prognosis in critically ill patients than systemic or macrovascular haemodynamic parameters. The RGB video camera and thermal camera used in the MOLLIE study provide an objective equivalent of the visual and tactile assessment performed by a clinician.

There are two strengths of the monitoring presented in this thesis.

Objectivity Both skin mottling and skin temperature are parameters that can be subjectively assessed at the bedside. The work presented in chapter 5 suggests a possible method of objectively detecting skin mottling and assessing its severity. Similarly, the decreased skin radiance in response to phenylephrine and the increased radiance in response to GTN offer a possible method of objectively detecting skin temperature changes.

Sensitivity In addition to objectivity, video camera monitoring provides sensitivity greater than that achieved by visual inspection or the examining hand. The increase in edges/contrast reported in chapter 5 was observed in a different skin region to the knee where one would expect mottling to occur first. The identified PPGi waveform amplitudes that change with phenylephrine and GTN infusions may be used for objective monitoring of perfusion changes.

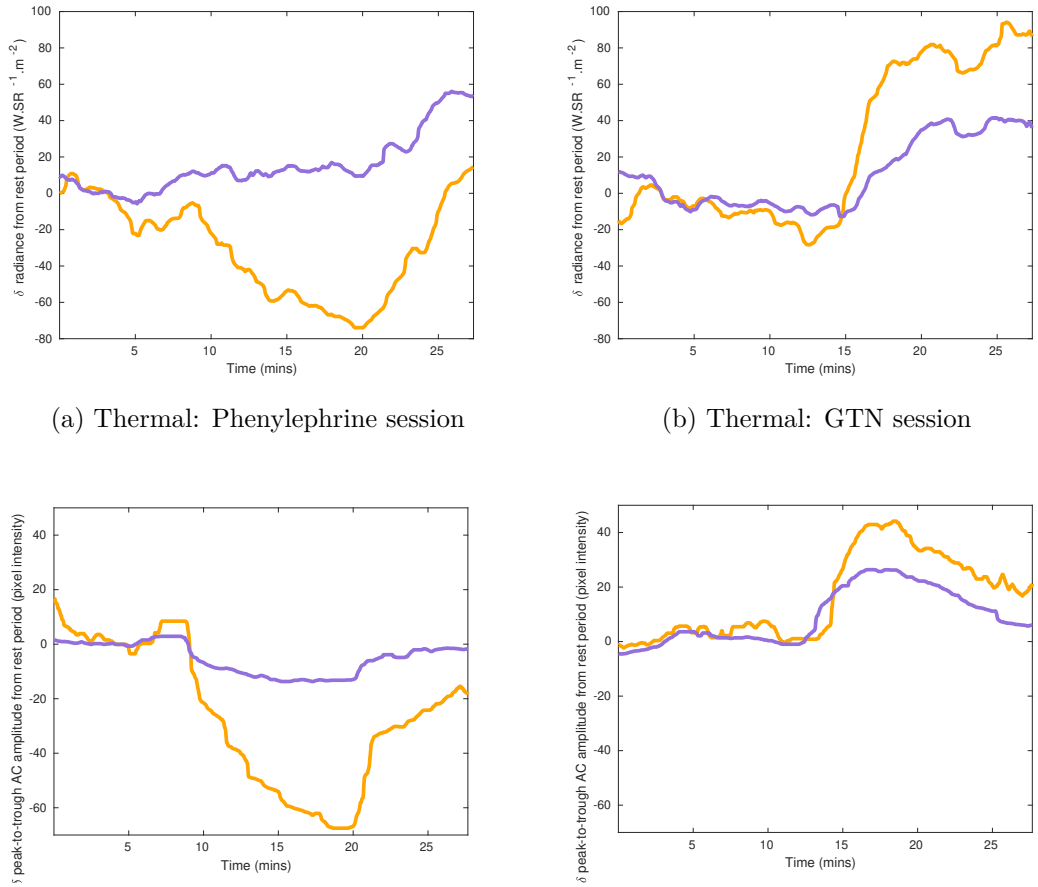
The results presented in chapter 5 further expand the potential use of video camera monitoring for skin mottling detection, using simple image processing tools. Furthermore, the opposite response induced via GTN suggested that it is possible to become 'less mottled' than at baseline. Skin mottling has previously been treated as a clinical sign that is either present or absent (with the only scale being provided by the size of the area affected), but the contrast results suggest that it is possible to quantify the degree of mottling in a given area.

The results presented in chapters 7 and 8 show that the skin surface is not uniform in its response to variation in the underlying haemodynamics. There were variations in response across a limited region of skin in the anterior thigh, a phenomenon observed with all three imaging modalities: RGB, thermal, and LSCI. In all three modalities, a baseline parameter (the AC amplitude of the pulsatile PPGi waveform for RGB imaging, skin radiance for thermal imaging, and skin perfusion flux for LSCI) was used to define regions of interest with opposite responses. There were

similar responses for all three top decile regions, labelled as ROI_{HIGH}, $ROI_{HIGH\text{-}TEMP}$, $ROI_{HIGH\text{-}FLUX}$ in RGB, thermal, and LSCI modalities respectively. These top decile regions all deviated further from the resting state measurements in response to phenylephrine when compared with the lower decile sub-regions. The two sub-region responses differed less in response to GTN. There is little prior work to offer an explanation of these differences. This observed pattern may be a result of a more selective effect of phenylephrine on the macrovasculature within the skin (where it is expected to exert larger effect via vasoconstriction of arterioles), whereas GTN may cause a more widespread response. The regions furthest away from the perforator vessels may better represent the status of the microvasculature. The results may also reflect the starting vascular or sympathetic tone of the participants. This in turn would be expected to be related to both participant factors (e.g., internal temperature and fluid balance status) and environmental factors (e.g., room temperature).

Throughout the thesis, I have presented population level data from the MOLLIE study. The trends and changes presented were average responses to the drug infusions across the 30 participants. Although this is important for demonstrating the applicability of this type of monitoring, the variation in baseline measurements among the participants (e.g., the absolute light intensity at baseline measured by the RGB camera from the skin of different participants) sometimes makes demonstration of average response across the population more difficult. Relative changes from baseline were reported in an attempt to standardise the magnitude of change across participants.

Whilst individual participant data was not presented in chapters 5 to 8, in a clinical scenario the monitoring technology presented may have a role as a trend monitor. An example of an individual response to the two drug infusions is shown in figure 9.1, which shows the variation in sub-region responses in one individual for both



(a) Thermal: Phenylephrine session

(b) Thermal: GTN session

(c) RGB: Phenylephrine session

(d) RGB: GTN session

Figure 9.1: Individual responses to phenylephrine (left column) and GTN (right column), recorded using a thermal camera (top row) and RGB camera (bottom row). Amber shows the response of the top decile sub-region ($ROI_{HIGH\text{-}TEMP}$ in thermal and ROI_{HIGH} in RGB) and purple shows the response of the bottom decile sub-region ($ROI_{LOW\text{-}TEMP}$ in thermal and ROI_{LOW} in RGB). The y-axis shows change in skin radiance (top row) or peak-to-trough amplitude of AC component (bottom row) from rest period (defined as mean of t = 2 to t = 4 minutes). All plots show absolute change from baseline.

thermal (top row) and RGB (bottom row) imaging. The first column shows the plots corresponding to the phenylephrine session, and the second column the plots corresponding to the GTN session. Each of the four plots shows the trend over the entire experimental period as demonstrated in figure 4.1, including the recovery period once the infusions were stopped (minutes t = 20 to t = 28). Monitoring of these trends in individuals in clinical practice may help target therapies.

9.1.1.2 Video-camera monitoring field

As discussed in section 3.3, physiological monitoring using video cameras has so far been limited to vital-sign monitoring. Much of this has been driven by the perceived value of non-contact systems in monitoring, and the widespread availability of smartphones with video camera functionality (section 3.2). There is also a growing interest in consumer health monitoring with increasing availability of wearable monitors. Most applications work by identifying/segmenting skin from non-skin zones, and extracting the PPGi waveform from the skin area [195, 258, 293], usually averaging across large skin areas to extract the vital-sign data.

In contrast, the overarching aim of this thesis has been to consider the PPGi signal available at the skin surface with regard to the locations of known underlying structures. In this way, interpretation of the signal becomes more physiologically relevant. If the PPGi waveform reflects vascular changes, the anatomy of the vascular system should not be ignored.

9.1.2 Limitations

The MOLLIE study and the analyses presented in this theses have several limitations.

9.1.2.1 Dataset

Although the MOLLIE study allowed us to explore hypotheses I had formulated, it is a single, limited dataset and there are several elements of the dataset that impose limitations. It was conducted using healthy volunteers with a median age of 29 years. Changes in vessel compliance occur with ageing [294, 295] and so there is likely to be a decrease in signal-to-noise ratio in an older population. The recruited population however represented a range of skin colours, measured using two recognised skin colour scales (section 4.10).

In the study, intravenous drug infusions were used to induce changes in skin perfusion. A standard weight-based dosing regimen was followed (up to tolerance by participants due to side effects, with maximum 30% variation in mean arterial pressure allowed for safety). Hence the variations in skin perfusion caused by the infusion protocol differ from the changes seen during acute illness when not driven by medication with a specific mechanism of action. For example, the body's feedback loop response to reduced central blood pressure during hypovolaemic shock is tachycardia and peripheral vasoconstriction, which means that low blood pressure, tachycardia, and reduced peripheral perfusion would co-exist. This is in contrast to our dataset for which phenylephrine induced peripheral vasoconstriction, which causes an increase in central blood pressure and bradycardia. How the results presented in chapters 5 to 8 apply to clinical scenarios requires further work. This also relates to the next section on the translation into clinical settings.

9.1.2.2 Translation into clinical practice

In the MOLLIE dataset, the *a priori* sub-region allocation/labelling could be performed because participants had normal physiology prior to the drug infusion. This is in contrast with critical care settings in which participants are frequently the least well upon arrival. Furthermore, any resuscitation measures for cardiovascular support may involve administration of inotropic and vasopressor agents, with known effect on peripheral perfusion. Vasopressors in particular are known to affect cutaneous perforator diameter (hence are avoided where possible post skin graft surgery to minimise the risk of graft ischaemia). It is possible, therefore, that identification of sub-regions may be more challenging in clinical settings. Whether local (sub-region) differences in PPGi waveform amplitude are reduced in magnitude or even exist in disease is unknown and requires further work.

In addition, a large proportion of patients admitted to the critical care unit have co-morbidites including cardiovascular disease and diabetes, both of which affect

peripheral perfusion. How the video camera-derived skin surface parameters behave in patients with abnormal baseline perfusion and how they respond to underlying haemodynamic changes also requires further work. This also raises the question of how chronic perfusion changes (where vascular anatomy is more directly affected) affect the PPGi signal.

9.1.2.3 Equipment

There are several implementation issues for the methodologies developed in this thesis that would need to be solved before they could be deployed in clinical settings. Addressing these issues is outside the scope of this thesis but the following represent initial considerations:

- Data size;
- Real-time analysis;
- Privacy concerns.

The MOLLIE study generated approximately 700Gb of imaging data for each participant (for approximately 60 minutes of recording). High-resolution images at high frame rates were collected for the study data. Any 'offline' analysis will be limited by the storage requirements for the generated images. This highlights the need for real-time analysis which is also important for clinical translation of this type of monitoring. The concept presented in chapters 7 and 8 whereby baseline metrics were used to select sub-regions *a priori* demonstrates the potential to limit the regions of interest being selected, allowing more selective storage and processing. Work towards real-time analysis will also address privacy concerns as this decreases the need to store images.

9.2 Future directions

In the remainder of this chapter and thesis, potential future directions for this work are presented. Immediate further questions that could be addressed with the current dataset from the MOLLIE study are described first. A related dataset that has been collected is then presented, and potential questions that could be explored using this dataset are set out. Following that, two future projects that have been planned using the findings from the work presented in this thesis are described.

9.2.1 PPGi waveform analysis from the MOLLIE study dataset

In chapters 6 and 8, two PPGi waveform metrics were used as outcome measures: the peak-to-trough amplitude of the AC component, and the DC component amplitude. These two metrics were selected based on their extensive use in cPPG analysis [165].

In the cPPG literature, several other waveform features have been described and their relationship with cardiovascular status have been explored. The pulse width (usually defined as the pulse width at the half-height of the systolic peak) and the pulse area (total area under the PPG waveform curve) have been investigated as alternative metrics [266, 267].

Preliminary analysis of the cPPG waveforms in the MOLLIE dataset has shown that these features also change with drug-induced blood pressure variations [206]. Further work is planned to investigate the corresponding PPGi waveform features.

9.2.2 Analyses from the Arterial Perforator Imaging study

A second dataset has been collected for 15 volunteers in a study titled "Arterial Perforator Imaging study" (Research Ethics Approval R80079/RE001 from University

of Oxford Interdivisional Research Ethics Committee, appendix B). Participants underwent video monitoring using the same RGB camera, thermal camera, and LSCI monitor (as described in sections 4.6.1 and 4.6.2.3). The same cameras set-up was used, but the thigh regions of interest were outlined using skin labels visible in all three modalities, clearly outlining the ROI_{GLOBAL} being measured. All participants underwent the tourniquet release procedure described in section 4.5.2. The study completed in June 2022. Two further analyses using the dataset are planned, as described below.

9.2.2.1 Alignment of multiple cameras

The three cameras in the MOLLIE study were positioned to record from the same anatomical area as much as possible (figure 4.3), but had to be placed at different locations and angles so that they could all include the same region of skin without generating shadow artefacts. I did not anticipate the significance of this and the subsequent challenge of aligning the images to enable direct comparison of the data acquired for the three imaging modalities. The skin labels used in this study will be used for further work on automated alignment of images collected by multiple cameras from different angles.

9.2.2.2 Persistence of hot spots

Of the 15 participants in the second study, 6 had also taken part in the MOLLIE study. I aimed to recruit from the same participants in order to study the persistence of the hot spots, hypothesised to indicate the perforator zones (section 7.4.1).

In the 6 participants who took part in both studies, two sets of tourniquet release monitoring images (with 2.5 year interval between the two sessions) are available. The persistence of $ROI_{HIGH\text{-}TEMP}$ and $ROI_{LOW\text{-}TEMP}$ will be analysed using the methodology described in section 7.3.2.2. If persistence of the hot spots can be

demonstrated, this would support an anatomical basis for their location.

9.2.3 Future clinical studies

Two clinical studies have been planned based on the hypotheses generated from the MOLLIE study analyses.

9.2.3.1 ICU

Skin mottling was introduced in chapter 1 as a clinical sign of microvascular failure and hypoperfusion. It is a skin appearance frequently observed in ICU patients [148]. Chapter 2 evidenced that skin mottling is linked to the odds of ICU mortality and hospital mortality. In the last decade, a mottling score to quantify the extent of mottling visually (from 0 to 5) has been shown to be associated with mortality risk [12, 144, 148]. No attempts have been made to either detect or quantify skin mottling using video cameras. Chapter 5 showed how this may be achieved using an edge-detection algorithm and quantifying the total amount of linear streaks at the skin surface. Phenylephrine infusion was associated with a significant increase in the mean Kirsch contrast in $\mathrm{ROI}_{\mathrm{GLOBAL}}$. In addition, the subgroup identified by clinicians as being mottled had a significantly higher increase in mean Kirsch contrast from baseline compared to those who were deemed not mottled.

I propose an observational study in patients admitted with septic shock, defined as sepsis and systolic blood pressure < 90 mmHg or mean arterial pressure < 65 mmHg despite fluids, requiring vasopressors on admission. These definitions have previously been used in other critical care studies in the septic population.

Patients would be monitored with RGB and thermal cameras, with a baseline measurement period followed by intermittent shorter measurements at set intervals (e.g., 6h and 24h after admission). This is in line with other critical care mottling

studies and the associated interval assessment protocol. In addition to video camera monitoring, I will aim to collect clinical observation of skin mottling including the mottling score. Other objective parameters of haemodynamic status (heart rate, systolic/mean/diastolic blood pressure, plasma lactate) would be collected in addition to details of intravenous medication and fluids given.

I hypothesise that changes in visually diagnosed skin mottling (measured using the mottling score [11]) would be correlated with the mean Kirsch operator contrast, with a reduction in contrast being associated with a reduction in visible mottling.

The currently known association between mottling score and mortality has not so far changed patient management. This proposed clinical study on skin mottling would aim to improve on current practice by making this assessment more objective (and it might also detect 'pre-visible-mottling' changes). In addition, rather than just showing an association between clinically visible mottling and mortality, the study would investigate whether a shorter-term or even contemporaneous relationship existed between haemodynamic status and mottling appearance.

9.2.3.2 Diabetes

Diabetes mellitus is a disorder resulting from the body's inability to produce insulin, and is a major global health issue with estimated prevalence of 9.3% [296]. The lifetime incidence of foot ulcers in patients with diabetes is between 15 and 25% [297]. Diabetic foot (ulceration from a combination of poor perfusion and peripheral neuropathy) is one of the commonest complications of diabetes and has a significant morbidity. Early diagnosis of peripheral arterial disease is critical and limb saving. Once diagnosed, a combination of better glycaemic control, pharmacological therapy (antiplatelets and statins), exercise programme, surgical revascularisation can all improve prognosis [298]. Diabetic foot clinic assessments usually include a visual assessment of feet, ankle-brachial pressure index (ABPI),

and monofilament assessment for neuropathy.

ABPI is used to quantify peripheral arterial disease. It is a ratio between ankle cuff pressure (the pressure at which the Doppler arterial pulsatile signal is first audible) and brachial cuff pressure. A value of 1.0 is normal; a value less than 1.0 indicates poorer lower limb perfusion. The measurement of ABPI has been shown to be highly subjective [299, 300]. Furthermore, many patients with peripheral arterial disease are asymptomatic and the value of ABPI assessment in the asymptomatic population is unknown [301]. Peripheral neuropathy in diabetes is thought to be secondary to small vessel disease in the peripheries – i.e., necrosis of peripheral nerves. Microvascular reactivity is impaired in those with type 2 diabetes, but to an even greater extent in those also affected by peripheral neuropathy [302].

Peripheral perfusion monitoring may allow indirect method of detecting the progress of diabetes. The BSP-ML Group has investigated the assessment of peripheral artery haemodynamics using infrared video thermography [280]. Laser speckle imaging of the lower limb skin in patients with diabetes to determine post-exercise recovery has also been reported [303]. In peripheral neuropathy/microvascular disease, there is a post-exercise decrease in skin perfusion, which then recovers over a period of approximately 20 minutes [304]. A prolonging of this recovery period has been shown in patients with peripheral neuropathy, presumed to be related to diabetic neuropathy in the autonomic nervous system. Even patients with sub-clinical neuropathy show delayed recovery [303].

A video camera could allow foot monitoring before and after exercise (quantifying the decrease in perfusion and subsequent perfusion recovery). Both the ROI_{GLOBAL} PPGi parameters presented in chapter 6 or the sub-region monitoring described in chapter 8 could provide clinically useful information. As both macro- and microvascular disease are present in diabetes, I hypothesise that dual monitoring of

the perforator and watershed zones (and the ratio between the two) may help to quantify the severity of disease.

I anticipate that the study would take place in primary or secondary care diabetes foot clinics, with a protocolised exercise test (e.g., six minute walk test). Pre-existing diabetes foot assessments would be carried out alongside the camera imaging.

The association between perfusion changes/response and the degree of vascular disease/neuropathy has previously been explored with laser speckle imaging [303] but not with RGB cameras. The latter offers the potential of developing an app for home measurement of foot status using smartphone camera, with the outline of the foot shown on the screen to trigger recording by the patient followed by the 6-minute walk test (for which a smartphone app using the phone's accelerometer and GPS already exists – [305]). Post-exercise monitoring would then take place using the app and smartphone camera. Higher frequency assessment at home (e.g. 3-monthly rather than the annual foot check) would become possible.

9.3 Concluding remarks

The work presented in this thesis has explored how video cameras may provide insight into haemodynamic status by assessing skin perfusion. It is only by combining what is known about the skin as an organ and its blood supply that we can fully understand the information present in the measured parameters at the surface. Measuring perfusion using video cameras provides both an objective assessment similar to the subjective assessment made by clinicians, and a more sensitive monitor than the human visual system. The parameters of interest investigated in this thesis have the potential to provide valuable insights in the clinical domains in which skin perfusion is currently measured.

Appendices

A

Prognosis associated with skin mottling

Contents

A.1 Systematic review of skin mottling literature 208
A.1.1 Introduction 208
A.1.2 Methods 208
A.1.3 Results 209
A.1.4 Discussion 212

A.1 Systematic review of skin mottling literature

A.1.1 Introduction

I have performed a systematic review of the skin mottling literature in order to understand the current evidence for monitoring skin mottling and its associated outcomes.

A.1.2 Methods

I registered this study on PROSPERO (CRD42019147285). I searched MEDLINE, Embase, and the Cochrane library using truncated search terms (mottl*) and (critical* OR intensive* OR ICU OR sepsis OR septic) in July 2019.

A.1.2.1 Inclusion and exclusion criteria

I included any hospital-setting studies assessing critically ill or septic adult populations. I included any study with assessment of mottling status with or without the Mottling Score. I excluded any studies performed in neonatal or paediatric critical care units. I also excluded studies that included patients with other known causes of skin mottling (e.g., vasculitis) unless this group was clearly separated in the analysis.

A.1.2.2 Outcomes

The primary outcome of interest was mortality, which could be ICU/hospital, or time-limited (e.g., 7, 14, 28-day mortality). Secondary outcomes of interest were ICU length of stay, hospital length of stay, need for ventilatory or renal support, vasopressor use, and any associated reference haemodynamic measurements.

A.1.3 Results

415 titles were screened following duplicate entry removal. Following the article selection process as shown in Figure 5.3, 23 studies were included.

The majority of included studies (17/23, 74%) took place in ICUs or emergency departments in France. There were three further studies within Europe, and one from each of Asia, North America, and South America. Sixteen studies (16/23, 70%) were within populations with diagnosis of sepsis or septic shock. Two studies included all ICU patients while the remainder were in specific groups such as sepsis, liver cirrhosis, or patients undergoing weaning from mechanical ventilation.

The size of studies varied from 14 to 777 participants (median = 103, s.d. = 259).

Incidence of mottling estimates across the included studies vary from 2.5% [137] to 70% [11]. Across all studies reporting the incidence, mean incidence was 33% (averaged over 4726 subjects in 21 studies). Among patients with sepsis or septic shock, incidence was higher at 44%. Within the septic population, Cheng et al.

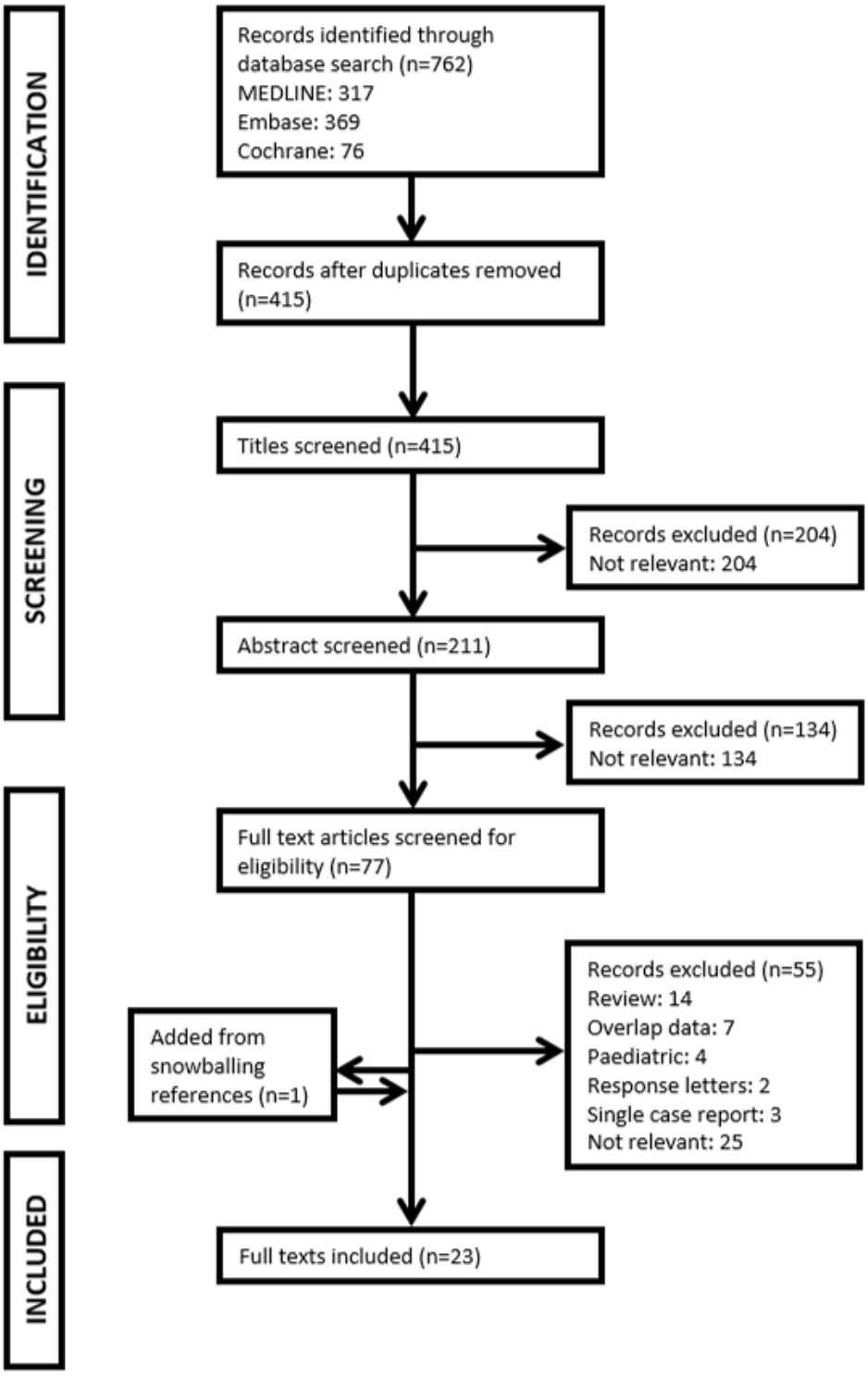


Figure A.1: PRISMA flow diagram.

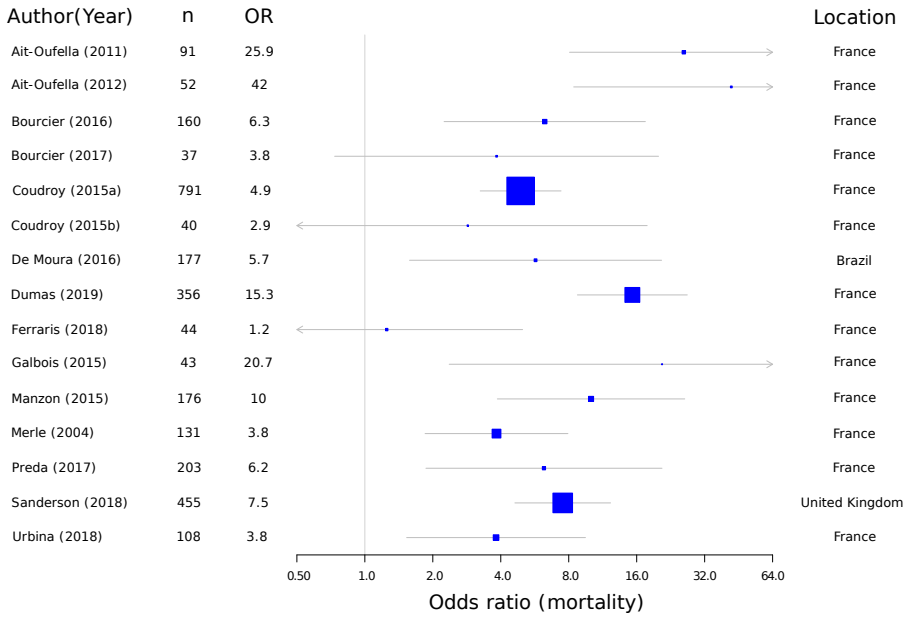


Figure A.2: Forest plot of mortality odds ratio associated with skin mottling. n = number of subjects, OR = odds ratio

[306] found mottling incidence of 4.8% within two hospitals in Taiwan. This latter study also found no significant mortality association with mottling. This may have been secondary to the low incidence in both survivor and non-survivor groups. It may also be secondary to difficulty in diagnosing mottling in this different racial population. Several studies [11, 12, 115, 139, 148, 151, 307, 308] excluded patients with dark skin from their studies. Therefore, it is difficult to estimate the incidence of mottling across populations from the literature.

The mortality associated with skin mottling varied across the studies. Of 15 studies that reported the associated mortality, 12 showed a significant increase in mortality with any degree of mottling while 3 showed non-significant increase in mortality (Figure 5.4). Of the studies that used the Mottling Score and therefore could report the associated mortality depending on the severity of mottling, the unadjusted odds ratio for mortality between no mottling and most severely mottled groups ranged between 11 [151] and 74 [11].

A.1.4 Discussion

Mottling is a visible skin phenomenon which accompanies a severe degree of skin hypoperfusion and endothelial dysfunction. There has been a heightened interest in mottling studies within the critical care community over the last decade. A few studies that have adjusted the odds ratio have shown that the predictive mortality from mottling exceeds those expected from the illness severity scoring systems [144, 146].

It is notable that a large proportion of studies were performed in uniform settings within one country in Europe. Other studies in general ICU populations (not just septic patients) may provide further insight into this phenomenon.

B

Ethics approval documents

Included in this section:

1. Ethics approval for Mapping Of Lower Limb skIn pErfusion study
2. Ethics approval for Arterial Perforator Imaging study

MEDICAL SCIENCES INTERDIVISIONAL RESEARCH ETHICS COMMITTEE

Research Services, University of Oxford, Wellington Square, Oxford, OX1 2JD
Tel: +44(0)1865 616577 Fax: +44(0)1865 280467
ethics@medsci.ox.ac.uk

CONFIDENTIAL

Ref: R63796/RE001

Dr Mirae Harford
Critical Care Research Group (Kadoorie Centre)
Nuffield Department of Clinical Neurosciences
University of Oxford
Level 3, John Radcliffe Hospital
Oxford

16th July 2019

Dear Mirae

Research Ethics Approval - CUREC 3

Study Title: Video-based non-contact physiological monitoring using skin perfusion mapping of lower limbs

Short Title: Mapping Of Lower Limb skIn pErfusion (MOLLIE)

The above application has been considered by the Medical Sciences Interdivisional Research Ethics Committee (IDREC) in accordance with the procedures laid down by the University for Ethical Approval of all research involving human participants.

I am pleased to inform you that, on the basis of the information provided to the IDREC, the proposed research has been judged as meeting appropriate ethical standards, and approval has been granted for a period of **2 years**, commencing on **16th July 2019**. The reference number for this study is **R63796/RE001**.

This is **subject to:**

a) **it is your responsibility to comply with the requirements for administering any tests or questionnaires and if in doubt to contact the publisher of those tests or questionnaires.**

b) **if new research staff are engaged, the PI is responsible for ensuring they are suitably qualified by training and/or experience**

I would like to remind you that you will be required to submit an annual progress report on each anniversary of study approval, until the study is completed, and that your study may be selected for review by the MS IDREC during an annual audit.

Amendments

Should there be any subsequent changes to the study, you should first submit details to CTRG and, once approved by them, to the IDREC for consideration and approval. Details of changes must be listed on an amendment form.

Please do not hesitate to contact me if you have any queries.

Yours Sincerely

H. Barnby-Porritt

Dr. Helen Barnby-Porritt
Research Ethics Manager, Medical Sciences

MEDICAL SCIENCES INTERDIVISIONAL RESEARCH ETHICS COMMITTEE
Research Services, Boundary Brook House, Churchill Drive, Headington, Oxford, OX3 7GB
Tel: +44(0)1865 616575
ethics@medsci.ox.ac.uk

CONFIDENTIAL

Professor Lionel Tarassenko & Dr Mirae Harford
Institute of Biomedical Engineering
Department of Engineering Science
University of Oxford
Parks Road
Oxford

23 March 2022

Dear Professor Tarassenko and Dr Harford,

Research Ethics Approval - CUREC 2

Ethics Approval Reference: R80079/RE001

Study title: Isolation of arterial perforators using non-contact video cameras

Short title: Imaging arterial perforators

The above application has been considered on behalf of the Medical Sciences Interdivisional Research Ethics Committee (MS IDREC) in accordance with the University's procedures for ethical approval of all research involving human participants.

I am pleased to inform you that, on the basis of the information provided to the IDREC, the proposed research has been judged as meeting appropriate ethical standards, and approval has been granted for a period of **18 months**, commencing on **23rd March 2022.**

You will be required to submit an annual progress report on each anniversary of study approval, until the study is completed, and your study may be selected for review during an annual audit.

Amendments

Should there be any subsequent changes to the study, you should submit details to the MS IDREC for consideration and approval. Details of changes must be listed on an amendment form.

Yours Sincerely

DocuSigned by:
Leah Butts
9F14889D2BC549A...

Mrs Leah Butts
Research Ethics Administrator

for
Dr Helen Barnby-Porritt
Research Ethics Manager

C

MOLLIE study documents

Included in this section:

1. Participant information sheet
2. Consent form

Critical Care Research Group (Kadoorie Centre)
Level 3, John Radcliffe Hospital, Oxford
Nuffield Department of Clinical Neurosciences
Tel: +44 (0)1865 231449
Email: mirae.harford@ndcn.ox.ac.uk

PARTICIPANT INFORMATION SHEET

Mapping Of Lower Limb skIn pErfusion (MOLLIE)

Ethics Approval Reference: R63796/RE001
Version 2.0
Date: May 2019

We'd like to invite you to take part in our research study. Before you decide, it is important that you understand why the research is being done and what it would involve for you. Please take time to read this information, and discuss it with others if you wish. If there is anything that is not clear, or if you *would like more information, please ask us.*

What is the purpose of the study?

We are trialling a new approach to monitoring how well a patient's heart and their cardiovascular system is functioning. Many established methods of looking at this use invasive monitors or semi-invasive monitors. Non-invasive monitors are less uncomfortable for patients but still require direct contact with the patients with risks of infection and skin irritation. The new method uses video cameras that can detect the way blood arrives at the skin surface, which is not visible to the naked eye. We believe that using this method we may be able to develop a way we can monitor patients without any invasive lines or contacts to their skin.

In order to explore this further, we are aiming to study the way skin is perfused in health, followed by simulating some of the changes that may occur when patients are less well. We are particularly interested in leg skin perfusion and that is the focus of this study. We are planning on using two methods to study this:

- Increasing and decreasing the amount of blood delivered to your skin surface by changing the diameter of blood vessels close to the skin surface. This will be done by using two drugs called phenylephrine and glyceryl trinitrate (GTN). Both of these drugs have been used safely in healthy volunteers and they are frequently used in hospitals. After a recovery period, we will roll a tight-fitting doughnut-shaped balloon over the leg. It will feel like wearing tight-fitting socks or tights temporarily and should not be uncomfortable. We will then

inflate a thigh tourniquet for one minute. After one minute this tourniquet will be released and the re-filling of these vessels will be monitored using the video camera.

Why have I been invited?

You have been invited because you are a healthy adult, aged between 18 and 65, do not have any known pre-existing heart problems, not on any regular medication (except oral contraception), and have expressed interest in taking part in the study.

You will not be able to take part if:

- there are any reasons why you cannot use the monitoring equipment (camera monitor or monitors which are attached to your body via sticky adhesive pads) due to skin disorders such as eczema, scleroderma or psoriasis
- you have had any degree of leg amputation
- you have had any previous surgery to the thigh/knee/lower leg (except knee arthroscopy)
- you are allergic to silver chloride ECG pads
- you have hyperthyroidism
- you are pregnant or breastfeeding
- you have neurological conditions affecting blood flow to the leg
- you have known heart conditions
- you suffer from severe headaches

Do I have to take part?

No. It is up to you to decide if you want to take part in the study. We will describe the study and go through this information sheet with you to answer any questions you may have.

If you agree to take part, we will ask you to sign a consent form and give you a copy for you to keep.

If you change your mind, you are free to withdraw from the study at any time, without having to provide a reason.

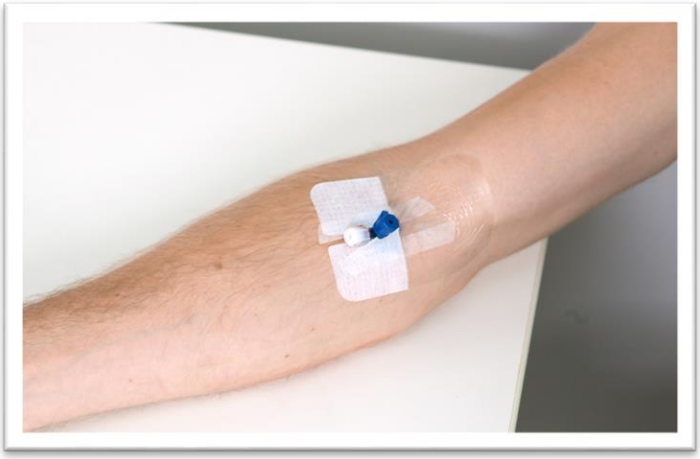
What will happen to me if I decide to take part?

The study will take part in the Cardiovascular Clinical Research Facility (John Radcliffe Hospital, Oxford) and will involve one single visit, unless we are unable to collect data needed on this visit or you ask us to discontinue the study and reschedule for another day. We expect one full session to take approximately 2.5 hours.

As we know that the video monitors are very sensitive to body hair, we will ask you to remove hair on your leg for the study. As shaving or waxing during the study visit may temporarily increase blood flow to the skin surface, we will ask you to do this at least 24 hours before the study visit. If you have hair removal equipment at home,

you can use your usual method. If not, we will discuss this with you before the study visit and agree on a plan. If required, we can supply body hair removal equipment (for shaving or waxing) that you can use.

Prior to starting, we will go through this information with you again and ask if you have any questions. Following that we will ask you some brief medical questions to ensure you are fit and well and examine your heart, lungs, and abdomen to make sure you are fit to take part in the study. Once we are happy that you can partake in the study, we will take some basic measurements from you. This will include your height, weight, and your skin colour from your arm according to a skin colour chart. This is so that the performance of the camera monitor can be compared to your skin tone. As we are recording from your legs, we will ask you to wear shorts so that the skin over your thigh is visible.



We will ask you to lie down on the bed and place a small drip on your arm. This is called a cannula and involves a small needle to ensure it sits inside your vein. The needle is removed after the drip is placed and a small plastic tube will then remain in your arm. The purpose of a cannula is to allow controlled infusion of the drugs to change the diameter of your blood vessels in a safe way. The cannulation will be completed by a trained doctor using sterile equipment. Once inserted, the cannula placement will be checked by flushing up to 10mls of normal saline (sterile fluid with small amount of salt to match the salt levels in the blood) and it will be secured using a specially designed plaster.

The cannula will then be connected to a flexible tube which will be connected to the drug infusion pump. At this point, the infusion will not be running.

The study will involve multiple methods of monitoring the heart and the circulation as described below:

- Video monitors: this is just like a normal video camera and will be mounted onto a trolley next to the examination bed where you will be lying. The camera will be set up after you are in the room and you will be warned when the recording is about to start. The camera is only recording your legs; your face and upper body will not be recorded. While the camera is recording we will ask you to maintain the same position as much as possible, as the monitor is very sensitive to movement. The camera will continue to record throughout the entire study visit and will be analysed at a later point.



- Thoracic bioimpedance monitor: This looks at the way your heart is pumping the blood around the body by measuring the total amount of water inside the chest cavity. The machine does this by passing a tiny amount of electrical signal between the leads which will be placed as sticky adhesives on either side of your neck and your lower chest. The amount of electrical signal passed is very small and you will not be aware of it. This is a continuous monitor and will continue to record throughout the study period.
- A non-invasive blood pressure monitor: This is a cuff that will be placed around your right arm which will intermittently inflate to measure your blood pressure.
- An oxygen saturation probe: This is an earlobe probe that will be placed on your left earlobe. The probe measures the amount of oxygen your blood is carrying using red and infrared light.
- Stowood Blackshadow monitor: This is a device which measures your breathing rate via two belts across your chest and a monitor placed just under your nostrils, and your heart rate and oxygen saturations using sticky adhesives on your chest and a finger probe.



Once all equipment is attached and we are ready to record, we will let you know when the study will start. For the first ten minutes, we will ask you to lie down as still as possible while we take some background measurements. We know from previous studies that talking during this period can cause fine movements in the body which reduces the quality of the images. Therefore, we will ask you to maintain silence during this period.

After ten minutes, we will administer one of the drugs. Each will last for 15 minutes and there will be a break of 20 minutes before the next drug is given. While the drug is being given, your blood pressure will be measured every minute. The drug infusion rate will slowly increase using our protocol, and we will stop increasing the rate once your blood pressure changes by 30% from baseline.

Once the drug infusions are complete and you have had a further break of 20 minutes, we will apply a tourniquet to one of your legs after passing a wrap balloon over your leg to empty out the blood vessels near the surface of your skin. After the

tourniquet is applied for approximately 30 seconds, we will let the cuff down while taking a video of your leg.

This is the end of the study and after safe removal of the cannula, we will observe you for a further five minutes. We will offer you some refreshments during this observation period. If you are feeling well, you will be free to go.

What drugs will I be given?

- Phenylephrine is a drug which has two effects; it can increase your blood pressure and lower your heart rate. It raises blood pressure by reducing the diameter of small blood vessels of arms and legs). The infusion is frequently used in women having caesarean sections under spinal anaesthetic to keep the blood pressure stable, and has been used at higher doses than planned in this study in other healthy volunteer studies.
- Glyceryl trinitrate (GTN) is a drug which has the opposite effect to that of phenylephrine. It reduces blood pressure by dilating the blood vessels. It is used in clinical settings to reduce blood pressure and to reduce the work of the heart when people have heart problems, and has been used in healthy volunteer studies at higher doses than planned in this study. Its main side effect is that in some people it can cause a headache. If this occurs, let us know and we will not further increase the dose.

Both of these drugs are short acting and will wash out of your system quickly once the infusions stop. It is very unlikely that you will have ongoing effects from the drug after leaving the study visit.

What should I consider?

You may participate in other research studies while you are taking part in this study.

Are there any possible disadvantages or risks from taking part?

The monitoring methods described are very safe and non-invasive. They have been trialled in healthy people and in patients without any problems.

The cannulation procedure and its presence may feel uncomfortable. We will not keep the cannula in for any longer than necessary. Once removed, the cannula may leave a small bruise but will heal quickly within 2-3 days.

There is a possibility that you may experience side effects from the drug infusions. The side effects occur because of the transient changes in blood pressure. More specifically, the most common side effects of the two drugs are headaches, flushing, and nausea. These effects should disappear once the drugs washout from your system. Approximately 95% of the drugs will be out of your system by the time you leave the study visit and the remainder (which is not enough to cause you any symptoms or harm) will leave your body over a few hours following the study visit.

Other risks associated with very high or low blood pressure will be minimised by monitoring your blood pressure closely at one minute intervals and making small step increases in drug doses being given. We will not allow your blood pressure to deviate more than 30% from baseline which falls within ranges expected during activities such as exercise and sleep.

The tourniquet placed on the thigh will be inflated to high pressure to stop blood flow. This can be uncomfortable but will only last for 30 seconds before the cuff is deflated.

What are the possible benefits of taking part?

There is no direct benefit for your participation in this study. We hope that the results from this research will help us develop a new method of monitoring critically unwell patients in the hospital in a more comfortable way.

Will my taking part in the study be kept confidential?

Yes. All study data will be entered on a spreadsheet and you will only be identifiable by a unique study specific number and/or code in any database. The name and any other identifying detail about you will not be included in any study data electronic file.

The raw video data of your legs will be stored in a format that is only readable by the review software and will be recorded onto a storage device that will be physically secured at Kadoorie Centre (behind two separate locked doors with restricted access) and the Institute of Biomedical Engineering (behind a locked door with restricted access and 24 hour CCTV monitoring). Access to this storage device will be limited to our research team. Video data analysis will be completed by our collaborators at the Oxford University Centre of Excellence for Medical Engineering who have designed the equipment being used for the study. They are based in the Institute of Biomedical Engineering.

Will I be reimbursed for taking part?

Should you incur any expenses as a result of the study, we will reimburse you as is reasonable (e.g. travel expenses). Additionally, once you complete the study we will give you a £50 voucher.

What will happen to my data?

The information you provide as part of the study is the **research data**. Any research data from which you can be identified (e.g. your name, date of birth), is known as **personal data**. This includes more sensitive categories of personal data (**special category data**) such as your racial or ethnic origin or data concerning your health. This does not include data where the identity has been removed (anonymous data).

We will minimise our use of personal and sensitive data in the study as much as possible.

Consent forms (which include your name) will be stored in the Kadoorie Centre for Critical Care Research and Education within the John Radcliffe Hospital, behind two restricted access doors. All other research data will be stored in the Kadoorie Centre or in the Institute of Biomedical Engineering in the Department of Engineering Science, University of Oxford on a secure local server. Access to this server is restricted to the members of our study team only and the Institute of Biomedical Engineering is accessed via two restricted access doors. Research data will be anonymised. Personal/sensitive data will be stored in the Kadoorie Centre.

The researcher and the research team will have access to personal/sensitive/research data.

We would like your permission to use anonymised images or videos of your legs in research publications. While it is not possible to fully anonymise images of legs, we will not use images with any distinguishing features (e.g. distinctive scar) which may make you identifiable from the image.

All research data and records will be stored for a minimum of 5 years after publication or public release of the work of the research.

We would like your permission to use anonymised data in future studies, and to share data with other researchers (e.g. online database) both inside and outside the European Union. All personal information that could identify you will be removed or changed before information is shared with other researchers or results are made public.

The University of Oxford is the data controller with respect to your personal data and, as such, will determine how your personal data is used in the study. The University will process your personal data for the purpose of the research outlined above. Research is a task that we perform in the public interest.

For further information about your rights with respect to your personal data is available http://www.admin.ox.ac.uk/councilsec/compliance/gdpr/individualrights/.

What will happen if I don't want to carry on with the study?

Participation is voluntary you may change your mind at any stage. If you withdraw from the study, unless you state otherwise, any non-identifiable video data which have been collected whilst you have been in the study will be used for research as

detailed in this participant information sheet. You are free to request that your video samples are destroyed at any time during or after the study.

What will happen to the results of this study?

It will not be possible to identify you from any report or publication placed in the public domain.

Once the study is complete including the analysis of results, the data will be used for publication in scientific journals and may be presented at conferences. It is also predicted that the current study will be used as basis for future similar studies.

Some of the research being undertaken will also contribute to the fulfilment of an educational requirement (i.e. a doctoral thesis).

What if we find something unexpected?

It is important to note that the examination and monitoring in the study are carried out for research purposes rather than for diagnosis. Therefore, participating in the study is not a substitute for a doctor's appointment. Occasionally, however, a possible abnormality may be detected. In this case, we will inform you of the findings and inform the lead investigator (Professor Peter Watkinson). If the lead investigator felt that the abnormality was medically important, you will be recommended to see your general practitioner. All information about you is kept strictly confidential.

There is no need to inform your General Practitioner/family doctor of your participation in the study unless you would like to. In the unlikely event that any findings need urgent treatment or investigation, we will inform you of this and may speak to your GP with your permission.

What if there is a problem?

If a participant in research is ever considered to have suffered harm through their participation, the University has arrangements in place to provide for compensation. If you have a concern about any aspect of this study, please speak to the relevant researcher (01865 231449) or their supervisor (01865 572609), who will do their best to answer your query. The researcher should acknowledge your concern within 10 working days and give you an indication of how they intend to deal with it. If you remain unhappy or wish to make a formal complaint, please contact the Chair of the Medical Sciences Interdivisional Research Ethics Committee (MS IDREC) at the University of Oxford who will seek to resolve the matter in a reasonably expeditious manner: Email: ethics@medsci.ox.ac.uk; Address: Research Services, University of Oxford, Wellington Square, Oxford OX1 2JD.

Who is organising and funding the study?

This study is being organised by a group of researchers specialising in critical care research at the Nuffield Department of Clinical Neuroscience, based at Kadoorie Centre in John Radcliffe Hospital.

The study is funded by the Oxford Biomedical Research Centre, which is a part of National Institute for Health Research (NIHR).

Who has reviewed the study?

This study has been reviewed by, and received ethics clearance through, the University of Oxford Central University Research Ethics Committee (Reference number: R63796/RE001).

Participation in future research:

We will not keep your contact details to contact you regarding future research. If you would like to know more about participating in future research projects, please contact Dr Mirae Harford.

Further information and contact details:

Please contact Dr Mirae Harford by email: mirae.harford@ndcn.ox.ac.uk.

Thank you for reading this information and for considering taking part.

Critical Care Research Group
Nuffield Department of Clinical Neurosciences
University of Oxford

Lead investigator: Professor Peter Watkinson
Peter.watkinson@ndcn.ox.ac.uk
Primary researcher: Mirae Harford
Oxford telephone number: 01865 231449
Oxford e-mail: mirae.harford@ndcn.ox.ac.uk

PARTICIPANT CONSENT FORM

CUREC Approval Reference: R63796/RE001

Mapping Of Lower Limb skIn pErfusion (MOLLIE)

Purpose of Study: To investigate leg skin perfusion at rest and changes created to the perfusion pattern in response to phenylephrine and glyceryl trinitrate (GTN) infusions.

		Please initial each box
1	I confirm that I have read and understand the information sheet version 2.0 dated May 2019 for the above study. I have had the opportunity to consider the information carefully, ask questions and have had these questions answered satisfactorily.	☐
2	I understand that my participation is voluntary and that I am free to withdraw at any time, without giving any reason, and without any adverse consequences or academic penalty.	☐
3	I have been advised about the potential risks associated with taking part in this research and have taken these into consideration before consenting to participate. I understand that the study visit involves video equipment and the recordings will be saved for subsequent analysis.	☐
4	I have been advised as to what I need to do for this research (especially with regard to the phenylephrine and GTN administration) and I agree to follow the instructions given to me. I understand that taking part will involve having a drip and application of a tourniquet on one leg which will stay inflated for one minute.	☐
5	To the best of my knowledge, I do not meet any of the exclusion criteria outlined in the information sheet for this research. If this changes at a later date during study participation, I agree to notify the researchers immediately.	☐
6	I understand that data collected during the study may be looked at by designated individuals from the University of Oxford. I give permission for these individuals to access my data.	☐
8	I understand who will have access to personal data provided, how the data will be stored and what will happen to the data at the end of the project.	☐
9	I agree for data collected in this study to be shared with other researchers, including those working outside of the EU, to be used in other research studies. I understand that any data shared will be fully anonymised so that I cannot be identified.	☐

10	I understand how this research will be written up and published. I agree to the use of anonymised data (including videos) in research publications.	☐
11	I understand that this project has been reviewed by, and received ethics clearance through, the University of Oxford Central University Research Ethics Committee.	☐
12	I understand how to raise a concern or make a complaint.	☐
13	I agree to take part in the study	☐

_____	dd / mm / yyyy	_____
Name of Participant	Date	Signature

_____	dd / mm / yyyy	_____
Name of person taking consent	Date	Signature

D

HemaClear® figures

Included in this section:

1. HemaClear® manufacturer instructions
2. HemaClear® pressure applied

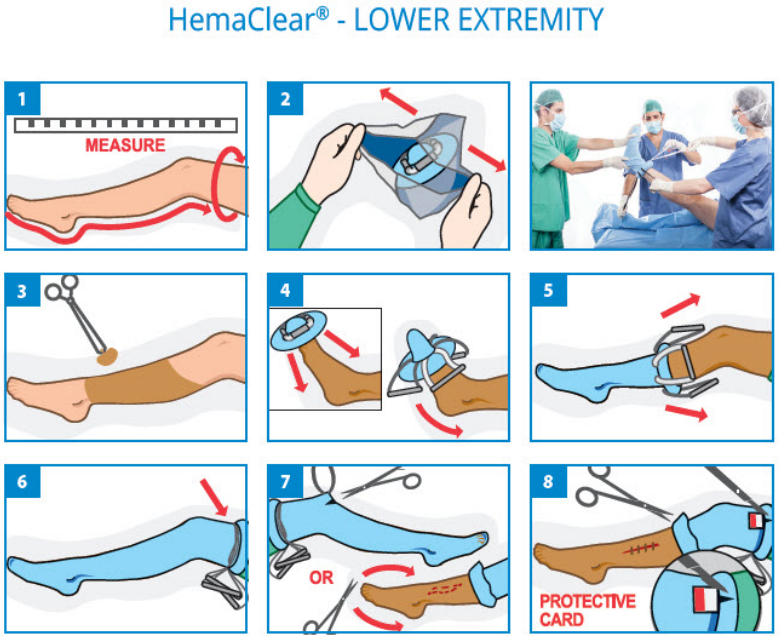


Figure D.1: HemaClear® instructions for lower extremity HemaClear® was applied according to these manufacturer instructions, except for: 1. Extra-large size HemaClear® was used for all participants; 3. The skin was not cleaned prior to the application; 7. The entire stockinette up to the level of the silicone ring were removed. Reproduced from manufacturer guidelines website [309].

HemaClear® EXTRA-LARGE BLACK & WHITE

HemaClear® Skin Pressure, mm Hg

HemaClear® EXTRA LARGE BLACK & WHITE <160 mm Hg PRH-090-BW-01A		Distance from Toes (cm)					
		60-70	71-80	81-90	91-100	101-110	111-120
LIMB CIRCUMFERENCE (cm)	50-54	300	296	292	289	285	281
	55-60	315	311	307	304	300	296
	61-66	327	323	320	316	313	310
	67-72	337	333	330	326	323	320
	73-78	345	342	338	335	331	328
	79-85	352	349	346	342	339	336



Figure D.2: Pressure applied by HemaClear® The skin pressure applied by HemaClear device is dependent on the limb circumference and the distance the tourniquet is unrolled over. Table reproduced from manufacturer website [309].

E

RGB to HSV conversion

Contents

E.1 Introduction 231
E.2 Conversion algorithm 231

E.1 Introduction

In chapter 6, the RGB video camera images were converted to HSV colour space in order to assess whether the observed changes in PPGi DC component was a change in skin colour.

The conversion used the de-bayer images (described in section 4.8.3) and used the originally described conversion formulae by Smith [260]. The same conversion may be performed using Matlab's image processing package 'rgb2hsv' [310].

E.2 Conversion algorithm

Inputs The RGB representation of each pixel is given as a number between 0 and 255. These are denoted 'R', 'G', and 'B'.

Intended outputs The HSV representation of each pixel is given as the following:

- Hue: an angular representation from 0 to 360 degrees. Here, it is denoted 'H'.
- Saturation: a percentage between 0 and 100%. Here, it is denoted 'S'.
- Value: a percentage between 0 and 100%. Here, it is denoted 'V'.

Conversion method Two terms are defined using the RGB values:

- M_{MAX}: maximum value among {R, G, B}
- M_{MIN}: minimum value among {R, G, B}

$V = M_{MAX}/255.$

$S = 1 - M_{MIN}/M_{MAX}$ if $M_{MAX} > 0$;

or

$S = 0$ if $M_{MAX} = 0$.

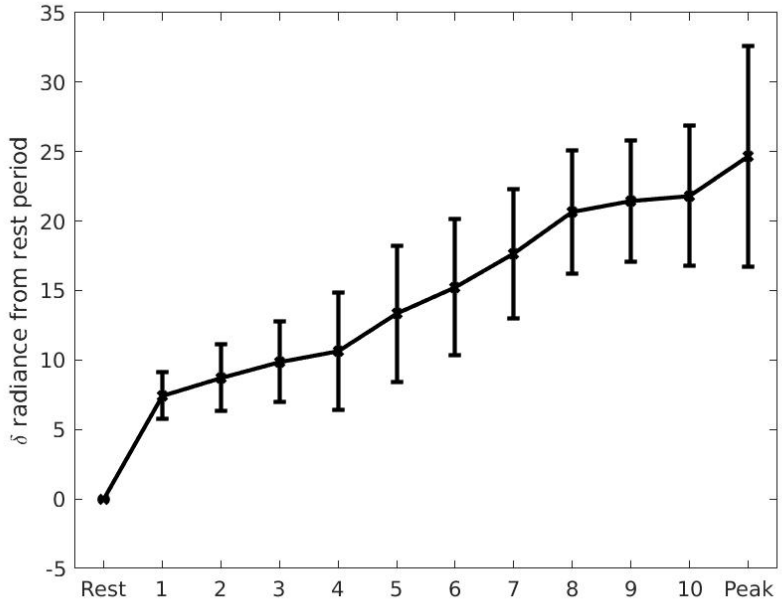
$H = cos^{-1}[(R - 0.5G - 0.5B)/\sqrt{(R^2 + G^2 + B^2 - RG - RB - GB)}]$ if $G \geq B$;

or

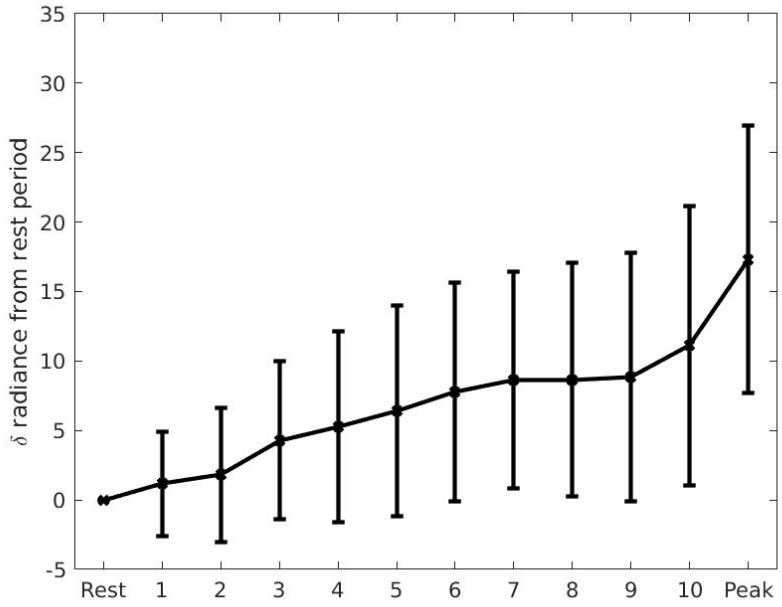
$H = 360 - cos^{-1}[(R - 0.5G - 0.5B)/\sqrt{(R^2 + G^2 + B^2 - RG - RB - GB)}]$ if $G > B$.

F

Background radiance change



(a) Phenylephrine session background radiance



(b) GTN session background radiance

Figure F.1: Background radiance change from baseline (during rest period) throughout phenylephrine (a) and GTN (b) sessions. Error bars indicate standard error across all participants. For each individual, three non-skin regions of equal size were selected from the image and the radiance change from baseline in the non-skin regions were tracked. An increase in radiance throughout the experimental session was observed during both sessions. For each participant, the background radiance change from baseline at each time point was subtracted from the skin ROI radiance.

G

Consistency of baseline skin surface radiance

Table G.1: Sørensen-Dice similarity index for $\mathbf{ROI_{HIGH\text{-}TEMP}}$ and $\mathbf{ROI_{LOW\text{-}TEMP}}$

Rank (low to high agreement)	$ROI_{HIGH\text{-}TEMP}$	$ROI_{LOW\text{-}TEMP}$
1	0.11	0.59
2	0.32	0.64
3	0.34	0.85
4	0.49	0.55
5	0.49	0.91
6	0.49	0.79
7	0.53	0.79
8	0.54	0.86
9	0.55	0.54
10	0.55	0.75
11	0.61	0.53
12	0.63	0.81
13	0.64	0.93
14	0.67	0.93
15	0.68*	0.77*
16	0.78	0.70
17	0.78	0.58
18	0.79	0.96
19	0.82	0.90
20	0.82	0.91
21	0.83	0.91
22	0.83	0.95
23	0.84	0.97
24	0.85	0.94
25	0.88	0.86
26	0.92	0.67
27	0.94	0.79
28	0.94	0.90

*Participant included in figure 7.4 to represent median agreement in $ROI_{HIGH\text{-}TEMP}$. This participant was chosen for demonstration instead of the 14th participant on the table as the 14th participant had a very high $ROI_{LOW\text{-}TEMP}$ agreement not felt to be representative of the true median.

H

Additional analyses from ICU databases: skin mottling

Contents

H.1 Included hospitals from eICU-CRD 237
H.2 Individual database results 238
H.3 UK versus US results 241

H.1 Included hospitals from eICU-CRD

Of the 208 hospitals included in eICU-CRD, I found skin assessment data in 12 hospitals' records. I was unable to isolate limb skin colour data from the other hospital records within eICU-CRD. The hospitals included a mix of teaching and non-teaching hospitals of variable sizes and regions. The characteristics of included hospitals from eICU-CRD are shown in table H.1.

Table H.1: Characteristics of included hospitals from eICU-CRD

Hospital ID	Numbers category	Region	Included (n)
188	>500	South	1627
194	100-249	South	324
394	250-499	West	981
399	<100	West	11
419	250-499	Northeast	439
420	>500	Northeast	3352
422	100-249	Northeast	298
423	<100	Northeast	177
424	<100	Northeast	341
429	Not known	South	10
436	100-249	South	280
440	250-499	South	1051

H.2 Individual database results

PICRAM

Unadjusted ICU mortality in the mottled group was 33.9% compared to 7.2% in the never-mottled group. Of the 914 patients who died in ICU, 380 (41.6%) had documented recording of mottling at some point during the length of stay. Within-ICU mortality was significantly higher in the mottled group (unadjusted OR 6.6, CI 5.7 - 7.7).

Adjusting for OASIS score and the therapies given in ICU (renal replacement therapy and vasopressor use) showed persistent significant association with mortality (OR 2.7, 95% CI 2.2 - 3.2). Upper limb mottling was associated with mortality OR 5.9 (4.7 - 7.4). Adjustment with the same three variables as above gave mortality OR of 2.1 (1.6 - 2.7).

The median length of stay in mottled group was 5.1 (2.3 - 12.0) days. Never-mottled patients' median length of stay was 1.7 (1.0 - 3.3) days.

Patients with at least one episode of mottling were more likely to require vasopressor therapy (44.6% vs 18.4%, $p<0.001$), more likely to be ventilated (79% vs 53.8%,

$p<0.001$), and more likely to require renal replacement therapy (27.3% vs 6.4%, $p<0.001$).

MIMIC

Unadjusted ICU mortality in the mottled group was 37.3% compared to 5.9% in the never-mottled group. Of the 3704 patients who died on ICU, 660 (17.8%) were documented as having been mottled at some point during their ICU stay. Within-ICU mortality was significantly higher in the mottled group (unadjusted OR 9.4, CI 8.5 - 10.5). When adjusted for severity of illness using OASIS, vasopressor use, and RRT, ICU mortality risk in mottled patients remained significantly elevated (adjusted OR 2.3, 95% CI 2.0 - 2.6)).
Upper limb mottling was associated with mortality OR 12.1 (10.6 - 13.8). Adjustment with the same three variables as above gave mortality OR of 2.7 (95% CI 2.3 - 3.1).

The median length of ICU stay in mottled group was 6.1 (2.9 - 12.8) days. Never-mottled patients' median length of stay was 1.8 (1.1 - 3.3) days.

Patients with at least one episode of lower limb mottling were more likely to require vasopressor therapy (78.2% vs 30.9%, $p<0.001$), more likely to be ventilated (82.5% vs 40.9%, $p<0.001$), and more likely to require renal replacement therapy (20.2% vs 1.6%, $p<0.001$).

eICU-CRD

Unadjusted ICU mortality in the mottled group was 43.3% compared to 5.0% in the never-mottled group. Of the 554 patients who died on ICU, 122 (22.0%) were documented as having been mottled at some point during their ICU stay. Within-ICU mortality was significantly higher in the mottled group (unadjusted OR 14.4, CI 11.2 - 18.6). When adjusted for severity of illness using OASIS, vasopressor use, and RRT, ICU mortality risk in mottled patients remained significantly elevated (adjusted OR 6.0, 95% CI 4.5 - 8.1)).

The median length of ICU stay in mottled group was 4.1 (2.1 - 8.3) days. Never-mottled patients' median length of stay was 1.9 (1.1 - 3.6) days.

Patients with at least one episode of mottling were more likely to require vasopressor therapy (51.1% vs 42.2%, p=0.003) and more likely to be ventilated (51.4% vs 21.2%, p<0.001). Rates of renal replacement therapy were not significantly different (0.4% vs 0.9%, p=0.38).

Table H.2: Skin mottling: UK versus US results

Variable		**UK: PICRAM**	**US: MIMIC-IV and eICU-CRD**
N		8555	62041
Age	Median (IQR)	63 (47-73)	66 (54-78)
Sex	Male (%)	5053 (59.1)	34735 (56.0)
	Female (%)	3495 (40.9)	27296 (44.0)
	Not coded (%)	3 (0.0)	10 (0.0)
Organ support	Ventilation (%)	4886 (57.1)	24420 (39.4)
	RRT (%)	783 (9.2)	1271 (2.0)
	Vasopressor use (%)	2052 (24.0)	21036 (33.9)
ICU score	OASIS (IQR)	33 (25-42)	30 (24-36)
Mottled		1120 (13.1)	2053 (3.3)
ICU LOS*	Median (IQR)	1.9 (1.0-3.9)	1.9 (1.1-3.4)
ICU mortality	(%)	914 (10.7)	4258 (6.9)
Hosp mortality	(%)	1328 (15.5)**	6318 (10.2)

*ICU length of stay (LOS) calculated from patients discharged from ICU alive only.
**No record of hospital mortality in 453 cases. Calculated from the 8102 records (94.7%) with hospital mortality data.

H.3 UK versus US results

I observed higher incidence of mottling on ICU in the UK-based database (13.1%) compared to the two based in the US (4.0% and 3.2%). These differences between the databases may be due to higher illness severity in the UK ICU patient cohort, supported by higher ICU mortality, OASIS, and rates of vasopressor and renal support. Table H.2 compares the UK (PICRAM) and US (MIMIC-IV and eICU-CRD) databases.

I

Perforator locations on RGB imaging: further results

Contents

I.1 Absolute change in PPGi amplitude in the sub-regions 242
I.1.1 Red channel 242
I.1.2 Blue channel 243
I.2 Percentage change in PPGi amplitude in the sub-regions 243
I.2.1 Green channel 243
I.2.2 Red channel 245
I.2.3 Blue channel 245

I.1 Absolute change in PPGi amplitude in the sub-regions

I.1.1 Red channel

During peak phenylephrine effect (period defined in section 4.8.1), the median absolute change in peak-to-trough amplitude of the AC waveform in ROI_{HIGH} was a decrease of 5.6 (IQR 2.0 - 11.7) pixel units ($p < 0.001$) from baseline. The corresponding change in ROI_{LOW} was a decrease of 0.03 (IQR -1.4 to 0.6) pixel units ($p = 0.63$) from baseline. The two responses were significantly different from

each other ($p < 0.001$). The mean absolute changes are shown in table 8.1.

During peak GTN effect (period defined in section 4.8.1), the median absolute change in peak-to-trough amplitude of the AC waveform in ROI_{HIGH} was an increase of 4.7 (IQR 1.8 - 10.6) pixel units ($p < 0.001$) from baseline. The corresponding change in ROI_{LOW} was an increase of 2.3 (IQR 1.2 - 6.8) pixel units ($p < 0.001$) from baseline. The two responses were not significantly different ($p = 0.16$). The mean absolute changes are shown in table 8.2.

I.1.2 Blue channel

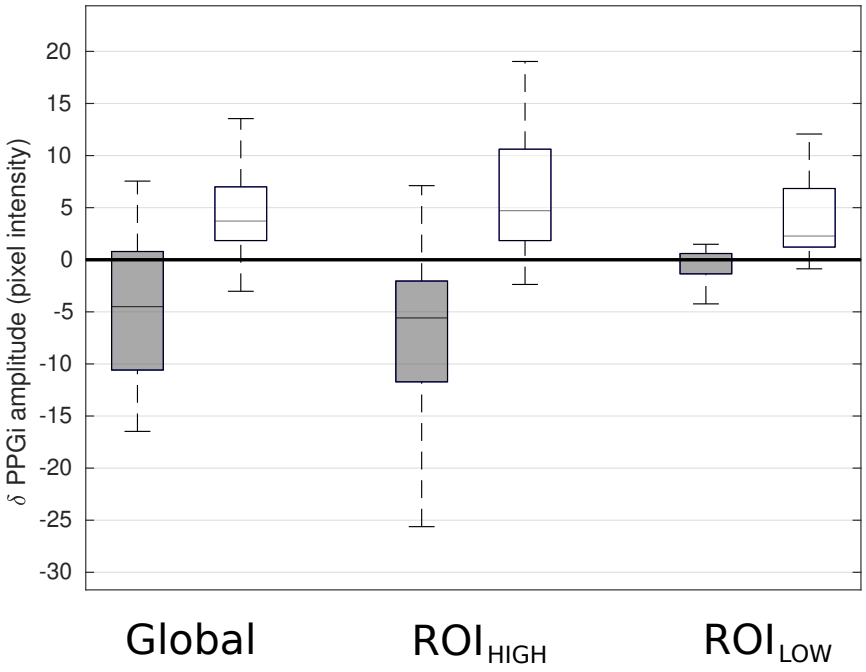
During peak phenylephrine effect (period defined in section 4.8.1), the median absolute change in peak-to-trough amplitude of the AC waveform in ROI_{HIGH} was a decrease of 3.2 (IQR 1.0 - 8.3) pixel units ($p < 0.001$) from baseline. The corresponding change in ROI_{LOW} was a decrease of 0.3 (IQR -1.4 to 0.02) pixel units ($p = 0.01$) from baseline. The two responses were significantly different from each other ($p < 0.001$). The mean absolute changes are shown in table 8.1.

During peak GTN effect (period defined in section 4.8.1), the median absolute change in peak-to-trough amplitude of the AC waveform in ROI_{HIGH} was an increase of 2.8 (IQR 1.1 - 9.5) pixel units ($p < 0.001$) from baseline. The corresponding change in ROI_{LOW} was an increase of 1.3 (IQR 0.6 - 4.5) pixel units ($p < 0.001$) from baseline. The two responses were not significantly different ($p = 0.11$). The mean absolute changes are shown in table 8.2.

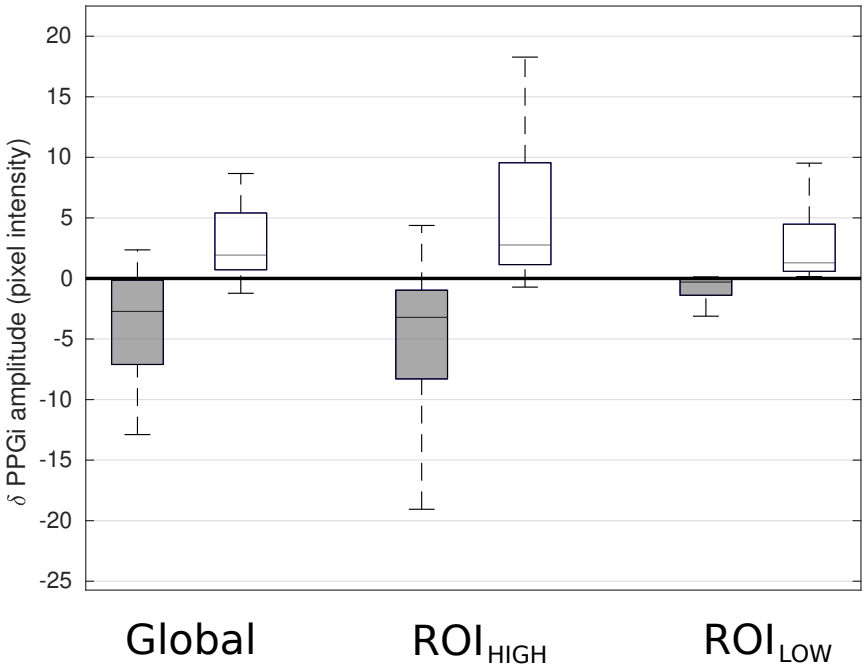
I.2 Percentage change in PPGi amplitude in the sub-regions

I.2.1 Green channel

During peak phenylephrine effect (period defined in section 4.8.1), the median percentage change in peak-to-trough amplitude of the AC waveform in ROI_{HIGH} was



(a) Red channel



(b) Blue channel

Figure I.1: Differential response in RGB sub-regions: Pre-to-peak absolute change in PPGi waveform amplitude. Phenylephrine session results are shown in grey, GTN session results are shown in white. The $\mathrm{ROI}_{\mathrm{GLOBAL}}$ response which was presented in chapter 6 is shown first on the left. The PPGi amplitude changes in the two sub-regions are shown as $\mathrm{ROI}_{\mathrm{HIGH}}$ and $\mathrm{ROI}_{\mathrm{LOW}}$. The two sub-regions defined using baseline/resting state PPGi waveform amplitude show differing response to both phenylephrine and GTN.

a decrease of 48.0 % (IQR 20.8 - 57.3) ($p < 0.001$) from baseline. The corresponding change in ROI_{LOW} was a decrease of 10.3 % (IQR -35.0 to 10.2) ($p = 0.25$) from baseline. The two responses were significantly different from each other ($p < 0.001$).

During peak GTN effect (period defined in section 4.8.1), the median percentage change in peak-to-trough amplitude of the AC waveform in ROI_{HIGH} was an increase of 22.3 % (IQR 8.2 - 27.9) ($p < 0.001$) from baseline. The corresponding change in ROI_{LOW} was an increase of 37.9 % (IQR 22.6 - 67.9) ($p < 0.001$) from baseline. The two responses were significantly different ($p = 0.001$).

I.2.2 Red channel

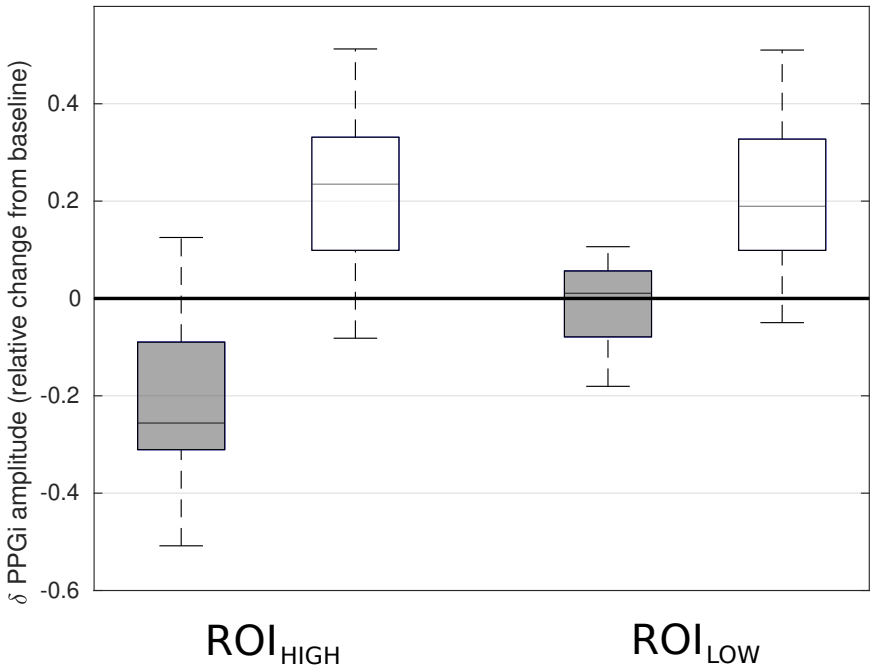
During peak phenylephrine effect (period defined in section 4.8.1), the median percentage change in peak-to-trough amplitude of the AC waveform in ROI_{HIGH} was a decrease of 25.6 % (IQR 9.0 - 31.1) ($p < 0.001$) from baseline. The corresponding change in ROI_{LOW} was a decrease of 1.1 % (IQR -7.9 to 5.7) ($p = 0.93$) from baseline. The two responses were significantly different from each other ($p < 0.001$).

During peak GTN effect (period defined in section 4.8.1), the median percentage change in peak-to-trough amplitude of the AC waveform in ROI_{HIGH} was an increase of 23.5 % (IQR 9.9 - 33.1) ($p < 0.001$) from baseline. The corresponding change in ROI_{LOW} was an increase of 18.9 % (IQR 9.9 - 32.7) ($p < 0.001$) from baseline. The two responses were not significantly different ($p = 0.87$).

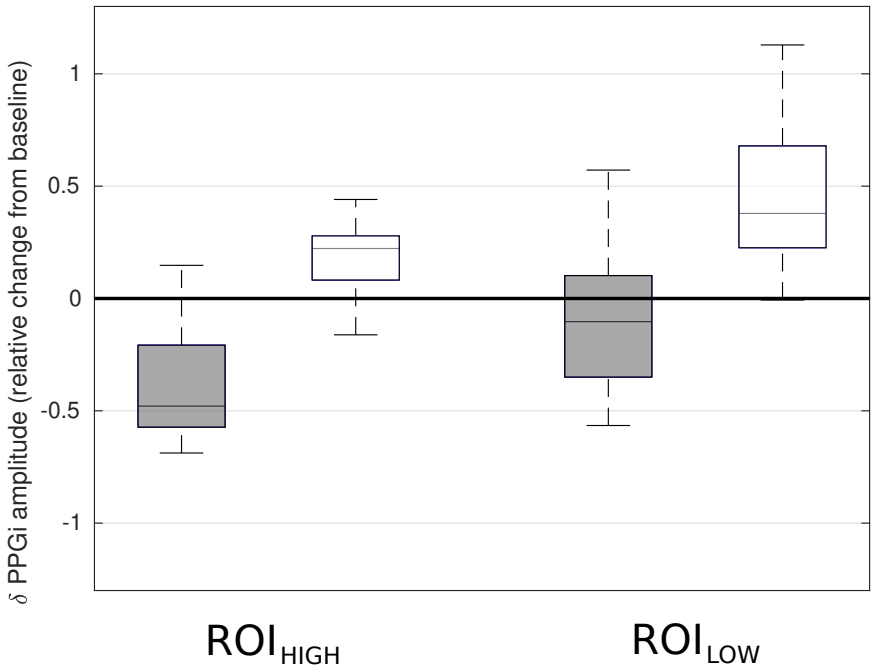
I.2.3 Blue channel

During peak phenylephrine effect (period defined in section 4.8.1), the median percentage change in peak-to-trough amplitude of the AC waveform in ROI_{HIGH} was a decrease of 24.6 % (IQR 10.6 - 36.0) ($p < 0.001$) from baseline. The corresponding change in ROI_{LOW} was a decrease of 4.1 % (IQR -12.6 to 0.4) ($p = 0.02$) from baseline. The two responses were not significantly different from each other ($p < 0.001$).

During peak GTN effect (period defined in section 4.8.1), the median percentage change in peak-to-trough amplitude of the AC waveform in ROI_{HIGH} was an increase of 20.9.3 % (IQR 10.1 - 35.4) ($p < 0.001$) from baseline. The corresponding change in ROI_{LOW} was an increase of 14.1 % (IQR 9.2 - 38.8) ($p < 0.001$) from baseline. The two responses were not significantly different ($p = 0.87$).

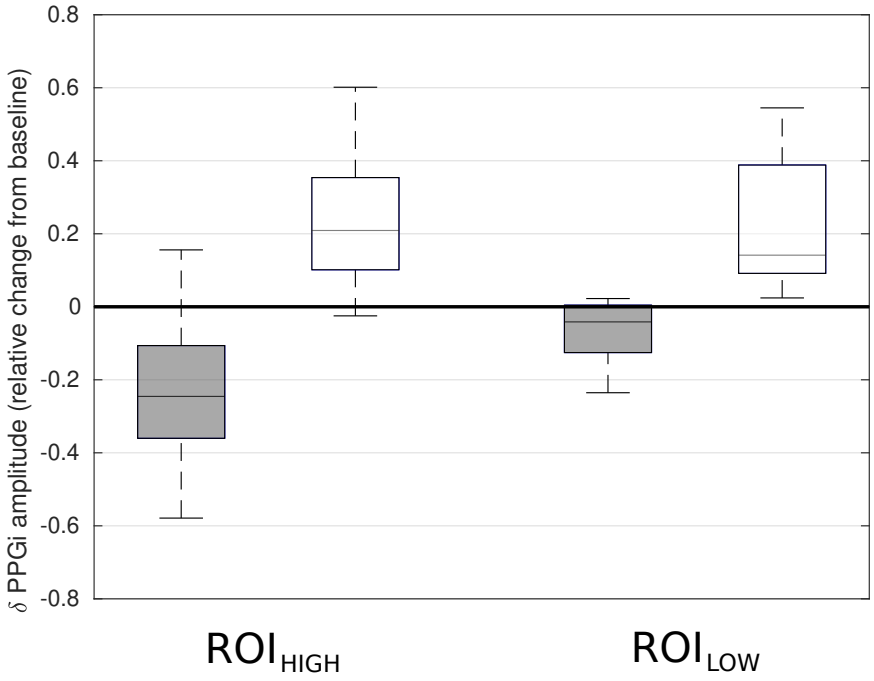


(a) Red channel



(b) Green channel

Figure I.2: Differential response in RGB sub-regions (contd.)



(c) Blue channel

Figure I.2: Differential response in RGB sub-regions: Pre-to-peak relative change in PPGi waveform amplitude. Phenylephrine session results are shown in grey, GTN session results are shown in white. The relative PPGi amplitude changes in the two sub-regions are shown as $\mathrm{ROI}_{\mathrm{HIGH}}$ and $\mathrm{ROI}_{\mathrm{LOW}}$. The two sub-regions defined using baseline/resting state PPGi waveform amplitude show differing response to both phenylephrine and GTN.

J
Permissions

Included in this section:

1. Permission figure 1.2
2. Permission figure 1.4
3. Permission figure 5.1

JOHN WILEY AND SONS LICENSE
TERMS AND CONDITIONS

Aug 26, 2022

This Agreement between Dr. Mirae Harford ("You") and John Wiley and Sons ("John Wiley and Sons") consists of your license details and the terms and conditions provided by John Wiley and Sons and Copyright Clearance Center.

License Number	5376480923735
License date	Aug 26, 2022
Licensed Content Publisher	John Wiley and Sons
Licensed Content Publication	Wiley Books
Licensed Content Title	Shimizu's Dermatology, 2nd Edition
Licensed Content Author	Hiroshi Shimizu
Licensed Content Date	Feb 1, 2017
Licensed Content Pages	1
Type of use	Dissertation/Thesis
Requestor type	University/Academic
Format	Print and electronic
Portion	Figure/table
Number of figures/tables	1
Will you be translating?	No

Title	Physiological Monitoring Using Skin Perfusion Mapping
Institution name	n/a
Expected presentation date	Sep 2022
Portions	Figure 1.1, Chapter 1, page 1
Requestor Location	Dr. Mirae Harford Kadoorie Centre John Radcliffe Hospital Oxford, Oxfordshire OX3 9DU United Kingdom Attn: Dr. Mirae Harford
Publisher Tax ID	EU826007151
Total	0.00 GBP

Terms and Conditions

TERMS AND CONDITIONS

This copyrighted material is owned by or exclusively licensed to John Wiley & Sons, Inc. or one of its group companies (each a"Wiley Company") or handled on behalf of a society with which a Wiley Company has exclusive publishing rights in relation to a particular work (collectively "WILEY"). By clicking "accept" in connection with completing this licensing transaction, you agree that the following terms and conditions apply to this transaction (along with the billing and payment terms and conditions established by the Copyright Clearance Center Inc., ("CCC's Billing and Payment terms and conditions"), at the time that you opened your RightsLink account (these are available at any time at http://myaccount.copyright.com).

Terms and Conditions

- The materials you have requested permission to reproduce or reuse (the "Wiley Materials") are protected by copyright.
- You are hereby granted a personal, non-exclusive, non-sub licensable (on a stand-alone basis), non-transferable, worldwide, limited license to reproduce the Wiley Materials for the purpose specified in the licensing process. This license, **and any CONTENT (PDF or image file) purchased as part of your order,** is for a one-time use only and limited to any maximum distribution number specified in the license. The first instance of republication or reuse granted by this license must be completed within two years of the date of the grant of this license (although copies prepared before the end date may be distributed thereafter). The Wiley Materials shall not be used in any other manner or for any other purpose, beyond what is granted in the license. Permission is granted subject to an appropriate acknowledgement given to the

author, title of the material/book/journal and the publisher. You shall also duplicate the copyright notice that appears in the Wiley publication in your use of the Wiley Material. Permission is also granted on the understanding that nowhere in the text is a previously published source acknowledged for all or part of this Wiley Material. Any third party content is expressly excluded from this permission.

- With respect to the Wiley Materials, all rights are reserved. Except as expressly granted by the terms of the license, no part of the Wiley Materials may be copied, modified, adapted (except for minor reformatting required by the new Publication), translated, reproduced, transferred or distributed, in any form or by any means, and no derivative works may be made based on the Wiley Materials without the prior permission of the respective copyright owner.**For STM Signatory Publishers clearing permission under the terms of the STM Permissions Guidelines only, the terms of the license are extended to include subsequent editions and for editions in other languages, provided such editions are for the work as a whole in situ and does not involve the separate exploitation of the permitted figures or extracts,** You may not alter, remove or suppress in any manner any copyright, trademark or other notices displayed by the Wiley Materials. You may not license, rent, sell, loan, lease, pledge, offer as security, transfer or assign the Wiley Materials on a stand-alone basis, or any of the rights granted to you hereunder to any other person.

- The Wiley Materials and all of the intellectual property rights therein shall at all times remain the exclusive property of John Wiley & Sons Inc, the Wiley Companies, or their respective licensors, and your interest therein is only that of having possession of and the right to reproduce the Wiley Materials pursuant to Section 2 herein during the continuance of this Agreement. You agree that you own no right, title or interest in or to the Wiley Materials or any of the intellectual property rights therein. You shall have no rights hereunder other than the license as provided for above in Section 2. No right, license or interest to any trademark, trade name, service mark or other branding ("Marks") of WILEY or its licensors is granted hereunder, and you agree that you shall not assert any such right, license or interest with respect thereto

- NEITHER WILEY NOR ITS LICENSORS MAKES ANY WARRANTY OR REPRESENTATION OF ANY KIND TO YOU OR ANY THIRD PARTY, EXPRESS, IMPLIED OR STATUTORY, WITH RESPECT TO THE MATERIALS OR THE ACCURACY OF ANY INFORMATION CONTAINED IN THE MATERIALS, INCLUDING, WITHOUT LIMITATION, ANY IMPLIED WARRANTY OF MERCHANTABILITY, ACCURACY, SATISFACTORY QUALITY, FITNESS FOR A PARTICULAR PURPOSE, USABILITY, INTEGRATION OR NON-INFRINGEMENT AND ALL SUCH WARRANTIES ARE HEREBY EXCLUDED BY WILEY AND ITS LICENSORS AND WAIVED BY YOU.

- WILEY shall have the right to terminate this Agreement immediately upon breach of this Agreement by you.

- You shall indemnify, defend and hold harmless WILEY, its Licensors and their respective directors, officers, agents and employees, from and against any actual or threatened claims, demands, causes of action or proceedings arising from any breach of this Agreement by you.

- IN NO EVENT SHALL WILEY OR ITS LICENSORS BE LIABLE TO YOU OR ANY OTHER PARTY OR ANY OTHER PERSON OR ENTITY FOR ANY SPECIAL, CONSEQUENTIAL, INCIDENTAL, INDIRECT, EXEMPLARY OR PUNITIVE DAMAGES, HOWEVER CAUSED, ARISING OUT OF OR IN CONNECTION WITH THE DOWNLOADING, PROVISIONING, VIEWING OR USE OF THE MATERIALS REGARDLESS OF THE FORM OF ACTION, WHETHER FOR BREACH OF CONTRACT, BREACH OF WARRANTY, TORT,

NEGLIGENCE, INFRINGEMENT OR OTHERWISE (INCLUDING, WITHOUT LIMITATION, DAMAGES BASED ON LOSS OF PROFITS, DATA, FILES, USE, BUSINESS OPPORTUNITY OR CLAIMS OF THIRD PARTIES), AND WHETHER OR NOT THE PARTY HAS BEEN ADVISED OF THE POSSIBILITY OF SUCH DAMAGES. THIS LIMITATION SHALL APPLY NOTWITHSTANDING ANY FAILURE OF ESSENTIAL PURPOSE OF ANY LIMITED REMEDY PROVIDED HEREIN.

- Should any provision of this Agreement be held by a court of competent jurisdiction to be illegal, invalid, or unenforceable, that provision shall be deemed amended to achieve as nearly as possible the same economic effect as the original provision, and the legality, validity and enforceability of the remaining provisions of this Agreement shall not be affected or impaired thereby.

- The failure of either party to enforce any term or condition of this Agreement shall not constitute a waiver of either party's right to enforce each and every term and condition of this Agreement. No breach under this agreement shall be deemed waived or excused by either party unless such waiver or consent is in writing signed by the party granting such waiver or consent. The waiver by or consent of a party to a breach of any provision of this Agreement shall not operate or be construed as a waiver of or consent to any other or subsequent breach by such other party.

- This Agreement may not be assigned (including by operation of law or otherwise) by you without WILEY's prior written consent.

- Any fee required for this permission shall be non-refundable after thirty (30) days from receipt by the CCC.

- These terms and conditions together with CCC's Billing and Payment terms and conditions (which are incorporated herein) form the entire agreement between you and WILEY concerning this licensing transaction and (in the absence of fraud) supersedes all prior agreements and representations of the parties, oral or written. This Agreement may not be amended except in writing signed by both parties. This Agreement shall be binding upon and inure to the benefit of the parties' successors, legal representatives, and authorized assigns.

- In the event of any conflict between your obligations established by these terms and conditions and those established by CCC's Billing and Payment terms and conditions, these terms and conditions shall prevail.

- WILEY expressly reserves all rights not specifically granted in the combination of (i) the license details provided by you and accepted in the course of this licensing transaction, (ii) these terms and conditions and (iii) CCC's Billing and Payment terms and conditions.

- This Agreement will be void if the Type of Use, Format, Circulation, or Requestor Type was misrepresented during the licensing process.

- This Agreement shall be governed by and construed in accordance with the laws of the State of New York, USA, without regards to such state's conflict of law rules. Any legal action, suit or proceeding arising out of or relating to these Terms and Conditions or the breach thereof shall be instituted in a court of competent jurisdiction in New York County in the State of New York in the United States of America and each party hereby consents and submits to the personal jurisdiction of such court, waives any objection to venue in such court and consents to service of process by registered or certified mail, return receipt requested, at the last known address of such party.

WILEY OPEN ACCESS TERMS AND CONDITIONS

Wiley Publishes Open Access Articles in fully Open Access Journals and in Subscription journals offering Online Open. Although most of the fully Open Access journals publish open access articles under the terms of the Creative Commons Attribution (CC BY) License only, the subscription journals and a few of the Open Access Journals offer a choice of Creative Commons Licenses. The license type is clearly identified on the article.

The Creative Commons Attribution License

The Creative Commons Attribution License (CC-BY) allows users to copy, distribute and transmit an article, adapt the article and make commercial use of the article. The CC-BY license permits commercial and non-

Creative Commons Attribution Non-Commercial License

The Creative Commons Attribution Non-Commercial (CC-BY-NC)License permits use, distribution and reproduction in any medium, provided the original work is properly cited and is not used for commercial purposes.(see below)

Creative Commons Attribution-Non-Commercial-NoDerivs License

The Creative Commons Attribution Non-Commercial-NoDerivs License (CC-BY-NC-ND) permits use, distribution and reproduction in any medium, provided the original work is properly cited, is not used for commercial purposes and no modifications or adaptations are made. (see below)

Use by commercial "for-profit" organizations

Use of Wiley Open Access articles for commercial, promotional, or marketing purposes requires further explicit permission from Wiley and will be subject to a fee.

Further details can be found on Wiley Online Library
http://olabout.wiley.com/WileyCDA/Section/id-410895.html

Other Terms and Conditions:

v1.10 Last updated September 2015

Questions? customercare@copyright.com or +1-855-239-3415 (toll free in the US) or +1-978-646-2777.

WOLTERS KLUWER HEALTH, INC. LICENSE
TERMS AND CONDITIONS

Mar 01, 2023

This Agreement between Dr. Mirae Harford ("You") and Wolters Kluwer Health, Inc. ("Wolters Kluwer Health, Inc.") consists of your license details and the terms and conditions provided by Wolters Kluwer Health, Inc. and Copyright Clearance Center.

License Number	5500201191640
License date	Mar 01, 2023
Licensed Content Publisher	Wolters Kluwer Health, Inc.
Licensed Content Publication	Plastic and Reconstructive Surgery
Licensed Content Title	The Anatomical (Angiosome) and Clinical Territories of Cutaneous Perforating Arteries: Development of the Concept and Designing Safe Flaps
Licensed Content Author	G. Ian Taylor, Russell J. Corlett, Shymal C. Dhar, et al
Licensed Content Date	Apr 1, 2011
Licensed Content Volume	127

Licensed Content Issue	4
Type of Use	Dissertation/Thesis
Requestor type	University/College
Sponsorship	No Sponsorship
Format	Print and electronic
Will this be posted online?	Yes, on an unrestricted website
Portion	Figures/tables/illustrations
Number of figures/tables/illustrations	1
Author of this Wolters Kluwer article	No
Will you be translating?	No
Intend to modify/change the content	No
Title	Non-contact Monitoring of Skin Perfusion as a Proxy for Haemodynamic Status

Institution name	University of Oxford
Expected presentation date	Mar 2023
Portions	Figure2, page 1449
Requestor Location	Dr. Mirae Harford Kadoorie Centre John Radcliffe Hospital Oxford, Oxfordshire OX3 9DU United Kingdom Attn: Dr. Mirae Harford
Publisher Tax ID	13-2932696
Total	0.00 GBP

Terms and Conditions

Wolters Kluwer Health Inc. Terms and Conditions

1. **Duration of License:** Permission is granted for a one time use only. Rights herein do not apply to future reproductions, editions, revisions, or other derivative works. This permission shall be effective as of the date of execution by the parties for the maximum period of 12 months and should be renewed after the term expires.
    i. When content is to be republished in a book or journal the validity of this agreement should be the life of the book edition or journal issue.

ii. When content is licensed for use on a website, internet, intranet, or any publicly accessible site (not including a journal or book), you agree to remove the material from such site after 12 months, or request to renew your permission license

2. **Credit Line:** A credit line must be prominently placed and include: For book content: the author(s), title of book, edition, copyright holder, year of publication; For journal content: the author(s), titles of article, title of journal, volume number, issue number, inclusive pages and website URL to the journal page; If a journal is published by a learned society the credit line must include the details of that society.
3. **Warranties:** The requestor warrants that the material shall not be used in any manner which may be considered derogatory to the title, content, authors of the material, or to Wolters Kluwer Health, Inc.
4. **Indemnity:** You hereby indemnify and hold harmless Wolters Kluwer Health, Inc. and its respective officers, directors, employees and agents, from and against any and all claims, costs, proceeding or demands arising out of your unauthorized use of the Licensed Material
5. **Geographical Scope:** Permission granted is non-exclusive and is valid throughout the world in the English language and the languages specified in the license.
6. **Copy of Content:** Wolters Kluwer Health, Inc. cannot supply the requestor with the original artwork, high-resolution images, electronic files or a clean copy of content.
7. **Validity:** Permission is valid if the borrowed material is original to a Wolters Kluwer Health, Inc. imprint (J.B Lippincott, Lippincott-Raven Publishers, Williams & Wilkins, Lea & Febiger, Harwal, Rapid Science, Little Brown & Company, Harper & Row Medical, American Journal of Nursing Co, and Urban & Schwarzenberg - English Language, Raven Press, Paul Hoeber, Springhouse, Ovid), and the Anatomical Chart Company
8. **Third Party Material:** This permission does not apply to content that is credited to publications other than Wolters Kluwer Health, Inc. or its Societies. For images credited to non-Wolters Kluwer Health, Inc. books or journals, you must obtain permission from the source referenced in the figure or table legend or credit line before making any use of the image(s), table(s) or other content.
9. **Adaptations:** Adaptations are protected by copyright. For images that have been adapted, permission must be sought from the rightsholder of the original material and the rightsholder of the adapted material.
10. **Modifications:** Wolters Kluwer Health, Inc. material is not permitted to be modified or adapted without written approval from Wolters Kluwer Health, Inc. with the exception of text size or color. The adaptation should be credited as follows: Adapted with permission from Wolters Kluwer Health, Inc.: [the author(s), title of book, edition, copyright holder, year of publication] or [the author(s), titles of article, title of

journal, volume number, issue number, inclusive pages and website URL to the journal page].

11. **Full Text Articles:** Republication of full articles in English is prohibited.
12. **Branding and Marketing:** No drug name, trade name, drug logo, or trade logo can be included on the same page as material borrowed from *Diseases of the Colon & Rectum, Plastic Reconstructive Surgery, Obstetrics & Gynecology (The Green Journal), Critical Care Medicine, Pediatric Critical Care Medicine, the American Heart Association publications and the American Academy of Neurology publications.*
13. **Open Access:** Unless you are publishing content under the same Creative Commons license, the following statement must be added when reprinting material in Open Access journals: "The Creative Commons license does not apply to this content. Use of the material in any format is prohibited without written permission from the publisher, Wolters Kluwer Health, Inc. Please contact permissions@lww.com for further information."
14. **Translations:** The following disclaimer must appear on all translated copies: Wolters Kluwer Health, Inc. and its Societies take no responsibility for the accuracy of the translation from the published English original and are not liable for any errors which may occur.
15. **Published Ahead of Print (PAP):** Articles in the PAP stage of publication can be cited using the online publication date and the unique DOI number.
    i. Disclaimer: Articles appearing in the PAP section have been peer-reviewed and accepted for publication in the relevant journal and posted online before print publication. Articles appearing as PAP may contain statements, opinions, and information that have errors in facts, figures, or interpretation. Any final changes in manuscripts will be made at the time of print publication and will be reflected in the final electronic version of the issue. Accordingly, Wolters Kluwer Health, Inc., the editors, authors and their respective employees are not responsible or liable for the use of any such inaccurate or misleading data, opinion or information contained in the articles in this section.
16. **Termination of Contract:** Wolters Kluwer Health, Inc. must be notified within 90 days of the original license date if you opt not to use the requested material.
17. **Waived Permission Fee:** Permission fees that have been waived are not subject to future waivers, including similar requests or renewing a license.
18. **Contingent on payment:** You may exercise these rights licensed immediately upon issuance of the license, however until full payment is received either by the publisher or our authorized vendor, this license is not valid. If full payment is not received on a timely basis, then any license preliminarily granted shall be deemed automatically revoked and shall be void as if never granted. Further, in the event that you breach any of these terms and conditions or any of Wolters Kluwer Health, Inc.'s other billing and

payment terms and conditions, the license is automatically revoked and shall be void as if never granted. Use of materials as described in a revoked license, as well as any use of the materials beyond the scope of an unrevoked license, may constitute copyright infringement and publisher reserves the right to take any and all action to protect its copyright in the materials.

19. **STM Signatories Only:** Any permission granted for a particular edition will apply to subsequent editions and for editions in other languages, provided such editions are for the work as a whole in situ and do not involve the separate exploitation of the permitted illustrations or excerpts. Please view: STM Permissions Guidelines
20. **Warranties and Obligations:** LICENSOR further represents and warrants that, to the best of its knowledge and belief, LICENSEE's contemplated use of the Content as represented to LICENSOR does not infringe any valid rights to any third party.
21. **Breach:** If LICENSEE fails to comply with any provisions of this agreement, LICENSOR may serve written notice of breach of LICENSEE and, unless such breach is fully cured within fifteen (15) days from the receipt of notice by LICENSEE, LICENSOR may thereupon, at its option, serve notice of cancellation on LICENSEE, whereupon this Agreement shall immediately terminate.
22. **Assignment:** License conveyed hereunder by the LICENSOR shall not be assigned or granted in any manner conveyed to any third party by the LICENSEE without the consent in writing to the LICENSOR.
23. **Governing Law:** The laws of The State of New York shall govern interpretation of this Agreement and all rights and liabilities arising hereunder.
24. **Unlawful:** If any provision of this Agreement shall be found unlawful or otherwise legally unenforceable, all other conditions and provisions of this Agreement shall remain in full force and effect.

For Copyright Clearance Center / RightsLink Only:

1. **Service Description for Content Services:** Subject to these terms of use, any terms set forth on the particular order, and payment of the applicable fee, you may make the following uses of the ordered materials:
    i. **Content Rental:** You may access and view a single electronic copy of the materials ordered for the time period designated at the time the order is placed. Access to the materials will be provided through a dedicated content viewer or other portal, and access will be discontinued upon expiration of the designated time period. An order for Content Rental does not include any rights to print, download, save, create additional copies, to distribute or to reuse in any way the full text or parts of the materials.

ii. **Content Purchase:** You may access and download a single electronic copy of the materials ordered. Copies will be provided by email or by such other means as publisher may make available from time to time. An order for Content Purchase does not include any rights to create additional copies or to distribute copies of the materials

Other Terms and Conditions:

v1.18

Questions? customercare@copyright.com.

SPRINGER NATURE LICENSE
TERMS AND CONDITIONS

Mar 01, 2023

This Agreement between Dr. Mirae Harford ("You") and Springer Nature ("Springer Nature") consists of your license details and the terms and conditions provided by Springer Nature and Copyright Clearance Center.

License Number	5500050164492
License date	Mar 01, 2023
Licensed Content Publisher	Springer Nature
Licensed Content Publication	Intensive Care Medicine
Licensed Content Title	Mottling score predicts survival in septic shock
Licensed Content Author	H. Ait-Oufella et al
Licensed Content Date	Mar 4, 2011
Type of Use	Thesis/Dissertation
Requestor type	academic/university or research institute
Format	electronic
Portion	figures/tables/illustrations
Number of figures/tables/illustrations	1
Will you be translating?	no
Circulation/distribution	1 - 29

Author of this Springer Nature content	no
Title	Non-contact Monitoring of Skin Perfusion as a Proxy for Haemodynamic Status
Institution name	University of Oxford
Expected presentation date	Mar 2023
Portions	Figure 1, page 803
Requestor Location	Dr. Mirae Harford Kadoorie Centre John Radcliffe Hospital Oxford, Oxfordshire OX3 9DU United Kingdom Attn: Dr. Mirae Harford
Total	0.00 GBP

Terms and Conditions

Springer Nature Customer Service Centre GmbH Terms and Conditions

The following terms and conditions ("Terms and Conditions") together with the terms specified in your [RightsLink] constitute the License ("License") between you as Licensee and Springer Nature Customer Service Centre GmbH as Licensor. By clicking 'accept' and completing the transaction for your use of the material ("Licensed Material"), you confirm your acceptance of and obligation to be bound by these Terms and Conditions.

1. Grant and Scope of License

1. 1. The Licensor grants you a personal, non-exclusive, non-transferable, non-sublicensable, revocable, world-wide License to reproduce, distribute, communicate to the public, make available, broadcast, electronically transmit or create derivative works using the Licensed Material for the purpose(s) specified in your RightsLink Licence Details only. Licenses are granted for the specific use requested in the order and for no other use, subject to these Terms and Conditions. You acknowledge and agree that the rights granted to you under this License do not include the right to modify, edit, translate, include in collective works, or create derivative works of the Licensed Material in whole or in part unless expressly stated in your RightsLink Licence Details. You may use the Licensed Material only as permitted under this Agreement and will not reproduce, distribute, display, perform, or otherwise use or exploit any Licensed Material in any way, in whole or in part, except as expressly permitted by this License.

1. 2. You may only use the Licensed Content in the manner and to the extent permitted by these Terms and Conditions, by your RightsLink Licence Details and by any applicable laws.

1. 3. A separate license may be required for any additional use of the Licensed Material, e.g. where a license has been purchased for print use only, separate permission must be obtained for electronic re-use. Similarly, a License is only valid in the language selected and does not apply for editions in other languages unless additional translation rights have been granted separately in the License.

1. 4. Any content within the Licensed Material that is owned by third parties is expressly excluded from the License.

1. 5. Rights for additional reuses such as custom editions, computer/mobile applications, film or TV reuses and/or any other derivative rights requests require additional permission and may be subject to an additional fee. Please apply to journalpermissions@springernature.com or bookpermissions@springernature.com for these rights.

2. Reservation of Rights

Licensor reserves all rights not expressly granted to you under this License. You acknowledge and agree that nothing in this License limits or restricts Licensor's rights in or use of the Licensed Material in any way. Neither this License, nor any act, omission, or statement by Licensor or you, conveys any ownership right to you in any Licensed Material, or to any element or portion thereof. As between Licensor and you, Licensor owns and retains all right, title, and interest in and to the Licensed Material subject to the license granted in Section 1.1. Your permission to use the Licensed Material is expressly conditioned on you not impairing Licensor's or the applicable copyright owner's rights in the Licensed Material in any way.

3. Restrictions on use

3. 1. Minor editing privileges are allowed for adaptations for stylistic purposes or formatting purposes provided such alterations do not alter the original meaning or intention of the Licensed Material and the new figure(s) are still accurate and representative of the Licensed Material. Any other changes including but not limited to, cropping, adapting, and/or omitting material that affect the meaning, intention or moral rights of the author(s) are strictly prohibited.

3. 2. You must not use any Licensed Material as part of any design or trademark.

3. 3. Licensed Material may be used in Open Access Publications (OAP), but any such reuse must include a clear acknowledgment of this permission visible at the same time as the figures/tables/illustration or abstract and which must indicate that the Licensed Material is not part of the governing OA license but has been reproduced with permission. This may be indicated according to any standard referencing system but must include at a minimum 'Book/Journal title, Author, Journal Name (if applicable), Volume (if applicable), Publisher, Year, reproduced with permission from SNCSC'.

4. STM Permission Guidelines

4. 1. An alternative scope of license may apply to signatories of the STM Permissions Guidelines ("STM PG") as amended from time to time and made available at https://www.stm-assoc.org/intellectual-property/permissions/permissions-guidelines/.

4. 2. For content reuse requests that qualify for permission under the STM PG, and which may be updated from time to time, the STM PG supersede the terms and

conditions contained in this License.

4. 3. If a License has been granted under the STM PG, but the STM PG no longer apply at the time of publication, further permission must be sought from the Rightsholder. Contact journalpermissions@springernature.com or bookpermissions@springernature.com for these rights.

5. Duration of License

5. 1. Unless otherwise indicated on your License, a License is valid from the date of purchase ("License Date") until the end of the relevant period in the below table:

Reuse in a medical communications project	Reuse up to distribution or time period indicated in License
Reuse in a dissertation/thesis	Lifetime of thesis
Reuse in a journal/magazine	Lifetime of journal/magazine
Reuse in a book/textbook	Lifetime of edition
Reuse on a website	1 year unless otherwise specified in the License
Reuse in a presentation/slide kit/poster	Lifetime of presentation/slide kit/poster. Note: publication whether electronic or in print of presentation/slide kit/poster may require further permission.
Reuse in conference proceedings	Lifetime of conference proceedings
Reuse in an annual report	Lifetime of annual report
Reuse in training/CME materials	Reuse up to distribution or time period indicated in License
Reuse in newsmedia	Lifetime of newsmedia
Reuse in coursepack/classroom materials	Reuse up to distribution and/or time period indicated in license

6. Acknowledgement

6. 1. The Licensor's permission must be acknowledged next to the Licensed Material in print. In electronic form, this acknowledgement must be visible at the same time as the figures/tables/illustrations or abstract and must be hyperlinked to the journal/book's homepage.

6. 2. Acknowledgement may be provided according to any standard referencing system and at a minimum should include "Author, Article/Book Title, Journal name/Book imprint, volume, page number, year, Springer Nature".

7. Reuse in a dissertation or thesis

7. 1. Where 'reuse in a dissertation/thesis' has been selected, the following terms apply: Print rights of the Version of Record are provided for; electronic rights for use only on institutional repository as defined by the Sherpa guideline (www.sherpa.ac.uk/romeo/) and only up to what is required by the awarding institution.

7. 2. For theses published under an ISBN or ISSN, separate permission is required. Please contact journalpermissions@springernature.com or bookpermissions@springernature.com for these rights.

7. 3. Authors must properly cite the published manuscript in their thesis according to current citation standards and include the following acknowledgement: '*Reproduced with permission from Springer Nature*'.

8. License Fee

You must pay the fee set forth in the License Agreement (the "License Fees"). All amounts payable by you under this License are exclusive of any sales, use, withholding, value added or similar taxes, government fees or levies or other assessments. Collection and/or remittance of such taxes to the relevant tax authority shall be the responsibility of the party who has the legal obligation to do so.

9. Warranty

9. 1. The Licensor warrants that it has, to the best of its knowledge, the rights to license reuse of the Licensed Material. **You are solely responsible for ensuring that the material you wish to license is original to the Licensor and does not carry the copyright of another entity or third party (as credited in the published version).** If the credit line on any part of the Licensed Material indicates that it was reprinted or adapted with permission from another source, then you should seek additional permission from that source to reuse the material.

9. 2. EXCEPT FOR THE EXPRESS WARRANTY STATED HEREIN AND TO THE EXTENT PERMITTED BY APPLICABLE LAW, LICENSOR PROVIDES THE LICENSED MATERIAL "AS IS" AND MAKES NO OTHER REPRESENTATION OR WARRANTY. LICENSOR EXPRESSLY DISCLAIMS ANY LIABILITY FOR ANY CLAIM ARISING FROM OR OUT OF THE CONTENT, INCLUDING BUT NOT LIMITED TO ANY ERRORS, INACCURACIES, OMISSIONS, OR DEFECTS CONTAINED THEREIN, AND ANY IMPLIED OR EXPRESS WARRANTY AS TO MERCHANTABILITY OR FITNESS FOR A PARTICULAR PURPOSE. IN NO EVENT SHALL LICENSOR BE LIABLE TO YOU OR ANY OTHER PARTY OR ANY OTHER PERSON OR FOR ANY SPECIAL, CONSEQUENTIAL, INCIDENTAL, INDIRECT, PUNITIVE, OR EXEMPLARY DAMAGES, HOWEVER CAUSED, ARISING OUT OF OR IN CONNECTION WITH THE DOWNLOADING, VIEWING OR USE OF THE LICENSED MATERIAL REGARDLESS OF THE FORM OF ACTION, WHETHER FOR BREACH OF CONTRACT, BREACH OF WARRANTY, TORT, NEGLIGENCE, INFRINGEMENT OR OTHERWISE (INCLUDING, WITHOUT LIMITATION, DAMAGES BASED ON LOSS OF PROFITS, DATA, FILES, USE, BUSINESS OPPORTUNITY OR CLAIMS OF THIRD PARTIES), AND WHETHER OR NOT THE PARTY HAS BEEN ADVISED OF THE POSSIBILITY OF SUCH DAMAGES. THIS LIMITATION APPLIES NOTWITHSTANDING ANY FAILURE OF ESSENTIAL PURPOSE OF ANY LIMITED REMEDY PROVIDED HEREIN.

10. Termination and Cancellation

10. 1. The License and all rights granted hereunder will continue until the end of the applicable period shown in Clause 5.1 above. Thereafter, this license will be terminated and all rights granted hereunder will cease.

10. 2. Licensor reserves the right to terminate the License in the event that payment is not received in full or if you breach the terms of this License.

11. General

11. 1. The License and the rights and obligations of the parties hereto shall be construed, interpreted and determined in accordance with the laws of the Federal

Republic of Germany without reference to the stipulations of the CISG (United Nations Convention on Contracts for the International Sale of Goods) or to Germany´s choice-of-law principle.

11. 2. The parties acknowledge and agree that any controversies and disputes arising out of this License shall be decided exclusively by the courts of or having jurisdiction for Heidelberg, Germany, as far as legally permissible.

11. 3. This License is solely for Licensor's and Licensee's benefit. It is not for the benefit of any other person or entity.

Questions? For questions on Copyright Clearance Center accounts or website issues please contact springernaturesupport@copyright.com or +1-855-239-3415 (toll free in the US) or +1-978-646-2777. For questions on Springer Nature licensing please visit https://www.springernature.com/gp/partners/rights-permissions-third-party-distribution

Other Conditions:

Version 1.4 - Dec 2022

Questions? customercare@copyright.com.

Bibliography

[1] Cheng TO. The true father of circulation: Harvey or Hippocrates? The Annals of Thoracic Surgery. 2001 4;71(4):1399.

[2] Makrantonaki E, Jiang D, Hossini AM, Nikolakis G, Wlaschek M, Scharffetter-Kochanek K, et al. Diabetes mellitus and the skin. Reviews in Endocrine and Metabolic Disorders. 2016 9;17(3):269–282.

[3] Cutolo M, Smith V. Detection of microvascular changes in systemic sclerosis and other rheumatic diseases. Nature Reviews Rheumatology. 2021 11;17(11):665–677.

[4] Lima A, Takala J. Clinical significance of monitoring perfusion in non-vital organs. Intensive Care Med. 2014;40:1052–1054.

[5] Misra S, Shishehbor MH, Takahashi EA, Aronow HD, Brewster LP, Bunte MC, et al. Perfusion Assessment in Critical Limb Ischemia: Principles for Understanding and the Development of Evidence and Evaluation of Devices: A Scientific Statement From the American Heart Association. Circulation. 2019 9;140(12).

[6] Millet C, Roustit M, Blaise S, Cracowski JL. Comparison between laser speckle contrast imaging and laser Doppler imaging to assess skin blood flow in humans. Microvascular Research. 2011;82(2):147–151.

[7] Heeman W, Steenbergen W, van Dam G, Boerma EC. Clinical applications of laser speckle contrast imaging: a review. Journal of biomedical optics. 2019 8;24(8):1–11. Available from: `https://pubmed.ncbi.nlm.nih.gov/31385481https://www.ncbi.nlm.nih.gov/pmc/articles/PMC6983474/`.

[8] Deegan AJ, Wang RK. Microvascular imaging of the skin. Physics in Medicine & Biology. 2019 3;64(7):07TR01.

[9] Lima A, Bakker J. Clinical assessment of peripheral circulation. Current opinion in critical care. 2015;21(3):226–231.

[10] Tafner PFdA, Chen FK, Rabello Filho R, Corrêa TD, Chaves RCdF, Serpa Neto A. Recent advances in bedside microcirculation assessment in critically ill patients. Revista Brasileira de Terapia Intensiva. 2017;29(2).

[11] Ait-Oufella H, Lemoinne S, Boelle PY, Galbois A, Baudel JL, Lemant J, et al. Mottling score predicts survival in septic shock. Intensive Care Med. 2011;37(5):801–807.

[12] Bourcier S, Joffre J, Dubee V, Preda G, Baudel JL, Bige N, et al. Marked regional endothelial dysfunction in mottled skin area in patients with severe infections. Crit Care. 2017;21(1):155.

[13] Levick JR. An introduction to cardiovascular physiology. Butterworth-Heinemann; 2013.

[14] NICE. Monitoring patients in hospital and caring for them if their health becomes worse; 2007. Available from: https://www.nice.org.uk/guidance/cg50/resources/monitoring-patients-in-hospital-and-caring-for-them-if-their-health-becomes-worse-pdf-253000512709.

[15] Bellomo R, Uchino S. Cardiovascular monitoring tools: use and misuse. Current Opinion in Critical Care. 2003;9(3). Available from: https://journals.lww.com/co-criticalcare/Fulltext/2003/06000/Cardiovascular_monitoring_tools__use_and_misuse.10.aspx.

[16] Forrester JS, Ganz W, Diamond G, McHugh T, Chonette DW, Swan HJC. Thermodilution cardiac output determination with a single flow-directed catheter. American Heart Journal. 1972 3;83(3):306–311.

[17] Shah MR, Hasselblad V, Stevenson LW, Binanay C, O'Connor CM, Sopko G, et al. Impact of the Pulmonary Artery Catheter in Critically Ill Patients. JAMA. 2005 10;294(13):1664.

[18] Kobe J, Mishra N, Arya V, Al-Moustadi W, Nates W, Kumar B. Cardiac output monitoring: Technology and choice. Annals of Cardiac Anaesthesia. 2019;22(1):6.

[19] Arya VK, Al-Moustadi W, Dutta V. Cardiac output monitoring-invasive and noninvasive. Current Opinion in Critical Care. 2022 3;Available from: www.co-criticalcare.com.

[20] van Genderen ME, Paauwe J, de Jonge J, van der Valk RJP, Lima A, Bakker J, et al. Clinical assessment of peripheral perfusion to predict postoperative complications after major abdominal surgery early: a prospective observational study in adults. Critical care (London, England). 2014;18(3):R114–R114.

[21] Kara A, Akin S, Ince C. Monitoring microcirculation in critical illness. Current opinion in critical care. 2016;22(5):444–452.

[22] Ince C. Hemodynamic coherence and the rationale for monitoring the microcirculation. Critical Care. 2015;19(3):S8.

[23] De Backer D, Donadello K, Sakr Y, Ospina-Tascon G, Salgado D, Scolletta S, et al. Microcirculatory Alterations in Patients With Severe Sepsis. Critical Care Medicine. 2013 3;41(3):791–799.

[24] Tahvanainen J, Meretoja O, Nikki P. Can central venous blood replace mixed venous blood samples? Critical Care Medicine. 1982 11;10(11):758–761.

[25] Hayden RA. CE Credit: What Keeps Oxygenation on Track? The American Journal of Nursing. 1992 12;92(12):32.

[26] Russell A, Rivers EP, Giri PC, Jaehne AK, Nguyen HB. A Physiologic Approach to Hemodynamic Monitoring and Optimizing Oxygen Delivery in Shock Resuscitation. Journal of Clinical Medicine. 2020 6;9(7):2052.

[27] Bisarya R, Shaath D, Pirzad A, Satterwhite L, He J, Simpson SQ. Serum lactate poorly predicts central venous oxygen saturation in critically ill patients: A retrospective cohort study. Journal of Intensive Care. 2019 9;7(1).

[28] Squara P. Central venous oxygenation: when physiology explains apparent discrepancies. Critical Care. 2014 12;18(5):579.

[29] Andersen LW, Mackenhauer J, Roberts JC, Berg KM, Cocchi MN, Donnino MW. Etiology and therapeutic approach to elevated lactate levels. In: Mayo Clinic Proceedings. vol. 88. Elsevier; 2013. p. 1127–1140.

[30] Tuma RF, Durán WN, Ley K. Microcirculation. Elsevier Inc.; 2008.

[31] Guven G, Hilty M, Ince C. Microcirculation: Physiology, Pathophysiology, and Clinical Application. Blood Purification. 2020;49(1-2):143–150.

[32] Zweifach BW. General principles governing the behavior of the microcirculation. The American Journal of Medicine. 1957 11;23(5):684–696.

[33] Jackson WF. Microcirculation. In: Muscle. Elsevier; 2012. p. 1197–1206.

[34] Gul F, Boran OF, Arslantas R. Microcirculation and Hyperbaric Oxygen Treatment. In: Hyperbaric Oxygen Treatment in Research and Clinical Practice - Mechanisms of Action in Focus. InTech; 2018. .

[35] Gattinoni L, Carlesso E. Supporting hemodynamics: what should we target? What treatments should we use? Critical Care. 2013;17(1):S4.

[36] Moranville MP, Mieure KD, Santayana EM. Evaluation and Management of Shock States: Hypovolemic, Distributive, and Cardiogenic Shock. Journal of Pharmacy Practice. 2010 11;24(1):44–60. Available from: `https://doi.org/10.1177/0897190010388150`.

[37] Lat I, Coopersmith CM, De Backer D. The surviving sepsis campaign: fluid resuscitation and vasopressor therapy research priorities in adult patients. Intensive Care Medicine Experimental. 2021;9(1):1–16.

[38] Singer M. Management of fluid balance. Current Opinion in Anaesthesiology. 2012 2;25(1):96–101.

[39] Hall DP, Jordan H, Alam S, Gillies MA. The impact of focused echocardiography using the Focused Intensive Care Echo protocol on the management of critically ill patients, and comparison with full echocardiographic studies by BSE-accredited sonographers. Journal of the Intensive Care Society. 2017 8;18(3):206–211.

[40] Dünser MW, Dankl D, Petros S, Mer M. Clinical Examination Skills in the Adult Critically Ill Patient. Springer; 2018.

[41] Cormack GC, Lamberty BGH, Miranda Bromage SK. The arterial anatomy of skin flaps. 2nd ed. Churchill Livingstone; 1994.

[42] Agache P. Skin Blood Flow: Histophysiology. In: Agache's Measuring the Skin. Cham: Springer International Publishing; 2017. p. 513–519.

[43] Charkoudian N. Skin blood flow in adult human thermoregulation: how it works, when it does not, and why. Mayo Clinic Proceedings. 2003;78(5):603–612.

[44] Bajwa EK, Malhotra A, Thompson BT. Methods of Monitoring Shock. Seminars in Respiratory and Critical Care Medicine. 2004 12;25(06):629–644.

[45] Taylor RM, Tujios S, Jinjuvadia K, Davern T, Shaikh OS, Han S, et al. Short and long-term outcomes in patients with acute liver failure due to ischemic hepatitis. Digestive diseases and sciences. 2012;57(3):777–785.

[46] Doyle JF, Forni LG. Acute kidney injury: short-term and long-term effects. Critical Care. 2016;20(1):188.

[47] Boyd O, Bennett ED. Enhancement of perioperative tissue perfusion as a therapeutic strategy for major surgery. New horizons (Baltimore, Md). 1996;4(4):453–465.

[48] Klabunde R. Cardiovascular physiology concepts. Lippincott Williams & Wilkins; 2011.

[49] Armstead WM. Cerebral Blood Flow Autoregulation and Dysautoregulation. Anesthesiology Clinics. 2016 9;34(3):465–477.

[50] Fantini S, Sassaroli A, Tgavalekos KT, Kornbluth J. Cerebral blood flow and autoregulation: current measurement techniques and prospects for noninvasive optical methods. Neurophotonics. 2016 6;3(3):031411.

[51] Hemmings HC, Hopkins PM. Foundations of anesthesia: basic sciences for clinical practice. Elsevier Health Sciences; 2006.

[52] Korthuis RJ. Skeletal muscle circulation. In: Colloquium Series on Integrated Systems Physiology: From Molecule to Function. vol. 3. Morgan & Claypool Life Sciences; 2011. p. 1–144.

[53] Johnson PC. Autoregulation of blood flow. Circulation research. 1986;59(5):483–495.

[54] Johnson JM. The cutaneous circulation. In: Laser-Doppler blood flowmetry. Springer; 1990. p. 121–139.

[55] Tuma RF. The Cerebral Microcirculation. In: Microcirculation. Elsevier; 2008. p. 485–520.

[56] Schneider AG, Goodwin MD, Bellomo R. Measurement of kidney perfusion in critically ill Patients. Critical Care. 2013 4;17(2):220.

[57] Yeong Brigitte WF, Childs C. A systematic review on the role of extremity skin temperature as a non-invasive marker for hypoperfusion in critically ill adults in the intensive care setting. JBI Database of Systematic Reviews and Implementation Reports. 2012;10(26).

[58] Strauch B, de Moura W. Arterial system of the fingers. The Journal of Hand Surgery. 1990 1;15(1):148–154.

[59] Lee CM, Jin SP, Doh EJ, Lee DH, Chung JH. Regional Variation of Human Skin Surface Temperature. Annals of Dermatology. 2019;31(3):349.

[60] Douglas G, Nicol F, Robertson C. Macleod's clinical examination. Thirteenth ed. Edinburgh, Scotland: Churchill Livingstone; 2013.

[61] Lima A, Bakker J. Clinical monitoring of peripheral perfusion: there is more to learn. Critical Care. 2014;18(1):113.

[62] van Genderen ME, van Bommel J, Lima A. Monitoring peripheral perfusion in critically ill patients at the bedside. Current opinion in critical care. 2012;18(3):273–279.

[63] van Genderen ME, Lima A, Akkerhuis M, Bakker J, van Bommel J. Persistent peripheral and microcirculatory perfusion alterations after out-of-hospital cardiac arrest are associated with poor survival*. Critical Care Medicine. 2012 8;40(8):2287–2294.

[64] Vincent JL, De Backer D. Circulatory shock. New England Journal of Medicine. 2013;369(18):1726–1734.

[65] Yeh YC, Chiu CT. Association and dissociation of microcirculation and macrocirculation in critically ill patients with shock. Journal of Emergency and Critical Care Medicine. 2019 12;3:60–60.

[66] Lima R, Villela N, Castiglione R, de Souza MdGC, Bouskela E. Dissociation between macro- and microvascular parameters in the early phase of hemorrhagic shock. Microvascular Research. 2019 11;126:103909.

[67] Hariri G, Joffre J, Leblanc G, Bonsey M, Lavillegrand JRR, Urbina T, et al. Narrative review: clinical assessment of peripheral tissue perfusion in septic shock. Annals of intensive care. 2019;9(1):37. Available from: `https://doi.org/10.1186/s13613-019-0511-1`.

[68] Humbert P, Fanian F, Maibach HI, Agache P. Agache's Measuring the Skin. 2nd ed. Springer; 2016.

[69] Nafisi S, Maibach HI. Skin penetration of nanoparticles. In: Emerging Nanotechnologies in Immunology. Elsevier; 2018. p. 47–88.

[70] Stücker M, Struk A, Altmeyer P, Herde M, Baumgärtl H, Lübbers DW. The cutaneous uptake of atmospheric oxygen contributes significantly to the oxygen supply of human dermis and epidermis. The Journal of Physiology. 2002 2;538(3):985–994.

[71] Shimizu H. Shimizu's Dermatology. 2nd ed. New York, UNITED KINGDOM: John Wiley & Sons, Incorporated; 2016.

[72] Taylor GI, Corlett RJ, Dhar SC, Ashton MW. The anatomical (angiosome) and clinical territories of cutaneous perforating arteries: development of the concept and designing safe flaps. Plastic and reconstructive surgery. 2011;127(4):1447–1459.

[73] Pan WR, Taylor GI. The Angiosomes of the Thigh and Buttock. Plastic & Reconstructive Surgery. 2009 1;123(1):236–249.

[74] Buntic R. Atlas of Microsurgery Techniques and Principles; 2022. Available from: `https://www.microsurgeon.org/index`.

[75] Morris SF, Tang M, Almutari K, Geddes C, Yang D. The Anatomic Basis of Perforator Flaps. Clinics in Plastic Surgery. 2010 10;37(4).

[76] Prasetyono TOH, Menna C. Cutaneous Perforators and Their Clinical Implications on Intrinsic Hand Flaps: A Systematic Review. Plastic and Reconstructive Surgery - Global Open. 2022 4;10(4):e4154.

[77] Berner JE, Pereira N, Troisi L, Will P, Nanchahal J, Jain A. Accuracy of infrared thermography for perforator mapping: A systematic review and meta-analysis of diagnostic studies. Journal of Plastic, Reconstructive & Aesthetic Surgery. 2021;74(6):1173–1179. Available from: https://www.sciencedirect.com/science/article/pii/S1748681521000280.

[78] Chubb DP, Taylor GI, Ashton MW. True and "Choke" Anastomoses between Perforator Angiosomes: Part II. Dynamic Thermographic Identification. Plastic and Reconstructive Surgery. 2013;132(6). Available from: https://journals.lww.com/plasreconsurg/Fulltext/2013/12000/True_and__Choke__Anastomoses_between_Perforator.14.aspx.

[79] Amini A, Nagalli S. Bowel Ischemia; 2022.

[80] Momjian-Mayor I, Baron JC. The Pathophysiology of Watershed Infarction in Internal Carotid Artery Disease. Stroke. 2005 3;36(3):567–577. Available from: https://doi.org/10.1161/01.STR.0000155727.82242.e1.

[81] McGregor IA, Morgan G. Axial and random pattern flaps. British Journal of Plastic Surgery. 1973;26(3):202–213.

[82] Weum S, Mercer JB, de Weerd L. Evaluation of dynamic infrared thermography as an alternative to CT angiography for perforator mapping in breast reconstruction: A clinical study. BMC Medical Imaging. 2016 7;16(1).

[83] Hennessy O, Potter SM. Use of infrared thermography for the assessment of free flap perforators in autologous breast reconstruction: A systematic review. Elsevier Ltd; 2020.

[84] de Weerd L, Mercer JB, Weum S. Dynamic Infrared Thermography. Clinics in Plastic Surgery. 2011;38(2):277–292. Available from: http://www.sciencedirect.com/science/article/pii/S0094129811000228.

[85] Blondeel PN, Beyens G, Verhaeghe R, Van Landuyt K, Tonnard P, Monstrey SJ, et al. Doppler flowmetry in the planning of perforator flaps. British Journal of Plastic Surgery. 1998;51(3):202–209.

[86] Lam DL, Mitsumori LM, Neligan PC, Warren BH, Shuman WP, Dubinsky TJ. Pre-operative CT angiography and three-dimensional image post processing for deep inferior epigastric perforator flap breast reconstructive surgery. The British Journal of Radiology. 2012 12;85(1020):e1293–e1297.

[87] Wei Fc, Jain V, Celik N, Chen Hc, Chuang DCC, Lin Ch. Have We Found an Ideal Soft-Tissue Flap? An Experience with 672 Anterolateral Thigh Flaps. Plastic and Reconstructive Surgery. 2002;109(7). Available from: https://journals.lww.com/plasreconsurg/Fulltext/2002/06000/Have_We_Found_an_Ideal_Soft_Tissue_Flap__An.7.aspx.

[88] Yu P, Youssef A. Efficacy of the Handheld Doppler in Preoperative Identification of the Cutaneous Perforators in the Anterolateral Thigh Flap. Plastic and Reconstructive Surgery. 2006 9;118(4):928–933.

[89] Kehrer A, Sachanadani NS, da Silva NPB, Lonic D, Heidekrueger P, Taeger CD, et al. Step-by-step guide to ultrasound-based design of alt flaps by the microsurgeon – Basic and advanced applications and device settings. Journal of Plastic, Reconstructive & Aesthetic Surgery. 2020 6;73(6):1081–1090.

[90] Rozen WM, Phillips TJ, Ashton MW, Stella DL, Gibson RN, Taylor GI. Preoperative Imaging for DIEA Perforator Flaps: A Comparative Study of Computed Tomographic Angiography and Doppler Ultrasound. Plastic and Reconstructive Surgery. 2008 1;121(MOC-PS CME Coll):1–8.

[91] Kumamaru KK, Hoppel BE, Mather RT, Rybicki FJ. CT Angiography: Current Technology and Clinical Use. Radiologic Clinics of North America. 2010 3;48(2):213–235.

[92] Hoffmann KR, Dmochowski J, Nazareth DP, Miskolczi L, Nemes B, Gopal A, et al. Vessel size measurements in angiograms: Manual measurements. Medical Physics. 2003 3;30(4):681–688.

[93] Waldman DL, Cantos AJ. Angiography. Complications in Endovascular Surgery. 2022;p. 279–284. Available from: https://linkinghub.elsevier.com/retrieve/pii/B9780323554480000437.

[94] Pereira N, Valenzuela D, Mangelsdorff G, Kufeke M, Roa R. Detection of Perforators for Free Flap Planning Using Smartphone Thermal Imaging: A Concordance Study with Computed Tomographic Angiography in 120 Perforators. Plastic and Reconstructive Surgery. 2018;141(3). Available from: https://journals.lww.com/plasreconsurg/Fulltext/2018/03000/Detection_of_Perforators_for_Free_Flap_Planning.38.aspx.

[95] Tenorio X, Mahajan AL, Elias B, van Riempst JS, Wettstein R, Harder Y, et al. Locating Perforator Vessels by Dynamic Infrared Imaging and Flow Doppler With No Thermal Cold Challenge. Annals of Plastic Surgery. 2011;67(2). Available from: https://journals.lww.com/annalsplasticsurgery/Fulltext/2011/08000/Locating_Perforator_Vessels_by_Dynamic_Infrared.14.aspx.

[96] Xiao W, Li K, Kiu-Huen NG S, Feng S, Zhou H, Nicoli F, et al. A Prospective Comparative Study of Color Doppler Ultrasound and Infrared Thermography in the Detection of Perforators for Anterolateral Thigh Flaps. Annals of Plastic Surgery. 2020;84(5S). Available from: https://journals.lww.com/annalsplasticsurgery/Fulltext/2020/05003/A_Prospective_Comparative_Study_of_Color_Doppler.6.aspx.

[97] Chen Q, Zhang L, Ge S, He W, Zeng M. Prognosis predictive value of the Oxford Acute Severity of Illness Score for sepsis: a retrospective cohort study. PeerJ. 2019 6;7:e7083.

[98] Donadio V, Nolano M, Provitera V, Stancanelli A, Lullo F, Liguori R, et al. Skin sympathetic adrenergic innervation: an immunofluorescence confocal study. Annals of Neurology: Official Journal of the American Neurological Association and the Child Neurology Society. 2006;59(2):376–381.

[99] Folkow B. Nervous control of the blood vessels. Physiological Reviews. 1955;35(3):629–663.

[100] Zweifach BW, Nagler AL, Thomas L. The role of epinephrine in the reactions produced by the endotoxins of Gram-negative bacteria. Journal of Experimental Medicine. 1956 12;104(6):881–896.

[101] Duval A, Pouchot J. Livedo: from pathophysiology to diagnosis. Rev Med Interne. 2008;29(5):380–392.

[102] Ait-Oufella H, Bourcier S, Alves M, Galbois A, Baudel JL, Margetis D, et al. Alteration of skin perfusion in mottling area during septic shock. Annals of intensive care. 2013;3(1):31.

[103] Charkoudian N. Mechanisms and modifiers of reflex induced cutaneous vasodilation and vasoconstriction in humans. Journal of Applied Physiology. 2010 10;109(4):1221–1228.

[104] Ahlquist R. A study of the adrenotropic receptors. American Journal of Physiology. 1948;153(3):586–600. Available from: `https://www.physiology.org/doi/pdf/10.1152/ajplegacy.1948.153.3.586`.

[105] VanValkinburgh D, Kerndt CC, Hashmi MF. Inotropes and vasopressors. 2018;.

[106] Kellogg DL. In vivo mechanisms of cutaneous vasodilation and vasoconstriction in humans during thermoregulatory challenges. Journal of Applied Physiology. 2006 5;100(5):1709–1718.

[107] Vinnakota S, Chen HH. The Importance of Natriuretic Peptides in Cardiometabolic Diseases. Journal of the Endocrine Society. 2020 6;4(6).

[108] Nishiyama SK, Zhao J, Wray DW, Richardson RS. Vascular function and endothelin-1: tipping the balance between vasodilation and vasoconstriction. Journal of Applied Physiology. 2017 2;122(2):354–360.

[109] Thomas HM. Effect of thyroid hormone on circulation. Journal of the American Medical Association. 1957 2;163(5):337.

[110] Fromy B, Merzeau S, Abraham P, Saumet JL. Mechanisms of the cutaneous vasodilator response to local external pressure application in rats: involvement of CGRP, neurokinins, prostaglandins and NO. British Journal of Pharmacology. 2000 11;131(6):1161–1171.

[111] Chen K, Pittman RN, Popel AS. Nitric Oxide in the Vasculature: Where Does It Come From and Where Does It Go? A Quantitative Perspective. Antioxidants & Redox Signaling. 2008 7;10(7):1185–1198.

[112] Moor Instruments. Laser Speckle Contrast Imager; 2022. Available from: `https://www.moor.co.uk/products/imaging/laser-speckle-contrast-imager/`.

[113] Law J, Martin EA. Concise Medical Dictionary. Law J, Martin E, editors. Oxford University Press; 2020.

[114] Holmes SR, King S, Stott JRR, Clemes S. Facial Skin Pallor Increases During Motion Sickness. Journal of Psychophysiology. 2002;16:150–157.

[115] Ferraris A, Bouisse C, Mottard N, Thiolliere F, Anselin S, Piriou V, et al. Mottling score and skin temperature in septic shock: Relation and impact on prognosis in ICU. PLoS One. 2018;13(8):e0202329.

[116] Yamazaki F, Yuge N. Limb-specific differences in the skin vascular responsiveness to adrenergic agonists. Journal of Applied Physiology. 2011;111(1):170–176.

[117] Owen VS, Rosgen BK, Cherak SJ, Ferland A, Stelfox HT, Fiest KM, et al. Adverse events associated with administration of vasopressor medications through a peripheral intravenous catheter: a systematic review and meta-analysis. Critical Care. 2021 12;25(1):146.

[118] Joly HR, Weil MH. Temperature of the great toe as an indication of the severity of shock. Circulation. 1969;39(1):131–138.

[119] Kaplan LJ, McPartland K, Santora TA, Trooskin SZ. Start with a subjective assessment of skin temperature to identify hypoperfusion in intensive care unit patients. Journal of Trauma and Acute Care Surgery. 2001;50(4):620–628.

[120] Schey BM, Williams DY, Bucknall T. Skin temperature and core-peripheral temperature gradient as markers of hemodynamic status in critically ill patients: A review. Heart & Lung. 2010 1;39(1).

[121] WOODS I, WILKINS RG, EDWARDS JD, MARTIN PD, FARAGHER EB. Danger of using core/peripheral temperature gradient as a guide to therapy in shock. Critical Care Medicine. 1987 9;15(9).

[122] Sommers MS, Stevenson JS, Hamlin RL, Ivey TD. Skin Temperature and Limb Blood Flow as Predictors of Cardiac Index. Clinical Nursing Research. 1995 2;4(1).

[123] MacRae BA, Annaheim S, Spengler CM, Rossi RM. Skin Temperature Measurement Using Contact Thermometry: A Systematic Review of Setup Variables and Their Effects on Measured Values. Frontiers in Physiology. 2018 1;9.

[124] Falotico JM, Shinozaki K, Saeki K, Becker LB. Advances in the Approaches Using Peripheral Perfusion for Monitoring Hemodynamic Status. Frontiers Media S.A.; 2020.

[125] Lara B, Enberg L, Ortega M, Leon P, Kripper C, Aguilera P, et al. Capillary refill time during fluid resuscitation in patients with sepsis-related hyperlactatemia at the emergency department is related to mortality. PLOS ONE. 2017 11;12(11):e0188548.

[126] Murray AK. Laser Doppler imaging: a developing technique for application in the rheumatic diseases. Rheumatology. 2004 7;43(10):1210–1218.

[127] Khatib M, Jabir S, Fitzgerald O'Connor E, Philp B. A Systematic Review of the Evolution of Laser Doppler Techniques in Burn Depth Assessment. Plastic Surgery International. 2014 8;2014:1–13.

[128] Boyle NH, Manifold D, Jordan MH, Mason RC. Intraoperative assessment of colonic perfusion using scanning laser doppler flowmetry during colonic resection11No competing interests declared. Journal of the American College of Surgeons. 2000 11;191(5):504–510.

[129] Forrester KR, Stewart C, Tulip J, Leonard C, Bray RC. Comparison of laser speckle and laser Doppler perfusion imaging: Measurement in human skin and rabbit articular tissue. Medical & Biological Engineering & Computing. 2002 11;40(6):687–697.

[130] Ruaro B, Sulli A, Alessandri E, Pizzorni C, Ferrari G, Cutolo M. Laser speckle contrast analysis: a new method to evaluate peripheral blood perfusion in systemic sclerosis patients. Annals of the Rheumatic Diseases. 2014 6;73(6):1181–1185.

[131] Lindahl F, Tesselaar E, Sjöberg F. Assessing paediatric scald injuries using Laser Speckle Contrast Imaging. Burns. 2013;39(4):662–666.

[132] Van Genderen ME, Bartels SA, Lima A, Bezemer R, Ince C, Bakker J, et al. Peripheral perfusion index as an early predictor for central hypovolemia in awake healthy volunteers. Anesthesia & Analgesia. 2013;116(2):351–356.

[133] Hui D, dos Santos R, Chisholm G, Bansal S, Souza Crovador C, Bruera E. Bedside clinical signs associated with impending death in patients with advanced cancer: Preliminary findings of a prospective, longitudinal cohort study. Cancer. 2015 3;121(6):960–967.

[134] De Backer D, Creteur J, Dubois MJJ, Sakr Y, Vincent JLL. Microvascular alterations in patients with acute severe heart failure and cardiogenic shock. American Heart Journal. 2004;147(1):91–99.

[135] Revier J. Étude descriptive de la vascularisation dermique superficielle au niveau de la malléole interne; 1981.

[136] Sakr Y, Dubois MJ, De Backer D, Creteur J, Vincent JL. Persistent microcirculatory alterations are associated with organ failure and death in patients with septic shock. Critical care medicine. 2004;32(9):1825–1831.

[137] Grissom CK, Morris AH, Lanken PN, Ancukiewicz M, Orme Jr JF, Schoenfeld DA, et al. Association of physical examination with pulmonary artery catheter parameters in acute lung injury. Critical care medicine. 2009;37(10):2720–2726.

[138] Coudroy R, Jamet A, Thille AW. Is skin mottling a predictor of high mortality in non-selected patients with cirrhosis admitted to intensive care unit? Journal of hepatology. 2015;63(3):770–771.

[139] Galbois A, Bigé N, Pichereau C, Boëlle PY, Baudel JL, Bourcier S, et al. Exploration of skin perfusion in cirrhotic patients with septic shock. Journal of hepatology. 2015;62(3):549–555.

[140] Gerber K. Basic Priniciples of Intensive Care Nursing; 2020. Available from: `https://www.baccn.org/media/resources/Basic_principles_of_Intensive_Care_Nursing.pdf`.

[141] Benchimol EI, Smeeth L, Guttmann A, Harron K, Moher D, Petersen I, et al. The REporting of studies Conducted using Observational Routinely-collected health Data (RECORD) statement. PLoS medicine. 2015;12(10):e1001885.

[142] Johnson AEW, Burgess J, Pimentel MAF, Clifton DA, Young JD, Watkinson PJ, et al. Physiological trajectory of patients pre and post ICU discharge. In: 2014 36th Annual International Conference of the IEEE Engineering in Medicine and Biology Society. IEEE; 2014. p. 3160–3163.

[143] Johnson AEW, Kramer AA, Clifford GD. A new severity of illness scale using a subset of acute physiology and chronic health evaluation data elements shows comparable predictive accuracy. Critical care medicine. 2013;41(7):1711–1718.

[144] Dumas G, Lavillegrand JR, Joffre J, Bigé N, De-Moura EB, Baudel JL, et al. Mottling score is a strong predictor of 14-day mortality in septic patients whatever vasopressor doses and other tissue perfusion parameters. Critical Care. 2019;23(1):211.

[145] R Core Team. R: A Language and Environment for Statistical Computing. Vienna, Austria: R Foundation for Statistical Computing; 2021.

[146] Coudroy R, Jamet A, Frat JP, Veinstein A, Chatellier D, Goudet V, et al. Incidence and impact of skin mottling over the knee and its duration on outcome in critically ill patients. Intensive Care Med. 2015;41(3):452–459.

[147] Hiemstra B, Koster G, Wiersema R, Hummel YM, van der Harst P, Snieder H, et al. The diagnostic accuracy of clinical examination for estimating cardiac index in critically ill patients: the Simple Intensive Care Studies-I. Intensive care medicine. 2019;45(2):190–200. Available from: `https://link.springer.com/content/pdf/10.1007%2Fs00134-019-05527-y.pdf`.

[148] Ait-Oufella H, Joffre J, Boelle PY, Galbois A, Bourcier S, Baudel JL, et al. Knee area tissue oxygen saturation is predictive of 14-day mortality in septic shock. Intensive Care Med. 2012;38(6):976–983.

[149] Boulain T, Boisrame-Helms J, Ehrmann S, Lascarrou JB, Bouglé A, Chiche A, et al. Volume expansion in the first 4 days of shock: a prospective multicentre study in 19 French intensive care units. Intensive care medicine. 2015;41(2):248–256.

[150] Cheng J, Chen X, Xu L, Wang ZJ. Illumination Variation-Resistant Video-Based Heart Rate Measurement Using Joint Blind Source Separation and Ensemble Empirical Mode Decomposition. IEEE J Biomed Health Inform. 2017;21(5):1422–1433.

[151] de Moura EB, Amorim FF, da Cruz Santana AN, Kanhouche G, de Souza Godoy LG, de Jesus Almeida L, et al. Skin mottling score as a predictor of 28-day mortality in patients with septic shock. Intensive Care Med. 2016;42(3):479–480.

[152] Sanderson M, Chikhani M, Blyth E, Wood S, Moppett IK, McKeever T, et al. Predicting 30-day mortality in patients with sepsis: An exploratory analysis of process of care and patient characteristics. Journal of the Intensive Care Society. 2018;19(4):299–304.

[153] Lima A, Jansen TC, van Bommel J, Ince C, Bakker J. The prognostic value of the subjective assessment of peripheral perfusion in critically ill patients. Critical care medicine. 2009;37(3):934–938.

[154] Sun Y, Thakor N. Photoplethysmography revisited: from contact to noncontact, from point to imaging. IEEE Trans Biomed Eng. 2016;63(3):463–477.

[155] Filingeri D, Zhang H, Arens EA. Thermosensory micromapping of warm and cold sensitivity across glabrous and hairy skin of male and female hands and feet. Journal of Applied Physiology. 2018 9;125(3):723–736.

[156] FLIR. FLIR A6750sc MWIR;. Available from: `http://www.flirmedia.com/MMC/THG/Brochures/RND_033/RND_033_US.pdf`.

[157] de Haan G, Verkruysse W. Editorial for Special Issue: Contactless Vital Signs Monitoring. Applied Sciences. 2019 12;10(1):166.

[158] Parry R, Pino M, Faull C, Feathers L. Acceptability and design of video-based research on healthcare communication: Evidence and recommendations. Patient Education and Counseling. 2016 8;99(8):1271–1284.

[159] Doberstein C, Charbonneau Morin G, Despatie S. Measuring the Acceptability of Facial Recognition-Enabled Work Surveillance Cameras in the Public and Private Sector. Public Performance & Management Review. 2022 1;45(1):198–227.

[160] Omboni S, Padwal RS, Alessa T, Benczúr B, Green BB, Hubbard I, et al. The worldwide impact of telemedicine during COVID-19: current evidence and recommendations for the future. Connected Health. 2022;.

[161] Harford M, Catherall J, Gerry S, Young JD, Watkinson P. Availability and performance of image-based, non-contact methods of monitoring heart rate, blood pressure, respiratory rate, and oxygen saturation: A systematic review. Physiological Measurement. 2019 6;40(6).

[162] ANSI/AAMI. Cardiac monitors, heart rate meters, and alarms. American National Standard (ANSI/AAMI EC13: 2002) Arlington, VA. 2002;p. 1–87.

[163] Severinghaus JW. Takuo Aoyagi: discovery of pulse oximetry. Anesthesia & Analgesia. 2007;105(6):S1–S4.

[164] Sun Y, Hu S, Azorin-Peris V, Greenwald S, Chambers J, Zhu Y. Motion-compensated noncontact imaging photoplethysmography to monitor cardiorespiratory status during exercise. J Biomed Opt. 2011;16(7):77010.

[165] Allen J, Zheng D, Kyriacou PA, Elgendi M. Photoplethysmography (PPG): state-of-the-art methods and applications. Physiological Measurement. 2021 10;42(10):100301.

[166] Hartmann V, Liu H, Chen F, Qiu Q, Hughes S, Zheng D. Quantitative Comparison of Photoplethysmographic Waveform Characteristics: Effect of Measurement Site. Frontiers in Physiology. 2019 3;10.

[167] Westerhof N, Lankhaar JW, Westerhof BE. The arterial Windkessel. Medical & Biological Engineering & Computing. 2009 2;47(2):131–141.

[168] Chan ED, Chan MM, Chan MM. Pulse oximetry: Understanding its basic principles facilitates appreciation of its limitations. Respiratory Medicine. 2013 6;107(6).

[169] Wieringa FP, Mastik F, van der Steen AFW. Contactless multiple wavelength photoplethysmographic imaging: a first step toward "SpO2 camera" technology. Ann Biomed Eng. 2005;33(8):1034–1041.

[170] Goodell TT. An in vitro quantification of pressures exerted by earlobe pulse oximeter probes following reports of device-related pressure ulcers in ICU patients. Ostomy/wound Management. 2012;58(11):30–34.

[171] Kim JY, Lee YJ. Medical device-related pressure ulcer (MDRPU) in acute care hospitals and its perceived importance and prevention performance by clinical nurses. International Wound Journal. 2019 3;16:51–61.

[172] Kamshilin AA, Nippolainen E, Sidorov IS, Vasilev PV, Erofeev NP, Podolian NP, et al. A new look at the essence of the imaging photoplethysmography. Scientific reports. 2015;5:10494. Available from: `http://dx.doi.org/10.1038/srep10494`.

[173] Moço AV, Stuijk S, de Haan G. New insights into the origin of remote PPG signals in visible light and infrared. Scientific Reports. 2018;8(1):8501. Available from: `https://doi.org/10.1038/s41598-018-26068-2`.

[174] Wu HY, Rubinstein M, Shih E, Guttag J, Durand F, Freeman W. Eulerian video magnification for revealing subtle changes in the world. ACM transactions on graphics (TOG). 2012;31(4):1–8.

[175] He X, Goubran RA, Liu XP. Wrist pulse measurement and analysis using Eulerian video magnification. In: 2016 IEEE-EMBS International Conference on Biomedical and Health Informatics (BHI). IEEE; 2016. p. 41–44.

[176] McDuff D, Gontarek S, Picard RW. Remote detection of photoplethysmographic systolic and diastolic peaks using a digital camera. IEEE Trans Biomed Eng. 2014;61(12):2948–2954.

[177] Van Gastel M, Stuijk S, de Haan G. Motion Robust Remote-PPG in Infrared. IEEE Trans Biomed Eng. 2015;62(5):1425–1433.

[178] Yang Y, Liu C, Yu H, Shao D, Tsow F, Tao N. Motion robust remote photoplethysmography in CIELab color space. J Biomed Opt. 2016;21(11):117001.

[179] Secerbegovic A, Bergsland J, Halvorsen PS, Suljanovic N, Mujcic A, Balasingham I. Blood pressure estimation using video plethysmography. Prague, Czech Republic: IEEE; 2016.

[180] Jain M, Deb S, Subramanyam AV. Face Video Based Touchless Blood Pressure and Heart Rate Estimation. Montreal, Canada: IEEE; 2017.

[181] Khong WL, Rao NSVK, Mariappan M. Blood pressure measurements using non-contact video imaging techniques. In: 2017 IEEE 2nd International Conference on Automatic Control and Intelligent Systems (I2CACIS). IEEE; 2017. p. 35–40.

[182] Rong M, Li K. A Blood Pressure Prediction Method Based on Imaging Photoplethysmography in combination with Machine Learning. Biomedical Signal Processing and Control. 2021 2;64:102328.

[183] Mukkamala R, Hahn JO, Inan OT, Mestha LK, Kim CS, Töreyin H, et al. Toward ubiquitous blood pressure monitoring via pulse transit time: theory and practice. IEEE Transactions on Biomedical Engineering. 2015;62(8):1879–1901.

[184] Stergiou GS, Alpert B, Mieke S, Asmar R, Atkins N, Eckert S, et al. A universal standard for the validation of blood pressure measuring devices. Journal of Hypertension. 2018 3;36(3):472–478.

[185] Steinman J, Barszczyk A, Sun HS, Lee K, Feng ZP. Smartphones and Video Cameras: Future Methods for Blood Pressure Measurement. Frontiers in Digital Health. 2021 11;3.

[186] Tran DN, Lee H, Kim C. A robust real time system for remote heart rate measurement via camera. 2015 IEEE International Conference on Multimedia and Expo (ICME). 2015;p. 1–6.

[187] Gupta O, McDuff D, Raskar R. Real-time physiological measurement and visualization using a synchronized multi-camera system. Las Vegas, USA: IEEE; 2016.

[188] Fallet S, Mirmohamadsadeghi L, Moser V, Braun F, Vesin JM. Real-time approaches for heart rate monitoring using imaging photoplethysmography. Vancouver, Canada: IEEE; 2016.

[189] Bai G, Huang J, Liu H. Real-time robust noncontact heart rate monitoring with a camera. IEEE Access. 2018;6:33682–33691.

[190] Ede J, Vollam S, Darbyshire JL, Gibson O, Tarassenko L, Watkinson P. Non-contact vital sign monitoring of patients in an intensive care unit: A human factors analysis of staff expectations. Applied Ergonomics. 2021 1;90.

[191] Coppetti T, Brauchlin A, Muggler S, Attinger-Toller A, Templin C, Schonrath F, et al. Accuracy of smartphone apps for heart rate measurement. Eur J Prev Cardiol. 2017;24(12):1287–1293.

[192] Tarassenko L, Villarroel M, Guazzi A, Jorge J, Clifton DA, Pugh C. Non-contact video-based vital sign monitoring using ambient light and auto-regressive models. Physiol Meas. 2014;35(5):807–831.

[193] Aarts LAM, Jeanne V, Cleary JP, Lieber C, Nelson JS, Bambang Oetomo S, et al. Non-contact heart rate monitoring utilizing camera photoplethysmography in the neonatal intensive care unit - a pilot study. Early Hum Dev. 2013;89(12):943–948. Available from: `http://dx.doi.org/10.1016/j.earlhumdev.2013.09.016`.

[194] Villarroel M, Guazzi A, Jorge J, Davis S, Watkinson P, Green G, et al. Continuous non-contact vital sign monitoring in neonatal intensive care unit. Healthc Technol Lett. 2014;1(3):87–91.

[195] Jorge J, Villarroel M, Chaichulee S, Guazzi A, Davis S, Green G, et al.. Non-Contact Monitoring of Respiration in the Neonatal Intensive Care Unit. Washington, USA: IEEE; 2017.

[196] Mestha LK, Kyal S, Xu B, Lewis LE, Kumar V. Towards continuous monitoring of pulse rate in neonatal intensive care unit with a webcam. In: Engineering in Medicine and Biology Society (EMBC), 2014 36th Annual International Conference of the IEEE. vol. 2014. Chicago, USA: IEEE; 2014. p. 3817–3820.

[197] Jorge J, Villarroel M, Tomlinson H, Gibson O, Darbyshire JL, Ede J, et al. Non-contact physiological monitoring of post-operative patients in the intensive care unit. npj Digital Medicine. 2022 12;5(1):4.

[198] Kumar M, Suliburk JW, Veeraraghavan A, Sabharwal A. PulseCam: a camera-based, motion-robust and highly sensitive blood perfusion imaging modality. Scientific Reports. 2020 12;10(1).

[199] Jensen J. Camera-based Heart Rate Monitoring. Denmark; 2014.

[200] Koprowski R. Blood pulsation measurement using cameras operating in visible light: limitations. Biomed Eng Online. 2016;15(1):111.

[201] Chen W, Hernandez J, Picard RW. Estimating carotid pulse and breathing rate from near-infrared video of the neck. Physiological measurement. 2018;39(10):10NT01.

[202] Al-Naji A, Gibson K, Lee SH, Chahl J. Monitoring of Cardiorespiratory Signal: Principles of Remote Measurements and Review of Methods. IEEE Access. 2017;5:15776–15790.

[203] Harford M, Areia C, Villarroel M, Jorge J, Finnegan E, Davidson S, et al. Study protocol for an exploratory interventional study investigating the feasibility of video-based non-contact physiological monitoring in healthy volunteers by Mapping of Lower Limb skIn pErfusion (MOLLIE). BMJ Open. 2020 6;10(6).

[204] Casiglia E, Bongiovi S, Paleari CD, Petucco S, Boni M, Colangeli G, et al. Haemodynamic effects of coffee and caffeine in normal volunteers: a placebo-controlled clinical study. Journal of Internal Medicine. 1991 6;229(6):501–504.

[205] Mills DL. Internet time synchronization: the network time protocol. IEEE Transactions on Communications. 1991;39(10):1482–1493.

[206] Finnegan E, Davidson S, Harford M, Jorge J, Watkinson P, Young D, et al. Pulse arrival time as a surrogate of blood pressure. Scientific Reports. 2021 12;11(1):22767.

[207] Reed MJ. Administering a glyceryl trinitrate infusion: big is not always best. Emergency Medicine Journal. 2007 6;24(6):423–424.

[208] Cooper BE. Review and Update on Inotropes and Vasopressors. AACN Advanced Critical Care. 2008 1;19(1):5–13.

[209] Hashimoto S, Kobayashi A. Clinical Pharmacokinetics and Pharmacodynamics of Glyceryl Trinitrate and its Metabolites. Clinical Pharmacokinetics. 2003;42(3):205–221. Available from: `https://doi.org/10.2165/00003088-200342030-00001`.

[210] Theuvenet WJ, Koeyers GF, Borghouts MHM. Thermographic assessment of perforating arteries. Scandinavian Journal of Plastic and Reconstructive Surgery and Hand Surgery. 1986;20(1):25–29.

[211] Tsuyoshi C, Arai K, Miyazaki N, Igota S, Yamamoto N. Making of a Facial Perforator Map by Thermography. Annals of Plastic Surgery. 2000;44(6):596–600.

[212] Muntean MV, Strilciuc S, Ardelean F, Pestean C, Lacatus R, Badea AF, et al. Using dynamic infrared thermography to optimize color doppler ultrasound mapping of cutaneous perforators. Medical Ultrasonography. 2015;17(4):503–508.

[213] National Institute for Health and Care Excellence. HemaClear for bloodless surgical field during limb surgery; 2019. Available from: `https://www.nice.org.uk/advice/mib187/chapter/The-technology`.

[214] NICE. HemaClear for bloodless surgical field during limb surgery; 2019. Available from: https://www.nice.org.uk/advice/mib187/resources/hemaclear-for-bloodless-surgical-field-during-limb-surgery-pdf-2285963703068101.

[215] Tang D, Olesnicky, Eby M, Heiskell. Auto-transfusion tourniquets: the next evolution of tourniquets. Open Access Emergency Medicine. 2013 12;p. 29.

[216] FLIR. Using colour interpolation; 2017. Available from: https://www.flir.com/globalassets/support/iis/application-notes/tan2017004-color-interpolation.pdf.

[217] Teledyne FLIR. How Does Emissivity Affect Thermal Imaging?; 2022. Available from: https://www.flir.co.uk/discover/professional-tools/how-does-emissivity-affect-thermal-imaging/.

[218] Charlton M, Stanley SA, Whitman Z, Wenn V, Coats TJ, Sims M, et al. The effect of constitutive pigmentation on the measured emissivity of human skin. PLOS ONE. 2020 11;15(11):e0241843.

[219] Funk DJ, Moretti EW, Gan TJ. Minimally Invasive Cardiac Output Monitoring in the Perioperative Setting. Anesthesia & Analgesia. 2009 3;108(3):887–897.

[220] Harford M, Clark SH, Smythe JF, Gerry S, Villarroel M, Jorge J, et al. Non-invasive stroke volume estimation by transthoracic electrical bioimpedance versus Doppler echocardiography in healthy volunteers. Journal of medical engineering & technology. 2019;43(1):33–37.

[221] Mangraviti A, Volpin F, Cha J, Cunningham SI, Raje K, Brooke MJ, et al. Intraoperative Laser Speckle Contrast Imaging For Real-Time Visualization of Cerebral Blood Flow in Cerebrovascular Surgery: Results From Pre-Clinical Studies. Scientific Reports. 2020 12;10(1):7614.

[222] Lucas BD, Kanade T. An iterative image registration technique with an application to stereo vision. vol. 81. Vancouver, British Columbia; 1981.

[223] Tomasi C, Kanade T. Detection and tracking of point features. Int J Comput Vis. 1991;9:137–154.

[224] Hartley R, Zisserman A. Multiple view geometry in computer vision. Cambridge university press; 2003.

[225] Büscher R, Herrmann V, Ring KM, Kailasam MT, O'Connor DT, Parmer RJ, et al. Variability in phenylephrine response and essential hypertension: a search for human alpha(1B)-adrenergic receptor polymorphisms. The Journal of pharmacology and experimental therapeutics. 1999 11;291(2):793–8.

[226] McPhee I, Levac B, Pyke K. Within Subject Variability and Duration of Brachial Artery Dilation in Response to GTN. The FASEB Journal. 2015 4;29(S1).

[227] Schmetterer L, Wolzt M, Salomon A, Rheinberger A, Unfried C, Zanaschka G, et al. Effect of isoproterenol, phenylephrine, and sodium nitroprusside on fundus pulsations in healthy volunteers. British Journal of Ophthalmology. 1996 3;80(3).

[228] Stewart JM, Suggs M, Merchant S, Sutton R, Terilli C, Visintainer P, et al. Postsynaptic α-Adrenergic Vasoconstriction Is Impaired in Young Patients With Vasovagal Syncope and Is Corrected by Nitric Oxide Synthase Inhibition. Circulation: Arrhythmia and Electrophysiology. 2016 8;9(8).

[229] Vargas Pelaez AF, Gao Z, Ahmad TA, Leuenberger UA, Proctor DN, Maman SR, et al. Effect of adrenergic agonists on coronary blood flow: a laboratory study in healthy volunteers. Physiological Reports. 2016 5;4(10).

[230] Moppett IK, Sherman RW, Wild MJ, Latter JA, Mahajan RP. Effects of norepinephrine and glyceryl trinitrate on cerebral haemodynamics: transcranial Doppler study in healthy volunteers. British Journal of Anaesthesia. 2008 2;100(2).

[231] Bashir A, Lewis M, Henderson A. Pharmacokinetic studies of various preparations of glyceryl trinitrate. British Journal of Clinical Pharmacology. 1982 12;14(6).

[232] Clark R. Notes on the resolution and other details of the human eye; 2018. Available from: `https://clarkvision.com/articles/eye-resolution.html`.

[233] Schlaffke L, Golisch A, Haag LM, Lenz M, Heba S, Lissek S, et al. The Brains Dress Code: How The Dress allows to decode the neuronal pathway of an optical illusion. Journal of Vision. 2016;16(12):747.

[234] Orujov F, Maskeliūnas R, Damaševičius R, Wei W. Fuzzy based image edge detection algorithm for blood vessel detection in retinal images. Applied Soft Computing. 2020;94:106452.

[235] WilliamThomas HM, Kumar SCP. A review of segmentation and edge detection methods for real time image processing used to detect brain tumour. In: 2015 IEEE International Conference on Computational Intelligence and Computing Research (ICCIC). IEEE; 2015. p. 1–4.

[236] Zhao Yu-qian, Gui Wei-hua, Chen Zhen-cheng, Tang Jing-tian, Li Ling-yun. Medical Images Edge Detection Based on Mathematical Morphology. In: 2005 IEEE Engineering in Medicine and Biology 27th Annual Conference. IEEE; 2005. p. 6492–6495.

[237] Preda G, Bourcier S, Joffre J, Boelle PY, Dubee V, Baudel JL, et al. Mottling score is associated with 28-day mortality in critically ill patients with sepsis. Minerva anestesiologica. 2017;83(6):664.

[238] Haebisch EMAB. Transdermal glyceryl trinitrate (nitroglycerin) in healthy persons: acute effects on skin temperature and hemodynamic orthostatic response. Sao Paulo Medical Journal. 1995 10;113(5):973–982.

[239] Legrand M, De Backer D, Dépret F, Oufella HA. Recruiting the microcirculation in septic shock. Springer Verlag; 2019.

[240] Kirsch RA. Computer determination of the constituent structure of biological images. Computers and Biomedical Research. 1971 6;4(3):315–328.

[241] Karasulu B. Automatic extraction of retinal blood vessels: a software implementation. European Scientific Journal. 2012;8(30).

[242] Allen J. Photoplethysmography and its application in clinical physiological measurement; 2007.

[243] Elgendi M. On the analysis of fingertip photoplethysmogram signals. Current cardiology reviews. 2012;8(1):14–25.

[244] Reisner A, Shaltis P, McCombie D, Asada H, Warner D, Warner M. Utility of the Photoplethysmogram in Circulatory Monitoring. Anesthesiology. 2008 5;108(5).

[245] Townsend N. Pulse Oximetry; 2001. Available from: `https://www.robots.ox.ac.uk/~neil/teaching/lectures/med_elec/notes6.pdf`.

[246] Lopez S, Americas R. Pulse oximeter fundamentals and design. Free scale semiconductor. 2012;p. 23.

[247] Harford M, Villarroel M, Jorge J, Redfern O, Finnegan E, Davidson S, et al. Contactless skin perfusion monitoring with video cameras: tracking pharmacological vasoconstriction and vasodilation using photoplethysmographic changes. Physiological Measurement. 2022;43(11):115001.

[248] Kamshilin AA, Margaryants NB. Origin of Photoplethysmographic Waveform at Green Light. Physics Procedia. 2017;86:72–80.

[249] Volynsky M, Margaryants N, Mamontov O, Kamshilin A. Contactless Monitoring of Microcirculation Reaction on Local Temperature Changes. Applied Sciences. 2019 11;9(22):4947.

[250] Zahedi E, Jaafar R, Mohd Ali MA, Mohamed AL, Maskon O. Finger photoplethysmogram pulse amplitude changes induced by flow-mediated dilation. Physiological Measurement. 2008 5;29(5):625–637.

[251] Sniecinski RM, Wright S, Levy JH. Cardiovascular pharmacology. Elsevier Inc; 2007.

[252] Villarroel M, Chaichulee S, Jorge J, Davis S, Green G, Arteta C, et al. Non-contact physiological monitoring of preterm infants in the Neonatal Intensive Care Unit. npj Digital Medicine. 2019;2(1):1–18. Available from: `http://dx.doi.org/10.1038/s41746-019-0199-5`.

[253] Verkruysse W, Svaasand LO, Nelson JS. Remote plethysmographic imaging using ambient light. Opt Express. 2008;16(26):21434–21445.

[254] Poh MZZ, McDuff DJ, Picard RW. Non-contact, automated cardiac pulse measurements using video imaging and blind source separation. Opt Express. 2010;18(10):10762–10774.

[255] Daly J. Video camera monitoring to detect changes in haemodynamics. University of Oxford; 2016.

[256] Zong W, Heldt T, Moody GB, Mark RG. An open-source algorithm to detect onset of arterial blood pressure pulses. In: Computers in Cardiology, 2003. IEEE; 2003. p. 259–262.

[257] Chaichulee S. Non-contact vital sign monitoring in pre-term infants. University of Oxford; 2018.

[258] Chaichulee S, Villarroel M, Jorge J, Arteta C, Green G, McCormick K, et al. Localised photoplethysmography imaging for heart rate estimation of pre-term infants in the clinic. In: Coté GL, editor. Optical Diagnostics and Sensing XVIII: Toward Point-of-Care Diagnostics. SPIE; 2018. p. 26.

[259] Villarroel M. Non-contact vital sign monitoring in the clinic. Department of Engineering Science. 2017;DPhil.

[260] Smith A. Color Gamut Transform Pairs. ACM Siggraph Computer Graphics. 1978 8;12:12–19.

[261] Walsh JA, Topol EJ, Steinhubl SR. Novel Wireless Devices for Cardiac Monitoring. Circulation. 2014 8;130(7):573–581.

[262] Chaves-González JM, Vega-Rodríguez MA, Gómez-Pulido JA, Sánchez-Pérez JM. Detecting skin in face recognition systems: A colour spaces study. Digital Signal Processing. 2010 5;20(3):806–823.

[263] Ricciuti M, Ciattaglia G, De Santis A, Gambi E, Senigagliesi L. Contactless Heart Rate Measurements using RGB-camera and Radar. In: ICT4AWE; 2020. p. 121–129.

[264] Jeong IC, Finkelstein J. Introducing Contactless Blood Pressure Assessment Using a High Speed Video Camera. J Med Syst. 2016;40(4):77.

[265] Sugita N, Obara K, Yoshizawa M, Abe M, Tanaka A, Homma N. Techniques for estimating blood pressure variation using video images. In: Engineering in Medicine and Biology Society (EMBC), 2015 37th Annual International Conference of the IEEE. Milan, Italy: IEEE; 2015. p. 4218–4221.

[266] Awad AA, Haddadin AS, Tantawy H, Badr TM, Stout RG, Silverman DG, et al. The relationship between the photoplethysmographic waveform and systemic vascular resistance. Journal of clinical monitoring and computing. 2007;21(6):365–372.

[267] Seitsonen ERJ, Korhonen IKJ, Van Gils MJ, Huiku M, Lötjönen JMP, Korttila KT, et al. EEG spectral entropy, heart rate, photoplethysmography and motor responses to skin incision during sevoflurane anaesthesia. Acta Anaesthesiologica Scandinavica. 2005;49(3):284–292.

[268] Jiang XJ. Quantification of glyceryl trinitrate effect through analysis of the synthesised ascending aortic pressure waveform. Heart. 2002 8;88(2):143–148.

[269] Paul M, Mota AF, Antink CH, Blazek V, Leonhardt S. Modeling photoplethysmographic signals in camera-based perfusion measurements: optoelectronic skin phantom. Biomedical Optics Express. 2019;10(9):4353–4368.

[270] De Weerd L, Weum S, Mercer J. Preoperative perforator mapping with dynamic infrared thermography in breast reconstruction with a DIEP flaps; 2012.

[271] Estebe JP, Davies JM, Richebe P. The pneumatic tourniquet: mechanical, ischaemia–reperfusion and systemic effects. European Journal of Anaesthesiology. 2011 6;28(6):404–411.

[272] Paul SP. Using a thermal imaging camera to locate perforators on the lower limb. Archives of Plastic Surgery. 2017;44(3):243–247.

[273] De Weerd L, Mercer JB, Setså LB. Intraoperative dynamic infrared thermography and free-flap surgery. Annals of Plastic Surgery. 2006 9;57(3):279–284.

[274] Unger M, Markfort M, Halama D, Chalopin C. Automatic detection of perforator vessels using infrared thermography in reconstructive surgery. International Journal of Computer Assisted Radiology and Surgery. 2019 3;14(3):501–507.

[275] Pajula J, Kauppi JP, Tohka J. Inter-Subject Correlation in fMRI: Method Validation against Stimulus-Model Based Analysis. PLoS ONE. 2012 8;8(8):e41196.

[276] Sorensen TA. A method of establishing groups of equal amplitude in plant sociology based on similarity of species content and its application to analyses of the vegetation on Danish commons. Biol Skar. 1948;5:1–34.

[277] Dice LR. Measures of the Amount of Ecologic Association Between Species. Ecology. 1945 7;26(3):297–302.

[278] Carass A, Roy S, Gherman A, Reinhold JC, Jesson A, Arbel T, et al. Evaluating White Matter Lesion Segmentations with Refined Sørensen-Dice Analysis. Scientific Reports. 2020 12;10(1):8242.

[279] Gault TR, Farag AA. A fully automatic method to extract the heart rate from thermal video. Portland, USA: IEEE; 2013.

[280] Jorge J, Harford M, Villarroel M, Chaichulee S, Davidson S, Finnegan E, et al. Non-invasive assessment of peripheral artery haemodynamics using infrared thermography. Transactions on Medical Imaging. 2019;.

[281] Zhou K. Observations concerning the mechanism of action of Glyceryl Trinitrate. University of Toronto. Toronto; 2018.

[282] Mellodge P. A practical approach to dynamical systems for engineers. Woodhead Publishing; 2015.

[283] Escolar JD, Escolar A. Lung hysteresis: a morphological view. Histology and histopathology. 2004;19(1):159–66.

[284] Camasão DB, Mantovani D. The mechanical characterization of blood vessels and their substitutes in the continuous quest for physiological-relevant performances. A critical review. Materials Today Bio. 2021 3;10:100106.

[285] Sullivan G, Edmondson C. Heat and temperature. Continuing Education in Anaesthesia Critical Care & Pain. 2008 6;8(3):104–107.

[286] Behem CR, Graessler MF, Friedheim T, Kluttig R, Pinnschmidt HO, Duprée A, et al. The use of pulse pressure variation for predicting impairment of microcirculatory blood flow. Scientific Reports. 2021 12;11(1):9215.

[287] Lundborg G, Rosen B. The Two-Point Discrimination Test – Time For a Re-Appraisal? Journal of Hand Surgery. 2004 10;29(5):418–422.

[288] Tong J, Mao O, Goldreich D. Two-Point Orientation Discrimination Versus the Traditional Two-Point Test for Tactile Spatial Acuity Assessment. Frontiers in Human Neuroscience. 2013;7.

[289] Craig JC, Lyle KB. A comparison of tactile spatial sensitivity on the palm and fingerpad. Perception & Psychophysics. 2001 2;63(2):337–347.

[290] Bakker J, Ince C. Monitoring coherence between the macro and microcirculation in septic shock. Current Opinion in Critical Care. 2020 6;26(3):267–272.

[291] Zaunseder S, Vehkaoja A, Fleischhauer V, Hoog Antink C. Signal-to-noise ratio is more important than sampling rate in beat-to-beat interval estimation from optical sensors. Biomedical Signal Processing and Control. 2022 4;74:103538.

[292] Cracowski JL, Roustit M. Human skin microcirculation. Comprehensive Physiology. 2020 7;10(3):1105–1154.

[293] Bobbia S, Macwan R, Benezeth Y, Mansouri A, Dubois J. Unsupervised skin tissue segmentation for remote photoplethysmography. Pattern Recognition Letters. 2019 6;124:82–90.

[294] Thijssen DHJ, Carter SE, Green DJ. Arterial structure and function in vascular ageing: are you as old as your arteries? The Journal of physiology. 2016;594(8):2275–2284.

[295] O'rourke MF, Hashimoto J. Mechanical factors in arterial aging: a clinical perspective. Journal of the American College of Cardiology. 2007;50(1):1–13.

[296] Saeedi P, Petersohn I, Salpea P, Malanda B, Karuranga S, Unwin N, et al. Global and regional diabetes prevalence estimates for 2019 and projections for 2030 and 2045: Results from the International Diabetes Federation Diabetes Atlas, 9th edition. Diabetes Research and Clinical Practice. 2019 11;157:107843.

[297] Schaper NC, Van Netten JJ, Apelqvist J, Lipsky BA, Bakker K. Prevention and management of foot problems in diabetes: a Summary Guidance for Daily Practice 2015, based on the IWGDF Guidance Documents. Diabetes/Metabolism Research and Reviews. 2016 1;32:7–15.

[298] Savill P. Early diagnosis of peripheral arterial disease can save limbs. The Practitioner. 2012 10;256(1755):19–21.

[299] Ray SA, Srodon PD, Taylor RS, Dormandy JA. Reliability of ankle: Brachial pressure index measurement by junior doctors. British Journal of Surgery. 1994 12;81(2):188–190.

[300] Caruana MF, Bradbury AW, Adam DJ. The Validity, Reliability, Reproducibility and Extended Utility of Ankle to Brachial Pressure Index in Current Vascular Surgical Practice. European Journal of Vascular and Endovascular Surgery. 2005 5;29(5):443–451.

[301] Al-Qaisi M. Ankle Brachial Pressure Index (ABPI): An update for practitioners. Vascular Health and Risk Management. 2009 9;p. 833.

[302] Loader J, Khouri C, Taylor F, Stewart S, Lorenzen C, Cracowski J, et al. The continuums of impairment in vascular reactivity across the spectrum of cardiometabolic health: A systematic review and network meta-analysis. Obesity Reviews. 2019 6;20(6):906–920.

[303] Reynès C, Beaume JB, Latil-Plat F, Ennaifer H, Rocher L, Antoine-Jonville S, et al. Concomitant Peripheral Neuropathy and Type 2 Diabetes Impairs Postexercise Cutaneous Perfusion and Flowmotion. The Journal of Clinical Endocrinology & Metabolism. 2021 6;.

[304] Potočnik N, Lenasi H. The responses of glabrous and nonglabrous skin microcirculation to graded dynamic exercise and its recovery. Clinical Hemorheology and Microcirculation. 2016 11;64(1):65–75.

[305] Salvi D, Poffley E, Orchard E, Tarassenko L. The Mobile-Based 6-Minute Walk Test: Usability Study and Algorithm Development and Validation. JMIR mHealth and uHealth. 2020 1;8(1):e13756.

[306] Cheng Yy, Lin SJs, Chang Ch, Lin Cj, Tsai Cc, Su Yc. Cool extremities, a diagnostic sign recorded in Shang Han Lun, still good prognosis index for septic patients in today's medical intensive care unit. Chinese journal of integrative medicine. 2014;p. 1–8.

[307] Margetis D, Maury E, Boelle PY, Alves M, Galbois A, Baudel JL, et al. Peripheral microcirculatory exploration during mechanical ventilation weaning. Minerva Anestesiol. 2014;80(11):1188–1197.

[308] Bourcier S, Pichereau C, Boelle PY, Nemlaghi S, Dubée V, Lejour G, et al. Toe-to-room temperature gradient correlates with tissue perfusion and predicts outcome in selected critically ill patients with severe infections. Annals of intensive care. 2016;6(1):63.

[309] OHK Medical Devices. HemaClear: Directions for Use; 2015. Available from: `https://www.hemaclear.com/hemaclear-products/hemaclear-product-line/hemaclear-medium-yellow/`.

[310] Mathworks inc. Matlab rgb2hsv documentation; 2020. Available from: `https://www.mathworks.com/help/matlab/ref/rgb2hsv.html`.